Vol. 59 JANUARY, 1955 No. 1

THE JOURNAL OF PHYSICAL CHEMISTRY

(Registered in U. S. Patent Office)

THE JOURNAL OF PHYSICAL CHEMISTRY

(Registered in U. S. Patent Office)

Published monthly by the American Chemical Society at 20th and Northampton Sts., Easton, Pa.

Entered as second-class matter at the Post Office at Easton, Pennsylvania.

The *Journal of Physical Chemistry* is devoted to the publication of selected symposia in the broad field of physical chemistry and to other contributed papers.

Manuscripts originating in the British Isles, Europe and Africa should be sent to F. C. Tompkins, The Faraday Society, 6 Gray's Inn Square, London W. C. 1, England.

Manuscripts originating elsewhere should be sent to W. Albert Noyes, Jr., Department of Chemistry, University of Rochester, Rochester 3, N. Y.

Correspondence regarding accepted copy, proofs and reprints should be directed to Assistant Editor, Allen D. Bliss, Department of Chemistry, Simmons College, 300 The Fenway, Boston 15, Mass.

Business Office: American Chemical Society, 1155 Sixteenth St., N. W., Washington 6, D. C.

Advertising Office: Reinhold Publishing Corporation, 430 Park Avenue, New York 22, N. Y.

Articles must be submitted in duplicate, typed and double spaced. They should have at the beginning a brief Abstract, in no case exceeding 300 words. Original drawings should accompany the manuscript. Lettering at the sides of graphs (black on white or blue) may be pencilled in, and will be typeset. Figures and tables should be held to a minimum consistent with adequate presentation of information. Photographs will not be printed on glossy paper except by special arrangement. All footnotes and references to the literature should be numbered consecutively and placed in the manuscript at the proper places. Initials of authors referred to in citations should be given. Nomenclature should conform to that used in *Chemical Abstracts*, mathematical characters marked for italic, Greek letters carefully made or annotated, and subscripts and superscripts clearly shown. Articles should be written as briefly as possible consistent with clarity and should avoid historical background unnecessary for specialists.

Symposium papers should be sent in all cases to Secretaries of Divisions sponsoring the symposium, who will be responsible for their transmittal to the Editor. The Secretary of the Division by agreement with the Editor will specify a time after which symposium papers cannot be accepted. The Editor reserves the right to refuse to publish symposium articles, for valid scientific reasons. Each symposium paper may not exceed four printed pages (about sixteen double spaced typewritten pages) in length except by prior arrangement with the Editor.

Remittances and orders for subscriptions and for single copies, notices of changes of address and new professional connections, and claims for missing numbers should be sent to the American Chemical Society, 1155 Sixteenth St., N. W., Washington 6, D. C. Changes of address for the *Journal of Physical Chemistry* must be received on or before the 30th of the preceding month.

Claims for missing numbers will not be allowed (1) if received more than sixty days from date of issue (because of delivery hazards, no claims can be honored from subscribers in Central Europe, Asia, or Pacific Islands other than Hawaii), (2) if loss was due to failure of notice of change of address to be received before the date specified in the preceding paragraph, or (3) if the reason for the claim is "missing from files."

Subscription Rates: to members of the American Chemical Society, $8.00 for 1 year, $15.00 for 2 years, $22.00 for 3 years; to non-members, $10.00 for 1 year, $18.00 for 2 years, $26.00 for 3 years. Postage free to countries in the Pan American Union; Canada, $0.40; all other countries, $1.20. $12.50 per volume, foreign postage $1.20, Canadian postage $0.40; special rates for A.C.S. members supplied on request. Single copies, current volume, $1.00; foreign postage, $0.15; Canadian postage $0.05. Back issue rates (starting with Vol. 56): non-member, $1.50 per issue, foreign postage $0.15, Canadian postage $0.05.

The American Chemical Society and the Editors of the *Journal of Physical Chemistry* assume no responsibility for the statements and opinions advanced by contributors to THIS JOURNAL.

The American Chemical Society also publishes *Journal of the American Chemical Society, Chemical Abstracts, Industrial and Engineering Chemistry, Chemical and Engineering News, Analytical Chemistry*, and *Journal of Agricultural and Food Chemistry*. Rates on request.

THE JOURNAL OF
PHYSICAL CHEMISTRY

(Registered in U. S. Patent Office) (Copyright, 1955, by the American Chemical Society)

VOLUME 59 JANUARY 14, 1955 NUMBER 1

KINETICS OF PHASE TRANSFORMATION IN SUPERCOOLED SOLUTIONS

BY R. P. RASTOGI AND A. C. CHATTERJI

Department of Chemistry, Lucknow University, India

Received September 28, 1953

The linear velocity of crystallization in supercooled solutions of solids in liquids has been measured at various degrees of supersaturation. The phenomenon of maximum velocity is also observed in solutions. At high degrees of supersaturation, the velocity is uniform while at low degrees of supersaturation gradually diminishing velocity is observed. Attempt has been made to explain the results on the basis of Frenkel's theory of two-dimensional crystallization velocity.

1. Introduction

The initiation and separation of a new phase is attended by two rate processes, namely, the rate of formation of nuclei and the rate of growth of these crystal germs. Considerable amount of theoretical as well as experimental work has been done on the kinetics of these processes in uni-component systems.[1-3] The particular case of liquid solutions seems not to have received sufficient attention although attempts have been made to study phase transitions in supercooled mixed vapors and alloys. In spite of the elegant technique developed by Vonnegut[4] for the measurement of the rate of nucleation in supercooled liquids, it is still difficult to determine the rates in solutions. Accordingly an effort has been made to measure the linear velocity of crystallization of the solutes in supersaturated solutions for which the data are recorded in this paper.

In the over-all picture of crystallization in solutions, the kinetics of linear crystal growth has an important place. Although it can yield no crystallographic information, yet it has been shown that in a straight tube, the rate at which the solid front of crystallization moves forward is not usually far removed from the velocity of crystal growth along the longer diagonal.[5] The linear velocity of crystallization of supercooled liquids has been extensively studied by Tamman and his school. It has been reported that the velocity increases as the temperature is lowered until it attains the maximum value after which the velocity decreases with further supercooling. The pronounced effect of the viscosity of the medium has also been stressed.[6] The phenomenon has been theoretically treated by Volmer and Marder[7] and Frenkel[8] for unicomponent systems. Following Frenkel, an expression for the two-dimensional crystallization velocity for the analogous case of supersaturated solution can be easily deduced. In the case of solutions, diffusion is an important factor to be considered. For the molecules of the solute have to diffuse through the solution to get adsorbed on the growing crystal boundary. As usual for rate processes, the diffusion of solute molecules will require a certain activation energy $\Delta u'$. The activation energy of self-diffusion is related to viscosity of the medium. Thus the velocity is given by the following expression if we neglect the surface diffusion on the crystal

$$I = \text{Const} \times e^{-1/kT\left[\Delta u' + \frac{B}{T_s - T}\right]} \qquad (1)$$

where

$$B = \frac{1}{4} \times \frac{\alpha'^2 T_s}{\lambda}$$

α' = surface tension over the boundary of plane embryo.
Ts = saturation temp.
λ = heat of solution

Equation 1 yields the maximum velocity

$$I_{max} = \text{Const} \times e^{-\Delta u'/k(2T_{max} - T_s)} \qquad (2)$$

(1) M. Volmer, "Kinetik der Phasenbildung," T. Steinkoff, Dresden, 1939.

(2) G. M. Pound and V. K. La Mer, *J. Am. Chem. Soc.*, **74**, 2323 (1952).

(3) W. J. Dunning, "Crystal Growth," *Discs. Trans. Faraday Soc.*, **79**, 183 (1949).

(4) B. Vonnegut, *J. Coll. Sci.*, **3**, 563 (1948).

(5) H. E. Buckley, "Crystal Growth," John Wiley and Sons, Inc., New York, N. Y., 1951.

(6) J. H. Hildebrand and G. J. Rotariu, *J. Am. Chem. Soc.*, **73**, 2524 (1951); R. E. Powell, T. S. Gilman and J. H. Hildebrand, *ibid.*, **73**, 2525 (1951).

(7) M. Volmer and Marder, *Z. physik. Chem.*, **154**, 97 (1931).

(8) J. Frenkel, "Kinetic Theory of Liquids," Oxford University Press, London, 1946, p. 434.

by putting $dI/dt = 0$. From the condition of maxima, the value of B is found to be given by

$$B = \Delta u'(T_s - T_{max})^2/(2T_{max} - T_s) \qquad (3)$$

where T_{max} is the temperature at which the velocity is maximum.

2. Experimental

The experimental arrangement was similar to that adopted by Walton and co-workers.[9] The use of U-tube as employed by Tamman was avoided since that would vitiate the results both because the velocity would be different at bends as shown by Buckley[5] and also because the gravity would affect the rate. Consequently we have employed straight horizontal tubes in our experiments. The experimental Pyrex tube was about one meter long having a diameter of one cm. It was glass-stoppered at both the ends. The tube, filled with the supersaturated solution to be investigated, was placed in a specially constructed air-thermostat which had a glass-pane parallel to the tube and a meter scale attached to it. With a powerful beam of light the movement of the crystal boundary could be marked very conveniently. In preparing the solution, care was taken to free it from dust particles and other possible forms of nuclei. The crystallization was induced by freshly prepared seed crystals. As soon as the crystallization started, the time taken by the crystal boundary to traverse a known distance was noted after regular intervals of time to see whether the velocity was uniform or not. In most of the cases, at high degrees of supersaturation it was found to be uniform. Several such readings were taken at the particular temperature of the thermostat, which were found to be similar. In a similar manner the rate of growth was determined at various temperatures. For determining the rate at temperatures well below the room temperature, ice-cold water was circulated in a similar tube enclosed in a glass-jacket from a big reservoir whose temperature was adjusted by adding requisite quantities of ice.

In such experiments the heat of crystallization will enhance the temperature at the crystal boundary, and consequently the measured rates may not be isothermal. The solutions cannot be stirred and hence the heat developed is still more localized. To have an idea about the magnitude of heat developed mention may be made of the experiments of Dunning[3] in which the increase of temperature at the crystal boundary is of the order of 10^{-4} °, but the solutions were constantly stirred. In our experiments, the temperature increase will be rather significant. However, it appears that a steady state is reached and the temperature remains constant throughout the tube, although somewhat higher than the temperature of the thermostat. This is supported by the fact that for high degree of supersaturation, the velocity remains the same at all points of the tube which could not have been uniform otherwise.

Standardized thermometers and stop-watches were used in the experiment. The mean observations are recorded below. The temperatures are given in degrees centigrade and the velocity in cm./min.

Discussion

From the results given in the Tables I–IV, it is clear that the velocity increases very rapidly with increase in supercooling. The velocity passes through maximum only in the case of sodium thiosulfate. The phenomenon of maximum velocity has also been shown to occur in aqueous solutions of sodium and potassium acetates[1] by Chatterji and Rastogi.[10] This clearly establishes that the phenomenon of maximum velocity occurs in solutions also, about the existence of which doubt had been cast previously. In the rest of the cases, the spontaneous crystallization occurs before the temperature of maximum velocity is reached.

(9) Walton and co-workers, *J. Am. Chem. Soc.*, **38**, 317 (1916); **40**, 1168 (1918).

(10) A. C. Chatterji and R. P. Rastogi, *J. Ind. Chem. Soc.*, **28**, 599 (1951).

It is not possible to apply various theories to the experimental data as the quantities involved in the expression for velocity cannot be determined easily. Therefore, we shall attempt only to see how far the observed facts can be explained, rather in a qualitative way. Consider equation (1) *viz.*

$$I = \text{Const} \times e^{-1/kT\left[\Delta u' + \frac{B}{T_s - T}\right]}$$

TABLE I

Temp., °C.	Velocity, cm./min.	Temp., °C.	Velocity, cm./min.
(1) System acetanilide–chloroform, satn. temp. 50°		(2) System acenaphthene–toluene, satn. temp. 40°	
42.5	[a]	39.0	[a]
40.0	0.56	38.0	0.52
37.5	1.05	35.5	1.35
35.0	2.55	33.0	1.80
32.5	4.53	31.0	2.02
30.0	7.07	27.5	5.40
26.4	8.02	25.0	6.00
(3) System naphthalene–toluene, satn. temp. 40°		(4) System diphenylamine–methyl alcohol, satn. temp. 40°	
38.5	[a]	38.0	0.14
37.0	0.55	34.5	1.18
36.0	1.03	33.5	3.60
35.0	2.34	32.5	4.40
34.0	[b]	31.5	5.23
(5) System diphenylamine–toluene, satn. temp. 40°		30.5	6.00
35.0	[a]	28.5	7.21
33.0	0.10	27.5	7.60
31.5	0.40	26.0	7.81
30.0	0.75	24.0	8.40
29.0	1.40	(6) System diphenylamine–ethyl alcohol, satn. temp 40°	
28.0	2.15	37.5	[a]
26.0	2.91	36.5	0.70
24.0	3.39	34.0	2.40
(7) System diphenylamine–benzene, satn. temp. 40°		32.0	4.50
35.0	[a]	30.0	5.80
34.0	0.21	27.0	6.80
32.0	.30	24.0	7.40
30.0	.40	(8) System diphenylamine–*m*-xylene, satn. temp. 40°	
28.0	.65	37.0	[a]
26.0	.90	36.0	0.08
25.0	.96	34.0	.16
24.0	1.06	32.0	.31
(9) System urea–water, satn. temp. 40°		30.0	.45
37.5	[a]	27.5	.62
35.5	1.75	24.0	3.10
33.0	2.59	(10) System sodium thiosulfate–water, satn. temp. 70° (?)	
31.0	3.70	30.0	[a]
28.5	5.70	25.0	0.60
26.0	8.10	15.0	2.00
24.0	[b]	12.5	3.00
		10.0	3.80
		7.8	5.31[c]
		6.0	5.00
		2.0	4.01

[a] Irregular velocity, *i.e.*, velocity continually diminishing with time. [b] Spontaneous crystallization. [c] Maximum velocity.

TABLE II

In the following cases the velocity was slower than the previous cases even at large degrees of supercooling, hence the effect of supercooling could not be studied.

System	T_s	Obsd. temp., °C.	Velocity, cm./min.
Manganese chloride–water	40	5.0	0.013
Calcium nitrate–water	32	10.0	0.42
		−2.0	0.81
		−6.0	1.05
Sodium formate–water	54	32.0	0.10

TABLE III

In the following systems the velocity of crystallization was found to be very slow and sometimes only vigorous shaking brought about crystallization. T_s was 40° in each case.

1. Resorcinol–methyl alcohol
2. Resorcinol–ethyl alcohol
3. Sodium benzoate–water
4. Acetanilide–water

TABLE IV

For the aqueous solutions of following substances, there is no linear velocity of crystallization, probably due to lack of definite crystal boundary and the occurrence of spontaneous crystallization.

1. Potassium chloride
2. Potassium bromide
3. Potassium nitrate
4. Potassium nitrite

where

$$B = \frac{1}{4} \times \frac{\alpha'^2 T_s}{\lambda}$$

The exponential term contains one term due to viscosity and other due to supercooling. As the temperature of the solution is lowered, viscosity increases rapidly and hence the first term increases while the other one decreases. The role at the temperature of maximum velocity as played by viscosity is revealed by the expression

$$I_{max} = \text{Const} \times e^{-\Delta u'/k(2T_{max} - T_s)}$$

The role of viscosity has been clearly demonstrated by Michnevitch.[11] It was found by him that the product of velocity of crystallization and the viscosity rises monotonically as the temperature is lowered below the standard crystallization point. Consequently those solutions will display a maximum whose energy of self-diffusion is comparable to the energy required to form new nets of adsorbed layers since at the temperature of maximum velocity we have the relation

$$\Delta u' = B(2T_{max} - T_s)/(T_s - T_{max})^2$$

Since the solutions of sodium and potassium acetates are highly viscous in comparison to others studied here, it is quite possible that the activation energy of self-diffusion may be sufficiently high to cause the phenomenon of maximum velocity to occur in these cases. It may be pointed out here, that provided the value of $\Delta u'$ is known from viscosity measurements, the value of interfacial tension can be calculated from the above expression.

As regards the solutions represented in Table III, since the order of factors occurring in B is the same and the velocity is not large, it can be conceived that the constant ought to be small for such cases. The thermodynamic theory cannot give an estimate of the constant. Although Reiss[12] has tried to deduce expressions for the constant, yet it is not possible to have an exact estimate because of certain factors which cannot be evaluated. One reason for the low value of velocity may be ascribed to the fact that the crystals which grow are not perfect and their imperfections provide the steps required, making two-dimensional nucleation unnecessary. Thus the low value of velocity may be due to the absence of dislocations in the surface or to the presence of so many that the mean distance between them is much smaller than the crystal nucleus. Burton, Cabrera and Frank[13] have shown that the latter alternative is not possible.

In certain solutions represented in Table I, the velocity along the tube for low degree of supersaturation diminishes continuously as the boundary moves forward. Consider equation 1. The equation suggests that at a particular temperature the velocity would remain constant provided the saturation temperature all along the tube does not vary appreciably. If there is quick diffusion rather more significant than the movement of the crystal boundary, the saturation temperature will decrease as the crystal boundary moves forward and hence the factor $e^{-1/kT \times B/(T_s - T)}$ and the velocity will diminish gradually. Reiss and La Mer[14] have theoretically solved the problem of diffusion which involves moving boundaries. They have deduced expressions for the case when the flux of material through any surface in the diffusional field is considerably greater than the rate of change of concentration on that surface and *vice versa*. The interpretation of the results on the basis of such a procedure may yield interesting results and will be attempted in a future communication.

Lastly it has been shown that the linear velocity of crystallization would occur when a sharp crystal boundary is formed. No such boundary is formed in aqueous solutions of most of the electrolytes probably because the solubility and the temperature coefficient is not so high.

(11) Michnevitch, Dissertation, Odessa, 1941.

(12) H. Reiss, *J. Chem. Phys.*, **18**, 840 (1950).

(13) W. K. Burton, N. Cabrera and F. C. Frank, *Phil. Trans. Roy. Soc.* (London), **A243**, 299 (1951).

(14) H. Reiss and V. K. La Mer, *J. Chem. Phys.*, **18**, 1 (1950).

SOME THERMAL PROPERTIES OF 1-MONOSTEARIN, 1-ACETO-3-STEARIN AND 1,2-DIACETO-3-STEARIN[1]

BY T. L. WARD, E. J. VICKNAIR, W. S. SINGLETON AND R. O. FEUGE

Southern Regional Research Laboratory,[2] New Orleans, Louisiana

Received December 28, 1953

Pure 1-monostearin, 1-aceto-3-stearin and 1,2-diaceto-3-stearin have been examined calorimetrically over a temperature range of −73 to 100°. The properties investigated were specific heat (C_p), heat of fusion, accumulated heat content and heat of transition upon changing polymorphic form.

The acetylated glycerides 1-aceto-3-stearin and 1,2-diaceto-3-stearin possess the unique property of solidifying in a very pliable and stretchable form when cooled under normal conditions.[3] This form has been identified as the alpha modification[4,5] which is stable for many practical purposes, even though it is not thermodynamically stable.

The polymorphism and certain other physical properties of both the triglyceride 1,2-diaceto-3-stearin and the diglyceride 1-aceto-3-stearin have been described by Vicknair, *et al.*[5] The polymorphism of the triglyceride has also been described by Jackson and Lutton.[4]

Melting points and other constants of 1-monostearin have been reported by a number of workers,[6–9] but apparently there have been no previous report of specific heats and heat of fusion.

In the present investigation pure 1-monostearin, 1-aceto-3-stearin and 1,2-diaceto-3-stearin were examined calorimetrically over a temperature range of −73 to 100°. Specific heats, heat contents, latent heats of fusion, and heats of transition when polymorphic transformations occurred were either measured experimentally or calculated from the experimental data.

Experimental

Preparation of Glycerides.—The 1-monostearin was prepared by esterifying stearic acid in the presence of an excess of glycerol and a small amount of soap and then purifying the reaction product, principally by fractional crystallization from solvents, as described by Singleton and Vicknair.[9] The purity of the 1-monostearin obtained was better than 99%, as indicated by its melting curve and the periodic acid method of analysis.[10]

Both the 1-aceto-3-stearin and 1,2-diaceto-3-stearin were prepared by a modification of the method of Malkin, *et al.*[11] Briefly, the procedure consisted of the direct esterification of 1-monostearin with acetyl chloride and purification of the product by fractional crystallization from solvent. Analytical data for the two samples of mixed glycerides were as follows: Calcd. for $C_{23}H_{44}O_5$ (1-aceto-3-stearin): C, 68.96; H, 11.20; hydroxyl value, 140. Found: C, 69.04; H, 11.19; hydroxyl value, 142; m.p., 50.3°. Calcd. for $C_{25}H_{46}O_6$ (1,2-diaceto-3-stearin): C, 67.84; H, 10.48. Found: C, 67.99; H, 10.61; m.p., 48.6°.

Heating and cooling curves obtained by the method of Smit[12] indicated that the two acetoglycerides were at least 98% pure.

Apparatus and Procedure.—The calorimetric apparatus and procedure and the calculations employed have been described in a previous publication.[13] The calorimeter used was a modification of the vacuum enclosed aneroid type modified specifically for use with vegetable fats and oils. The instantaneous values for specific heat at the midpoint of approximately three degree intervals were measured directly in the calorimeter as was the latent heat of fusion. Heat content curves and other thermal data were obtained by calculation using the specific heat and heat of fusion data. The samples were placed in the calorimeter in the melted state and cooled to −73° at a moderate rate (3 to 5 degrees per minute).

The thermochemical calorie (4.180 absolute joules) was used in all calculations.

The results obtained are believed to be accurate to within 1%.

In identifying the polymorphic forms of 1-monostearin the nomenclature employed by Lutton and Jackson[8] was used.

Lutton and Jackson[8] reported that the melting and resolidification of 1-monostearin always resulted in the formation of the α-form, which on further cooling reversibly transformed to the sub-α-form. Therefore, the initial determinations of the thermal properties of 1-monostearin were obtained on the sub-α-form while later determinations probably tended more toward the α-form as the transition temperature (49°) was approached. The β- and β'-forms were not investigated because for all practical purposes they must be obtained by crystallization from solvent,[5] and hence could not be formed in the type of calorimeter which was employed.

Three polymorphic forms of solid 1-aceto-3-stearin have been identified by Vicknair, *et al.*,[5] on the basis of crystal spacings obtained from X-ray diffraction patterns. They are β', α and sub-α. The α-form is the plastic, stretchable form whereas the β'-form behaves more like a conventional hard fat. Vicknair, *et al.*, found that 1-aceto-3-stearin solidified in the α-form when the melt was cooled at an ordinary rate. They also found the capillary melting point of this form to be 47.5°. However, the α-form apparently transformed in the dilatometer to the β'-form at some temperature below 47.5°. By a very rapid determination of this transformation, they placed it at about 36°.

In the present investigation, data were assembled for the two forms of the solid 1-aceto-3-stearin identified as the sub-α and α. No data were obtained for the β'-form because only ten degrees in temperature separated the transition point of the α-form and the melting point of the β'-form. Premelting began within that interval.

It has been observed[8] that on solidifying 1,2-diaceto-3-stearin at a moderate rate the α-modification is obtained and that further cooling results in a transition to the sub-α-

(1) Presented at the 9th Southwest Regional Meeting of the American Chemical Society, New Orleans, Louisiana, December 10–12, 1953.

(2) One of the laboratories of the Bureau of Agricultural and Industrial Chemistry, Agricultural Research Service, U. S. Department of Agriculture. Article not copyrighted.

(3) R. O. Feuge, E. J. Vicknair and N. V. Lovegren, *J. Am. Oil Chemists' Soc.*, **29**, 29 (1952).

(4) F. L. Jackson and E. S. Lutton, *J. Am. Chem. Soc.*, **74**, 4827 (1952).

(5) E. J. Vicknair, W. S. Singleton and R. O. Feuge, THIS JOURNAL, **58**, 64 (1954).

(6) R. S. Rewadikar and H. E. Watson, *J. Indian Inst. Sci.*, **13A**, Pt. 11, 128 (1930).

(7) T. Malkin and M. R. el Shurbagy, *J. Chem. Soc.*, 1628 (1936).

(8) E. S. Lutton and F. L. Jackson, *J. Am. Chem. Soc.*, **70**, 2445 (1948).

(9) W. S. Singleton and E. J. Vicknair, *J. Am. Oil Chemists' Soc.*, **28**, 342 (1951).

(10) E. Handschumaker and E. Linteris, *ibid.*, **24**, 143 (1947).

(11) T. Malkin, M. R. el Shurbagy and M. L. Meara, *J. Chem. Soc.*, 1409 (1937).

(12) W. M. Smit, "A Tentative Investigation Concerning Fatty Acids and Fatty Acid Methyl Esters," Hilversum, Drukkerig "De Mercuser," 1946.

(13) A. E. Bailey, S. S. Todd, W. S. Singleton and G. D. Oliver, *Oil & Soap*, **21**, 293 (1944).

form. In the present work these lower melting polymorphic forms were produced by this treatment. As an extension of this treatment, the 1,2-diaceto-3-stearin was tempered just below the melting point of the α-form in an effort to obtain the high-melting β-form. This tempering had effected transformation in dilatometers[6] but failed to do so in the calorimeter.

Results and Discussion

Specific Heat.—The specific heats of 1-monostearin, 1-aceto-3-stearin and 1,2-diaceto-3-stearin were determined from the calorimetric data and the values obtained were used to develop equations for calculating the specific heat of these glycerides in the liquid and various solid states over the temperature range of 200 to 370°K. Each equation is valid only for the state or polymorphic form and temperature interval indicated. Where specific heat was determined on two polymorphic forms two equations were developed for calculating the specific heat, one equation for each crystalline form. These equations, which relate specific heat (C_p) in calories per gram per degree to the temperature (t) in degrees centigrade (using the proper sign) are:

1-Monostearin: solid state, sub-α-form, (-13 to 40°), $C_p = 0.4977 + 0.00318t$; liquid state, (87 to 100°), $C_p = 0.5118 + 0.00182t$.

1-Aceto-3-stearin: solid state, sub-α-form, (-73 to -1°), $C_p = 0.4471 + 0.00133t$; α-form, (-1 to 27°), $C_p = 0.4513 + 0.00434t$; liquid state, (57 to 87°), $C_p = 0.2290 + 0.0068t$.

1,2-Diaceto-3-stearin: solid state, sub-α-form, (-73 to -3°), $C_p = 0.4315 + 0.00104t$; α-form, (-3 to 33°), $C_p = 0.4349 + 0.00213t$; liquid state, (77 to 97°), $C_p = 0.3790 + 0.00195t$.

The specific heats observed are given in Table I.

At -73° the specific heats of the three compounds were approximately the same. As the temperature increased the specific heat values gradually increased with that for 1-monostearin increasing the most. The value for 1-aceto-3-stearin increased an intermediate amount, while that for 1,2-diaceto-3-stearin increased the least.

At 0° the temperature of transition of the sub-α-form of 1-aceto-3-stearin to the α-form, the C_p of 1-aceto-3-stearin was 0.05 cal./g./deg. lower than that of 1-monostearin. At 0° which is 3.1° above the temperature at which the sub-α-form of 1,2-diaceto-3-stearin transformed to the α-form, the C_p of the 1,2-diaceto-3-stearin was 0.015 cal./g./deg. lower than that of 1-monostearin. At temperatures above the point of transition of the α-form of 1-aceto-3-stearin the C_p values increase at a rate approaching that for 1-monostearin. At the melting point of the 1-aceto-3-stearin the values are about equal. The difference in specific heats of the α-forms of 1-aceto-3-stearin and 1,2-diaceto-3-stearin increases as the temperature increases.

The C_p of 1-monostearin is approximately 20% higher than that of stearic acid within the temperature range of 0 to 50°.

It would appear from the data that the presence of an acetic acid group in the glyceride molecule causes a lowering of the specific heat of the solid.

The C_p of liquid 1,2-diaceto-3-stearin is about 0.1 cal./g./deg. lower than that of liquid 1-monostearin and approximately 0.2 cal./g./deg. lower than that of 1-aceto-3-stearin.

TABLE I

OBSERVED SPECIFIC HEATS OF 1-MONOSTEARIN, 1-ACETO-3-STEARIN AND 1,2-DIACETO-3-STEARIN

Temp., °C.	C_p 1-Monostearin, cal./g.	Temp., °C.	C_p 1-Aceto-3-stearin, cal./g.	Temp., °C.	C_p 1,2-Diaceto-3-stearin, cal./g.
−74.3	0.336	−71.4	0.351	−69.1	0.360
−70.8	.348	−64.9	.361	−61.6	.369
−67.2	.359	−61.1	.364	−59.4	.370
−63.0	.361	−57.8	.371	−57.0	.373
−59.1	.368	−53.6	.375	−51.9	.377
−53.6	.405	−47.7	.390	−47.9	.380
−49.9	.382	−44.1	.389	−43.5	.386
−46.9	.388	−39.5	.401	−40.8	.385
−42.4	.394	−34.9	.402	−36.3	.393
−36.9	.404	−27.9	.411	−34.3	.398
−32.6	.415	−24.5	.416	−31.7	.399
−28.3	.422	−20.6	.419	−28.6	.402
−23.0	.434	−17.0	.424	−26.0	.405
−18.6	.444	−12.7	.435	−22.3	.420
−12.4	.462	−10.2	.345	−19.4	.412
− 9.1	.470	− 5.9	.441	−18.1	.413
− 3.2	.491	− 3.1	.355	−14.4	.418
4.8	.514	0.6	.291	−12.1	.415
7.3	.521	5.6	.464	− 8.6	.422
11.5	.534	10.1	.502	− 5.9	.426
15.1	.543	14.0	.512	− 2.8	.433
18.8	.557	19.3	.540	0.9	.927
21.1	.565	22.2	.547	4.2	.444
24.8	.576	27.7	.568	8.0	.450
27.2	.584	28.8	.575	11.5	.463
32.0	.597	33.1	1.194	14.4	.465
39.3	.623	40.8	1.680	16.9	.466
42.2	.630	43.5	1.997	19.8	.477
46.1	1.156	60.0	0.637	23.3	.484
50.3	0.613	64.0	.671	25.5	.489
55.0	.691	67.5	.686	29.2	.498
61.2	.727	72.1	.719	32.3	.505
65.6	.771			35.5	.508
70.9	1.348			38.1	.570
87.4	0.656			41.6	.821
90.9	.677			61.3	.612
96.9	.688			66.4	.589
103.0	.700			70.2	.550
107.8	.707			73.1	.538
114.3	.722			77.1	.530
				80.1	.535
				83.3	.542
				88.9	.553
				94.6	.563
				96.9	.568

Heat of Fusion.—The heats of fusion were found to be as follows: 1-monostearin, 39.39 cal./g. (14.12°K. cal./mole) at 74.0°; 1-aceto-3-stearin, 24.87 cal./g. (9.96°K. cal./mole) at 46.7°; 1,2-diaceto-3-stearin, 24.60 cal./g. (10.89°K. cal./mole) at 35.1°.

The calorimetric melting points of the compounds, as determined from fusion data, agreed within 1 degree with those found dilatometrically[6,9] for the α-forms. Therefore, it can be assumed that each of the fusion determinations was made on the α-form.

For both 1-aceto-3-stearin and 1,2-diaceto-3-stearin the heats of fusion, on a gram basis, were ap-

proximately 63% of the corresponding value for 1-monostearin, which in turn was approximately 63% of the value reported previously for stearic acid.[14] It is therefore apparent that the introduction of one acetyl radical into the monostearin molecule lowers the heat of fusion to a considerable extent, but the introduction of a second acetyl radical causes no appreciable additional change. It is possible that this relationship holds for the monoglycerides of other saturated, fat-forming acids and their aceto derivatives.

If the heat of fusion of stearic acid is multiplied by the proportion by weight of stearoyl group in the monostearin, which is 0.746, a value of 42.9 cal./g. is obtained. This value is about 8% above the experimentally determined heat of fusion for monostearin. The relationship of melting dilation, which corresponds to heat of fusion, to content of the stearoyl group has been shown to hold in the case of stearic acid, 1-monostearin and tristearin.[9]

A plot of the heat of fusion of 1,2-diaceto-3-stearin *versus* the melting dilation of this compound[4] falls very close to but a little below the graphical representation of these same values for simple triglycerides, as illustrated by Bailey.[15] This indicates that the melting of this mixed triglyceride follows the pattern of the simple triglycerides of the saturated acids.

Heat Contents and Heats of Transition.—The accumulated heat contents of 1-monostearin, 1-aceto-3-stearin and 1,2-diaceto-3-stearin were calculated at the mid-temperature of the experimental determinations and are shown in Table II.

The data from Table II are illustrated graphically in Fig. 1.

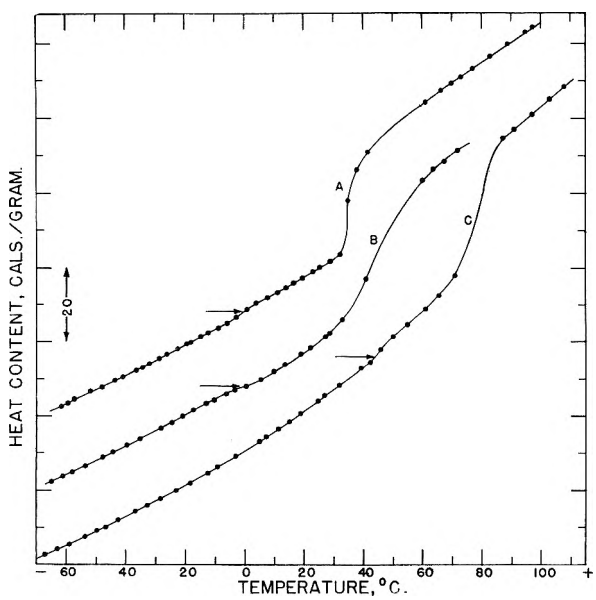

Fig. 1.—Heat of content curves: A, 1-monostearin; B, 1-aceto-3-stearin; C, 1,2-diaceto-3-stearin.

Points of possible polymorphic transformation are indicated by arrows in Fig. 1. In each of the three cases the heat content curve was so nearly smooth at the transition point that it precluded accurate measurement of the heat of transition. The heats of transition agree with dilation data[5,9] reported for these compounds in that a small transition contraction was reported for 1-aceto-3-stearin and small transition expansions were reported for 1-monostearin and 1,2-diaceto-3-stearin at the same temperatures indicated here. The loss in heat for 1-aceto-3-stearin and the gain in heat for 1,2-diaceto-3-stearin are the opposite of what would have been expected since a loss in heat content upon

TABLE II

ACCUMULATED HEAT CONTENTS OF 1-MONOSTEARIN, 1-ACETO-3-STEARIN AND 1,2-DIACETO-3-STEARIN

1-Monostearin		1-Aceto-3-stearin		1,2-Diaceto-3-stearin	
Temp., °C.	Heat content accumulated, cal./g.	Temp., °C.	Heat content accumulated, cal./g.	Temp., °C.	Heat content accumulated, cal./g.
−74.3	0.000	−71.4	0.000	−69.1	0.000
−70.8	1.197	−64.9	2.314	−61.6	2.738
−67.2	2.471	−61.1	3.690	−59.4	3.552
−63.0	3.983	−57.8	4.901	−57.0	4.445
−59.1	5.407	−53.6	6.468	−51.9	6.358
−53.6	7.519	−47.7	8.722	−47.9	7.874
−49.9	8.977	−44.1	10.122	−43.5	9.559
−46.9	10.132	−39.5	11.939	−40.8	10.601
−42.4	11.892	−34.9	13.784	−36.3	12.352
−36.9	14.087	−27.9	16.626	−34.3	13.144
−32.6	15.850	−24.5	18.030	−31.7	14.181
−28.3	17.652	−20.6	19.660	−28.6	15.424
−23.0	19.920	−17.0	21.179	−26.0	16.474
−18.6	21.852	−12.7	23.028	−22.3	18.002
−12.4	24.661	−10.2	24.003	−19.4	19.208
− 9.1	26.199	− 5.9	25.692	−18.1	19.745
− 3.2	29.037	− 3.1	26.807	−14.4	21.284
4.8	33.061	0.6	28.001	−12.1	22.243
7.3	34.356	5.6	29.891	− 8.6	23.710
11.5	36.574	10.1	32.060	− 5.9	24.855
15.1	38.514	14.0	34.037	− 2.8	26.179
18.8	40.549	19.3	36.825	0.9	28.695
21.1	41.839	22.2	38.400	4.2	30.147
24.8	43.952	27.7	41.469	8.0	31.846
27.2	45.344	28.8	42.098	11.5	33.446
32.0	48.181	33.1	45.904	14.4	34.792
39.3	52.634	40.8	56.969	16.9	35.957
42.2	54.452	43.5	61.934	19.8	37.326
46.1	57.936	60.0	83.657	23.3	39.006
50.3	61.653	64.0	86.273	25.5	40.077
55.0	64.717	67.5	88.307	29.2	41.905
61.2	69.113	72.1	91.536	32.3	43.461
65.6	72.409			35.5	58.000
70.9	78.032			38.1	66.201
87.4	94.575			41.6	71.121
90.9	96.910			61.3	84.415
96.9	101.008			66.4	87.475
103.0	105.241			70.3	89.698
107.8	108.620			73.1	91.221
114.3	113.268			77.1	93.357
				80.1	94.953
				83.3	96.678
				88.9	99.747
				94.6	102.928
				96.9	104.230

(14) W. S. Singleton, T. L. Ward and F. G. Dollear, *J. Am. Oil Chemists' Soc.*, **27**, 143 (1950).

(15) A. E. Bailey, "Melting and Solidification of Fats," Interscience Publishers, Inc., New York, N. Y., p. 179.

transition to a higher form usually occurs in triglycerides.

A comparison of the heat content curves with the specific heat data reveals that the transitions indicated are first-order phase changes, *i.e.*, changes in lattice structure.

THE LIQUID PHASE HYDROGENATION OF OLEFINS OVER ADAMS PLATINUM[1]

BY GEORGE W. WATT AND M. T. WALLING, JR.

Contribution from the Department of Chemistry of The University of Texas, Austin, Texas

Received May 18, 1954

The rates of hydrogenation of allyl alcohol and hexene-1 over Adams platinum in ethanol have been measured as a function of temperature, hydrogen pressure, agitation frequency, concentration of acceptor and product, and the ratio of catalyst to acceptor. The data indicate that the most probable rate-controlling process is the diffusion of hydrogen to the catalyst surface. On the assumption of a diffusion-controlled process, an equation relating the mode of variation of rate with weight of catalyst has been derived and has been used to correlate the data obtained using Adams platinum and related data obtained previously for W-6 Raney nickel, and for rhodium and palladium catalysts prepared by reduction of their salts with solutions of alkali metals in liquid ammonia.

For several years there have been in progress in these laboratories studies on the catalytic activity of Group VIII transitional metals produced by the reduction of salts with solutions of alkali metals in liquid ammonia.[2] In all of the cases studied thus far, catalysts prepared in ammonia have been compared with corresponding conventional catalysts and in certain instances particular attention has been given to the nature of the dependence of hydrogenation rates upon the weights of catalyst employed. All of the rate measurements have been made in the liquid phase with ethanol as the reaction medium, temperatures of the order of 30°, and hydrogen pressures at or below 2 atm.

Studies have been made using Adams platinum as a basis of comparison with platinum prepared by the reduction of tetrammineplatinum(II) bromide with potassium in ammonia.[3] The purpose of this paper is to present data in support of the view that the rate-determining process in the hydrogenation of allyl alcohol and hexene-1 over Adams platinum and certain other catalysts is the diffusion of hydrogen through the bulk liquid phase. Since the study of most of the usual variables led to results essentially no different from those reported by earlier workers, these results are summarized only briefly and primary emphasis is placed upon results having a major bearing upon the importance of the diffusional process.

Experimental

Materials.—Some samples of catalyst were prepared by the method of Adams, Voorhees and Shriner,[4] others as described by Frampton, Edwards and Henze.[5] The platinum content of these products ranged from 77.7 to 79.8% and the average was 79.0 (calcd. for $PtO_2 \cdot H_2O$:Pt, 79.6). It has been reported previously[4] that the activity of this type of catalyst varies as a function of the quantity prepared in a given batch and decreases upon storage. These characteristics were observed in the present work, and precautions were taken to ensure that the studies of each variable were conducted with catalyst from the same lot and over a period during which the activity of the stock sample did not undergo significant change. In addition, cross comparisons were made in enough cases to ensure that the results obtained were not unique to a particular sample of catalyst.

The hydrogen acceptors used were of the same origin and quality as those described previously.[2a]

Procedures.—The apparatus used for hydrogenation rate measurements differed from that described earlier[2a] in that an automatic pressure regulator was used to deliver hydrogen to the reactor at a known and constant pressure. Hydrogenation was effected either in the reactor employed previously[2a] and operated at 930 r.p.m. or in a mechanical shaker of conventional design and operated at 60, 115, 200 or 380 oscillations/min. Unless otherwise indicated, 1.0 ml. of allyl alcohol (0.85 g., 14.6 mmoles) in 10 ml. of ethanol, or 2.0 ml. of hexene-1 (1.35 g., 16.0 mmoles) in 9 ml. of ethanol was hydrogenated at 30.0 ± 0.5° at a hydrogen pressure of 1450 ± 25 mm. and an agitation frequency of 930 r.p.m.

At the start of a run, the catalyst sample was introduced into the reactor, covered and thoroughly wetted with a known volume of ethanol, and the oxide was reduced with hydrogen for 15 min. with agitation at a low rate. No uptake of hydrogen was ever observed after the first 3 or 4 min. of this treatment. The acceptor and sufficient ethanol to bring the total volume to that indicated above was then added in a manner which obviated exposure of the reduced catalyst to the atmosphere.

For computation of rates of hydrogenation from experimentally observed rates of change in the volume of the gas phase, the vapor pressure of solutions of the compositions involved in the various experiments were determined[6] and the corresponding corrections applied. Since the vapor pressures of these solutions changed only slightly during a run, a single average correction was applied to the data over the entire range of the run.

Rate *vs.* Hydrogen Pressure.—The dependence of rate of hydrogenation of both acceptors upon hydrogen pressure was determined over the pressure range 200–1500 mm. using several different lots of catalyst. The weights of catalyst employed were within the range 50–100 mg., *i.e.*, weights selected so that the rate was not dependent upon the weight of catalyst (*vide infra*). For both acceptors and all catalyst samples, the observed rates were linear with respect to hydrogen pressure.

(1) This work was supported in part by the Office of Naval Research, Contract N6onr-26610.

(2) (a) G. W. Watt, W. F. Roper and S. G. Parker, *J. Am. Chem. Soc.*, **73**, 5791 (1951); (b) G. W. Watt, A. Broodo, W. A. Jenkins and S. G. Parker, *ibid.*, **76**, 5989 (1954).

(3) G. W. Watt, M. T. Walling, Jr., and P. I. Mayfield, *ibid.*, **75**, 6175 (1953).

(4) R. Adams, V. Voorhees and R. L. Shriner, *Org. Syntheses*, **8**, 92 (1928).

(5) V. L. Frampton, J. D. Edwards and H. R. Henze, *J. Am. Chem. Soc.*, **73**, 4432 (1951).

(6) The vapor pressures found for ethanol–allyl alcohol solutions were in good agreement with values computed by assuming ideal solution behavior. For ethanol–hexene-1 solutions the values were higher than expected on the same basis. This is indicative of a low-boiling azeotrope comparable to that formed by ethanol and *n*-hexane [*cf.*, L. H. Horsley, *Anal. Chem.*, **19**, 508 (1947)].

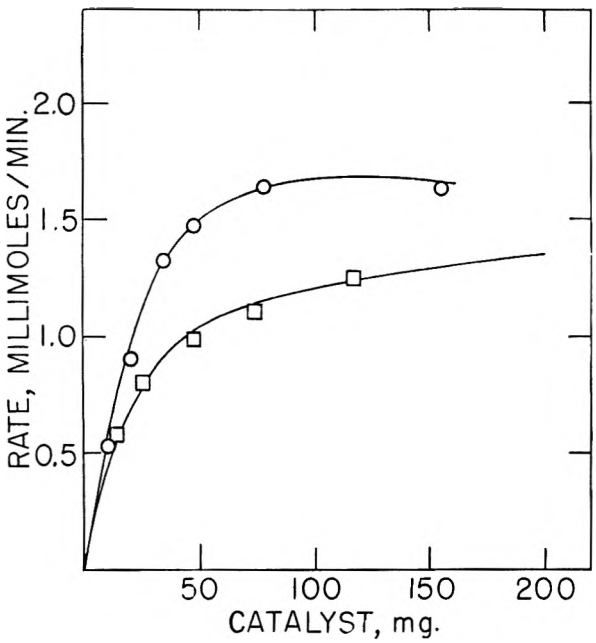

Fig. 1.—Effect of weight of catalyst upon rate of hydrogenation over Adams platinum: O, hexene-1; □, allyl alcohol.

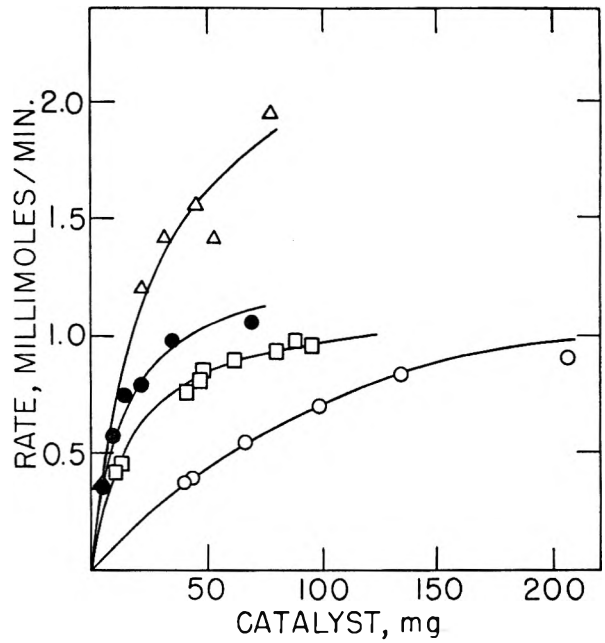

Fig. 2.—Effect of weight of catalyst upon rates of hydrogenation over W-6 Raney nickel, rhodium and palladium: O, allyl alcohol, W-6 Raney nickel; △, ●, hexene-1, rhodium; □, allyl alcohol, palladium.

Rate *vs.* Temperature.—Values for energy of activation were computed from data on rates of hydrogenation at 2 and 30°. Both acceptors were used in reactions catalyzed by 20–100 mg. of several different lots of catalyst. The linear dependence upon hydrogen pressure indicates that the rates must be proportional to the saturation concentration of hydrogen in the solutions. Accordingly, the observed temperature coefficients were corrected to take into account the solubility of hydrogen at the temperatures involved.[7] Values for energy of activation were found to range from 1000 to 2000 cal./mole for catalyst weights of 20–100 mg. and hydrogen pressures of 800–1500 mm.

Rate *vs.* Concentration of Acceptor and/or Product.—Replacement of 10% of the ethanol solvent with *n*-propanol did not alter the rate of hydrogenation of allyl alcohol. Complete replacement of the ethanol by *n*-propanol gave a rate 40% lower than with ethanol as the solvent. The rates were zero order with respect to acceptor. With increase in the initial concentration of acceptor, the rate of hydrogenation of allyl alcohol decreases and the reaction is no longer zero order with respect to acceptor. At the higher concentrations of acceptor, the reaction is between zero and first order.

Rate *vs.* Agitation Frequency.—The influence of mode and frequency of agitation upon the rate of hydrogenation of allyl alcohol was determined for several different lots of catalyst using the magnetic stirrer at 930 r.p.m. in comparison with the mechanical shaker operated at a frequency of 200 and 380 oscillations/min. The resulting data showed that the use of the mechanical shaker gave increased rates of hydrogenation for all weights of catalyst, that this effect is more pronounced for larger weights of catalyst, but that the nature of the dependence of rate upon other variables is not altered.

Rate *vs.* Weight of Catalyst.—With all other conditions held constant, the dependence of rate of hydrogenation upon the weight of catalyst used with a fixed initial quantity of acceptor was determined for five different lots of Adams platinum, three different lots of allyl alcohol, and one lot of hexene-1. Typical data are shown in Fig. 1; data obtained in earlier work with other catalysts[2] are shown in Fig. 2.

With Adams platinum in experiments involving low ratios of catalyst to acceptor, the rate reaches a maximum in the early stages of the reaction and thereafter decreases at a steadily diminishing rate. As the weight of catalyst is increased (other variables being held fixed) the maximum broadens until a condition is reached wherein the rate rises rapidly to a maximum which is maintained throughout the remainder of the reaction. At low catalyst to acceptor ratios the reaction order is between zero and first with respect to acceptor; at higher ratios the reaction becomes zero order with respect to acceptor. The transition to zero-order reactions occurred generally with *ca.* 20 mg. of catalyst (with 1 ml. of allyl alcohol in 11 ml. of solution, or with 2 ml. of hexene-1 in 11 ml. of solution). This effect was observed only with Adams platinum. With the other catalysts studied in earlier work, these reactions were zero order with respect to acceptor over the entire range of catalyst weights studied.

Discussion

The first-order dependence of rate upon hydrogen pressure, the zero-order dependence upon acceptor and product concentrations (over certain concentration ranges), the low activation energies, and the marked dependence of rate upon agitation frequency suggest that the rate-limiting process involved in these experiments is the diffusion of hydrogen to the surface of the catalyst. It is the purpose of the discussion that follows to show that the rates observed in the present work with Adams platinum and in earlier work[2] with W-6 Raney nickel, rhodium and palladium catalysts may be expressed by an equation of the form

$$R_0 = \frac{AWP_{H_2}}{1 + BW} \qquad (1)$$

where R_0 is the rate of the zero-order reaction, W is the weight of catalyst, P_{H_2} is the hydrogen pressure, and A and B are constants.

The mode of variation of rate with weight of catalyst suggests that the rate is linear with the weight of catalyst for small weights, but approaches a limiting rate independent of the amount of catalyst as the weight of catalyst is increased. This behavior is to be expected if the rate is determined by two

(7) Since data on the solubility of hydrogen in ethanol–allyl alcohol and ethanol–hexene-1 mixtures were not available, the data given by Seidell (A. Seidell, "Solubilities of Inorganic and Metal Organic Compounds," 3rd Ed., Vol. 1, D. van Nostrand Co., Inc., New York, N. Y., 1940, p. 565) for the solubility of hydrogen in ethanol were used; the mole fraction of ethanol in both cases was ca. 0.92.

consecutive processes, one of which proceeds at a rate proportional to the first power of the weight of catalyst and is hence the dominant process as the weight of catalyst approaches zero; the rate of the other is independent of the weight of catalyst so that it becomes the slower process as the weight of catalyst is increased. This mode of variation obtains if it is assumed that the rate of the surface-catalyzed reaction by which hydrogen is consumed is limited by the rate of diffusion of hydrogen through the liquid phase to the catalyst surface.

The net rate of diffusion of a solute in the positive (x) direction across a surface of area A is given by the Fick's law expression

$$R_d = -DA\ dc/dx \qquad (2)$$

where R_d is the rate of diffusion in moles/unit time, D is the diffusivity of the diffusing species in the medium in question, A is the cross-sectional area of the diffusion path (measured normal to the direction of diffusion), and dc/dx is the concentration gradient for the diffusing species, measured in the direction of diffusion. For steady-state diffusion, the term $A\ dc/dx$ is constant; and the rate of diffusion can, therefore, be expressed in terms of the terminal values of the concentration and the coördinate x, thus

$$R_d = \frac{D(c_1 - c_2)}{\int_{x_1}^{x_2} dx/A} \qquad (3)$$

We shall assume that the transport of hydrogen from the gas phase to the catalyst involves diffusion through regions of two types in the liquid phase. The effective diffusion area and path length of the first are assumed to be fixed constants for fixed conditions of agitation and independent of the type or quantity of catalyst present. The second region is considered to be that portion of the liquid in the immediate neighborhood of the catalyst. It is further assumed that the effective diffusional area of this second region is proportional to the total surface area of the catalyst. For steady state diffusion through the first of these regions the term $\int_{x_1}^{x_2} dx/A$ is a constant (M) for fixed conditions of agitation, so that the rate of diffusion through this region is given by

$$R_d' = (D_{H_2}/M)(c_{H_2}^* - c_{H_2}') \qquad (4)$$

where $c_{H_2}^*$ is the concentration of hydrogen at its point of entry into this region and c_{H_2}' is the concentration of hydrogen at the terminus. We shall assume that the hydrogen enters this region from either the gas phase or a turbulent region fronting on the gas phase; in either case $c_{H_2}^*$ is the saturation concentration of hydrogen in equilibrium with the gas phase. By Henry's law, this is proportional to the partial pressure of hydrogen in the gas phase; and we may set $c_{H_2}^* = HP_{H_2}$ and write

$$R_d' = (D_{H_2}/M)(HP_{H_2} - c_{H_2}') \qquad (5)$$

Since the concentration of hydrogen remains constant throughout any turbulent regions intervening between the two diffusional regions, c_{H_2}' is the concentration of hydrogen at its point of entry into the second diffusional region. Since the effective diffusional area in this second region is proportional to the total surface area of the catalyst, which in turn is proportional to the total weight of catalyst for a given catalyst (assuming equal radii or porosity, and no close-packing) we may set the denominator of equation 3 equal to a function N_c/W, where N_c is a constant for a given catalyst for fixed conditions of agitation, and W is the weight of catalyst. The rate of diffusion through this second region is then given by the expression

$$R_d'' = (D_{H_2}W/N_c)(c_{H_2}' - c_{H_2i}) \qquad (6)$$

where c_{H_2i} is the concentration of hydrogen in the liquid phase adjacent to the catalyst.

Since the rates of diffusion through these two liquid regions must be equal for the postulated condition of steady state diffusion, c_{H_2}' may be eliminated from these two expressions; the result is an over-all rate equation for the diffusional process

$$R_d' = R_d'' = R_d \frac{D_{H_2}(HP_{H_2} - c_{H_2i})}{M + N_c/W} \qquad (7)$$

The term c_{H_2i} is the concentration of hydrogen of importance in determining the rate of the surface reaction. Since the zero-order reaction was found to be first order with respect to hydrogen pressure and since any probable surface mechanism would yield a rate proportional to the total weight of catalyst, it is assumed that the rate R_0 of the zero-order reaction may be expressed by

$$R_0 = kc_{H_2i}W \qquad (8)$$

where k is a constant. Since the consumption of

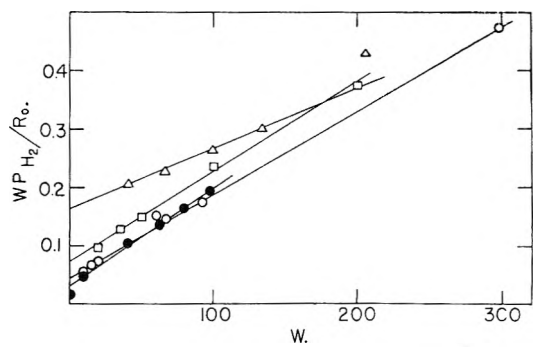

Fig. 3.—Test of equation $R_0 = AWP_{H_2}/(1 + BW)$ for hydrogenation of allyl alcohol: ○, □, Adams platinum; △, W-6 Raney nickel; ●, palladium.

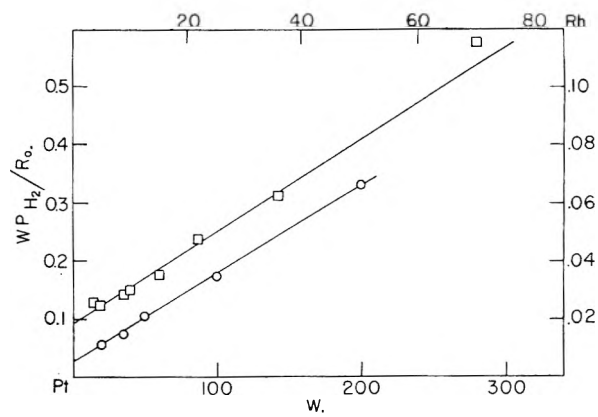

Fig. 4.—Test of equation $R_0 = AWP_{H_2}/(1 + BW)$ for hydrogenation of hexene-1: ○, Adams platinum; □, rhodium.

hydrogen by the surface reaction provides the sole impetus for the diffusion of hydrogen from the gas phase to the catalyst, it is apparent that the rates of these two processes must be equal, at least for the case of the zero-order reactions where the rates do not vary with time. Thus, the concentration of hydrogen at the catalyst surface, c_{H_2i}, must satisfy equations 7 and 8 for the condition that $R_d = R_0$. Using this condition to eliminate c_{H_2i} from equations 7 and 8 one obtains an equation which upon rearrangement may be written in the form

$$\frac{WP_{H_2}}{R_0} = \frac{MW}{D_{H_2}H} + \frac{N_c + D_{H_2}/k}{D_{H_2}H} \qquad (9)$$

from which it is apparent that a plot of WP_{H_2}/R_0 *vs.* W should be linear for systems for which equation 9 provides an accurate description of the manner of variation of the rate with the weight of catalyst. Typical experimental data for Adams platinum and several other catalysts studied previously are shown in the form of equation 9 in Figs. 3 and 4. It is seen that equation 9 provides a reasonably accurate representation of the manner in which the rate of hydrogenation varies with the weight of catalyst for two different acceptors and four different catalysts under these conditions of low pressure liquid phase hydrogenation. Gol'danskii and Elovich[8] have observed similar variations in rate with weight of catalyst in studies of the hydrogenation of oleic acid over supported platinum catalysts.

(8) V. I. Gol'danskii and S. Y. Elovich, *J. Phys. Chem.* (*U.S.S.R.*), **20**, 1085 (1946); *cf.* V. I. Gol'danskii, *Zhur. Fiz. Khim.*, **22**, 1374 (1948).

STUDIES ON ION-EXCHANGE RESINS. XII. SWELLING IN MIXED SOLVENTS

BY HARRY P. GREGOR, DEANA NOBEL AND MELVIN H. GOTTLIEB[1]

Contribution from the Department of Chemistry of the Polytechnic Institute of Brooklyn, Brooklyn, New York

Received June 1, 1954

The swelling of a polystyrene–sulfonic acid resin in the ammonium, quaternary ammonium and silver states in mixtures of water and methanol, ethanol, isopropyl alcohol and dioxane was studied. Total solvent uptake and distribution between resin and solution phases were determined. The more polar solvent (water) was sorbed preferentially, the degree of preference being greatest at low water contents. The cationic state of the resin influenced the selective sorption of solvent to a marked degree. Swelling appears to be determined largely by the dielectric constant of the sorbed solution; this behavior is similar to that predicted by Bjerrum's theory of ion-pair formation. Similar studies were carried out with a quaternary base anion exchanger in the chloride and acetate states in ethanol–water mixtures.

The swelling of ion-exchange resins in aqueous electrolytic solutions and at different relative humidities has been discussed in previous papers.[2,3] The swelling was considered as due primarily to the osmotic activity of the movable exchange ions, and opposed by the tension of the resin matrix. This paper describes the swelling of a polystyrene–sulfonic acid resin and of a quaternary ammonium resin in various mixed solvents; the equilibrium swelled volumes, weights and compositions of the resin phases were determined directly.

Experimental

Resins.—A sulfonated polystyrene–divinylbenzene cation-exchange resin (Dowex 50) was used; this material had a nominal divinylbenzene content of 8% and a capacity of 4.96 meq. per dry gram of hydrogen resin. This resin was specially prepared by pre-swelling before sulfonation to give perfect, low breakage, spherical beads.[4]

A strong base-anion exchanger of the quaternary ammonium type (Dowex 2) was also used; the exchange group is the benzyldimethylethanolammonium ion. This resin had a nominal divinylbenzene content of 8%, and an exchange capacity of 2.26 meq. per dry gram in the chloride state.

The resins were first conditioned in the conventional manner.[2] However, an additional conditioning procedure was required, namely, extraction with absolute methanol or ethanol for a few days. This resulted in slightly lowered wet weights and volumes, which were subsequently reproducible.

Swelling.—The swelling of the resins was determined in some cases by both weight and volume measurements. The swelled weight was determined by centrifugation,[2] and for these systems was reproducible to ±0.2%. The swelled volumes of the particles were determined microscopically. Diameters were measured using a filar micrometer microscope attachment which read to 0.001 mm. These diameter measurements were accurate to ±0.002 mm., and agreed with those determined by centrifugation within experimental error.[5] Measurements were made at room temperature (23–25°). Better temperature control was not needed because the solvent densities vary by only 0.1–0.2% per degree in this range, and the temperature coefficient of swelling of these resin systems is very small.[5]

For the microscopic measurements, three particles, of sufficiently different diameter to render them distinguishable, were placed in a flat-polished bottom cavity slide which was filled with solution and covered with a slide cover. (The relative swelling of each particle was substantially the same, within (0.3%). The solution was changed several times to ensure equilibrium. Rate experiments established that equilibrium was attained within 15 minutes.

Volumes of silver resin could not be determined microscopically because of the reduction of silver ions by the organic solvent in the presence of the strong light from the illuminating lamp of the microscope. A layer of a white precipitate was observed surrounding each particle.

Dioxane and isopropyl alcohol were dried over CaH_2 for 72 hours; methanol and ethanol were dried over magnesium turnings and distilled. The resin particles were dried in a vacuum oven at 50° for 48 hours to constant weight. This presumably removes the last traces of water before equilibration with pure solvent.[2]

(1) Taken in part from the dissertation of M. H. Gottlieb, submitted in partial fulfillment of the requirements for the degree of Doctor of Philosophy in Chemistry, Polytechnic Institute of Brooklyn, August, 1953.

(2) H. P. Gregor, F. Gutoff and J. I. Bregman, *J. Colloid Sci.*, **6**, 245 (1951).

(3) B. R. Sundheim, M. H. Waxman and H. P. Gregor, THIS JOURNAL, **57**, 974 (1953).

(4) R. M. Wheaton and D. F. Harrington, *Ind. Eng. Chem.*, **44**, 1796 (1952).

(5) H. P. Gregor, F. C. Collins and M. Pope, *J. Colloid Sci.*, **6**, 304 (1951).

TABLE I

DISTRIBUTION COEFFICIENTS FOR WATER–NON-AQUEOUS SOLVENT FOR A POLYSTYRENE–SULFONIC ACID RESIN (DVB 8) SYSTEM

Wt. % of water in soln. phase	NH_4^+ State			$(CH_3)_4N^+$ State			$(C_2H_5)_4N^+$ State			$(C_4H_9)_4N^+$ State			Ag^+ State
	Methanol	Ethanol	Dioxane	Methanol	Ethanol	Dioxane	Methanol	Ethanol	Dioxane	Methanol	Ethanol	Dioxane	Ethanol
80	1.4	1.5		1.5	2.3		1.9	3.2		1.4	0.83		1.7
60		1.9	3.0		3.5	4.7			9.6		1.2	3.0	2.1
40	1.0	2.6		1.5	5.0		1.7	5.3		1.3	1.6		4.3
20		5.8	11.0		11.0	15.5		8.5	38.1		2.6	7.6	9.8
5		8.2			13.2			4.8			4.8		

Solvent Uptake.—Two methods for the determination of the composition of the solution sorbed by the resin were used. For the first, the resin equilibrated with water–alcohol solutions was centrifuged, weighed, eluted with distilled water and then dried to constant weight. The alcohol in the eluate was determined colorimetrically.[6,7] For the second method, after centrifugation the sorbed solvents were completely distilled at 80° and 5 mm. directly from the resin contained in the centrifuge basket, and determined refractometrically; the validity of this method was established using pure solvents and by comparison with the first method. Distribution coefficients determined by these methods were accurate to within about 5%.

Results

Only selected, typical data are presented in this paper; the reader is referred to the Thesis[1] for details. Table I gives selectivity coefficients for solvent exchange, defined as

$$K_s^w = \left(\frac{n_w}{n_s}\right)^r \left(\frac{n_s}{n_w}\right)$$

where n_w is the moles of water, n_s moles of organic solvent, and where the superscript r designates the resin phase; the solution phase is not designated. Data are given in Table I for three non-aqueous solvent–water systems and the sulfonic acid resin in the ammonium, substituted ammonium and silver states. Figure 1 is a plot of the distribution of ethanol and water between solution and resin phases. Figure 2 shows the swelled volume of the tetramethylammonium form of the sulfonate resin in mixtures of water with methanol, ethanol and dioxane, plotted against the weight per cent. of water in the solution phase. Similar results were obtained with the resin in other cationic states.

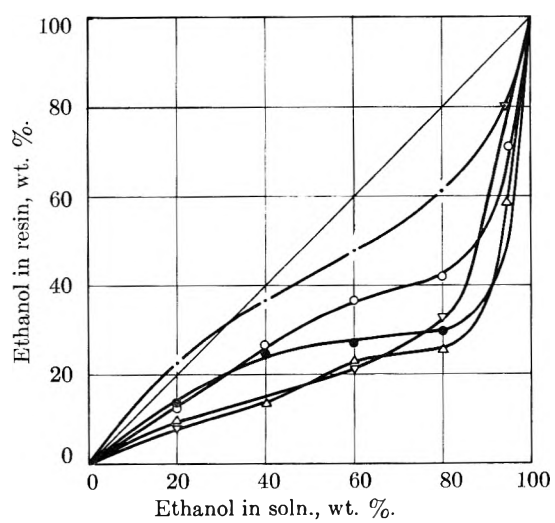

Fig. 1.—Distribution of water and ethanol between solution phase and polystyrene sulfonate resin phase, with the resin in the following states: $(C_4H_9)_4N^+$ (.); NH_4^+ (○); Ag^+ (●); $(CH_3)_4N^+$ (△); $(C_2H_5)_4N^+$ (▽).

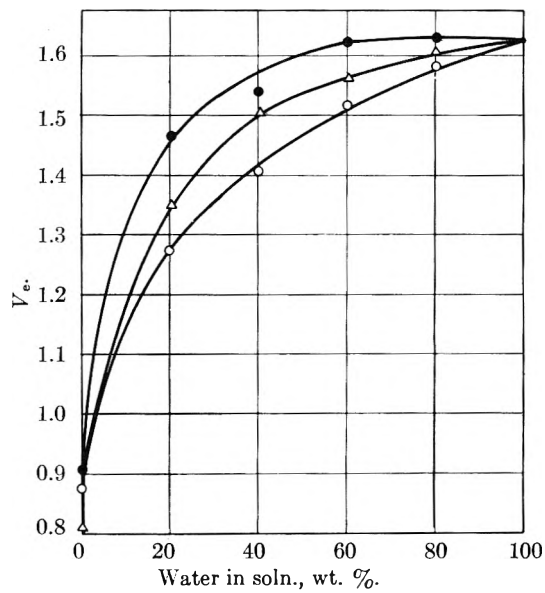

Fig. 2.—Specific swelled volume (V_e) of tetramethylammonium sulfonate resin in water–methanol (○), ethanol (△), and dioxane (●) solutions.

Discussion

The two principal effects observed with the cation-exchange resin systems are that there is a selective uptake of the more polar solvent (water), and that the systems deswell upon going from polar to less polar solvents. The discussion which follows takes up first the sorption of solvents by the polymer system as a whole, and then considers the osmotic activity of exchange ions.

Distribution of Solvent.—The resin systems sorb water selectively from solvent mixtures, this selectivity being greatest at low mole fractions of water and also increasing as the dielectric constant of the other solvent decreases. The distribution plot (Fig. 1) is for ethanol–water mixtures; similar effects are found with the other systems, shown in Table I.

The nature of the exchange cation also influences the selective uptake of water, which is preferred by resins in the sequence: $(CH_3)_4N^+ \cong (C_2H_5)_4N^+ > NH_4^+ > (C_4H_9)_4N^+$. These results are comparable to those for the sorption of water vapor by these systems, where the order of increasing sorption is exactly the same.[8] For a dis-

(6) F. Milton and R. Waters, "Quantitative Microanalysis," Arnold and Co., London, 1949, p. 317.

(7) D. A. Webb, *Sci. Proc. Roy. Dublin Soc.*, **21**, 281 (1936).

(8) B. R. Sundheim, M. H. Waxman and H. P. Gregor, THIS JOURNAL, **57**, 974 (1953).

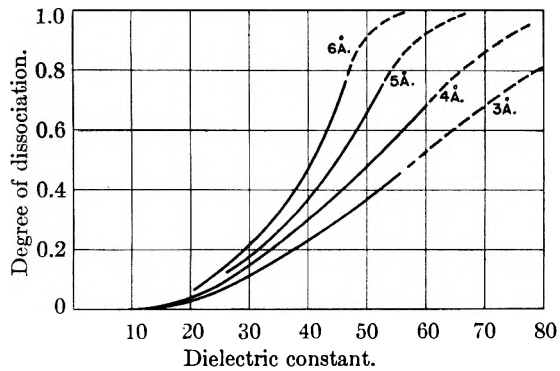

Fig. 3.—Calculated degree of dissociation of ion-pairs of varying $\mathring{a}$ values as a function of dielectric constant of solvent.

cussion of the various factors which may be operative, the reader is referred to the earlier paper.[8]

Osmotic Activity of Exchange Cations. Ion exchange resins are osmotic systems[9] in which the cross-linked matrix, which restricts the fixed ions to the resin phase, has a function analogous to that of the membrane in a Donnan system. The system is thus treated as a polyelectrolyte where the spring entropy of the chain restrains the swelling. The exchange ion is restricted to the resin phase by electro-neutrality conditions, so that the (membrane) system is permeable only to the solvent. For this system in equilibrium, $\pi \bar{V}_1 = RT \ln a_1/a_1^r$, where a_1^r and a_1 are the activities of permeable species 1 in the resin (r) and equilibrating phases, respectively, $\bar{V}_1$ the partial molar volume of species 1 and π the thermodynamic osmotic pressure.

A simplified equation of state which relates the external volume of a resin system V_e with the osmotic swelling pressure π has been proposed by Gregor,[9] $V_e = m\pi + b$. Here b is the "rest volume" or volume when π is zero, and is made up of the sum of the matrix volume V_M and V_s^0, the volume of sorbed solvent when π is zero. If the total sorbed solvent volume is V_s, then

$$V_e = V_M + V_s = m\pi + V_M + V_s^0$$

Considering a reasonable dilute and ideal system so that $\pi V_s = n_i RT$, where n_i is the moles of osmotically active ions, and neglecting V_s^0 (which is small compared to V_s), $V_s^2 = mn_i RT$. Thus, V_s is a function only of the concentration of osmotically active ions and the elastic modulus. This relationship applies also to mixed solvent systems.

It can be readily shown that pressure–volume effects will make for the selective uptake of the solvent having a smaller partial molar volume. Using values of π as calculated by Gregor and Frederick[10] from vapor pressure data, $K_{EtOH}^{H_2O}$ would equal only about 1.2.

The deswelling of the resin on going to a less polar solvent can be interpreted in terms of the formation of ion-pairs as a result of the lowered dielectric constant of the sorbed solvent in this osmotic system. However, lowering the dielectric constant also increases the repulsive forces between fixed ions; this latter effect by itself would decrease the

(9) H. P. Gregor, *J. Am. Chem. Soc.*, **70**, 1293 (1948).

(10) H. P. Gregor and M. Frederick, *Ann. N. Y. Acad. Sci.*, **57**, 87 (1953).

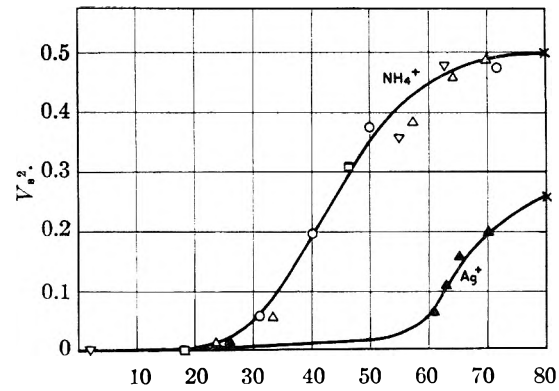

Fig. 4.—Plot of square of sorbed solvent volume (V_s^2) as a function of (calculated) dielectric constant of sorbed solvent for an ammonium sulfonate resin in mixtures of water and the following solvents: water (×); methanol (○); ethanol (△); isopropyl alcohol (□); dioxane (▽). Data for a silver sulfonate resin and water–ethanol mixtures shown (▲).

chain entropy and cause the resin to swell. Fuoss and Cathers[11] have observed a decrease in the viscosity of butylpolyvinylpyridinium bromide solutions with decreasing dielectric constant. This indicated that the decrease in dissociation of the polyelectrolyte more than offset the increased repulsion along the chain.

The method of Bjerrum considers the formation of ion-pairs in media of low dielectric constant.[12] This theory correlates the degree of association or ion-pair formation with the dielectric constant and closest distance of approach $\mathring{a}$ of the ion-pair. Figure 3 shows calculated values of the degree of dissociation of a 1 molar solution at 25° for a 1-1 electrolyte for different values of $\mathring{a}$. Activity coefficients are assumed to be unity. These calculations become increasingly inaccurate with increasing values of the dielectric constant.

The square of the solution volume contained in the resin phase (V_s^2), which is presumably proportional to the number of osmotically active ions present, was plotted against the dielectric constant of the sorbed solution in Fig. 4. The solution volumes were calculated either from the resin volumes and resin matrix volumes, or from wet weight measurements. The dielectric constant of the sorbed solution was obtained from the composition of the resin phase, assuming the dielectric constant to be the same as for an ordinary solution of the same composition.[12]

In Fig. 4, the curve for the ammonium resin is strikingly similar to the Bjerrum plots of Fig. 3. It should be noted that each point on this curve is for either different compositions of the same solvent pairs, or for different solvent pairs. The dielectric constant of the sorbed solution is obviously quite different from that of the entire resin phase. Interactions between a fixed sulfonate group and a movable exchange cation are primarily a function of the dielectric constant of the sorbed solution.[13]

(11) R. M. Fuoss and G. I. Cathers, *J. Polymer Sci.*, **4**, 97 (1949).

(12) H. S. Harned and B. B. Owen, "Physical Chemistry of Electrolytic Solutions," Reinhold Publ. Corp., New York, N. Y., 1950.

(13) See *e.g.*, J. G. Kirkwood and F. H. Westheimer, *J. Chem. Phys.*, **6**, 506 (1938).

The observed strong similarity between the plot of V_s^2 *vs.* D and the Bjerrum plot suggests indeed that ion-pair formation is the primary effect here. The horizontal portion of the experimental plot at high dielectric constants leads to the conclusion that little if any association has taken place. This is corroborated by the work of Heymann and O'Donnell,[14] who found that the equivalent conductances of alkali metal cations in exchange resins are proportional to their values in aqueous solution. If association is present in these systems, the conductivity data would require that all of the alkali metal sulfonates have the same dissociation constants, which is highly unlikely. Ion-pair formation constants for the alkali metals and the doubly charged sulfate ion, as calculated by Davies and others (see ref. 12, p. 147) are not the same, but vary by a factor of 1.5 between lithium and potassium. Therefore, it is not valid to ascribe ion selectivities to differences in ion association constants with the alkali metal cations and sulfonate resins.

Consider now the analogous curve for the silver resin in Fig. 4. Heymann[14] observed from conductance data that the silver resinate is apparently one-third associated. This can also be inferred from the selectivity of this resin for silver, as observed for example by Hogfeldt, Ekedahl and Sillen.[15] Where ion-pair formation already exists in aqueous solution, lowering the dielectric constant will cause a sharp decrease in dissociation as shown in Fig. 3. This is observed in Fig. 4 for the silver resinate system, where in water the silver sulfonate ion-pair is apparently more than 40% dissociated, being more or less completely associated at values of $D < 50$.

Plots of V_s^2 *vs.* D for the tetrabutyl- and tetramethylammonium resinates are shown in Fig. 5; the dotted line is for the ammonium resin, taken from Fig. 4. The same, general deswelling behavior shown by the ammonium form resin is observed; the V_s^2 values are in the sequence $NH_4^+ > Me_4N^+ > Et_4N^+ > Bu_4N^+$. The swelled volumes in water of the tetrabutylammonium and the silver resins are the same, but the slopes of the deswelling curves indicate that association is small in the former case. With increasing size of the exchange cation the solvent volume decreases; this can be the result of increasing association and also of exclusion of the solvent by the high osmotic pressure which obtains in the presence of large exchange ions. While less ion-pair formation should result in systems involving large exchange cations, one must also consider that the van der Waals forces, which increase with molecular weight and act here to reinforce coulombic attraction, can cause a net increase in association. Gregor and Bregman[16] have shown that for loosely cross-linked resins (where osmotic effects are small), the resin preferentially adsorbs organic ions in the order of increasing molecular weight.

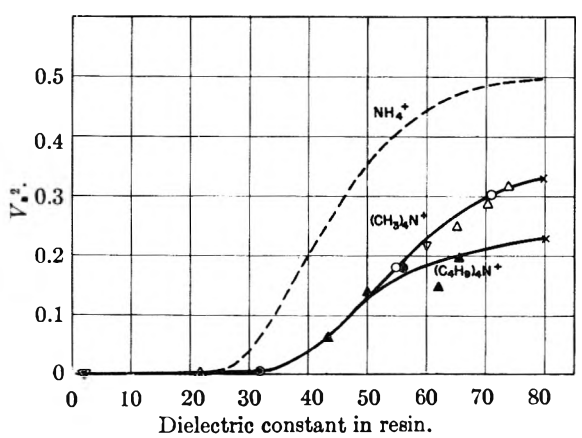

Fig. 5.—Plot of square of sorbed solvent volume (V_s^2) as a function of (calculated) dielectric constant of sorbed solvent for a tetramethylammonium and a tetrabutylammonium sulfonate resin for mixtures of water and the following solvents: water (×); methanol (○); ethanol (△); dioxane (▽). Points for tetrabutylammonium resin shown solid; dotted line for ammonium resin is from Fig. 4.

(14) E. Heymann and I. J. O'Donnell, *J. Colloid Sci.*, **4**, 405 (1949).

(15) E. Hogfeldt, E. Ekedahl and L. G. Sillen, *Acta Chem. Scand.*, **4**, 1471 (1950).

Results with Anion-exchange Resins.—The anion-exchange resin–mixed solvent systems showed similar behavior to that of the sulfonic acid resins, but also significant differences. Chloride and acetate state resins were studied, and found to behave similarly. These resins sorb water preferentially, but to a much lesser extent than the sulfonic resins. For example, at solution phase water weight percentages of 80, 60 and 20, the distribution coefficient for water over ethanol was 0.95, 1.16 and 2.90 for the chloride state resin; corresponding values for the tetramethylammonium sulfonate resin were 2.3, 3.5 and 11.0.

From Fig. 6 it is seen that the weight of the anion-resin phase (specific wet weight W_e) increases as the percentage of ethanol in the solution (and also in resin) phase increases, reaches a maximum, and then decreases. Also plotted in Fig. 6 are the total *moles* of solvent sorbed, and it is seen that the molar sorption is fairly constant down to 50:50 mixtures. No explanation is offered for this behavior.

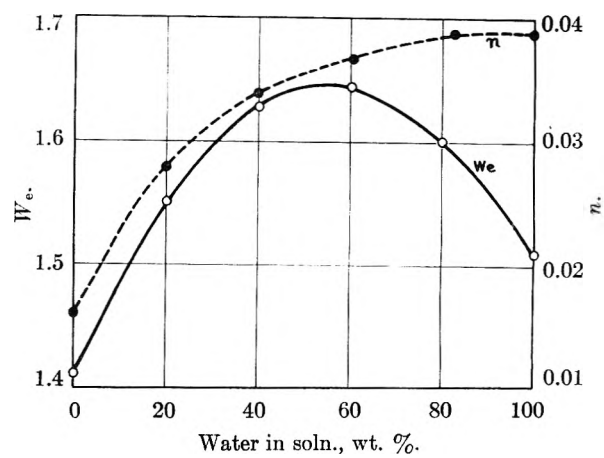

Fig. 6.—Wet weight (W_e) and moles of solvent sorbed (n) of a quaternary ammonium anion-exchange resin in the chloride state, in equilibrium with different water–ethanol solutions.

The authors wish to thank the Office of Naval Research for the support given this work.

(16) H. P. Gregor and J. I. Bregman, *J. Colloid Sci.*, **6**, 323 (1951).

VELOCITY AND ABSORPTION OF ULTRASONICS IN LIQUID SULFUR

BY A. W. PRYOR AND E. G. RICHARDSON

King's College, Newcastle upon Tyne, England

Received June 17, 1954

In order to derive some of the visco-elastic properties of liquid sulfur, particularly in the transition region where polymerization takes place, measurements of ultrasonic velocity and attenuation over the range of temperature 100 to 250° have been made. Comparison is made between the "ultrasonic viscosity" deduced from such measurements and those derived in a conventional viscometer. A model is suggested to account for the acoustic behavior of sulfur above 160°.

Introduction

A number of measurements of the viscosity of sulfur in the molten state have been made over the past fifty years, using simple transpiration or slow oscillatory motion. Sulfur melts at 111° and in this state the element exists in the form of 8 atom rings. At 160° polymerization occurs and the viscosity rapidly rises. The sulfur in this stage exists in long chains and traces of hydrocarbons by terminating the chain have, according to Gee,[1] a marked effect on the viscosity. Farr and McLeod[2] found that the viscosity varies with time. The object of the present research was to measure the velocity and attenuation of ultrasonics of megacycle frequencies in sulfur over this transition region and to deduce therefrom values of compressibility and ultrasonic viscosity. In view of the known difficulty of removing small traces of impurities and their effects on the flow properties, only the more usual efforts at purification, *e.g.*, boiling, as recommended by Bacon and Fanelli,[3] were made, it being considered sufficient for our purpose to compare viscosities deduced from absorption with those obtained in a conventional viscometer on another sample of the same specimen.

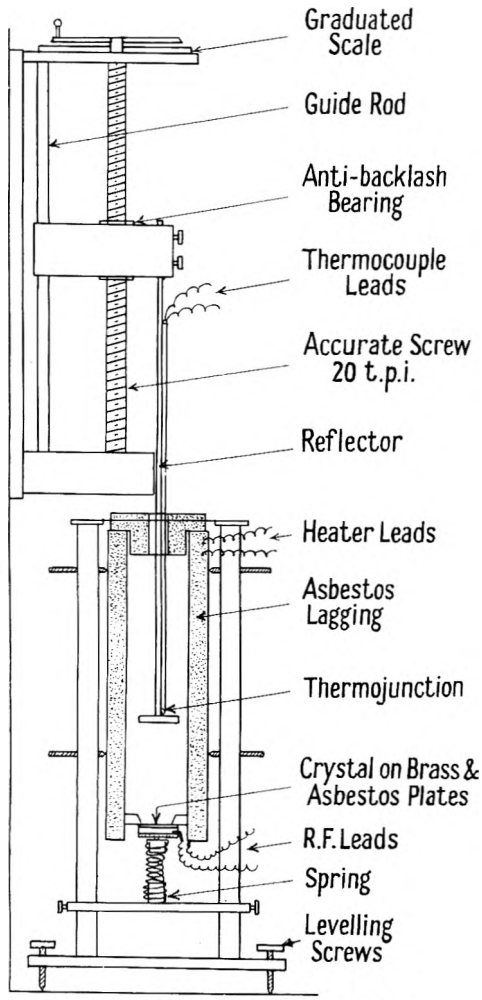

Fig. 1.—Ultrasonic interferometer.

Ultrasonic Apparatus.—The interferometer built for these measurements is shown in Fig. 1. The container of the specimen is a brass tube 1.38 in. diameter and 7.5 in. long, heavily chrome-plated on the inside to prevent contamination. The tube is covered externally by a layer of asbestos and wound with a heating coil, over which a further layer of asbestos is placed.

The transducer (a 1-in. quartz crystal), spring-loaded against a collar with hole 0.88 in. diameter soldered near the lower end of the tube, is mounted on a brass disc insulated from the (earthed) furnace by an asbestos disc. The crystals were coated above and below by evaporated aluminum or baked silver paste.

The steel screw which carries the reflector is of high accuracy, has a pitch of 20 turns per inch and is fitted with anti-backlash bearings of brass. It has a dial at its upper end. Calibration showed the screw to be accurate to better than 1 in 1000.

The reflector is of aluminum and also carries the iron-constantan thermocouple which gives the temperature of the enclosure. In order that the reflector and transducer can be adjusted in parallelism—a very important point—the interferometer tube is supported on the base of the screw-carrier through three levelling screws, which are adjusted until a good signal echo is returned.

An automatic temperature control assures the temperature of the furnace to ±1°.

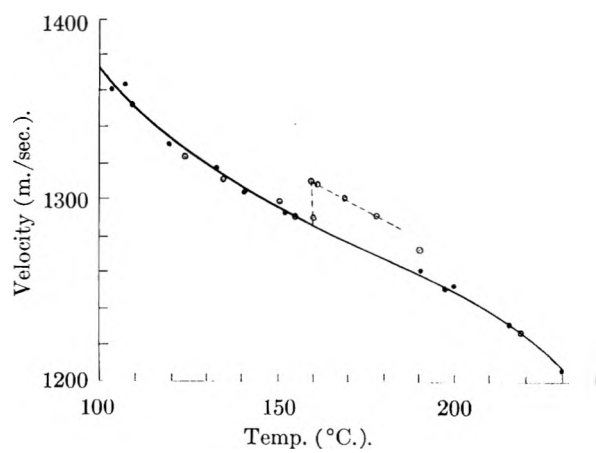

Fig. 2.—Velocities of sound at various temperatures: ●, 4 Mc./sec.; ○, 0.4 Mc./sec.

(1) G. Gee, *Trans. Faraday Soc.*, **48**, 515 (1952).

(2) C. C. Farr and D. B. McLeod, *Proc. Roy. Soc.* (*London*), **A97**, 80 (1920); **A118**, 534 (1928).

(3) R. F. Bacon and R. Fanelli, *Ind. Eng. Chem.*, **34**, 1043 (1942).

Electronic Circuits.—A pulse signal was employed. Oscillations from a Hartley oscillator are excited by a multi-vibrator. These are gated in the form of short pulses of oscillations and applied to the transducer, which then launches a short train of waves to be reflected. The echo, again energizing the transducer, is amplified at constant gain in the receiver. (During the emission of the signal the latter must be put out of action by a "blanking pulse"). The echo is exhibited on a cathode ray oscillograph and brought to a determined level through the operation of an attenuator in the receiver circuit. The determination of the absorption coefficient therefore consists in moving the reflector away from the source while adjusting and reading the attenuator.

To measure the wave length—and so, the velocity—the echo is mixed with a fraction of the original oscillations. The superposed amplitude, displayed on the oscilloscope, will vary as the relative phase of signal and echo varies with relative position of source and reflector. This method is very useful when—as in the present instance—a highly absorbent liquid is in question.

The frequency is checked to a high degree of precision on a heterodyne wave-meter.

Velocity Results.—Figure 2 shows the results of velocity measurements at two frequencies, 0.4 and 4 Mc./sec. Those at 4 Mc./sec. showed no marked change at the transition temperature; but at the lower frequency, a jump of some 20 m./sec. occurred at 160° which eventually subsided into the 4 Mc./sec. curve above 200°. This effect seemed to be a sort of hysteresis and was not apparent coming down in temperature. The velocity in liquid sulfur was earlier measured by Kleppa[4] but our results are higher than his by 10 to 20 m./s.

The density of sulfur at 115° is 1.82, of polymerized sulfur 1.93 g./cm.^{3} making the adiabatic compressibilities at 115 and 160° 32.5 × 10^6 and 31.5 × 10^6 dynes/cm.^{2}, respectively. Natta and Baccareda[5] have shown that the ratio velocity of sound/density is an important index for the lengths of chains in polymers. At the two temperatures noted, this ratio has values 0.74 and 0.66, respectively, in their units.

Absorption Results.—Results in the form amplitude–absorption coefficient (α) *vs.* temperature at frequencies 5.8, 12 and 15 Mc./sec. are given in Fig. 3. All show a rise beginning at 160° and leveling off at about 200°. Initially, the absorption could be as much as 0.1 above the final value on standing. In order to get steady readings it was necessary to wait some time at each temperature. Even so, at the higher temperatures difficulties were experienced through fluctuating echos, attributed to the formation and collapse of vapor bubbles in the liquid.

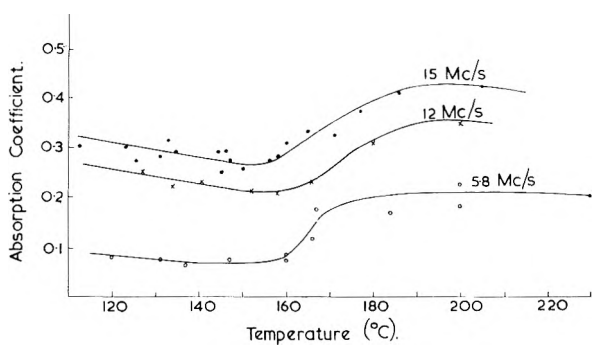

Fig. 3.—Absorption coefficients of sound at various temperatures.

In order to make a comparison between the viscous behavior of sulfur at high and near-zero frequencies an oscillating cylinder viscometer was set up, equipped with a furnace, and the viscosities—which also showed a tendency to after-effects—determined. The results, which agree with the measurements of Farr and McLeod (1920), are shown in Fig. 4.

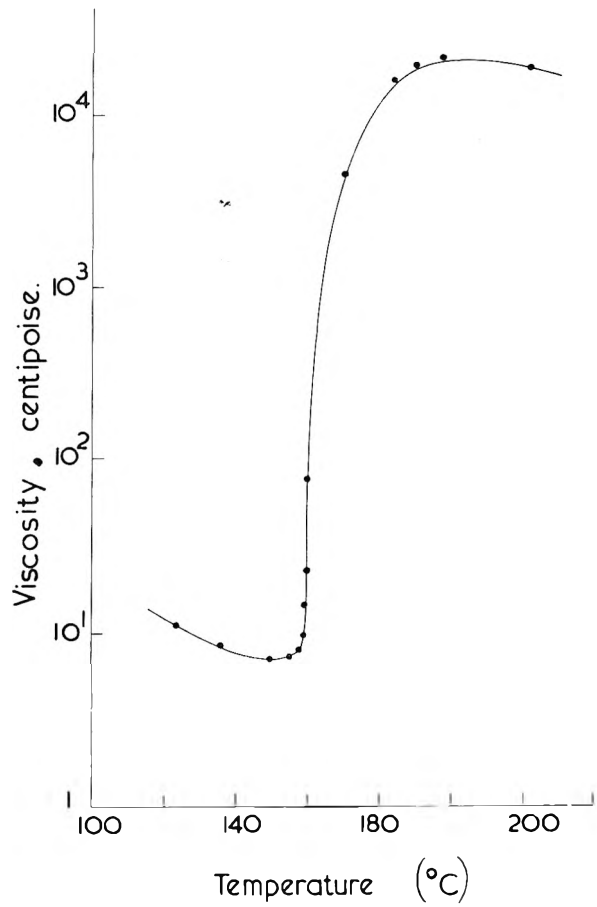

Fig. 4.—Viscosity coefficients at various temperatures.

Discussion of Results

According to the well-known theory of Stokes[6] the absorption of plane waves of sound in a liquid should follow the formula

$$\alpha = \frac{8\pi^2}{3} \times \frac{\nu f^2}{c^3}$$

where f is the frequency, c the velocity and ν the kinematic viscosity. The latter being the common coefficient of viscosity ν divided by the density ρ we may divide the data of Fig. 4 by 1.9 approximately to obtain ν values for sulfur.

This formula fits few fluids but it is so far true that in many liquids α/f^2 is constant. Figure 5 shows that in sulfur at 180°, α rises steadily with f^2 in the megacycle gamut, though with a factor which has changed after about an hour's standing. Working back from the formula given above, substituting our values of α/f^2, we can deduce values of ν which we might call "ultrasonic viscosity."

(4) O. J. Kleppa, *J. Chem. Phys.*, **18**, 1303 (1949).

(5) G. Natta and M. Baccareda, *J. Polymer Sci.*, **3**, 829 (1948).

(6) Sir G. Stokes, *Trans. Camb. Phil. Soc.*, **3** (1845).

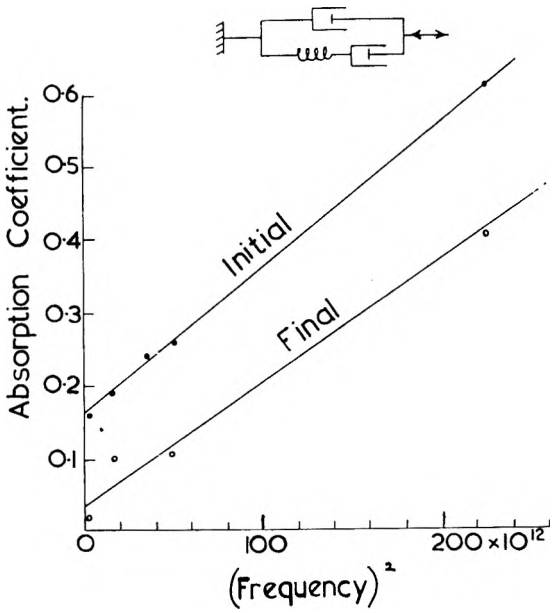

Fig. 5.—Absorption coefficients *vs.* (frequency)².

Doing this for the whole range of temperature to the results of Fig. 3, we can show that below transition the flow viscosity is about one third and above transition about one thousand times the ultrasonic viscosity.

In order to explain this we assume that above 160° we are dealing with a visco-elastic fluid, whose elasticity at high frequencies far outweighs the true viscosity. The model shown as inset to Fig. 5 will serve our purpose. Here a dashpot of viscosity η is in parallel with another dashpot η' and a spring of elasticity n'.

In Fig. 5 the slope of the lines gives the ultrasonic viscosity η' while $\eta + \eta'$ represents the "steady viscosity." The intercept, absorption at zero frequency, enables the elasticity n' to be calculated.

Thus, the model has a resonant pulsatance $\omega_0 = n'/\eta'$, $= RC'$ in electrical symbols, and the attenuation can be written

$$\alpha = \frac{2}{3}\frac{\omega^2}{\rho c^3}\left[\eta + \frac{\eta'}{1 + (\omega/\omega_0)^2}\right] = \omega^2\left[B + \frac{A}{1 + (\omega/\omega_0)^2}\right]$$

Thus, on a graph of α against f^2, the slope $B = 8\pi^2/3 \times \eta/\rho c^3$, and the intercept on the ordinate axis where $f \longrightarrow 0$

$$= \frac{2}{3} \times \frac{\eta'\omega_0^2}{\rho c^3} = \frac{2}{3} \times \frac{n'^2}{\rho c^3 \eta'}$$

Inserting the slopes and intercepts, we find for example at 180° the following initial and final approximate values for the elements of the model: η, 0.32 to 0.27; η', 300 to 200; n', 5 to 1.7 $\times$ 10^8 in c.g.s. units.

THE CONDUCTANCES OF SOME POTASSIUM AND SODIUM SALTS IN DIMETHYLFORMAMIDE AT 25°

BY DONALD P. AMES AND PAUL G. SEARS

Contribution from the Department of Chemistry, University of Kentucky, Lexington, Ky.

Received June 18, 1954

The conductances of dilute dimethylformamide solutions of ten potassium and sodium salts having univalent anions have been measured at 25°. For the concentration range of 1–20 $\times$ 10^{-4} N, relatively good agreement exists between the observed and theoretical Onsager behavior for all salts studied except the nitrates. The limiting equivalent conductances indicate a potassium salt to be 0.7 $\pm$ 0.4 ohm^{-1} cm.^{2} more conducting than the corresponding sodium salt and substantiate the Kohlrausch law of independent ion migration in dimethylformamide.

Introduction

Although dimethylformamide has become important in the non-aqueous solvent field, there exists in the literature[1,2] a paucity of information concerning the conductance of salts in this solvent. The purpose of this investigation has been to obtain some additional information concerning the conductance behavior of several pairs of potassium and sodium salts having the same univalent anion and to test the validity of the Kohlrausch law of independent ion migration in dimethylformamide.

Experimental

1. **Purification of Solvent.**—Dimethylformamide (Eastman White Label) was dried over solid potassium hydroxide and fractionally distilled at 5 mm. pressure. The retained middle fractions had conductivities ranging from 0.6–2.0 $\times$ 10^{-7} ohm^{-1} cm.$^{-1}$ at 25°.

2. **Purification of Salts.**—Reagent grade potassium and sodium nitrates and bromides were recrystallized three times from redistilled water and dried for 12 hours *in vacuo* at 70°. Reagent grade potassium and sodium iodides were recrystallized three times from water–ethanol solutions and dried for 12 hours *in vacuo* at 70°. Reagent grade potassium and sodium perchlorates were recrystallized three times from redistilled water and dried *in vacuo* for 10 hours at 100° and an additional 12 hours at 130°. Reagent grade potassium and sodium thiocyanates were recrystallized three times from redistilled water and dried 48 hours *in vacuo* at 60°.

3. **Apparatus and Procedure.**—Resistance measurements were made with a Jones bridge (manufactured by the Leeds and Northrup Company) at a frequency of 1000 cycles per second. Periodic resistance measurements were made also at 500 and 2000 cycles per second; however, no significant frequency dependence for resistance was observed. For resistances greater than 30,000 ohms, 30,000 ohms of the bridge resistance was shunted in parallel with the cell and the series cell resistance was computed from the measured parallel resistance.

Three flask cells with lightly platinized electrodes, similar to those designed by Daggett, Blair and Kraus,[3] were em-

(1) L. R. Dawson, M. Golben, G. R. Leader and H. K. Zimmerman, Jr., *J. Electrochem. Soc.*, **99**, 28 (1952).

(2) L. R. Dawson, M. Golben, G. R. Leader and H. K. Zimmerman, Jr., *Trans. Kentucky Acad. Sci.*, **13**, 221 (1952).

(3) H. M. Daggett, Jr., E. J. Blair and C. A. Kraus, *J. Am. Chem. Soc.*, **73**, 799 (1951).

TABLE I

CONDUCTANCE OF SOME POTASSIUM AND SODIUM SALTS IN DIMETHYLFORMAMIDE AT 25°

$C \times 10^4$	Λ	$C \times 10^4$	Λ	$C \times 10^4$	Λ	$C \times 10^4$	Λ	$C \times 10^4$	Λ
(a) Potassium iodide		(c) Potassium perchlorate		(e) Potassium thiocyanate		(g) Potassium bromide		(i) Potassium nitrate	
1.237	81.1	0.374	81.9	1.256	88.5	0.730	82.8	0.833	86.4
3.616	79.9	1.112	81.4	3.435	87.4	3.614	81.4	1.881	85.5
6.542	79.0	2.757	80.6	7.204	86.0	13.32	78.5	7.184	82.8
11.71	77.8	6.745	79.2	13.50	84.4	22.94	76.7	13.41	80.6
18.48	76.7	12.49	78.0	21.52	83.1	37.66	74.8	25.39	77.6
28.51	75.3	22.85	76.2	32.35	81.6			39.12	74.7
38.37	74.3	35.15	74.8	46.84	80.0				
48.87	73.4								
(b) Sodium iodide		(d) Sodium perchlorate		(f) Sodium thiocyanate		(h) Sodium bromide		(j) Sodium nitrate	
1.661	80.1	0.969	80.7	1.502	87.4	1.059	81.7	0.945	84.9
2.887	79.5	2.919	79.5	2.459	86.8	2.847	80.7	6.778	81.2
8.375	77.8	6.124	78.5	7.772	84.7	5.599	79.6	14.22	78.0
15.54	76.4	11.69	77.1	14.22	83.0	8.976	78.5	28.72	73.7
26.25	74.8	20.33	75.6	21.80	81.5	14.25	77.2	39.64	71.3
38.64	73.5	26.73	74.8	35.93	79.6	22.92	75.4		
		32.08	74.2	53.80	77.6	31.76	74.1		

ployed in the resistance measurements. The cell constants of 0.4204, 0.4224 and 0.4443 cm.$^{-1}$ were determined by the intercomparison of these cells with two Jones cells having constants of 1.0312 and 1.0606 cm.$^{-1}$ which were evaluated using the accepted value for the specific conductance of a 0.01 demal aqueous solution of potassium chloride at 25° as given by Jones and Bradshaw.[4] Resistance measurements were carried out in an oil-filled thermostat at 25.00 ± 0.03°. The temperature of the bath was established with a thermometer calibrated by the National Bureau of Standards.

Although the resistance of the more dilute solutions would decrease slightly (in some cases as much as 0.2%) with time, even though temperature equilibrium had been established, it was found that the measured resistance was reproducible if the immersed cells were manually manipulated in a manner so as to change the solution between the electrodes immediately prior to measuring the resistance. A mean of 3 to 5 resistances, each of which was determined after changing the solution between the electrodes, was used in the calculation of the conductivity of a given solution.

The weight dilution method was used for the preparation of the solution in the flask cells. The preparation of the stock solutions, the filling of the cells and the Friedman–LaMer weighing pipets were performed in a dry-box; however, the rapid additions of stock solutions to the conductance cells were made under natural laboratory conditions after it had been established that very brief exposures of the solvent or solutions to the atmosphere caused no observable change in the resistance. In calculating concentrations on a volume basis, it was assumed that the densities of the solutions were the same as that of the solvent. All weights were corrected to vacuum. The conductivity of a salt was obtained by subtracting the conductivity of the solvent from that of the solution.

The following data for dimethylformamide at 25° were used in the calculations: density, 0.9443 g./ml.[5]; viscosity, 7.96×10^{-3} poise[5]; dielectric constant, 36.71.[6] The values of the fundamental constants were taken from the latest report of the Subcommittee on Fundamental Constants.[7]

Results

Values of the equivalent conductance, Λ, and the concentration in gram equivalents per liter, C, for one of three independent series of measurements for each salt are presented in Table I.[8]

Discussion

A plot of the equivalent conductance against the square root of the concentration for each salt studied in dimethylformamide is given in Figs. 1 or 2. The radii of the circles representing experimental points on these plots are equivalent to 0.2 Λ unit or approximately 0.25% of the ordinate value. Linear plots were obtained for all salts for concentrations less than 0.002 N. For greater concentrations, the plots either remain linear or become convex to the concentration axis. The extrapolated values of the limiting equivalent conductance and the limiting experimental slopes are listed in Table II together with the theoretical slopes calculated by

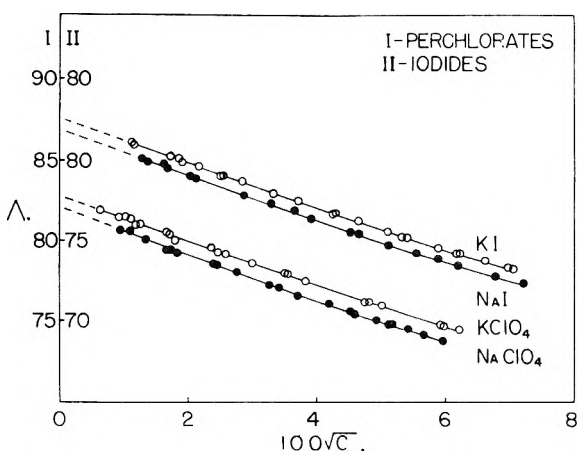

Fig. 1.—Equivalent conductance as a function of the square root of the concentration for some potassium and sodium salts in dimethylformamide at 25°.

(4) G. Jones and B. C. Bradshaw *J. Am. Chem. Soc.*, **55**, 1780 (1933).

(5) E. D. Wilhoit, unpublished data, University of Kentucky, 1954.

(6) G. R. Leader and J. F. Gormley, *J. Am. Chem. Soc.*, **73**, 5731 (1951).

(7) F. D. Rossini, F. T. Gucker, Jr., H. L. Johnston, L. Pauling and G. W. Vinal, *ibid.*, **74**, 2699 (1952).

(8) Material supplementary to this article has been deposited as Document number 4347 with the ADI Auxiliary Publications Project, Photoduplication Service, Library of Congress, Washington 25, D. C. A copy may be secured by citing the Document number and by remitting in advance $1.25 for photoprints, or $1.25 for 35 mm. microfilm, by check or money order payable to: Chief, Photoduplication Service, Library of Congress.

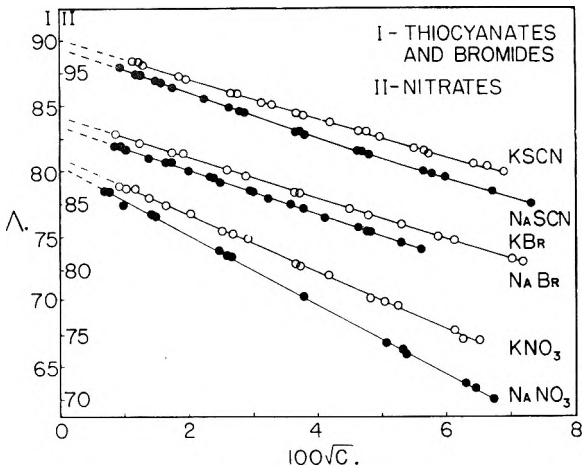

Fig. 2.—Equivalent conductance as a function of the square root of the concentration for some potassium and sodium salts in dimethylformamide at 25°.

the use of the Onsager equation[9] which may be written as follows for a univalent electrolyte

$$\Lambda = \Lambda_0 - \left[\frac{82.42}{(DT)^{1/2}\eta} + \frac{8.203 \times 10^5}{(DT)^{3/2}}\Lambda_0\right]\sqrt{C} \quad (1)$$

The substitution of the proper data simplifies this equation to give equation 2 for uni-univalent electrolytes in dimethylformamide at 25°

$$\Lambda = \Lambda_0 - [99.0 + 0.716\Lambda_0]\sqrt{C} \quad (2)$$

Compared to the theoretical slope, $-[99.0 + 0.716\ \Lambda_0]$, both more negative slopes (positive deviations) and less negative slopes (negative deviations) were observed.

TABLE II

TEST OF ONSAGER'S EQUATION FOR SOLUTIONS OF SOME POTASSIUM AND SODIUM SALTS IN DIMETHYLFORMAMIDE AT 25°

Salt	Λ_0	Theoretical slope (S_T)	Obsd. slope (S_E)	% Dev. $100(S_E - S_T)/S_T$
KI	82.6	−158	−137	−13
NaI	81.9	−158	−138	−13
$KClO_4$	82.7	−158	−137	−13
$NaClO_4$	82.1	−158	−145	− 8
KSCN	90.2	−164	−151	− 8
NaSCN	89.5	−163	−171	5
KBr	84.1	−159	−154	− 4
NaBr	83.4	−159	−165	4
KNO_3	88.5	−162	−214	32
$NaNO_3$	87.9	−162	−263	62

The conductance data for the salts exhibiting positive deviations were analyzed by the Shedlovsky extrapolation method[10] for incompletely dissociated electrolytes. The limiting equivalent conductances and dissociation constants obtained by this treatment are given in Table III. The Λ_0 values given in Table III should be more reliable than those for the same salts listed in Table II inasmuch as a more accurate extrapolation procedure was utilized.

It was observed that the semi-empirical Shedlovsky modification of the Onsager equation (equation 3) best describes the data for those salts for

(9) L. Onsager, *Physik. Z.*, **28**, 277 (1927).
(10) T. Shedlovsky, *J. Franklin Inst.*, **225**, 739 (1938).

TABLE III

LIMITING EQUIVALENT CONDUCTANCES AND DISSOCIATION CONSTANTS FOR SOME POTASSIUM AND SODIUM SALTS IN DIMETHYLFORMAMIDE DETERMINED BY THE SHEDLOVSKY METHOD

Salt	Λ_0	K
NaSCN	89.5	0.13
NaBr	83.4	0.13
KNO_3	88.1	0.043
$NaNO_3$	87.2	0.023

which the Kohlrausch plots become convex to the concentration axis. Equation 3 may be rearranged

$$\Lambda = \Lambda_0 - \frac{\Lambda}{\Lambda_0}[99.0 + 0.716\Lambda_0]\sqrt{C} \quad (3)$$

to give equation 4, which indicates that a plot of $1/\Lambda$ *versus* $\sqrt{C}$ should have an intercept of $1/\Lambda_0$ and a slope of $(99.0 + 0.716\,\Lambda_0)/\Lambda_0^2$. Figure 3 shows plots

$$\frac{1}{\Lambda} = \frac{1}{\Lambda_0} + \left[\frac{99.0 + 0.716\Lambda_0}{\Lambda_0^2}\right]\sqrt{C} \quad (4)$$

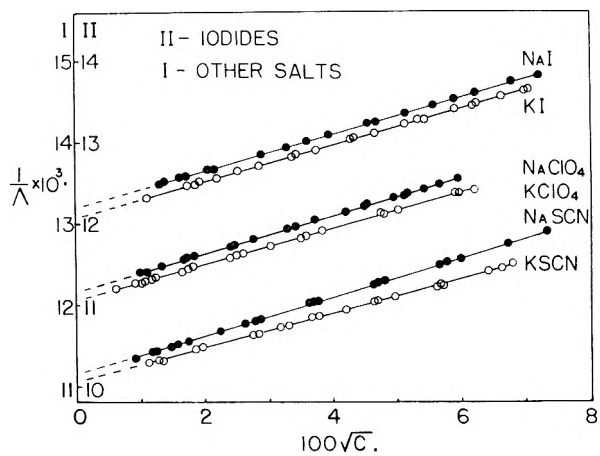

Fig. 3.—Plots of equation 4 for some potassium and sodium salts in dimethylformamide at 25°.

of this nature for six salts in dimethylformamide. The comparisons of the observed and calculated slopes for these plots are given in Table IV and show that equation 4 describes the conductance behavior of most of these salts for concentrations up to 0.005 *N*. Furthermore, except for sodium thiocyanate, the Λ_0 values obtained by this method agree with corresponding values reported in Table II.

TABLE IV

TEST OF EQUATION 4 FOR SOME POTASSIUM AND SODIUM SALTS IN DIMETHYLFORMAMIDE AT 25°

Salt	Λ_0	Theoretical slope (S_T)	Obsd. slope (S_E)	% Dev. $100(S_E - S_T)/S_T$
KI	82.6	0.220	0.231	5
NaI	82.0	.224	.235	5
$KClO_4$	82.8	.217	.231	6
$NaClO_4$	82.2	.232	.240	4
KSCN	90.3	.201	.207	3
NaSCN	89.8	.202	.237	17

The differences between the Λ_0 values for potassium and sodium salts having a common univalent anion may be deduced from the data listed in Tables II, III and IV.

A constant difference of 0.7 ± 0.4 ohm^{-1} cm.^{2} prevails within experimental and extrapolation errors for the five pairs of potassium and sodium salts studied, substantiating the reliability of the Kohlrausch law of independent ion migration in dimethylformamide.

THE SYSTEM LITHIUM OXIDE–BORIC OXIDE–WATER

BY WILLIAM T. REBURN AND WILLIAM A. GALE[1]

Contribution from the Research Department of American Potash & Chemical Corporation, Whittier, Calif.

Received June 22, 1954

Isotherms from 10 to 80° are presented for the ternary system Li_2O–B_2O_3–H_2O. Solubility data for the binary systems $Li_2B_4O_7$–H_2O and $LiBO_2$–H_2O, and the system $Li_2B_{10}O_{16}$–H_2O at temperatures above the transition interval of lithium pentaborate decahydrate, $Li_2B_{10}O_{16}\cdot 10H_2O$, are also given. The published data on the binary system $LiBO_2$–H_2O and the ternary system Li_2O–B_2O_3–H_2O at 30° are corrected to show the fields of existence of two additional compounds, $Li_2B_4C_7\cdot 3H_2O$ and $LiBO_2\cdot 2H_2O$. Lithium tetraborate pentahydrate, $Li_2B_4O_7\cdot 5H_2O$, did not appear in this investigation.

Data on the solubilities of lithium borates in aqueous solution are given by Dukelski[2] for the isotherm of the system Li_2O–B_2O_3–H_2O at 30° with H_3BO_3, $Li_2B_{10}O_{16}\cdot 10H_2O$, $Li_2B_4O_7\cdot xH_2O$, $LiBO_2\cdot 8H_2O$ and $LiOH\cdot H_2O$ as saturating solids. Rosenheim and Reglin,[3a] Menzel,[3b] and LeChatelier[4] present data for the system $LiBO_2$–H_2O, from the eutectic at −0.515° saturated with Ice + $LiBO_2\cdot 8H_2O$ to and beyond the congruent melting point of $LiBO_2\cdot 8H_2O$ at 47.1°. Only one hydrate, $LiBO_2\cdot 8H_2O$, is reported. The work of these authors has been summarized by Seidell[5] and by the International Critical Tables.[6] Data relative to the solubilities of lithium borates are also given in Mellor.[7]

The results of the present investigation agree with data of the previous authors only when allowance is made for supersaturation effects which apparently prevented the crystallization of two compounds, lithium tetraborate trihydrate, $Li_2B_4O_7\cdot 3H_2O$, and lithium metaborate dihydrate, $LiBO_2\cdot 2H_2O$, neither of which were known to these prior investigators. The solid phase borates found to be involved in the equilibrium relationships reported herein were $Li_2B_{10}O_{16}\cdot 10H_2O$, $Li_2B_4O_7\cdot 3H_2O$, $LiBO_2\cdot 8H_2O$ and $LiBO_2\cdot 2H_2O$.

Experimental

All available solubility data were used as guides in preparing the four lithium borates—$Li_2B_{10}O_{16}\cdot 10H_2O$, $Li_2B_4O_7\cdot 3H_2O$, $LiBO_2\cdot 8H_2O$ and $LiBO_2\cdot 2H_2O$ needed in this investigation.

Merck or Fisher reagent grade lithium hydroxide and boric acid of U.S.P. grade (99.95% H_3BO_3, produced by American Potash & Chemical Corp., Trona, California) were used as sources of Li_2O and B_2O_3. The amount of CO_2 present in these materials ranged from 0.03% for the boric acid to 0.16% for the lithium hydroxide.

A clear solution of lithium hydroxide was treated with a calculated amount of boric acid and brought to a temperature sufficiently high to ensure complete solution of all solids. After filtering, the resultant clear solution was cooled to a temperature that would cause the desired salt to crystallize. The compositions of some of the crops of the four borates as found by analysis are recorded in Table I.

TABLE I

INDIVIDUAL CROPS OF LITHIUM BORATES

	Four Crops of $Li_2B_{10}O_{16}\cdot 10H_2O$			
	Wt. %			Mole ratio
	Li_2O	B_2O_3	$Li_2B_{10}O_{16}$	B_2O_3/Li_2O
	5.34	62.09	67.43	4.989
	5.36	62.16	67.52	4.976
	5.34	62.00	67.34	4.981
	5.42	62.15	67.57	4.920
Av.	5.36	62.10	67.47	4.967
Theoretical	5.35	62.37	67.72	5.000

	Seven Crops of $Li_2B_4O_7\cdot 3H_2O$			
	Wt. %			Mole ratio
	Li_2O	B_2O_3	$Li_2B_4O_7$	B_2O_3/Li_2O
	13.32	62.33	75.65	2.008
	13.37	62.50	75.87	2.006
	13.34	62.20	75.54	2.001
	13.40	62.10	75.50	1.988
	13.19	62.10	75.29	2.020
	13.33	62.30	75.63	2.005
	13.41	62.33	75.75	1.994
Av.	13.34	62.27	75.60	2.003
Theoretical	13.39	62.40	75.79	2.000

	Four Crops of $LiBO_2\cdot 8H_2O$			
	Wt. %			Mole ratio
	Li_2O	B_2O_3	$LiBO_2$	B_2O_3/Li_2O
	7.73	18.06	25.79	1.002
	7.72	18.07	25.79	1.004
	7.77	18.27	26.04	1.009
	7.83	18.45	26.28	1.011
Av.	7.76	18.21	25.98	1.007
Theoretical	7.71	17.96	25.67	1.000

	Six Crops of $LiBO_2\cdot 2H_2O$			
	Wt. %			Mole ratio
	Li_2O	B_2O_3	$LiBO_2$	B_2O_3/Li_2O
	17.38	40.65	58.03	1.004
	17.33	40.60	57.93	1.005
	17.36	40.74	58.10	1.007
	17.33	40.89	58.22	1.012
	17.36	40.92	58.28	1.011
	17.38	40.91	58.29	1.010
Av.	17.36	40.79	58.14	1.008
Theoretical	17.42	40.59	58.01	1.000

(1) Correspondence regarding this manuscript should be addressed to William A. Gale, American Potash & Chemical Corp., 201 West Washington Boulevard, Whittier, California.

(2) M. P. Dukelski, *Z. anorg. Chem.*, **54**, 45 (1907).

(3) (a) A. Rosenheim and W. Reglin, *Z. anorg. allgem. Chem.*, **120**, 103 (1921); (b) H. Menzel, *ibid.*, **166**, 63 (1927).

(4) H. LeChatelier, *Compt. rend.*, **124**, 1091 (1897).

(5) A. Seidell, "Solubilities of Inorganic and Metal Organic Compounds," Vol. I, third ed., D. Van Nostrand, New York, N. Y., 1940, pp. 118, 897, 898, 929.

(6) "International Critical Tables," Vol. IV, ed. 1, McGraw-Hill Co., Inc., New York, N. Y., 1928, pp. 235, 380, 394.

(7) J. W. Mellor, "A Comprehensive Treatise on Inorganic and Theoretical Chemistry," Vol. V, Longmans, Green and Co., New York, N. Y., 1924, p. 66.

The solubility data were determined by the usual method of agitating complexes in a constant temperature bath until equilibrium was attained. This point was reached, in most cases, within 24 hours as shown by the constancy of analytical results on samples of the saturated solution taken on one or two following days. Samples were taken by filtering through a cotton plug attached to a pipet. Equilibrium was approached from below rather than from above in order to avoid supersaturation, a tendency exhibited particularly by the tetraborate and the metaborate.

A few sets of duplicate determinations on samples from the same complex, taken 24 hours apart, are shown in the tables as examples (indicated by "j"). However, all single values listed (exeept those quoted from other sources) are the average of at least two such determinations on samples from the same complex approximately 24 hours apart. In a few cases the points saturated with two solids were confirmed by analysis of the liquid phase from two separate complexes. These results are included in Table V with the notation "k."

The solid phases in the ternary systems were determined by Schreinemaker's method of wet residues where only one solid phase was known to be present. In those cases where two solid phases were present, however, the composition of the wet residue was not determined.

In the binary systems generated by a single lithium borate and water, an excess of the solid borate, known to be the saturating solid at the temperature in question was used. In some instances wet residues were taken. The analytical data for these wet residues along with the analyses of the corresponding saturated solutions are shown in the tables.

In a number of cases where only one solid phase was known to be present, an attempt was made to confirm its composition by direct analysis. The solid was filtered from the mother liquor using suction, and was then dried at a temperature such that the solid would not be decomposed. The analytical data for some of the solids recovered in this manner are recorded in Tables II, III and IV.

The samples were analyzed for alkali and borate by the usual titration methods, aliquot portions being titrated with standard acid (0.1 *N* HCl) to the methyl orange end-point, boiled to expel any CO_2, cooled and then back-titrated with standard alkali (0.1 *N* NaOH) to the phenolphthalein end-point in the presence of mannitol. The results were expressed in terms of wt. % Li_2O and B_2O_3. The lithium borate content was taken as the sum of the percentages of Li_2O and B_2O_3 present.

Results and Discussion

The System $Li_2B_{10}O_{16}$–H_2O.—Lithium pentaborate decahydrate, $Li_2B_{10}O_{16}\cdot 10H_2O$, was the only lithium borate found to show an incongruent solubility. It is stable in its own solution at temperatures above 40.5°.

This pentaborate is mentioned in the literature, but little solubility information is given. Dukelski[2] gives $Li_2B_{10}O_{16}\cdot 10H_2O$ for one of the saturating solids of the 30° isotherms of the system Li_2O–B_2O_3–H_2O. Table II gives the results of solubility determinations in the pure solution interval of this salt. These data are plotted in Fig. 1.

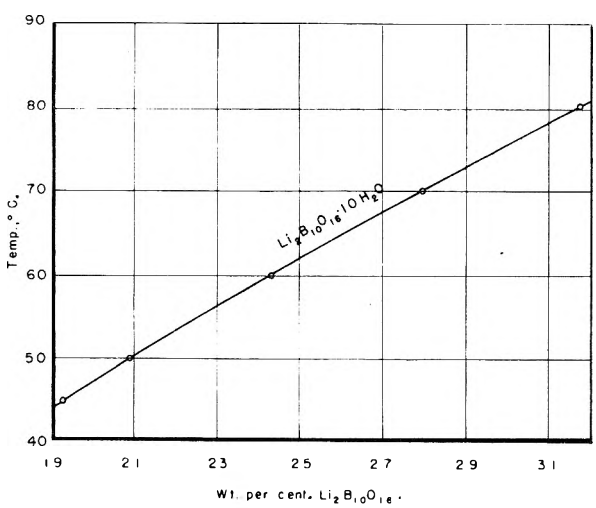

Fig. 1.—Solubility of $Li_2B_{10}O_{16}$ in the pure solution interval.

TABLE II

SOLUBILITY OF $Li_2B_{10}O_{16}\cdot 10H_2O$

Temp., °C.	Solution: wt. % $Li_2B_{10}O_{16}$	Dried solid phase, wt. % Li_2O	B_2O_3	$Li_2B_{10}O_{16}$
45	19.27	5.32	62.24	67.56
50	20.88	5.32	62.14	67.46
60	24.34	5.32	62.21	67.53
70	27.98	5.33	62.25	67.58
80	31.79	...	...	...
Theoretical composition of $Li_2B_{10}O_{16}\cdot 10H_2O$		5.35	62.37	67.72

The System $Li_2B_4O_7$–H_2O.—The literature does not give concordant information regarding the degree of hydration of $Li_2B_4O_7$. Dukelski[2] states that only a colloidal form of $Li_2B_4O_7$ could be obtained from aqueous solution and gives $Li_2B_4O_7\cdot xH_2O$ as the saturating tetraborate in the system Li_2O–B_2O_3–H_2O at 30°. He does mention, however, that he obtained a white powder which formed as a deposit after long standing from highly supersaturated solutions of lithium borates, and which analyzed close to the formula $Li_2B_4O_7\cdot 3H_2O$. This reference was the only mention of the trihydrate, as such, that was found in the literature. Mellor[7] states that in 1818 J. A. Arfvedson obtained a sirupy liquid by boiling an aqueous solution of boric acid with an excess of lithium carbonate. This sirup when treated with alcohol, furnished a white crystalline powder having the formula $Li_2B_4O_7\cdot 5H_2O$, which lost two-fifths of its water at 200°. This hydrate, $Li_2B_4O_7\cdot 5H_2O$, however, did not appear in the present investigation.

It was found that highly supersaturated solutions containing 20 to 25% $Li_2B_4O_7$ could be prepared by adding the calculated amount of boric acid to a known amount of lithium hydroxide solution. These solutions were not stable, and a gelatinous material of an indefinite degree of hydration, but having a mole ratio of B_2O_3 to Li_2O of 2, separated on standing.

It was found, however, that a definite hydrate of lithium tetraborate, $Li_2B_4O_7\cdot 3H_2O$, could be prepared from these supersaturated solutions by boiling. A clear solution containing about 10% $Li_2B_4O_7$, prepared by adding an equivalent amount of

TABLE III

SYSTEM $Li_2B_4O_7$–H_2O

Temp., °C.	$Li_2B_4O_7$, wt. %	Analysis of dried solid phase, wt. % Li_2O	B_2O_3	$Li_2B_4O_7$
0	2.20	13.29	61.95	75.24
10	2.55	...	...	...
20	2.81	13.25	62.15	75.50
30	3.01	...	...	...
40	3.26	13.33	62.30	75.63
60	3.76	13.32	62.27	75.59
80	4.35	13.33	62.26	75.59
100	5.17	...	...	...
Theoretical for $Li_2B_4O_7\cdot 3H_2O$		13.39	62.40	75.79

TABLE IV

SYSTEM $LiBO_2$–H_2O

Temp., °C.	Soln., wt. % $LiBO_2$	Dried solids, wt. % Li_2O	B_2O_3	$LiBO_2$	Solid phase (see Table V)
0	0.88	...	...	...	E
(0)[a]	(0.89)[a]	...	...	...	E
10	1.42	...	...	...	E
(18)[a]	(2.203)[a]	...	...	...	E
20	2.51	7.76	18.21	25.97	E
(25)[a]	(3.344)[a]	...	...	...	E
30	4.63	7.82	18.22	26.04	E
(30)[b]	(4.65)[b]	...	...	...	E
34	5.97	7.63	17.83	25.46	E
35	6.41	...	...	...	E
36	6.84	7.71	18.16	25.66	E
36.9 (extrp.)	7.2 (extrp.)	...	...	...	E + D
37	7.26	17.33	40.60	57.93	D
38	7.33	...	...	...	D
(38.8)[a]	(9.42)[a]	...	...	...	E (m)
39	7.34	...	...	...	D
40	7.40	...	...	...	D
40	9.40	...	...	...	E (m)
(42)[b]	(34.10)[b]	...	...	...	E (m)
(44.8)[a]	(14.7)[a]	...	...	...	E (m)
(46)[b]	(29.97)[b]	...	...	...	E (m)
(47.1)[b]	(25.67)[b]	...	...	...	E (m) (m.p.)
50	7.84	17.45	40.58	58.03	D
60	8.43	...	...	...	D
70	9.48	...	...	...	D
80	10.58	17.47	40.61	58.08	D
101.2	13.4	17.63	40.73	58.36	D
Theor. for $LiBO_2 \cdot 8H_2O$		7.71	17.96	25.67	
Theor. for $LiBO_2 \cdot 2H_2O$		17.42	40.59	58.01	

[a,b] See Table V.

boric acid to a solution of lithium hydroxide, was boiled for several hours. After about an hour of boiling the tetraborate began to precipitate. Three or four hours boiling was found to bring down most of the crystallizable salt from the supersaturated solution.

A large portion of Dukelski's points (Table V) given as saturated with $Li_2B_4O_7 \cdot xH_2O$, were found to be highly supersaturated. The stable hydrate was found to be $Li_2B_4O_7 \cdot 3H_2O$. The solubility data for this compound from 0 to 100° are shown in Table III and are plotted in Fig. 2.

The System $LiBO_2$–H_2O.—Table IV records the data determined in this investigation along with the relevant data of the previous investigators. These data are depicted in Fig. 3. This solubility curve shows two segments, one for solutions in equilibrium with lithium metaborate octahydrate, $LiBO_2 \cdot 8H_2O$, and the other for those in equilibrium with lithium metaborate dihydrate, $LiBO_2 \cdot 2H_2O$.

In the above mentioned references on this system, only one hydrate, $LiBO_2 \cdot 8H_2O$, is reported. However, Menzel[3] mentions that the octahydrate readily loses 6 moles of water by dehydration, while the existence of the dihydrate together with a little information regarding its solubility is reported by the Metalloy Corporation.[8]

The transition point, $LiBO_2 \cdot 8H_2O \rightleftarrows LiBO_2 \cdot 2H_2O$, was determined graphically from the intersection of the solubility curves as being at approximately 36.9° and at a solubility of 7.2% $LiBO_2$.

It is evident from Fig. 3 that the congruent

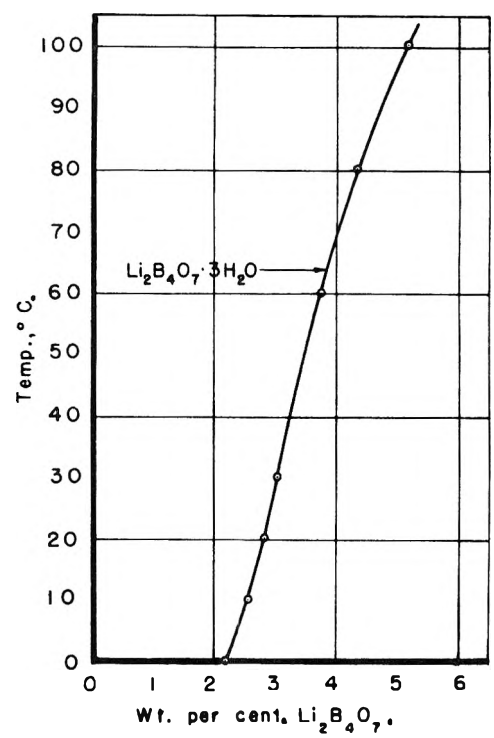

Fig. 2.—System $Li_2B_4O_7$–H_2O.

(8) "Lithium Data Sheets," Metalloy Corporation, Rand Tower, Minneapolis, Minn.

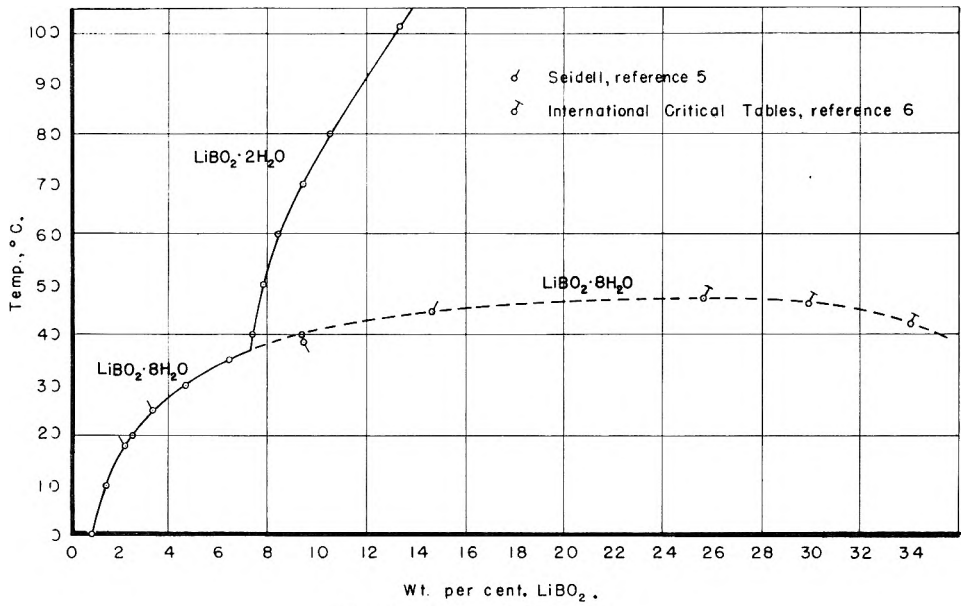

Fig. 3.—System $LiBO_2$–H_2O.

melting point of 47.1° for $LiBO_2 \cdot 8H_2O$ and the other points beyond 36.9° presented by the earlier investigators were actually metastable. The stable phase above 36.9° was found to be the dihydrate, $LiBO_2 \cdot 2H_2O$. This was confirmed by analysis of the dried solids at a few temperatures as shown in Table IV.

The System Li_2O–B_2O_3–H_2O.—The data for six ternary isotherms, from 10 to 80° are recorded in Table V. All points in this table were determined in the course of this investigation with the exception of those in parentheses. All values for the binary points saturated with H_3BO_3 or $LiOH \cdot H_2O$, are from Seidell.[5]

Only the 10, 40 and 80° isotherms have been plotted in Fig. 4 for purposes of illustration and comparison. The other isotherm given in Table V would form intermediate sets of curves. It will be noted that the 10° isotherm does not show the presence of $Li_2B_{10}O_{16} \cdot 10H_2O$ since this is below the ternary transition point $H_3BO_3 + Li_2B_4O_7 \cdot 3H_2O \rightleftarrows Li_2B_{10}O_{16} \cdot 10H_2O$ of the pentaborate. Above 40° the

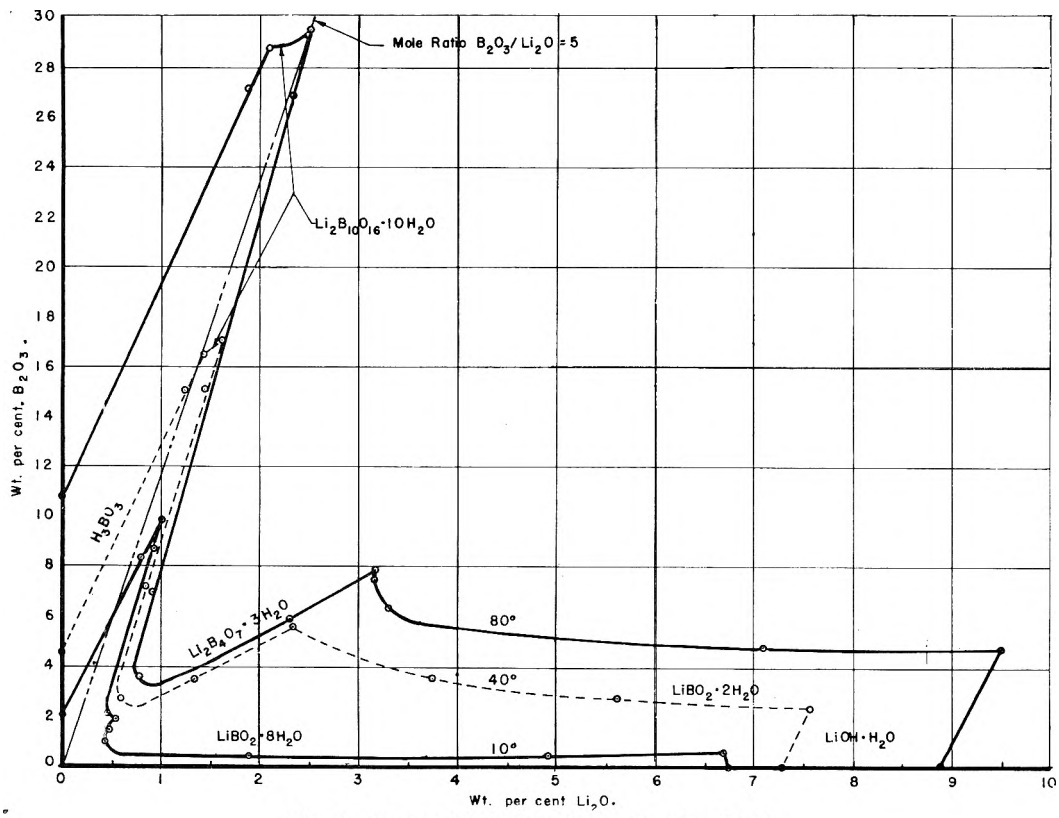

Fig. 4.—System Li_2O–B_2O_3–H_2O: 10, 40 and 80°.

isotherms are similar in form since these temperatures are above the transition points of the saturating solids and in the pure solution interval of the pentaborate, $Li_2B_{10}O_{16}\cdot 10H_2O$.

For purposes of comparison, the data for the 30° isotherm of Dukelski, as summarized in the International Critical Tables,[6] are included in Table V along with the values found in this investigation.

TABLE V

SYSTEM Li_2O–B_2O_3–H_2O

Solid Phases: A = H_3BO_3, B = $Li_2B_{10}O_{16}\cdot 10H_2O$, C = $Li_2B_4O_7\cdot 3H_2O$, D = $LiBO_2\cdot 2H_2O$, E = $LiBO_2\cdot 8H_2O$, F = $LiOH\cdot H_2O$, (x) = $Li_2B_4O_7\cdot xH_2O$ (Dukelski), (m) = Metastable.

Soln., wt. % Li_2O	Soln., wt. % B_2O_3	Wet residue, wt. % Li_2O	Wet residue, wt. % B_2O_3	Solid phase
		10°		
(0)[a]	(2.03)[a]	...	...	A
0.78	8.24	0.44	26.92	A
1.00	9.84	...	...	A + C
1.00	9.74			
0.92	8.65	7.23	35.95	C
.45	2.10	6.57	30.79	C
.53	1.88	...	...	C + E
.53	1.90			
.48	1.46	4.06	9.76	E
.42	1.00	3.85	9.01	E
1.88	0.46	4.60	8.59	E
4.91	0.41	6.26	8.77	E
6.71	0.50	...	...	E + F
6.67	0.50			
(6.74)[a]	(0)[a]	...	...	F
		20°		
(0)[a]	(2.70)[a]	...	...	A
1.04	11.11	0.85	19.03	A
1.18	12.19	...	...	A + B
1.18	12.23			
1.17	12.17			
1.21	12.30	...	...	B + C
1.21	12.25			
1.03	10.23	5.90	30.88	C
0.50	3.00	5.01	23.89	C
0.49	2.32	7.24	33.97	C
0.61	2.06	6.16	28.32	C
0.84	2.36	...	...	C + E
0.85	2.37			
0.74	1.77	...	...	E
2.22	1.05	3.61	5.33	E
4.94	1.00	5.79	6.14	E
6.94	1.18	...	...	E + F
6.98	1.17			
(6.86)[a]	(0)[a]	...	...	F
		30°		
(0)[a]	(3.55)[a]	...	...	A
0.60	8.67	0.21	38.77	A
1.30	14.26	...	...	A + B
1.29	14.29			
1.31	14.26			
(1.30)[b]	(14.14)[b]	...	...	A + B
1.38	14.49	3.60	41.52	B
1.39	14.64	...	...	B + C
1.38	14.57			
3.98	26.84	4.70	45.80	B
(5.06)[c]	(30.81)[c]	...	...	B + (x)
1.25	12.87	5.88	31.94	C
0.68	5.63	3.10	16.62	C
0.53	2.48	7.17	33.65	C
(0.53)[d]	(2.47)[d]	...	...	(x)
0.94	2.60	6.76	30.64	C
(0.95)[e]	(2.61)[e]	...	...	(x)
1.46	3.70	...	...	C + E
1.59	4.39	5.42	12.86	E
3.41	13.74	5.70	16.13	E
(5.63)[f]	(23.84)[f]	...	...	(x) + E
1.38	3.25	...	...	E
(1.58)[g]	(3.27)[g]	...	...	E
1.73	2.80	4.74	10.44	E
2.74	2.45	4.04	6.52	E
(2.94)[h]	(2.51)[h]	...	...	E
3.91	2.37	6.45	12.36	E
...	...	...	...	E + D
5.49	2.47	13.46	27.96	D
6.21	2.28	9.46	13.49	D
6.81	2.13	12.41	22.30	D
7.30	2.05	...	...	D + F
7.30	2.05			
5.92	2.66	6.73	9.54	E (m)
6.71	2.87	7.21	10.62	E (m)
7.45	3.04	...	...	E(m) + F
7.44	2.95			
(7.71)[i]	(3.38)[i]	...	...	E + F
(7.05)[a]	(0)[a]	...	...	F
		40°		
(0)[a]	(4.52)[a]	...	...	A
1.24	15.08	0.50	39.87	A
1.43	16.52	...	...	A + B
1.43	16.51			
1.56	17.04	...	...	B + C
1.58	17.03			
1.42	15.13	5.15	29.41	C
0.79	7.19	5.81	29.32	C
0.57	2.69	6.57	30.81	C
1.32	3.43	7.65	34.43	C
2.32	5.62	...	...	C + D
2.34	5.63			
3.74	3.52	10.88	23.01	D
5.60	2.78	10.50	18.51	D
7.56	2.32	...	...	D + F
7.56	2.34			
(7.29)[a]	(0)[a]	...	...	F
		60°		
(0)[a]	(7.26)[a]	...	...	A
1.46	20.31	...	...	A
1.73	21.87	...	...	A + B
1.73	22.03			
1.73	21.98			
1.93	22.41	...	...	B
2.00	22.70	...	...	B + C
2.00	22.72			
1.82	20.51	5.40	33.47	C
0.64	3.76	3.26	15.83	C
0.66	3.10	6.85	30.09	C
1.82	4.61	5.36	22.49	C
2.64	6.47	...	...	C + D
2.63	6.46			
2.52	5.91	...	...	D
3.83	4.34	...	...	D
5.88	3.55	...	...	D
8.22	3.23	...	...	D + F
8.29	3.23			
(7.96)[a]	(0)[a]	...	...	F

TABLE V (*Continued*)

Soln., wt. % Li_2O	Soln., wt. % B_2O_3	Wet residue, wt. % Li_2O	Wet residue, wt. % B_2O_3	Solid phase
		80°		
(0)[a]	(10.76)[a]	...	...	A
1.89	27.07	1.42	34.21	A
2.09	28.69	...	...	A + B
2.07	28.71			
2.47	29.32	...	...	B
2.53	29.47	...	...	B + C
2.45	29.41			
2.32	26.80	5.09	35.81	C
0.85	6.98	8.08	38.96	C
0.77	3.58	6.61	30.94	C
2.30	5.81	8.77	38.62	C
3.16	7.84	...	...	C + D
3.15	7.78			
3.15	7.41	...	...	D
3.24	6.30	10.85	24.37	D
7.08	4.74	12.13	21.80	D
9.48	4.67	...	...	D + F
9.48	4.71			
(8.87)[a]	(0)[a]	...	...	F

[a–i] Seidell,[5] and International Critical Tables.[6] [j] Samples taken 24 hours apart from same complex. [k] Samples taken from difference complexes.

It may be noted that Dukelski's isothermal invariant point b, given as saturated with the two solids H_3BO and $Li_2B_{10}O_{16}\cdot 10H_2O$, agrees with the results of the present investigation. However, the points c and f, given as saturated with the solids $Li_2B_{10}O_{16}\cdot 10H_2O$ + $Li_2B_4O_7\cdot xH_2O$ and $LiBO_2\cdot 8H_2O$ + $Li_2B_4O_7\cdot xH_2O$, respectively, are both highly supersaturated. The correct formula for the tetraborate is $Li_2B_4O_7\cdot 3H_2O$ and the two stable invariant points at 30° having the tetraborate for one of their saturating solids, are saturated with $Li_2B_{10}O_{16}\cdot 10H_2O$ + $Li_2B_4O_7\cdot 3H_2O$ and $LiBO_2\cdot 8H_2O$ + $Li_2B_4O_7\cdot 3H_2O$. The points d and e reported as saturated with $Li_2B_4O_7\cdot xH_2O$ lie on or near the saturation curve of $Li_2B_4O_7\cdot 3H_2O$ found in this investigation. The point i given as saturated with the two solids $LiBO_2\cdot 8H_2O$ + $LiOH\cdot H_2O$ by Dukelski was found to be metastable. It lies near a similarly metastable point found in this investigation. The stable invariant point in this region is saturated with $LiBO_2\cdot 2H_2O$ + $LiOH\cdot H_2O$. The remaining points of Dukelski, g and h, reported as saturated with $LiBO_2\cdot 8H_2O$ agree as to both solid phase and position on the isotherm with the results of the present investigation. Supersaturation effects had evidently prevented the crystallization of the two compounds $Li_2B_4O_7\cdot 3H_2O$ and $LiBO_2\cdot 2H_2O$ in their respective regions in Dukelski's work.

The phase diagrams of the system Li_2O–B_2O_3–H_2O show a rough similarity to the diagrams of the corresponding systems in which lithium oxide is replaced by sodium or potassium oxides. The J-like shape of the curve saturated with lithium tetraborate, $Li_2B_4O_7\cdot 3H_2O$, in the system Li_2O–B_2O_3–H_2O is also exhibited by the saturation curves of sodium tetraborate decahydrate, $Na_2B_4O_7\cdot 10H_2O$, and potassium tetraborate tetrahydrate, $K_2B_4O_7\cdot 4H_2O$, in the phase diagrams that may be constructed from the data Dukelski[9] gives for the systems Na_2O–B_2O_3–H_2O and K_2O–B_2O_3–H_2O at 30°.

Tie-lines and Residues.—These are not shown in the diagrams. In order to avoid the mechanical errors of plotting, the tie-line intersections were determined by an analytical method described by Dukelski.[9] In this method the intersections of tie-line pairs are found by solving their equations simultaneously. The tie-line equation, in the slope intercept form, is obtained from the analytical data of the solution and wet residue, two points whose compositions are known to lie on the tie-line.

The tie-lines for some points, particularly those saturated with lithium tetraborate trihydrate, $Li_2B_4O_7\cdot 3H_2O$, lie very close together. In these instances the tie-line pairs having the greatest possible angle were selected to determine the composition of the solid phase. In those cases where the solid phase was in equilibrium with its own solution, the solid phase was isolated by filtration and drying as previously described and its composition established by direct analysis.

Ternary Transition Points.—The solubility data indicate the approximate temperatures of three ternary transition points.

The 10 and 20° isotherms show that the transition point of lithium pentaborate decahydrate, $Li_2B_{10}O_{16}\cdot 10H_2O$, involving the solid phases H_3BO_3, $Li_2B_4O_7\cdot 3H_2O$, and $Li_2B_{10}O_{16}\cdot 10H_2O$ occurs between these temperatures.

The incongruent solubility of the pentaborate, $Li_2B_{10}O_{16}\cdot 10H_2O$, at 30° noted by Dukelski[2] was found to be consistent with the present investigation. That the pentaborate is incongruently soluble at this temperature was confirmed by the fact that the pentaborate mole ratio line of B_2O_3/Li_2O = 5 intersects the saturation curve of H_3BO_3 rather than the saturation curve of $Li_2B_{10}O_{16}\cdot 10H_2O$. The transition interval extends upwards from the transition point to approximately 40.5° as interpolated graphically from the following solubility data for points saturated with both H_3BO_3 and $Li_2B_{10}O_{16}\cdot 10H_2O$·

Temp., °C.	Mole ratio B_2O_3/Li_2O	Temp., °C.	Mole ratio B_2O_3/Li_2O
30	4.710	45	5.120
35	4.860	50	5.259
40	4.957		

Above 40.5° the pentaborate becomes stable in its own solution up to at least 80°. Above approximately this temperature it would seem, from the change in position of the point saturated with $Li_2B_{10}O_{16}\cdot 10H_2O$ and $Li_2B_4O_7\cdot 3H_2O$ with temperature, that the stable portion of the solubility curve will no longer intersect the line representing a B_2O_3/Li_2O mole ratio of 5. Thus it is probable that the pentaborate again becomes incongruently soluble.

(9) M. P. Dukelski, *Z. anorg. Chem.*, **60**, 38 (1906).

EQUILIBRIUM INHIBITION OF THE CATALASE–HYDROGEN PEROXIDE SYSTEM DURING THE STEADY STATE

BY ROLAND F. BEERS, JR.[1]

Division of Physical Biochemistry, Naval Medical Research Institute, Bethesda 14, Maryland

Received June 28, 1954

The possible effects of inhibitors on the kinetics of the steady state system of catalase and hydrogen peroxide have been examined analytically. The degree of association between either the free enzyme, the primary complex or both and the inhibitor is independent of the substrate concentration but is dependent on the steady state ratios of the free enzyme and primary complex. For this reason, except where the affinities of both enzyme forms for the inhibitor are the same, all reversible inhibitors display a competitive type of inhibition. This kind of inhibition can be described according to the relative affinities of the two enzyme forms for the inhibitor. The affinity of the primary complex for hydroxylamine, azide, fluoride and several monovalent salts is considerably greater than that of the free enzyme. In the special case of cyanide, the affinity of the free enzyme is greater than or equal to that of the primary complex. The hypothesis is suggested that the main mechanism of inhibition of the primary complex is through the formation of a compound with the inhibitor. This compound could be identical with the covalent secondary complex described by Chance.

Introduction

Until Chance[2] made the distinction between the catalytically active primary and catalytically inactive secondary complexes of catalase with hydrogen peroxide many of the possible mechanisms involved in the inhibition of catalase had not been fully realized or subjected to experimental study. The difficulties encountered by investigators in deriving suitable kinetic equations describing the inhibitory reactions with catalase have arisen primarily from faulty or inaccurate analytical solutions of the uninhibited catalase–hydrogen peroxide system. The recently derived analytical solutions of the steady state[3,4] and the transient state[3,5] systems of catalase and hydrogen peroxide provided for the first time a rational basis for analyzing the kinetics and thermodynamics of the reactions between catalase and inhibitors.

Chance, *et al.*,[3] have pointed out the interesting fact that the degree of inhibition of catalase by competitive inhibitors is not influenced by variations in the substrate concentration during the steady state, *i.e.*, when the concentrations of the primary complex and the free enzyme are independent of time and of the substrate concentration. A similar conclusion had been reached by Ogura, *et al.*,[6,7,8] but on the basis of a system in which all of the enzyme during the steady state is bound by the substrate (*cf.* Chance[9]).

It can be shown that the free enzyme and the primary complex, *i.e.*, the steady state components of the catalase–hydrogen peroxide system, may be in equilibrium with inhibitors, provided the time decay of the variable, the substrate, is first order. Under these conditions the concentrations of the steady state components are a function of the ratio of the velocity constants (specific reaction rates) of the catalyzed reaction, of the equilibrium constants and of the concentrations of the inhibitors in equilibrium with the various enzyme forms, but are independent of the time variable components. Conversely, the rate of decay of the substrate remains a function of the concentrations of the steady state components. By virtue of these facts we are able to calculate the concentrations of the free enzyme and the primary complex in equilibrium with given concentrations of inhibitor.

In the present paper we shall examine in greater detail the kinetics associated with the reactions of catalase with inhibitors during the period when the catalase–hydrogen peroxide system is in a steady state. The "non-competitive" character of catalase inhibition previously described by Chance, *et al.*,[3] is found to embrace many distinct types of inhibition which may be characterized according to the kinetics associated with them. Some of the experimental results published on catalase inhibition will be examined in the light of the concepts developed in this paper.

Theory

The reaction scheme under consideration is the following

$$E + S \overset{f \quad s \quad k_1}{\longrightarrow} ES \qquad (a)$$

$$ES + S \overset{p \quad s \quad k_4}{\longrightarrow} E + \text{products} \qquad (b)$$

The symbols used above the chemical equations are the concentrations of the various components in the system. Wherever practical the terminology introduced by Chance, *et al.*,[3] will be adopted in this paper, otherwise, the terminology used in previous papers by Beers and Sizer[4,10] will be used. In the discussion to follow it is assumed that no substrate–inhibitor interaction occurs in this system. The concentrations of the free or unbound inhibitor are assumed to be equal to the total inhibitor concentrations and, therefore, are constant. This is justified by the fact that in most studies the concentration of the inhibitor is several orders of magnitude greater than that of the enzyme. We will not make any distinction between activities and concentrations. As in previous papers[4,5] *e*, *f*, *p*, etc., refer to the molar concentrations of the reacting centers of the various forms of catalase complexes. In the present paper *e* is the total active

(1) Department of Biology, Massachusetts Institute of Technology, Cambridge 39, Massachusetts. The opinions expressed in this article are those of the author and do not necessarily reflect the opinions of the Navy Department or the Naval Service at large.

(2) B. Chance, *Acta Chem. Scand.*, **1**, 236 (1947).

(3) B. Chance, D. S. Greenstein and F. J. W. Roughton, *Arch. Biochem. Biophys.*, **37**, 301 (1952).

(4) R. F. Beers, Jr., and I. W. Sizer, THIS JOURNAL, **57**, 290 (1953).

(5) R. F. Beers, Jr., *ibid.*, **58**, 197 (1954).

(6) Y. Ogura, Y. Tonomura, S. Hino and H. Tamiya, *J. Biochem. (Japan)*, **37**, 153 (1950).

(7) Y. Ogura, Y. Tonomura, S. Hino and H. Tamiya, *ibid.*, **37**, 179 (1950).

(8) Y. Ogura, Y. Tonomura and S. Hino *ibid.*, 249 (1950).

(9) B. Chance, *J. Biol. Chem.*, **170**, 1311 (1949).

(10) R. F. Beers, Jr., and I. W. Sizer, *ibid.*, **195**, 133 (1952).

enzyme center concentration, *i.e.*, the sum of f and p.

For the postulated scheme (a) and (b) it has been shown elsewhere[4] that if the time decay of the substrate obeys the following equation

$$ds/dt = -k_0 s = -k_s es \qquad (1)$$

where k_0 is the observed first-order constant and k_s is the specific reaction rate of the over-all reaction, then the following holds during the steady state

$$R_k = f/p = k_4/k_1 \qquad (2)$$

where we define R_k as the steady-state constant of this system. The presence of inhibitors in equilibrium with E or ES does not alter the necessary conditions for simultaneous satisfaction of equations (1) and (2). Therefore, if in a given set of experimental conditions equation (1) is valid the steady state conditions have not been altered by the presence of an inhibitor. Where progressive inhibition of catalase occurs during the catalysis of the substrate equation 2 may be valid despite the absence of a steady state. This will be discussed in a forthcoming paper.[11] In general in the presence of reversible inhibitors or under conditions of partial and irreversible but constant inhibition of the catalase–hydrogen peroxide system from any number of causes, except at high pH,[12] the rate of catalysis has been found to follow equation 1.[10,13]

In the present paper we will abandon the conventional classification of inhibition according to whether it is competitive or non-competitive and adopt a classification based on the relative affinities of the inhibitor for the free enzyme and the primary complex. The reasons for this will become apparent as we proceed.

Inhibitor Complex Formation with Free Enzyme Only. (See Figure 1 for generalized reaction scheme.).—The possible reactions between inhibitor and enzyme are

$$E + I \underset{k_{-5}}{\overset{f \quad i \quad k_5}{\rightleftharpoons}} EI \qquad (c)$$

$$ES + I \underset{k'_{-5}}{\overset{p \quad i \quad k_5'}{\rightleftharpoons}} EI + S \qquad (d)$$

For the moment we exclude reaction (d) from further consideration; first, this reaction need not account for the displacement of S by I; second, we assume that the formation of ES is practically irreversible (reaction a) and, therefore, k_5' is negligible; and third, if we assume that EI is completely inactive with respect to S, k'_{-5} is negligible.

The dissociation constant, K_5, of reaction c is

$$K_5 = k_{-5}/k_5 = fi/q' \qquad (3)$$

At equilibrium

$$f = q'K_5/i \qquad (4)$$

Substituting equation 4 into 2, we obtain

$$p/q' = K_5/R_k i \qquad (5)$$

We observe that the ratio p/q' is independent of s (*cf.* Chance, *et al.*[3]). Therefore, the degree of inhibition does not vary with the substrate concentration. However, since some of the free enzyme is converted to the primary complex by the substrate a smaller fraction of the inhibited complex is formed in the presence than in the absence of the substrate. From the previously derived rate expression[4]

$$ds/dt = -2k_4 ps \qquad (6)$$

and equation 1 we have after appropriate substitutions from equation 6 the following

$$ds/dt = -2k_1 K_5 q'(s/i) = -k_0^* \qquad (7)$$

where k_0^* is the observed first-order constant in the presence of the inhibitor. From the conservation of material equations: $e = f + p$ and E (total active and inactive enzyme) $= e + q'$, we may make appropriate substitutions into equation 7 and solve directly for K_5 from the rate of catalysis of the substrate, *i.e.*, from the observed first-order constant

$$K_5 = \frac{k_s ei}{2k_1(E - e)} = \frac{R_k}{(R_k + 1)} \frac{ik_0^*}{(k_0^c - k_0^*)} \qquad (8)$$

k_0^c is the observed first-order constant in the absence of the inhibitor.

Inhibitor Complex Formation with Primary Complex Only.—The reaction between the inhibitor and the enzyme is

$$ES + I \underset{k_{-6}}{\overset{p \quad i \quad k_6}{\rightleftharpoons}} ESI \qquad (e)$$

(See below for discussion of reaction between inhibitor enzyme complexes and substrate.) The dissociation constant of reaction (e), K_6, is

$$K_6 \equiv k_{-6}/k_6 = pi/q'' \qquad (9)$$

The corresponding solution for K_6 from first-order constants is

$$K_6 = \frac{k_0^* i}{(R_k + 1)(k_0^c - k_0^*)} \qquad (10)$$

Equation 10 is of the same general form as equation 8 except that the factor, $R_k/(R_k + 1)$, now becomes

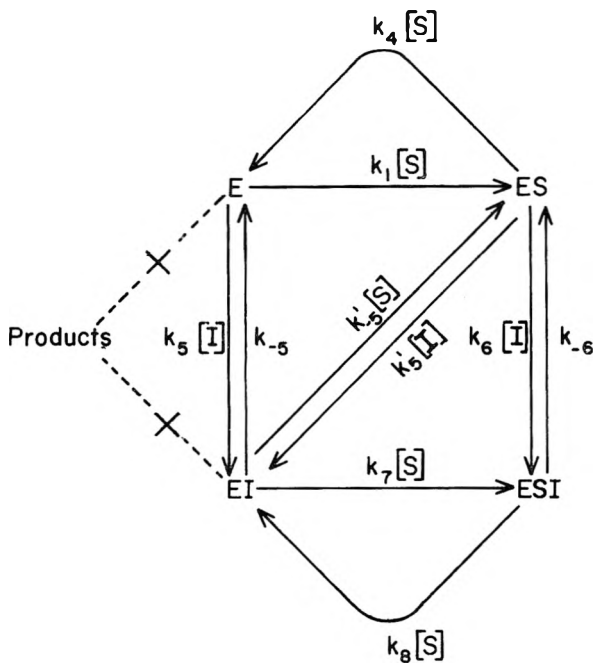

Fig. 1.

(11) R. F. Beers, Jr., in preparation.

(12) B. Chance, *J Biol. Chem.*, **194**, 471 (1952).

(13) R. K. Bonnischen, B. Chance and H. Theorell, *Acta Chem. Scand.*, **1**, 685 (1947).

$1/(R_k + 1)$. Obviously, from simple kinetic data equation 10 cannot be distinguished from equation 8. This type of inhibition is analogous to but not identical with "uncompetitive inhibition" as described by Ebersole, *et al.*[14] The inhibitor is reacting with the intermediate complex rather than with the free enzyme. However, the similarities extend no further. The distinction between the free enzyme and the primary complex is in this case rather arbitrary because both react with the substrate.

Inhibitor Complex Formation with Both Enzyme Species.—From reactions (a), (b), (c) and (e) three conditions are to be met: equations 2, 3 and 9. One consequence is the relation between q' and q''

$$q'/q'' = K_6R_k/K_5 \qquad (11)$$

In other words, the ratio of inhibited complexes is independent of both s and i. Following the same procedure adopted in the simpler cases, we obtain

$$\frac{k_0^*i}{k_0^e - k_0^*} = \frac{K_5(R_k + 1)}{R_k + K_5/K_6} \qquad (12)$$

We need know only K_5 independently in order to determine K_6 from kinetic data. Two limiting solutions are found by setting $K_5 \ll K_6$ or $K_5 \gg K_6$, in which case equation 12 reduces to equations 8 and 10, respectively. For the special case where $K_5 = K_6$, equation 12 reduces to equation 13

$$K_5 = K_6 = \frac{ei}{E - e} = \frac{ik_0^*}{k_0^e - k_0^*} \qquad (13)$$

Equation 13 is the usual form employed by most investigators for comparing inhibition constants determined from activity measurements and spectrophotometric data.[15] Equation 13 represents, in fact, a true case of non-competitive inhibition, *i.e.*, the affinities of the free enzyme and the enzyme–substrate complex for the inhibitor are identical. However, this does not imply that under the circumstance that the affinities are different the inhibitor is competitive in its mechanism. In particular, it is not necessary to assume that the inhibitor and the substrate are competing for the same locus of the enzyme. It is possible that the differences in the affinities may simply reflect the effects of site interaction as a result of binding of the substrate. In view of this possibility, it would appear desirable to substitute for the term "competitive," some quantitative relationship between the respective dissociation constants, K_5 and K_6.

One such relationship expresses the percentage difference in affinity of E and ES for I; which we will designate as D.A.

$$\text{D.A.} = 100[(K_5 - K_6)/(K_5 + K_6)] \qquad (14)$$

When the sign of equation 14 is positive, the affinity of the complex for the inhibitor is greater than that of the free enzyme by the above percentage. If the sign is negative, the affinity is correspondingly greater for the free enzyme. If the value is zero, the inhibition could be described as true non-competitive.

Reactions between Inhibited Complexes and Substrate.—If an inhibitor reacts with both forms of the enzyme, then the following reaction is also possible

$$\underset{q'}{\text{EI}} + \text{S} \underset{k_{-7}}{\overset{s \quad k_7}{\rightleftarrows}} \underset{q''}{\text{ESI}} \qquad (f)$$

A reasonable assumption to make is that $k_7 \gg k_{-7}$. The free energy drop which occurs in going from EI to ESI is of the same order of magnitude as that which occurs in reaction (a), an essentially irreversible reaction where k_1 exceeds k_2, the reverse reaction constant, by a factor of at least $10^{7.3}$ However, we cannot make any approximate assumptions regarding the value of k_7 since we know nothing about the free energy of activation of this potential reaction. It is, therefore, of considerable interest to ascertain whether we can detect this reaction from kinetic studies of the steady state system. The rate of destruction of the substrate is given by

$$ds/dt = -k_1fs - k_4ps - k_7q's \qquad (15)$$

which during the steady state can be integrated to yield

$$s = s_0e^{-(k_1f_1 + k_4p + k_7q')t} \qquad (16)$$

However, in order for q' to be constant in equation 16 the following equation must be satisfied

$$dq'/dt = k_5fi - k_{-5}q' - k_7q's = 0 \qquad (17)$$

But if the inhibitor is in equilibrium with the free enzyme (reaction c), then equation 17 becomes

$$dq'/dt = -k_7q's = 0 \qquad (17a)$$

In other words, if reaction (f) occurs to an appreciable extent, then during the steady state the inhibitor cannot be in equilibrium with the free enzyme. However, from equation 17 the ratio, q'/f, is

$$q'/f = k_5i/(k_7s + k_{-5}) \qquad (18)$$

But since s is a variable, q'/f must also be a variable. Therefore, under these conditions the catalase–hydrogen peroxide system cannot be in a steady state.

For the special case where $k_1 = k_7$, then

$$k_4/k_1 = k_7/k_1 = (q' + f)/p \qquad (19)$$

But since $k_4/k_1 = f/p = R_k$ in the absence of the inhibitor, the sum of q' and f must represent the effective or active fraction of the enzyme not bound as p or q''. In other words, EI is not an inhibited complex. However, the ratio, q'/f, continues to vary as a function of the substrate concentration.

In a similar manner to the above we may examine the possible effects of the reaction

$$\underset{q''}{\text{ESI}} + \text{S} \underset{k_{-8}}{\overset{s \quad k_8}{\rightleftarrows}} \underset{q'}{\text{EI}} + \text{products} \qquad (g)$$

where for the same reason as given above we may assume that $k_8 \gg k_{-8}$ The transient value of q''/p is

$$q''/p = k_6i/(k_8s + k_{-6}) \qquad (20)$$

and is found to vary inversely with the substrate concentration. Consequently reactions (f) and (g) cannot be distinguished by the observations on the effect of the substrate concentrations on the degree of inhibition.

For the more general case in which both $k_7 \neq 0$ and $k_8 \neq 0$, we have an example of two enzyme sys-

(14) E. R. C. Ebersole, C. Guttentag and P. W. Wilson, *Arch. Biochem.*, **3**, 399 (1944).

(15) B. Chance, *J. Biol. Chem.*, **179**, 1299 (1949).

tems, E and ES as well as EI and ESI, in equilibrium with each other and differing with respect to their kinetic constants. One requirement to be satisfied is

$$k_8/k_7 = R_k K_6/K_5 \qquad (21)$$

The observed degree of inhibition is found to be

$$1 - k_0^*/k_0^c = 1 - \frac{(k_1 + k_4)(k_4 + k_8 i/K_6)}{k_1 k_4 [R_k + 1 + i(k_8/k_7 + 1)/K_6]} \qquad (22)$$

where k_0^c, the control, is the observed velocity constant in the absence of I. With large i this reduces to

$$1 - k_0^*/k_0^c = 1 - \frac{(k_1 + k_4)k_7 k_8}{(k_7 + k_8)k_1 k_4} \qquad (23)$$

and with small i to

$$1 - k_0^*/k_0^c = 1 - \frac{(k_1 + k_4)k_4}{(R_k + 1)k_1 k_4} = 1 - 1 = 0 \qquad (24)$$

In other words, the degree of inhibition will vary from 0 to a maximum less than unity and independent of i. This type of inhibition of catalase has not been described and will not be considered further.

Discussion

Perhaps, the most unexpected result of this analysis of the kinetics of inhibition of the catalase–hydrogen peroxide system is the finding that the degree of inhibition bears a fixed relationship with the steady state ratio of the enzyme forms. The algebraic solutions presented above are identical with those of competing equilibria. Formally, there is no mathematical distinction between R_k as a steady state constant or as an equilibrium constant.

The steady state solutions of the catalase–hydrogen peroxide system have exposed a new area for theoretical and experimental investigations which could not be fully appreciated heretofore. Certain obvious experimental studies are suggested which have not been done. These can be appraised at the outset with respect to the precision required for identifying the various possible mechanisms of inhibition of the catalase–hydrogen peroxide system. This we can ascertain from the known values of R_k. The difference between K_5 and I_{50} calculated from the empirical quantity, $ik_0^*/(k_0^c - k_0^*)$, is only 40 to 25% for bacterial ($R_k = 1.5$)[16] and erythrocyte ($R_k = 3$)[13] catalase, respectively. The differences between K_6 and I_{50} are 60 and 75%. Fortunately, as illustrated below, most of the inhibitors have very large K_5/K_6 values. Therefore, the identification of the major mechanism of inhibition is no particular problem. The single and important exception is the inhibition by cyanide.

K_5 has been determined by several investigators with spectrophotometric methods based on changes in the absorption spectrum of the heme. These changes are proportional to the degree of association of the heme and inhibitor.[15] Conceivably, K_5 could be determined by this method both in the absence of and in the presence of the substrate. Only one such set of experimental studies has been done.[15]

Cyanide Inhibition.—The competitive mechanism of inhibition of cyanide was first observed by Chance[15] and Chance and Herbert[16] during the transient phase of the kinetics of this system. By varying the concentration of the substrate they were able to show spectrophotometrically a displacement of the cyanide from the catalase heme. They concluded that the mechanism but not the kinetics of inhibition by cyanide is competitive.

The value of K_5 in the absence of the substrate for horse erythrocyte catalase ($R_k = 3$) was found to be 4×10^{-6} M. Based on the hypothesis that the mechanism of inhibition is "competitive" for the free enzyme, the concentration of inhibitor necessary to produce 50% inhibition of the enzyme, I_{50}, may be calculated from equation 8, ($K_6 = \infty$), where the term, $k_0^*/(k_0^c - k_0^*)$, is unity. I_{50} turns out to be 5.33×10^{-6} M. The observed value was 4.7×10^{-6} M. Whether these differences are significant is not clear. The observed value happens to lie halfway between the extreme values of I_{50}, when $K_6 = K_5$ and $K_6 = \infty$.

Calculation of K_5 spectrophotometrically in the presence of the substrate, assuming that any spectral changes due to the formation of the primary complex are compensated for, can be obtained by making appropriate substitutions into equation 3

$$K_5 = R_k ei/(R_k + 1)q' \qquad (25)$$

The corresponding I_{50}, obtained by setting e/q' equal to unity, was found to be 1×10^{-6} M.[15] K_5 is, therefore, only 7.5×10^{-7} M. The discrepancy between the I_{50} values calculated spectrophotometrically and from activity measurements cannot be accounted for by the present theory, since regardless of the mechanism the two values should coincide. However, the I_{50} value determined from activity measurements is more consistent with K_5 calculated spectrophotometrically in the absence of the substrate. As indicated above, depending upon the value of K_6, I_{50} can have any value between 4×10^{-6} and 5.33×10^{-6} M. Unless there is a significant k_7 reaction, I_{50} can never be smaller than K_5, although it may be equal to K_5.

An alternate interpretation of cyanide inhibition is suggested by the results of Ogura, *et al.*[6] They report a value of 1.6×10^{-6} M for horse liver catalase ($R_k = 2$) for both K_5 and I_{50}. This suggests that $K_5 = K_6$. Such a conclusion need not necessarily conflict with the experimental observations of Chance during the transient phase when peroxide can displace the cyanide. However, it is necessary to make the assumption that during this transient phase the K_6 reaction does not occur to any extent. During the transient period the cyclic synthesis and breakdown of the primary complex results in a net increase in the concentration of this complex. This effectively removes some of the free enzyme from equilibrium with cyanide. Consequently, the cyanide complex dissociates. The probable sequence is

$$E + S \longrightarrow ES \qquad (h)$$

$$EI \rightleftharpoons E + I \qquad (i)$$

The net reaction is the sum of equations (h) and (i), which by virtue of reaction (h) is driven irreversibly in one direction, thus

$$EI + S \longrightarrow ES + I \qquad (d)$$

(16) B. Chance and D. Herbert, *Biochem. J.*, **46**, 402 (1950).

TABLE I

DISSOCIATION CONSTANTS OF THE CATALASE–INHIBITOR COMPLEXES

(See text for details)

Inhibitor	K_5, M	I_{50}, M	K_6, M	q'/q''	D.A., %	Ref.
Cyanide	4×10^{-6}	4.7×10^{-6}	9.9×10^{-6}	74.2	−42	15
Cyanide	4×10^{-6}	1×10^{-6}[a]	(-4.5×10^{-7})	...	...	15
Cyanide	1.6×10^{-6}	1.6×10^{-6}	1.6×10^{-6}	1.0	0	6
Azide	6.45×10^{-4}	6.3×10^{-8}	2.14×10^{-8}	6.6×10^{-5}	100	17
Azide	2×10^{-6}	5×10^{-8}	1.71×10^{-8}	2.56×10^{-2}	99	6
Hydroxylamine	1.08×10^{-3}	6.3×10^{-7}	2.1×10^{-7}	3.9×10^{-4}	100	17
Hydroxylamine	1×10^{-6}	1.25×10^{-7}	5.18×10^{-8}	1.55×10^{-2}	99	6
Fluoride	6.3×10^{-2}	2×10^{-3}	1×10^{-4}	4.8×10^{-3}	99	6

[a] Calculated spectrophotometrically in the presence of the substrate.

This may be the basis for the "competitive" nature of cyanide inhibition. In order to account for the fact that K_6 has some finite value, perhaps equal to K_5, we must also include reaction (e)

$$ES + I \longleftrightarrow ESI \qquad (e)$$

In contrast to the above sequence of reactions which results in a displacement, reaction (e) is an addition reaction. Either the time required for this reaction to reach equilibrium may be considerably longer than that allowed during the transient phase, or ESI may not be detected spectrophotometrically, a less likely possibility. Presumably, if such a complex exists it has a covalent structure with characteristic light absorption properties similar to those of the simple cyanide complex. According to this hypothesis, the ESI complex would not be detected during transient phase. An addition reaction between the catalase–cyanide complex and the substrate is not supported by the kinetics of the time decay of the substrate which remains first order throughout.

Azide Inhibition.—It has been known for many years that azide can inhibit catalase by two distinct mechanisms[17] through the formation of complexes with both the free enzyme and the primary complex. These phenomena can be observed spectrophotometrically and from activity measurements.[6,7,8,12,18] From spectrophotometric studies by Keilin and Hartree[17] on the affinity of azide for horse liver catalase ($R_k = 2$) we may calculate a reasonable value of K_5: 6.45×10^{-4} M (*p*H 6.8, room temperature).[19] From activity measurements they report an I_{50} value of 6.3×10^{-8} M. Therefore, $K_6 = 2.14 \times 10^{-8}$ M. A more recent value for K_5 has been reported by Ogura, *et al.*,[6] for the same enzyme: 2×10^{-6} M (*p*H 7.0, 0°). This compares favorably with that reported by Chance[21] for human erythrocyte catalase: 3×10^{-6} M (*p*H 6.8, 25°). I_{50} from their activity measurements was 5×10^{-8} M. The calculated value of K_6 is, therefore, 1.71×10^{-8} M.

Although there is a wide discrepancy between the K_5 values of the two groups of investigators, this has relatively little effect on the calculated value of K_6. According to equation 14, the main mechanism of inhibition is *via* the primary complex. According to the data of Ogura, *et al.*,[6] less than 2% of the inhibited enzyme is free from the substrate.

Similar results are reported by both groups of investigators for hydroxylamine. Table I summarizes the available data and computations based on the concepts developed in this paper. There is no gross distinction in the kinetics of any of these reactions. The mechanisms underlying the inhibitory phenomena appear to be very similar in each case.

Conclusions.—The catalase hydrogen peroxide system affords one more example of the necessity for classifying inhibition in accordance with kinetic thermodynamic principles. We have seen that a steric type of competitive inhibition, wherein the inhibitor and substrate compete for the same site, is not a necessary requirement to account for some of the competitive types of inhibition in this system. We have suggested that the inhibition be described by the relative magnitudes of the various enzyme–inhibitor dissociation constants. This provides us with a simple indicator of the modifying effect the substrate may have on the affinity of the enzyme for the inhibitor. A measurement of the effect of an inhibitor on the affinity of the enzyme for the substrate is impossible during the steady state, since it is implicitly assumed that the dissociation constants of ES and ESS are zero. In fact, ESS has never been identified.

In theoretical studies of the effects of modifiers on enzyme–substrate systems, where the modifier may be an activator, an inhibitor or a substrate, it has been assumed that the enzyme must be multivalent; *i.e.*, it must have two or more sites for binding of the substrate and the modifier. This has been treated with considerable detail by Botts and Morales[22] for the Michaelis–Menten enzyme–substrate system. By sites we mean simply forces of attraction or repulsion between the enzyme and the substrate and inhibitor which may or may not have any structural counterparts. In the catalase–hydrogen peroxide system the substrate is acting as a modifier for the inhibitor. It is entirely possible that the addition of the substrate to the heme site results in a suitable electronic and molecular rearrangement of the heme, such that a new site is

(17) D. Keilin and E. F. Hartree, *Biochem. J.*, **39**, 148 (1943).

(18) R. Lemberg and E. C. Foukes, *Nature*, **161**, 131 (1948).

(19) Estimated by the author from their relative affinity data of azide and cyanide for catalase, 1:150, respectively. Assuming that $K_5 = I_{50}$ for the cyanide inhibition, the dissociation constant of the azide complex is 4.3×10^{-6} $M \times 150$ (*cf.*, however, R. Lemberg and J. W. Legge).[20]

(20) R. Lemberg and J. W. Legge, "*Hematin Compounds and Bile Pigments*," Interscience Publishers, Inc., New York, N. Y., 1949, p. 409.

(21) B. Chance, *J. Biol. Chem.*, **194**, 483 (1952).

(22) J. Botts and M. Morales, *Trans. Faraday Soc.*, **49**, 696 (1953).

created. This new site may have a greater or less affinity for the inhibitor than the original site. A similar argument can be made for the affinity of the new site for the second substrate molecule.

We have suggested that cyanide may inhibit catalase by reacting directly with the primary complex at a rate too slow to be detected during the brief transient phase of the kinetics. The rates at which azide, hydroxylamine and other monovalent anions[23] react with the primary complex are sufficiently slow to be detected even during the steady state phase.[6-8,12,13,20,24] Because of the slow rates of inhibition, it is very probable that the main inhibitory reaction is not a simple addition complex of primary complex and inhibitor but the electronic rearrangement (oxidation–reduction, perhaps) which occurs within the ternary complex subsequent to its formation. This could result in a change in the bond type of the heme from essentially ionic to covalent in character.[25] Presumably, the secondary complex described by Chance[2] is spectrophotometric evidence for this covalent compound. However, the picture has been complicated by the recent discovery of another inactive complex by Keilin and Hartree.[26] There have as yet been no correlation studies between spectrophotometric properties of these inactive complexes and the inhibitory reactions between monovalent anions and the primary complex. Various aspects of this will be discussed in forthcoming papers.[12,27]

Should the main mechanism of inhibition of the primary complex be through the formation of a covalent structure, we would have to consider the following sequence of reactions

$$\mathrm{ES} + \mathrm{I} \overset{p \quad i}{\longleftrightarrow} \mathrm{ESI}^* \qquad (j)$$

$$K_6^* = pi/q''^* \qquad (26)$$

$$\mathrm{ESI}^* \overset{q''^* \quad q''}{\longleftrightarrow} \mathrm{ESI} \qquad (k)$$

$$K_6 = q''^*/q'' \qquad (27)$$

where ESI* and ESI are the ionic and covalent complexes, respectively. The correct value of K_6 is, therefore

$$K_6 = (pi/K_6^*)/q'' \qquad (28)$$

Acknowledgments.—The author wishes to thank Dr. M. F. Morales and Prof. Irwin W. Sizer for their helpful suggestions in the preparation of this paper.

(23) Recent studies by Chance[21] indicate that the reactive species of both the inhibitors and the substrate are the undissociated acids rather than the anions.

(24) R. F. Beers, Jr., and I. W. Sizer, *Science*, **120**, 32 (1954).

(25) H. Theorell and A. Ehrenberg, *Arch. Biochem. Biophys.*, **41**, 422 (1952).

(26) D. Keilin and E. F. Hartree, *Biochem. J.*, **49**, 88 (1951).

(27) R. F. Beers, Jr., in preparation.

X-RAY DIFFRACTION STUDIES OF ALUMINUM SOAPS

BY WALTER H. BAUER, JOSEPH FISHER, FREDERICK A. SCOTT AND STEPHEN E. WIBERLEY

Contribution from the Walker Laboratory of Rensselaer Polytechnic Institute, Troy, New York

Received June 29, 1954

X-Ray diffraction patterns have been obtained for two series of aluminum soaps. The first series consisted of aluminum di-soaps made from the following fatty acids, caproic, enanthic, caprylic, pelargonic, capric, lauric, myristic, palmitic and stearic. The second series was prepared from lauric acid with varying fatty acid–aluminum ratios. In the first series the most prominent characteristic is the presence of two or more definite orders of a long spacing which is proportional linearly to the number of carbon atoms in the hydrocarbon chain. A second feature is the appearance of a diffuse halo between 4.2 and 5.2 Å. units. In the second series, soaps having a fatty acid to aluminum ratio greater than that of the di-soap show sharp patterns and the presence of fatty acid lines while those below the di-soap show no new lines but less distinct patterns.

Introduction

In view of the importance of aluminum soaps as gelling agents for hydrocarbons it is surprising that so little X-ray diffraction work is available on these compounds. Ross and co-workers[1,2] have published X-ray diffraction data on aluminum dilaurate and aluminum distearate prepared by the addition of an aqueous solution of potassium laurate or stearate to a large excess of an aluminum chloride solution. The precipitates obtained were then extracted with boiling acetone to presumably form the corresponding di-soaps. These investigators reported the existence of free fatty acid spacings in the unextracted material. Mysels[3] studied the X-ray diffraction patterns of Napalm (a mixture of aluminum di-soaps) and aluminum dilaurate. He found the patterns to be strikingly similar, but that the sharpness of the patterns differed markedly depending upon the method of preparation. He also found that there was no indication in the Napalm pattern of the presence of an aluminum monosoap or any of the aluminum oxides.

Because infrared absorption measurements[4,5] on aluminum soaps made from different fatty acids and with varying fatty acid to aluminum ratios have been most helpful in establishing the structure and existence of the di-soaps as discrete chemical compounds, it was felt that X-ray diffraction studies on a similar series would also aid in further clarifying the structure of aluminum soaps.

Experimental

The fatty acids which are liquids at room temperature were purified by distillation and the neutralization equivalents were checked by titration. The purity of the solid acids used in this investigation has already been discussed[5] as well as the preparation and analysis of the aluminum soaps.

(1) S. Ross and J. W. McBain, *Oil and Soap*, **23**, 214 (1946).

(2) S. S. Marsden, K. J. Mysels, G. H. Smith and S. Ross, *J. Am. Oil Chemists Soc.*, **25**, 454 (1948).

(3) K. J. Mysels, *Ind. Eng. Chem.*, **41**, 1435 (1949).

(4) W. W. Harple, S. E. Wiberley and W. H. Bauer, *Anal. Chem.* **24**, 635 (1952).

(5) F. A. Scott, J. Goldenson, S. E. Wiberley and W. H. Bauer, THIS JOURNAL, **58**, 61 (1954).

TABLE II

COMPOSITION OF ALUMINUM LAURATE SOAPS

Sample Designation	Excess NaOH, %	Exp. wt. % Al	Moles of acid/mole of Al: Predicted from NaOH Used	Based on Al anal.	Extractable with isoöctane	Remaining: By diff.	By Al anal.
L-4.01	−25	3.21	4.00	4.01	1.8	2.21	2.01
L-2.89	0	4.34	3.00	2.89	0.87	2.02	1.94
L-2.60	10	4.81	2.67	2.60	0.58	2.02	1.94
L-2.03	45	6.05	2.07	2.03	0.05	1.98	1.85
L-1.29	100	8.60	1.00	1.29	0.00	1.29	1.2[illegible]

The X-ray diffraction measurements were made with a General Electric XRD-3 instrument using copper K_α radiation with a nickel filter. In some instances chromium K_α radiation was used. The soap samples were passed through a 100-mesh sieve and mounted on cellophane discs containing a hole slightly larger than the 0.010 mm. diameter pinhole collimator. The sample to film distance was 50 mm. in the case of the flat casette assembly. In the case of the circular camera the effective film diameter was 143.2 mm.

Results and Discussions

X-Ray diffraction patterns were obtained first for a series of aluminum di-soaps (*i.e.*, a fatty acid–aluminum mole ratio of 2:1) made from straight chain fatty acids containing 6, 7, 8, 9, 10, 12, 14, 16 and 18 carbon atoms. Table I contains the long spacings for this series of aluminum di-soaps. The short spacings were identical for the complete series. All of the di-soaps showed two strong lines corresponding to spacings of 3.90 and 7.8 Å., and a weak line giving a spacing of 3.00 Å. A diffuse halo was found in each case, corresponding to spacings from 4.2 to 5.2 Å.

TABLE I

INTERPLANAR SPACINGS ("*d*" VALUES) FOR ALUMINUM DI-SOAPS

Soap	Long spacing, Å. 1st Order	2nd Order	3rd Order	Av.
Aluminum dicaproate	15.2	7.8	5.1	15.4
Aluminum dienanthate	17.9	8.9	6.0	17.9
Aluminum dicaprylate	20.5	10.2	6.8	20.4
Aluminum dipelargonate	22.3	11.1	7.6	22.4
Aluminum dicaprate	25.5	12.3	8.1	24.8
Aluminum dilaurate	29.5	14.5	9.8	29.3
Aluminum dimyristate	32.0	16.8	11.2	33.1
Aluminum dipalmitate	...	18.5	12.3	37.0
Aluminum distearate	...	20.4	13.7	41.0

Figure 1 is a plot of the long spacings of the fatty acids and the aluminum soaps and the silver salts prepared from these same fatty acids. The data for the fatty acids and silver salts are taken from a previous paper.[5] The long spacings obtained for the fatty acids agree well with those obtained by Francis and Piper[6] for the crystalline form of the acids which they denote as the C-form. The long spacings obtained for the silver salts agree well with those obtained by Matthews, *et al.*[7]

It should be noted that the long spacings of the aluminum soaps and of the fatty acids are almost identical while those of the silver salts are considerably longer. Apparently the aluminum soaps are similar to the long chain acids, alcohols, esters, *n*-hydrocarbons and ketones in that the hydrocarbon chains are extended in the crystal. The regular increase in spacing of about 2 Å. per additional carbon atom is similar to that exhibited by the fatty acid crystals. The diffuse halo in the region corresponding to the "side-spacings" between 4.2 and 5.2 Å. indicates more random orientation in this dimension. The halo actually consists of two diffuse lines which are close to the ends of the halo.

The second series of soaps studied were prepared by precipitation of the soaps from sodium laurate solutions containing excess sodium hydroxide on addition of a solution of aluminum sulfate.[4,5] By control of the amount of sodium hydroxide, the ratio of moles of fatty acid to aluminum was controlled. Table II lists the composition of these soaps.

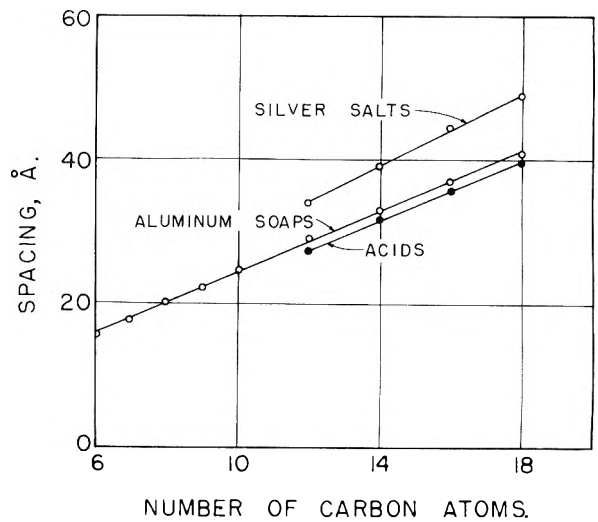

Fig. 1.

The X-ray diffraction patterns of these soaps showed the presence of lauric acid in samples L-4.01, L-2.89 and L-2.60. Both the long spacings of the soap and acid were readily distinguishable, and the characteristic 4.13 Å. spacing of lauric acid was very prominent in all these samples. Samples L-2.03 and L-1.29 did not show any lines attributable to acid spacings.

Samples L-4.01, L-2.89 and L-2.60 were extracted with cold isoöctane at 0 to 5°. X-Ray diffraction patterns of the extracted samples no longer showed lines ascribable to fatty acid. Only the diffraction pattern of the di-soap appeared. These results confirm those of previous workers[1,2,8] and are in excellent agreement with the infrared interpretation.[4] Evidently then, aluminum soaps prepared by an aqueous method having an analysis close to a tri-

(6) F. Francis and S. H. Piper, *J. Am. Chem. Soc.*, **61**, 577 (1939).

(7) F. W. Matthews, G. G. Warren and J. H. Michell, *Anal. Chem.* **22**, 514 (1950).

(8) J. D. Gross, "Ph.D. Thesis," Rensselaer Polytec. Inst., June, 1949.

soap consist of mixtures of di-soap plus fatty acid. It was shown in Fig. 1 that the long spacings of the aluminum soaps and of the fatty acids are almost identical. This fact explains why the fatty acid co-precipitates so readily with aluminum soap molecules to form materials of graded ratio of fatty acid to aluminum.

The X-ray diffraction pattern of soap L-1.29 showed no new spacings that could be attributed to either an aluminum mono-soap or to hydrated aluminum oxides. The diffraction pattern was considerably more diffuse than that of the di-soap L-2.03. This is a generally observed phenomenon. For any series of a single acid, as the acid to aluminum ratio increases, there is a sharpening of the diffraction pattern of the soap. Infrared studies on aluminum soaps containing a mole ratio of fatty acid to aluminum less than 2 show only bands attributable to aluminum di-soap and hydrated aluminum oxide. It is therefore concluded that aluminum mono-soaps are not present.

Acknowledgment.—This study was conducted under contract between the Chemical Corps, U. S. Army, and Rensselaer Polytechnic Institute.

DIELECTRIC PROPERTIES OF SOME ALKENES

BY AUBREY P. ALTSHULLER

National Advisory Committee for Aeronautics, Lewis Flight Propulsion Laboratory, Cleveland, Ohio

Received July 16, 1954

The dielectric constants of pentene-1, hexene-1, heptene-1, octene-1, 2-methylbutene-1, *trans*-hexene-3 and cyclohexene have been determined. The atomic polarizations of these compounds as well as *cis*-hexene-3 and the *cis*- and *trans*-isomers of octene-3, octene-4 and decene-5 have been calculated. The dipole moments of the polar alkenes have been calculated by means of the Onsager equation and are compared with the available dipole moments in the gaseous state. The relationship between the observed dipole moments and the bond moments in the alkenes is very briefly discussed.

Although the dielectric constants of several alkene-1 compounds have been determined,[1] the results obtained have been scattered and somewhat contradictory. Therefore, it seemed useful to determine the dielectric constants of highly purified samples of pentene-1, hexene-1, heptene-1 and octene-1 as representatives of the class $H_2C{=}CHR$. The dielectric constant of 2-methylbutene-1 was determined as a representative of compounds of the $H_2C{=}CR_2$ type. The dielectric constants of cyclohexene and *trans*-hexene-3 were also measured.

The dielectric constants, refractive indices and densities of four *cis*- and four *trans*-alkenes have been determined elsewhere.[2] The atomic polarizations, P_A, of the four *trans*-alkenes were calculated. The dielectric constant of *trans*-hexene-3 was redetermined because the literature value[2] gave an atomic polarization out of line with that of the three other *trans*-alkenes. An empirical relationship between P_A and n, the number of carbon atoms, was derived from the data for the four *trans*-alkenes and used to calculate P_A for the four *cis*-alkenes[2] and the six alkene-1 compounds measured in this investigation. The dipole moments of the ten polar alkenes were calculated by means of the Onsager equation.[3]

The bond moments which contribute to the overall molecular dipole moments are briefly discussed.

Experimental

Materials.—NBS samples of pentene-1, octene-1 of 99+% purity, and *trans*-hexene-3 were used. The 2-methylbutene-1 was obtained from API RP-45. Phillips Petroleum Co. samples of pentene-1 of 99+% purity and of research grade cyclohexene of 99.9+% purity were also used. The hexene-1 and heptene-1 used were prepared and purified at this Laboratory by fractional distillation of the products of the dehydration of the corresponding alcohols through Podbielniak columns. All of these materials were passed through silica gel columns before the measurements were made.

Dielectric Constants.—The dielectric constants were obtained using an apparatus and cell previously discussed.[4] The volume of liquid in the dielectric constant cell was 25 ml. The accuracy of the measurements is estimated to be ±0.2%.

Refractive Indices.—The indices of refraction were measured at 20.0 ± 0.1° with a Bausch and Lomb precision Abbe refractometer with an estimated accuracy of ±0.0001 units.

Results and Discussion

The refractive indices, $n^{20}D$, and the dielectric constants, ϵ^{20}, measured in this investigation along with previous literature values of ϵ are listed in Table I.

TABLE I

DIELECTRIC CONSTANTS AND REFRACTIVE INDICES OF SOME ALKENES

Compound	$n^{20}D$	ϵ^{20}	ϵ^{20} (lit. values)
Pentene-1 (NBS)	1.3714	2.017	2.100,[b] 1.92[c]
Pentene-1 (Phillips)	1.3712	2.017	
Hexene-1	1.3878	2.051[a]	...
Heptene-1	1.3996	2.071[a]	2.06[c]
Octene-1	1.4085	2.084	...
2-Methylbutene-1	1.3775	2.180	2.197[b]
trans-Hexene-3	1.3939	1.954	2.000[d] (25°)
Cyclohexene	1.4461	2.220	2.220[e] (25°)

[a] Hexene-1, $\epsilon^{30} = 2.035$; heptene-1, $\epsilon^{30} = 2.057$. [b] Ref. 5. [c] Ref. 6. [d] Ref. 2. [e] F. Fairbrother, *J. Chem. Soc.*, 1051 (1948).

The two values previously reported[5,6] for the di-

(1) A. A. Maryott and E. R. Smith, "Table of Dielectric Constants of Pure Liquids," NBS Circular 514, 1951.

(2) K. N. Campbell and L. T. Eby, *J. Am. Chem. Soc.*, **63**, 216, 2683 (1941).

(3) L. Onsager, *ibid.*, **58**, 1486 (1936).

(4) A. P. Altshuller, THIS JOURNAL, **58**, 392 (1954).

(5) A. E. van Arkel, P. Meerburg and C. R. v. d. Handel, *Rec. trav. chim.*, **61**, 767 (1942).

(6) M. L. Sherrill, K. E. Mayer and G. F. Walter, *J. Am. Chem. Soc.*, **56**, 926 (1934).

TABLE II

MOLAR REFRACTIONS, ATOMIC POLARIZATIONS AND DIPOLE MOMENTS OF SOME ALKENES

Compound	n^{20}_{∞}	R^{20}_{∞}, cm.^{3}	P^{25}_{CM},[b] cm.^{3}	P_A, cm.^{3}	n_{eff}	μ_1, D	μ_2, D
Pentene-1	1.3588	24.09	...	1.28	1.380	0.34	0.34
Hexene-1	1.3754	28.63	...	1.37	1.396	.32	.34
Heptene-1	1.3869	33.14	...	1.45	1.406	.31	.34
Octene-1	1.3958[a]	37.64	...	1.53	1.414	.29	.34
2-Methyl-butene-1	1.3652[a]	24.10	...	1.28	1.387	.51	.50
Cyclohexene	1.4319	26.26	...	1.37	1.458	.31	.28
cis-Hexene-3	1.3805	28.72	...	1.37	1.401	.33	.34
cis-Octene-3	1.3993	37.78	...	1.53	1.417	.25	.29
cis-Octene-4	1.4004	37.79	...	1.53	1.419	.22	.26
cis-Decene-5	1.4124	46.92	...	1.70	1.429	.19	.24
trans-Hexene-3	1.3813	28.88	30.19	1.31	...	0[c]	0[c]
trans-Octene-3	1.3992	37.97	39.51	1.54	...	0[c]	0[c]
trans-Octene-4	1.3987	37.99	39.63	1.64	...	0[c]	0[c]
trans-Decene-5	1.4108	47.03	48.67	1.64	...	0[c]	0[c]

[a] These values of n_∞ were obtained from the empirical relationship, $n_\infty/n_D = 0.9908 \pm 0.0001$, found by using the values of n for the other alkenes. [b] Values of ϵ were only available for the *trans*-alkenes at 25°, therefore P_{CM} is also given at 25°. The error involved in using R^{20}_∞ instead of R^{25}_∞ is negligible. [c] From molecular symmetry considerations. (*trans*-Octene-3 might possibly have an extremely small dipole moment.)

electric constant of pentene-1 are widely separated. The value of 2.100 for the dielectric constant[5] of pentene-1 exceeds even the dielectric constant of 2.06 reported[6] for heptene-1. The two different samples of pentene-1 used in the present work both gave dielectric constants of 2.017 at 20°. It is interesting to note that the density, refractive index, and b.p. reported[5] along with the dielectric constant of 2.100 are all higher than the values given by Rossini, *et al.*[7] Since the isomer, 2-methylbutene-1, has a higher density, refractive index, b.p. and ϵ^{20} than pentene-1, it is possible that appreciable amounts of this compound were present as an impurity. The low value for ϵ^{20} of pentene-1 of 1.92 units also given in the literature[6] would appear to indicate saturated hydrocarbons as impurities. The higher value of ϵ for *trans*-hexene-3 previously reported[2] may be the result of some contamination with the *cis*-isomer.

The differences in ϵ between the corresponding series of unsaturated and saturated hydrocarbons[8] (pentene-1 and pentane to octene-1 and octane) are 0.173, 0.161, 0.146 and 0.132. The decrease in the differences is in the direction expected for increasing length of the saturated hydrocarbon chain.

In order properly to evaluate μ_2, the dipole moment from the Onsager equation,[3] a refractive index, n_{eff}, which takes into account an infrared contribution is needed.

The values of n_∞ listed in Table II were obtained by extrapolating the refractive index data at various wave lengths given in several references[2,9] to infinite wave length by applying the least squares procedure to Cauchy's equation. The values of R_∞ were calculated from the Lorentz–Lorenz equation. The total polarizations, P_{CM}, for the non-polar *trans*-alkenes given in Table II were obtained from the Clausius–Mosotti equation. The atomic polarizations were computed for the *trans*-alkenes from the relationship $P_A = P_{CM} - R_\infty$. An empirical relationship between P_A and c, the number of carbon atoms, of the form $P_A = 0.87 + 0.083c$ was obtained by the method of least squares. The P_A values for the polar alkenes were computed from this empirical equation. The effective refractive indices, n_{eff}, given in Table II were obtained by solving for n_{eff} in the Lorentz–Lorenz equation with $R = R_\infty + P_A$. These values of n_{eff} were then used in the calculation of the dipole moments, μ_2, from the Onsager equation[3] given in Table II. The approximate dipole moments, μ_1, from the equation[10] $\mu_1 = (\epsilon - n^2_{eff})^{1/2}$ are also listed in Table II.

The dipole moments, μ_1, from the empirical equation[10] are in satisfactory agreement with the dipole moments, μ_2, from the Onsager equation. However, there is a small but definite trend toward increasing deviation of μ_1 values from μ_2 values with increasing molecular weight. For slightly polar substances, this empirical equation provides a convenient and rapid method of estimating μ.[4]

The μ_2 values of 0.34 D found in this investigation for the alkene-1 compounds (from pentene-1 to octene-1) are in satisfactory agreement with the average of the dipole moments from gas state measurements[11] of 0.34 D (for propene and butene-1). No appreciable increase in dipole moment for compounds of the type $H_2C{=}CHR$ beyond R = C_2H_5 or C_3H_7 for *n*-alkyl chains would be expected since any additional CH_2 groups would be too far removed from the remainder of the molecule to be subjected to appreciable induced moments. The value for 2-methylbutene-1 of 0.50 D calculated here is also in accord with the gas state moment[11] of 0.49 D for 2-methylpropene-1. The higher dipole

(7) F. D. Rossini, *et al.*, "Selected Values of Physical and Thermodynamic Properties of Hydrocarbons and Related Compounds," APIRP 44, Carnegie Press, Pittsburgh, Pa., 1953.

(8) A. Audsley and F. R. Goss, *J. Chem. Soc.*, 2989 (1950).

(9) J. Timmermans, "Physico-chemical Constants of Pure Organic Compounds," Elsevier Publishing Co., Inc., New York, N. Y., 1950.

(10) A. P. Altshuller, THIS JOURNAL, **57**, 538 (1953).

(11) A. A. Maryott and F. Buckley, "Table of Dielectric Constants and Electric Dipole Moments of Substances in the Gaseous State," NBS Circular 537, 1953

moments of 0.47 D for pentene-1 and 0.54 D for 2-methylbutene-1 reported in the literature,[5] which were also calculated from the Onsager equation, resulted from the larger dielectric constants reported by these investigators[5] along with their assumption that $\epsilon^{1/2} n_D$ would be the same for unsaturated and saturated hydrocarbons.

The dipole moment of 0.28 D for cyclohexene found in the present work is much smaller than the gas state value of 0.55 D.[11] Beckett, *et al.*,[12] have concluded that cyclohexene exists in two tautomeric forms similar to the chair and boat forms of cyclohexane. The chair form of cyclohexene is more stable at low temperatures, but increasing contributions from the boat form (*cis*-like form) might be expected as the temperature increases.[12] This tautomeric shift toward a more polar equilibrium mixture at higher temperatures may partially explain the differences in dipole moments between the liquid state measurements at 293°K. and the gas state measurements at from 308 to 480°K. It may be noted also that the dipole moment of 0.55 D for cyclohexene is about 0.2 D larger than the dipole moments of straight chain alkene-1 compounds. This difference may also be due to the higher polarity of the boat form of the cyclic compound compared with the *cis*-form of the straight-chain alkenes.

It is of considerable interest to attempt a semi-quantitative interpretation of the molecular dipole moments arrived at in this investigation and elsewhere[11] in terms of the bond moments which contribute to making up the molecular moments. If the simplest polar alkene, propene, is considered, it is clear that the molecule is made up of —C—H, =C—H, and =C—C— bonds which may be considered from the standpoint of orbital hybridization theory as C(sp³)–H, C(sp²)–H and C(sp²)–C(sp³) type bonds. The C(sp²)–H bond has a moment of around 0.6 D[13,14] with the probable direction $\overset{-}{\text{C}}(\text{sp}^2)\longrightarrow\overset{+}{\text{H}}$. Experimental data for C(sp³)–H give a moment of 0.3 to 0.4 D[15-17] and the probable direction C(sp³)–H. This difference between the magnitudes of the C(sp²)–H and the C(sp³)–H bond moments is probably responsible for the values of the molecular dipole moments which are arrived at from polarization measurements on propene and other alkenes. However, such additional factors as the small C(sp²)–C(sp³) bond moment of around 0.1 D, the effects of hyperconjugation of all three types of bonds, and the small contributions from induced moments also enter the picture.

Conclusion.—The atomic polarizations of a number of alkene-1, *cis*- and *trans*-alkene compounds have been determined. The dipole moments of the polar alkene compounds have been determined from the Onsager equation and satisfactory agreement with the dipole moments arrived at from gas state polarization measurements has been found. A semi-quantitative explanation of the origin of the molecular dipole moments in terms of the bond moments contributing to the over-all molecular moment has also been given.

(12) C. W. Beckett, N. K. Freeman and K. S. Pitzer, *J. Am. Chem. Soc.*, **70**, 4227 (1948).

(13) C. F. Hammer, Ph.D. thesis, Univ. of Wisconsin, 1948.

(14) R. L. Kelley, R. Rollefson and B. S. Schurin, *J. Chem. Phys.*, **19**, 1595 (1951).

(15) A. M. Thorndike, *ibid.*, **15**, 868 (1947).

(16) R. P. Bell, H. W. Thompson and E. E. Vago, *Proc. Roy. Soc. (London)*, **A192**, 498 (1948).

(17) G. M. Barrow and D. C. McKean, *ibid.*, **A213**, 27 (1952).

METAL–POLYELECTROLYTE COMPLEXES. I. THE POLYACRYLIC ACID–COPPER COMPLEX

BY HARRY P. GREGOR, LIONEL B. LUTTINGER[1] AND ERNST M. LOEBL

Contribution from the Department of Chemistry of the Polytechnic Institute of Brooklyn, New York

Received July 19, 1954

Formation constants for polyacrylic acid–copper complexes as obtained by a new adaptation of Bjerrum's method, are presented. Data taken at various ionic strengths indicate that in the presence of much neutral salt, the titration curve falls to a final, limiting value. The complexes formed are strong, and at least two carboxyl groups are involved simultaneously, as with simple dicarboxylic acids. The considerably greater stability of the polymer–copper complex as compared with that of a monomeric analog (glutaric acid) reflects the powerful field effect of the polyelectrolyte chain.

The potentiometric titration of polyacrylic and polymethacrylic acids has been studied by many investigators, principally Kern,[2] Katchalsky,[3] Overbeek[4] and Doty[5]; an excellent review of the recent literature has been made by Doty and Ehrlich.[6] In general, the experimental results for a single titration can be expressed by the modified Henderson–Hasselbalch equation, $pH = pK_a - n \log (1 - \alpha)/\alpha$, where α is the degree of neutralization, n a constant, and K_a the apparent ionization constant. For the same polymer, it has been shown that: (1) the values of K_a and n are independent of degree of polymerization (above a certain minimum); (2) the value of K_a increases with increasing ionic strength of neutral salt added; (3) the value of n, which is unity for a simple weak acid, *viz.*, acetic acid, varies from a value somewhat above 1 to about 2, approaching the higher value with increasing dilution, approaching the lower value at high ionic

(1) A portion of this work is abstracted from the Dissertation of Lionel B. Luttinger, submitted in partial fulfillment of the requirements for the degree of Doctor of Philosophy in Chemistry, Polytechnic Institute of Brooklyn, June, 1954.

(2) W. Kern, *Z. physik. Chem.*, **A181**, 249 (1938); *Biochem. Z.*, **301**, 338 (1939).

(3) A. Katchalsky and P. Spitnik, *J. Polymer Sci.*, **2**, 432 (1947).

(4) R. Arnold and J. T. G. Overbeek, *Rec. trav. chim.*, **69**, 192 (1950).

(5) A. Oth and P. M. Doty, THIS JOURNAL, **56**, 43 (1952).

(6) P. Doty and G. Ehrlich, *Ann. Rev. Phys. Chem.*, **III**, (1952).

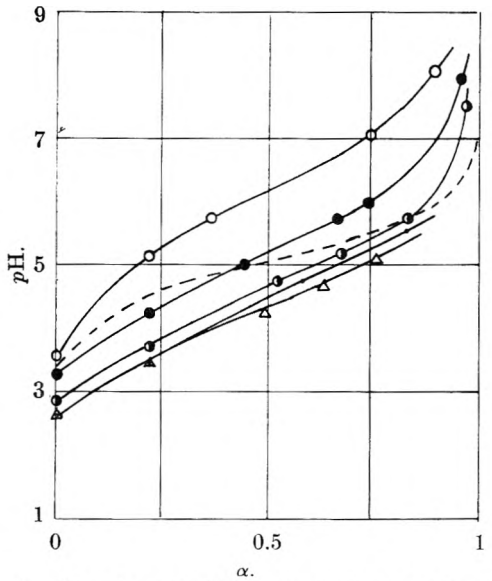

Fig. 1.—Titration of 0.01 *N* PAA in absence of: neutral salt (○); in 0.1 *M* KCl (●); in 1 *M* KCl (◑); in 3 *M* KCl (▲); in 2 *M* $NaNO_3$ (△). Dashed curve is for acetic acid.

strengths. Various statistical treatments of these systems have shown that the concepts of N. Bjerrum pertaining to the ionization of polybasic acids apply to the polymeric acids, and equations of the type of the Henderson–Hasselbalch relationship are obtained.

This paper describes titrations of a polymeric acid in the presence of copper salts, under different conditions of polymer acid concentration, ionic strength, and copper(II) concentration. The formation constants of the complexes formed are calculated using a modification of the methods of Bjerrum.[7]

Experimental

Methods.—A sample of pure polyacrylic acid (PAA) was first dialyzed using cellophane tubing. Only a negligible amount (<0.01%) of diffusible material was obtained; the molecular weight was estimated to be in the range 30,000–100,000. The polymer was completely soluble both as the free acid and in the presence of bases of the alkali metals, provided that the ionic strength is not too high.[8]

Titrations were performed in CO_2 free atmospheres with a Beckman *p*H meter at 24–26°. Plastic containers were used to avoid possible reactions with glass.

It was found that acid–base equilibrium was not always attained rapidly. Even in the absence of copper, a slow fall in *p*H with time was observed, particularly in the region beyond the half-neutralization point. The magnitude of this change was often between 0.10 and 0.30 of a *p*H unit over a period of several hours, and probably for this reason has often escaped detection. When gels were formed, as is the case in the presence of copper, and even, with high enough concentration of neutral salt (*e.g.*, 1 *M* potassium chloride) in the absence of copper, this effect was more pronounced. In all these experiments, a constant *p*H was attained after 24 hours. Routinely, all *p*H readings were taken after the sample had been shaken for 48 hours. All titrations were performed stepwise, *i.e.*, the sample was shaken after each addition of base.

When gel was present, the *p*H values were found to be identical whether the readings were made with the electrodes immersed only in the supernatant solution or in the gel phase. It was necessary to make the assumption that the equations used, derived for homogeneous solutions, hold when a gel phase is present as well. The intense field and high concentration within the gel phase would seem, at first thought, to preclude such a possibility. Yet we believe that the assumption is valid at high salt concentrations, since, as will be shown later, the Donnan potential appears to be swamped in 2 *M* $NaNO_3$. Further proof that this is so can be seen from a consideration of plots of *p*H *vs.* $\log (1 - \alpha)/\alpha$ in the absence of copper. This is an insensitive function, but data taken in the absence as well as in the presence of a gel phase fell on the same, straight lines. In 1 *M* KCl the gel phase appeared after the first point and disappeared after the third, yet all four points again fell on the same, straight line. If gel formation had caused a significant disturbance in the gegenion distribution, this could hardly be so.

The titer of the pure polymer acid was determined by titration in a large excess of potassium chloride. Concentrations are expressed as equivalents of carboxyl groups per liter (base molarity).

Titration Curves.—Figure 1 shows titration data for 0.01 *N* PAA in the presence of different concentrations of potassium chloride and sodium nitrate. With a given salt it is observed that the curves tend to approach an asymptotic limit as the salt concentration increases. Observable differences obtain with different salts. The same phenomenon has been observed by other authors. For example, Katchalsky[9] and others have shown that various physical-chemical properties of polyacrylic acid depend on whether KOH or NaOH are used to effect its partial neutralization. We have also found that the titration curve of the polymer is dependent upon the particular neutral salt taken (see Table I). The values of both pK_a and n are affected. As shown in Table I, these differences persist even at high concentrations of neutral salt. Table I also gives the decrease in *p*H in the presence of 0.00660 *M* copper at the half-neutralization point. It is evident that the effects in question cannot be attributed to the difference in activity coefficients of the neutral salts themselves. A complete discussion is deferred to a later paper.

In Fig. 2, we have plotted titration curves in the presence and absence of salt and in the presence of Cu(II) for acetic acid and glutaric acid, two monomeric analogs of polyacrylic acid. The *p*H is plotted as the ordinate and $\log (1 - \alpha)/\alpha$ as the abscissa. $(1 - \alpha)/\alpha$ is practically identical with $[HA]/[A^-]$ in the *absence* of complexation.

TABLE I

VARIATION IN pK_a AND n OF 0.01 *N* PAA WITH DIFFERENT NEUTRAL SALTS; DECREASE IN *p*H (ΔpH) IN THE PRESENCE OF 0.00660 *M* COPPER(II)

Salt	Concn. of salt (*M*)	pK_a	n	ΔpH
None	0	6.17	2.0	2.70
KCl	0.1	5.11	1.68	...
KCl	1	4.70	1.54	1.27
KCl	2	4.55	1.44	1.12
KCl	3	4.60	1.44	1.13
$NaNO_3$	0.2	4.91	1.69	...
$NaNO_3$	1	4.48	...	1.22
$NaNO_3$	2	4.30	1.39	1.13
$NaNO_3$	3	4.23	...	1.14
KNO_3	1	4.67	...	1.31
KNO_3	2	4.61	...	1.25
KNO_3	3	4.57	...	1.22

We see that the effect of the addition of neutral salt is small, also that comparable amounts of copper depress the curves only slightly, and that the plot of *p*H *vs.* $\log(1 - \alpha)\alpha$ is linear even when copper is present. This shows that complexation with both acetic and glutaric acid is very small, as will be discussed later.

The fact that acetic and glutaric acid produce an effect of the same magnitude is noteworthy; while greater complexation might be expected due to the formation of a chelate in the glutaric acid–copper complex, entropy considerations in forming the eight membered ring seem to obviate this.

(7) J. Bjerrum, "Metal Ammine Formation in Aqueous Solution," P. Haase, Copenhagen, 1941.

(8) S. H. Pinner, Dissertation, Polytechnic Institute of Brooklyn, 1951.

(9) A. Katchalsky, *J. Polymer Sci.*, **7**, 393 (1951).

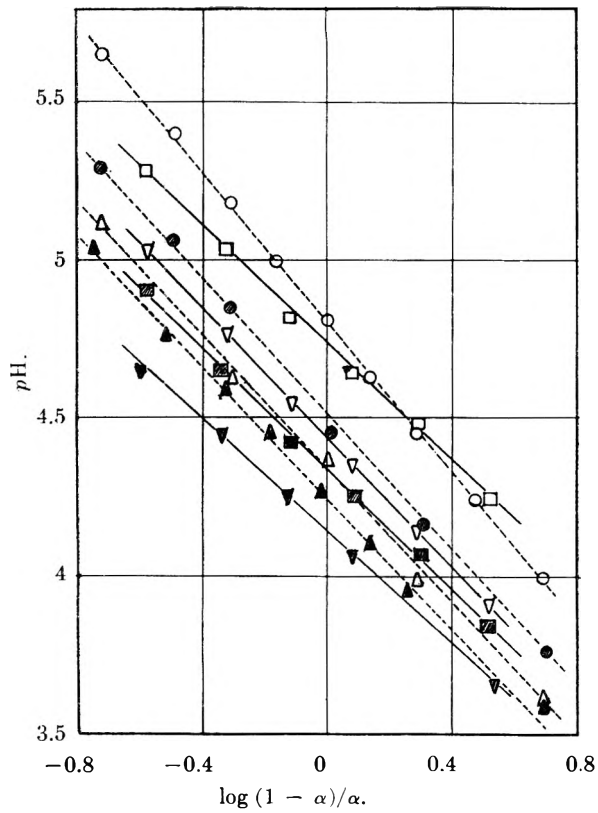

Fig. 2.—Plots of pH *vs.* log $(1 - \alpha)/\alpha$ for acetic and glutaric acids (0.01 N). Acetic acid (solid lines): no neutral salt, no Cu(II) (□); no neutral salt, 0.01285 M Cu(II) (■); 2 M $NaNC_3$, no Cu(II) (▽); 2 M $NaNO_3$, 0.01285 M Cu(II) (▼). Glutaric acid (dashed lines): no neutral salt, no Cu(II) (○); no neutral salt, 0.00643 M Cu(II) (●). 2 M $NaNO_3$, no Cu(II) (△); 2 M $NaNO_3$, 0.00643 M Cu(II) (▲).

In Fig. 3 plots of pH *vs.* log $(1 - \alpha)/\alpha$ are given for PAA, with and without neutral salt and with and without copper being present. In the presence of copper, the pH *vs.* log $(1 - \alpha)/\alpha$ plots show a pronounced curvature, indicating strong complex formation in this system. The pronounced effect of the addition of neutral salt is also shown. In the absence of neutral salt, pK_a for 0.01 N PAA is 5.92 and n is 2.0, while in the presence of 2 M sodium nitrate pK_a is 4.22 and n = 1.4. The same concentration of copper produces a much larger shift in the plot in the absence of neutral salt than when neutral salt is present. A typical set of data is given in Table II.

TABLE II

TITRATION OF 0.01 N POLYACRYLIC ACID IN 2 M SODIUM NITRATE

	pH	
α	No Cu(II)	0.00660 M Cu(II)
0	2.77	2.66
.2	3.51	2.87
.4	4.10	3.09
.6	4.61	3.45
.8	5.17	3.91

Since the addition of even a small amount of any salt has a pronounced effect on the titration curve of a polyelectrolyte and, further, since this effect approaches a limit at high salt concentrations, most of our experiments were performed in 1 or 2 M neutral salt. In solutions of such high ionic strength, the ionic strength effect of copper is negligible and therefore any pH changes produced may be attributed to complexation.

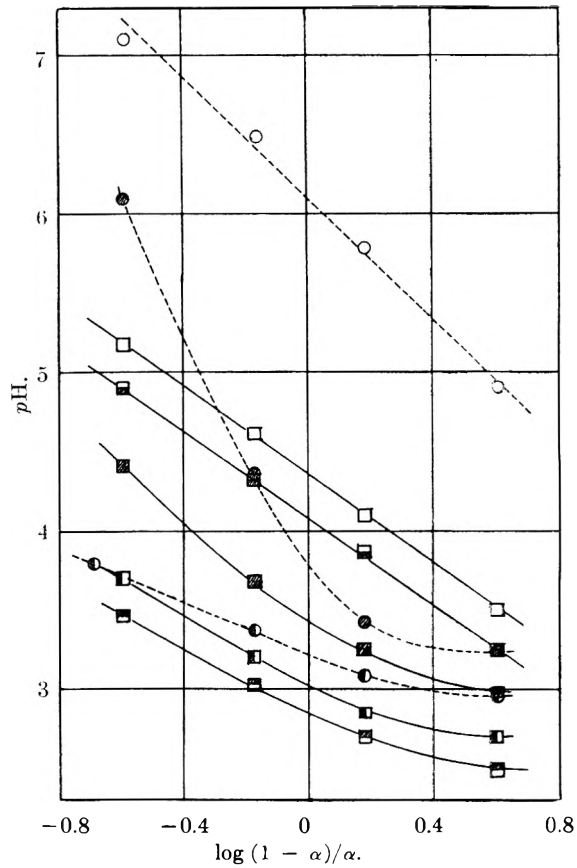

Fig. 3.—Plots of pH *vs.* log $(1 - \alpha)/\alpha$ for 0.01 N PAA. No neutral salt present (dashed lines): No Cu(II) (○); 0.00246 M Cu(II) (●); 0.00985 M Cu(II) (◐). In 2 M $NaNO_3$ (solid lines): No Cu(II) (□); 0.000493 M Cu(II) (▬); 0.00246 M Cu(II) (■); 0.00985 M Cu(II) (◧); 0.0246 M Cu(II) (▬).

Theory and Method of Calculation of the Complexity Constants

The method used to calculate complexation constants from the pH data was based on Bjerrum's method.[7] However, two modifications were necessitated by the polymeric nature of the acid. In Bjerrum's original method, $\bar{n}$, the average number of ligands (A) bound to the central group is determined experimentally and plotted against the ligand exponent $p[A] = -\log [A]$ giving the "formation curve" of the system. The functional relationship between $\bar{n}$ and [A] involves the successive complexation (formation) constants, k_1, k_2, . . . k_j, . . . k_N

$$\bar{n} = \frac{\sum_{i=1}^{N} iK_i[A]^i}{1 + \sum_{i=1}^{N} K_i[A]^i} \qquad (1)$$

$$K_i = \prod_{j=1}^{i} k_j \qquad (2)$$

$$k_j = \frac{[MA_j]}{[MA_{j-1}][A]} \qquad (3)$$

Here M is the central group or atom in a compound MA_j, j (or i) is the number of ligands in the compound MA_j (or MA_i) and N is the maximal value of j (or i), or the coördination number.

Because of this functional relationship, the formation curve makes it possible to determine the successive complexation constants, either directly by reading off the values of $p[A]$ at half integral values of $\bar{n}$ if the constants are sufficiently separated or through a method of iteration if they are not sufficiently separated. The formation curve also indicates the maximal values for $\bar{n}$ (the coördination number N) and through its slope the separation factor between successive constants. Sullivan and Hindman[10] review very succinctly some of the mathematical techniques associated with Bjerrum's and allied methods.

In the cases under discussion, namely, the complexation of metal ions (especially copper) with carboxylic acids, the complexation constants are the equilibrium constants for reactions of the type

$$R{-}COO^- + Cu^{++} \rightleftharpoons R{-}COOCu^+ \qquad (4)$$

i.e., the reaction of the *free* carboxylate ion with metal; the residue R may or may not carry other dissociated or undissociated carboxylic groups.

In the case of simple carboxylic acids the complexation constants k defined above and pertaining to reactions such as equation 4 may be expected to be constant within the limits of validity of the usual assumptions; however, in the case of a polymeric acid such as polyacrylic acid which contains a very large number of acid groups this can no longer be expected because of the fact that the reaction 4 involves a net change in the charge on the polymer chain and the well-known fact that the configuration and other properties of the polymer chain depend very markedly upon the charge on it.[9,11–13]

However, the reaction

$$R{-}COOH + M^+ \rightleftharpoons RCOOM + H^+ \qquad (5)$$

does not involve a net change in the charge of the polyelectrolyte and the equilibrium constant pertaining to it could therefore be expected to be effectively constant for both monomeric and polymeric acids. Let us write this equilibrium constant (b_j) in its general form

$$b_j = \frac{[MA_j][H^+]}{[MA_{j-1}][HA]} \qquad (3')$$

where [HA] refers to the concentration of undissociated carboxylic acid groups.

Another way of viewing this problem is the following. The relation between the constants b_j and k_j is given by

$$b_j = k_a k_j \qquad (6)$$

where k_a is either the single acid dissociation constant of a monobasic acid or the pertinent dissociation constant of a polybasic acid. Since in the case of a simple acid the k_a's are constant, well defined and known, both complexation constants b_j and k_j are equally constant and form an equally valid description of the system and the use of one or the other formulation is a matter of indifference. In the case of a *polymeric* acid, however, the dissociation "constant" k_a is of course not constant but varies with degree of neutralization, due to the change in chain potential.[4,5,9] The variations in k_j should be equal but opposite (k_a is a dissociation "constant," k_j a formation constant) since the same effects apply. It is therefore reasonable to expect from this point of view also that the b_j's should be constant and thus have a definite meaning as measuring the amount of complexation. On comparing polymeric and simple acids it is therefore the b_j's rather than the k_j's that should be compared.

By some simple manipulations, Bjerrum's formation function can be expressed in terms of the b_j's. Let

$$B_i = \prod_{j=1}^{i} b_j \qquad (2')$$

then

$$\bar{n} = \frac{\sum_{i=1}^{N} iB_i\left(\frac{[HA]}{[H^+]}\right)^i}{1 + \sum_{i=1}^{N} B_i\left(\frac{[HA]}{[H^+]}\right)^i} \qquad (1')$$

It is seen, therefore, that if the formation curve is plotted as $\bar{n}$ *vs.* p ($[HA]/[H^+]$) all the information that could be obtained in the original Bjerrum plot about the k_j's can now be obtained in exactly analogous fashion about the b_j's.

The other modification necessitated by the nature of the polymer is the following: $\bar{n}$ is given by its definition and from the stoichiometry of the problem as

$$\bar{n} = \frac{[A_t] - [HA] - [A]}{[M_t]} \qquad (7)$$

where $[A_t]$ and $[M_t]$ are the *total* acid and metal ion concentrations, respectively.

From the conservation equations and the electroneutrality relations [HA], the concentration of undissociated acid, is found to be

$$[HA] = [A_t](1 - \alpha) - [H^+] \qquad (8)$$

where α is the degree of neutralization.

The concentration of the carboxylate ion, [A], is connected with [HA] and $[H^+]$ through the functional relation describing the dissociation equilibrium of the acid groups. In the case of simple acids this relationship is determined by the set of dissociation constants which are presumed to be known and thus the concentration [A] can be calculated at each measured pH value. $\bar{n}$ is then determined through equation 7.

In the case of a polymeric acid, however, the relation between [HA], [A] and $[H^+]$ is less simple since it is governed by an almost continously varying dissociation "constant." A relationship

$$K_a = K_0 e^{-\Delta F_e/kT} \qquad (9)$$

should hold[14] where K_0 is an intrinsic dissociation constant and ΔF_e is the free energy change due to the displacement of the proton to infinity against the field of all the charges on the molecule. For a constant polymer and salt concentration, the term in equation 9 involving the free energy change should

(10) J. C. Sullivan and J. C. Hindman, *J. Am. Chem. Soc.*, **74**, 6091 (1952).

(11) J. J. Hermans and J. T. G. Overbeek, *Rec. trav. chim.*, **67**, 761 (1948).

(12) G. E. Kimball, M. Cutler and H. Samelson, THIS JOURNAL, **56**, 57 (1952).

(13) A. Katchalsky and S. Lifson, *J. Polymer Sci.*, **11**, 409 (1953).

(14) N. Bjerrum, *Z. physik. Chem.*, **106**, 219 (1923).

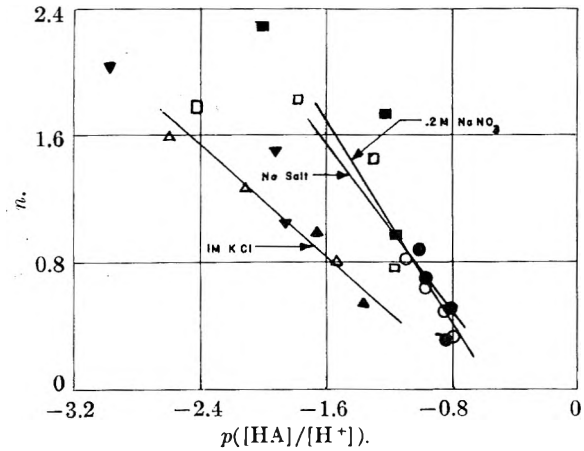

Fig. 4.—Modified Bjerrum plot for PAA (0.01 N)-copper(II) in the absence of salt, in 0.2 M $NaNO_3$ and in 1 M KCl. No neutral salt: 0.00246 M Cu(II) (■); 0.00985 M Cu(II) (●). In 0.2 M $NaNO_3$: 0.00246 M Cu(II) (□); 0.00985 M Cu(II) (○). In 1 M KCl: 0.00428 M Cu(II) (▼); 0.00214 M Cu(II) (△); 0.000500 M Cu(II) (▲).

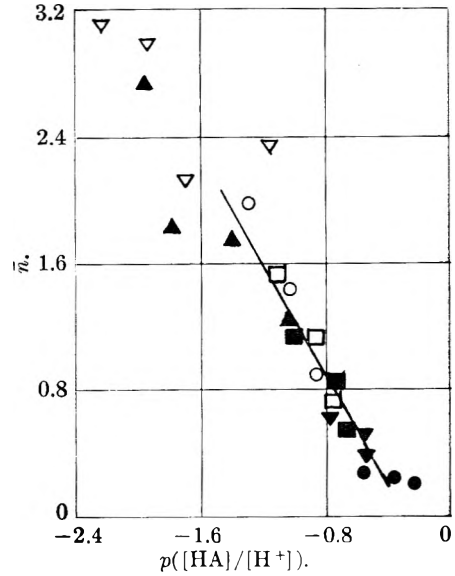

Fig. 5.—Modified Bjerrum plot for PAA (0.01 N)-copper(II) in 2 M $NaNO_3$: 0.000493 M Cu(II) (▽); 0.00131 M Cu(II) (▲); 0.00246 M Cu(II) (○); 0.00349 M Cu(II) (□); 0.00493 M Cu(II) (■); 0.00985 M Cu(II) (▼); 0.0246 M Cu(II) (●).

be a function of the degree of charging z only; z is the ratio of charged to uncharged groups, *i.e.*

$$z = \frac{[A]}{[A_t] - [A]}$$

Therefore

$$K_a = K_0 f(z) \qquad (10)$$

It has been shown[2,3,15] empirically that over a wide range of α, $f(z)$ can be expressed as $(z)^m$ where m is a constant. In a simple titration $[A_t] - [A] = [HA]$ and z becomes $[A]/[HA]$; equation 10 then takes the form

$$K_a = \frac{[H^+][A]}{[HA]}(z)^m = [H^+]\left(\frac{[A]}{[HA]}\right)^n \qquad (11)$$

where $n = m + 1$.

Some theoretical justification for equation 11 has been provided by Katchalsky and Gillis.[16]

It is now assumed that the occurrence of chelation does not in itself alter the dissociation relations of the acid, *i.e.*, that the first part of equation 11 still holds.

However, z is now no longer equal to $[A]/[HA]$, since the equation

$$[A_t] = [HA] + [A] \qquad (12)$$

no longer holds.

Equation 11 will then take the form

$$K_a = \frac{[H^+][A]}{[HA]}\left(\frac{[A]}{[A_t] - [A]}\right)^{n-1} \qquad (13)$$

where K_a and n have the same values as in the absence of chelation, *i.e.*, the values that are obtained from the logarithmic plot of the titration curve directly. Equation 13 can be solved by an iterative procedure, for the only unknown [A], and hence $\bar{n}$ can again be obtained through equation 7.

As indicated before, the logarithms of the complexation constants, log b_j, are the values of $p([HA]/[H^+])$ at successive half integral values of $\bar{n}$ provided that these constants are sufficiently separated. In any case, regardless of the separation between the constants, the value of $p([HA]/[H^+])$ at integral values of $\bar{n}$ gives an average constant, *e.g.*, at $\bar{n} = 1.0$ the average constant, $B_{av} = \sqrt{b_1 b_2}$ for a two-step process. The square of B_{av} is, of course, the constant for the over-all process

$$B_2 = \frac{[MA_2][H^+]^2}{[M][HA]^2} \qquad (14)$$

Results and Discussion

Figure 4 shows plots of $\bar{n}$ *vs.* $p([HA]/[H^+])$ for 0.01 N PAA and various amounts of copper in the absence of salt, and in the presence of 0.2 M $NaNO_3$ and 1 M KCl. Figure 5 shows the plot in 2 M $NaNO_3$; here seven different concentrations of copper were used. It is seen that all points fall on the same curve, attesting to the general validity of the approach used.

In principle the plot should yield the coördination number as the integral value approached by $\bar{n}$ as $p([HA]/[H^+])$ approaches $-\infty$. Such a flattening of the curve for PAA–copper systems is not observed. This may be due to the fact that the far left-hand corner of the plot is subject to several uncertainties. Values in this region are obtained: (a) at high degrees of neutralization, or (b) at very low total copper concentrations. In case (a), *e.g.*, $\alpha > 0.8$, equation 10 is inapplicable even in the absence of copper. In case (b) the decrease in pH upon the addition of small amounts of copper is small, and hence subject to much larger errors. It might be mentioned that ideal Bjerrum plots are often not obtained even for monomeric substances.

In this connection, it is interesting to compare these results with those found for a cross-linked polymer of acrylic acid. Here the plot tends to have the expected sigmoidal shape, approaching an $\bar{n}$ asymptote of 2, as will be shown in a subsequent paper in this series. Because of these uncertainties no effort was made to estimate the coördination number, nor was it felt to be possible to estimate complexation constants of greater than the second order.

(15) R. Speiser, C. H. Hills and C. R. Eddy, *J. Phys. and Colloid Chem.*, **49**, 334 (1945).

(16) A. Katchalsky and J. Gillis, *Rec. trav. chim.*, **68**, 879 (1949).

TABLE III

COMPLEXATION CONSTANTS OF COPPER(II) WITH CARBOXYLIC ACIDS

Acid	Neutral Salt	log B_{av}	B_2	b_1/b_2	K_2
PAA 0.01 N	...	−1.19	4.2×10^{-3}	2.1	9.1×10^{9}
PAA 0.01 N	0.2 M $NaNO_3$	−1.17	4.6×10^{-3}	0.76	3.0×10^{7}
PAA 0.01 N	2 M $NaNO_3$	−0.99	1.05×10^{-2}	0.33	9.6×10^{6}
PAA 0.01 N	1 M KCl	−1.78	2.8×10^{-4}	9.0	6.9×10^{5}
PAA 0.06 N	1 M KCl	−1.82	2.3×10^{-4}		6.0×10^{5}
PAA 0.1 N	1 M KCl	−1.7	4×10^{-4}		2×10^{6}
Acetic		−3.25	3.16×10^{-7}	14	5.5×10^{2}
Acetic	0.2 M $NaNO_3$	−3.09	6.6×10^{-7}		5.8×10^{2}
Acetic	2 M $NaNO_3$	−2.92	1.45×10^{-6}		6.0×10^{2}
Acetic[a]	1 M $NaClO_4$	−3.31	2.4×10^{-7}	4.5	4.4×10^{2}
Oxalic[b]			$\sim 10^{3}$		$\sim 10^{8}$
Malonic[c]	0.001 M	−1.37	1.82×10^{-3}		3.47×10^{5}
Methylmalonic[c]	0.001 M	−1.62	5.75×10^{-4}		1.55×10^{5}
Dimethylmalonic[c]	0.001 M	−2.02	8.91×10^{-5}		6.92×10^{4}
Succinic[b]		~ -2.5	$\sim 10^{-5}$		$\sim 10^{4}$
Glutaric 0.01 N	...	−2.88	1.74×10^{-5}	13	7.24×10^{3}
Glutaric 0.01 N	0.2 M $NaNO_3$	−2.8	2.5×10^{-5}		4.4×10^{3}
Glutaric 0.01 N	2 M $NaNO_3$	−2.92	1.45×10^{-5}	7	6.92×10^{2}
Glutaric 0.1 N	1 M KCl	−3.27	2.9×10^{-7}		2.51×10^{2}

[a] S. Fronaeus, *Acta Chem. Scand.*, 5, 859 (1951). [b] Estimated by interpolation from data in Martell and Calvin, "Chemistry of the Metal Chelate Compounds," John Wiley and Sons, Inc., New York, N. Y., 1952, Appendix 1. [c] From data in Martell and Calvin, Appendix 1.

The data for the PAA–copper system in the presence or absence of neutral salt can best be represented by a straight line over the range about $\bar{n} = 1$. The slope is quite large indicating a small spreading factor.[17]

That means $b_2 \sim b_1$, *i.e.*, the chance for a second ligand group attaching itself to the metal ion after one has attached itself is great. Because of the small spreading factor a separate evaluation of the two constants b_1 and b_2 cannot be conveniently and meaningfully performed; the significant constant is the over-all complexation constant $B_2 = b_1 b_2 = B_{av}^2$.

Formation constants for various systems are summarized in Table III. This table also lists complexation data for acetic acid and some simple dibasic acids; the data for acetic and glutaric acid were determined by us in a manner exactly analogous to that used for PAA and described above. The data for the other acids are taken from the literature.

The data show strikingly the enhancement of complexation in the polymer over the analogous monomer, glutaric acid. The table shows the considerable weakening of complexation with increasing ring size of the chelate (nine orders of magnitude in B_2 from oxalic acid—five-membered ring—to glutaric acid—eight-membered ring). It also shows the weakening effect of alkyl substitution on the complexation constant. In glutaric acid the complexation is hardly greater than in acetic acid. By comparison, the complexation constants of PAA itself are three to four orders of magnitude greater. This can only be because the enormous electrostatic attraction of the polyelectrolyte coil nullifies this steric effect, and allows the production of a complex as stable as those composed of five and six membered rings.

Comparing the values obtained for PAA under various conditions, it is seen that changing the salt concentration does not have a very large effect on the complexation constant B_2; this is not unexpected since the reaction described by this constant does not involve any net charge change. The values of K_2, by contrast, (obtained from B_2 by the use of equation 6) which are included here only for comparison and which are not very significant as was pointed out in the theoretical section, show a tremendous change with salt concentration. It is seen further that the complexation constant is practically unaffected by a change in the polymer concentration in the range 0.01 to 0.1 N.

It is also seen that complexation is weaker in chloride than in nitrate systems, probably because of the simultaneous formation of chloro complexes. The same phenomenon is observed with glutaric acid. The ratio of the individual constants, b_1/b_2, as estimated from the slope of the curve, shows in this case that it is the second step of the complexation which is repressed by chloride ions; the first one seems to be relatively unaffected.

A comparison of the spreading factors b_1/b_2 in the case of PAA, acetic and glutaric acids again shows up the fact that PAA has a much stronger preference for ring formation than its monomeric analog and is much closer in its chelation behavior to smaller dibasic acids like oxalic or malonic acid.

This investigation was supported in part by a research grant, RG 2934(C2) from the Division of Research Grants of the National Institutes of Health, Public Health Service. We also wish to express our gratitude to the Rohm and Haas Company which provided us with samples of the polyacrylic acid used in this investigation.

(17) Reference 7, p. 25.

DETERMINATION OF THE VAPOR PRESSURE OF SODIUM

BY M. M. MAKANSI, C. H. MUENDEL AND W. A. SELKE

Department of Chemical Engineering, Columbia University, New York, N. Y.

Received July 19, 1934

Experimental data on the vapor pressure of sodium in the pressure range 0.047 to 6.489 atm. have been obtained. The results are fitted by the equation $\log P = -5220/T + 4.521$, where P is in atm. and T is in degrees Kelvin.

Introduction

In the work being conducted in this Laboratory on the determination of the thermodynamic properties of sodium, the variation of the vapor pressure with temperature was of interest. The normal boiling point of sodium was determined by Ruff and Johannsen in 1905[1] to be 877.5 ± 5°. Another determination of the boiling point by Heycock and Lamplough in 1912[2] gave a value of 882.9°. Previous workers had obtained data in the pressure range of 0.00049 to 760 mm. These data were reviewed by Ditchburn and Gilmour.[3]

Rodebush and Walters[4] obtained experimental data in the pressure range of 48.82 to 482.5 mm., and fitted them with the equation

$$\log P = \frac{-5400}{T} + 4.6702 \qquad (1)$$

where P is in atm. and T in degrees Kelvin. Gordon[5] and Kelley[6] using spectroscopic information on the dissociation of sodium dimer together with some vapor pressure data observed by other workers derived the following equations for the vapor pressure of sodium atoms and of sodium vapor, respectively.

$$\log P_{(Na)} = -\frac{5702}{T} - 1.174 \log T + 8.4437 \qquad (2)$$

$$\log P_{(Na + Na_2)} = -\frac{5775}{T} - 1.274 \log T + 8.863 \qquad (3)$$

According to Gordon, when equation 2 is corrected for the presence of sodium dimer molecules, it is accurate to 0.5%. Ditchburn and Gilmour[3] correlating the experimental results of a number of workers, obtained the equation

$$\log P = -\frac{5567}{T} - 0.5 \log T + 6.354 \qquad (4)$$

According to them, the error in equation 4 is 5% in the range of 450 to 1200°K. and 10% in the range of 370 to 1250°K.

The purpose of the current work was to extend the range of the vapor pressure data beyond the existing limits and also to check the values obtained by other workers in the low pressure ranges.

Experimental

The method used consists of boiling sodium and refluxing it with a condenser in which pressure is maintained with purified argon. The pressure in the argon system was measured by means of a mercury manometer, which provided an indication of the vapor pressure of sodium at the measured temperature.

The Apparatus.—The boiler, consisting of a hollow vertical cylinder of inconel, 10 cm. by 2.5 cm., was welded to a one meter long section of one-quarter inch inconel pipe which served as a condenser. A piece of one-eighth inch inconel tubing, located axially inside the condenser down to the center of the boiler, served as a thermocouple well. The top end of the condenser was connected to the purified argon line. The boiler was heated by an alundum furnace wound with Kanthal alloy wire, designed to reach a temperature of 1300°. At the temperature and pressure conditions attainable in this experiment, the strength of the metals is greatly reduced. To offset this difficulty, the high temperature system was placed in a pressure vessel, the pressure in which was adjusted so as to balance the pressure in the boiler. Thus the net stress on the boiler and condenser walls was slight.

The sodium used was triply-distilled metal obtained in sealed and evacuated Pyrex flasks. These containers, each of which contained 25 cc. of sodium, were designed to allow the charging of sodium into the apparatus without contamination from the atmosphere.

Commercial argon was used. The traces of impurities that might react with sodium were removed by bubbling the gas through two columns filled with liquid sodium-potassium alloy (NaK).

Temperatures in the boiler were measured by a platinum–platinum 10% rhodium thermocouple inserted in the well extending into the sodium boiler so that the tip of the thermocouple touched the top surface of the liquid sodium before boiling commenced. The e.m.f. of the thermocouple was measured by a potentiometer. A series of auxiliary chromel–alumel thermocouples mounted at various points in the hot portion of the condenser served to indicate the height of the condensing ring of sodium, thus giving qualitative information about the rate of vaporization. These thermocouples were connected to continuously reading millivoltmeters so that the operation could be checked without delay.

Pressures in the high range were measured by a 13 foot mercury-filled manometer. Pressures lower than one foot of mercury gage were measured by a 100-cm. long U-tube mercury manometer. The difference between the boiler pressure and the balancing pressure was indicated by a U-tube differential mercury manometer. Auxiliary Bourdon gages were used to indicate the pressures in the argon supply lines.

Procedure.—Before a batch of sodium was charged into the apparatus, the boiler and condenser system were detached and cleaned several times, first with an aqueous mixture of 10% HF and 10% HNO_3, then with distilled water, and then dried. This ensured the removal of any oxides that might be present on the inner surface of the system. A Pyrex container of sodium was then sealed to the top end of the condenser. The system was then evacuated and flushed with purified argon several times at elevated temperatures to remove any traces of oxygen. Sodium oxides would affect the boiling point and cause the container to corrode at high rate. The seal in the pyrex container was then broken by a carbon steel ball inside the glass container manipulated by a permanent magnet outside the tube. The ball and the glass chips were collected in a pocket in the container provided for this purpose. The container was then heated externally by an asbestos mantle and the molten sodium was allowed to flow slowly into the boiler through the heated condenser by gradually reducing the argon pressure. The glass tube connecting the container to the condenser was then sealed and the empty container was removed.

The progress of boiling was followed by reading the po-

(1) O. Ruff and O. Johannsen, *Ber.*, **38**, 3601 (1905).

(2) C. T. Heycock and F. E. E. Lamplough, *Proc. Chem. Soc.*, **28**, 3 (1912).

(3) R. W. Ditchburn and J. C. Gilmour, *Rev. Modern Phys.*, **13**, 310 (1941).

(4) W. H. Rodebush and E. G. Walters, *J. Am. Chem. Soc.*, **52**, 2654 (1930).

(5) A. R. Gordon *J. Chem. Phys.*, **4**, 100 (1936).

(6) K. K. Kelley, U. S. Bur. of Mines Bull. 383, 1935.

tentiometer of the main thermocouple and the millivoltmeters of the chromel–alumel thermocouples which indicated the height of the condensing ring.

Data for a given pressure were taken when a steady state was indicated by the constancy of the readings of the potentiometer and the millivoltmeters for at least five minutes. The reading of the platinum–platinum 10% rhodium thermocouple was taken as the boiling point of sodium at that particular pressure.

Two loadings of sodium were used. One run was made with the first loading and three were made with second. The first run was not completed because the thermocouple was attacked by sodium vapor through a pin hole in the well.

Results

Table I shows the results of this work. Using the method of least squares the following equation was fitted to the data points

$$\log P = -\frac{5220}{T} + 4.521 \qquad (5)$$

The standard error in P as calculated from this equation is 0.9% in the experimental range 0.047 to 6.489 atm.

TABLE I

VAPOR PRESSURE OF SODIUM

Temp., °K.	Pressure, atm.	Temp., °K.	Pressure, atm.
Run no. 1		Run no. 2	
1169.0	1.108	1169.4	1.134
1195.6	1.428	1241.5	2.061
1195.8	1.420	1295.2	3.094
1201.2	1.459	1327.7	3.895
1249.5	2.287	1381.9	5.500
1251.8	2.253	1406.2	6.416
1245.2	2.083	1368.9	5.100
1240.7	2.059	1340.0	4.296
1291.2	2.927	1310.0	3.495
1288.0	3.013	1274.9	2.693
1280.0	2.728	1228.2	1.890
1331.0	4.035	Run no. 3	
1321.0	3.760	1158.8	1.027
1362.0	5.005	1139.0	0.866
1353.0	4.680	1118.4	0.710
Run no. 4		1100.8	0.594
893.6	0.047	1073.4	0.449
893.9	.050	948.7	0.115
896.7	.051	1111.4	0.656
898.4	.051	1172.5	1.180
958.0	.117	1297.7	3.078
954.2	.117	1341.3	4.281
956.8	.117	1381.3	5.486
958.7	.116	1392.9	5.888
958.0	.116	1408.3	6.489
958.2	.116	1402.4	6.289
958.5	.116	1378.8	5.486
958.4	.116	1364.8	5.085
1157.9	1.031	1291.8	3.079
1070.5	0.438		
1023.0	0.260		

Figure 1 is a semilog plot of the data as P *vs.* $1/T$ together with the line representing equation 5. The normal boiling point as calculated from the equation is 881.3°C.

Equations 1, 3, 4 and 5 for the vapor pressure of sodium were compared by computing the boiling points at several pressures from 1 to 10,000 mm. These computed values are listed in Table II.

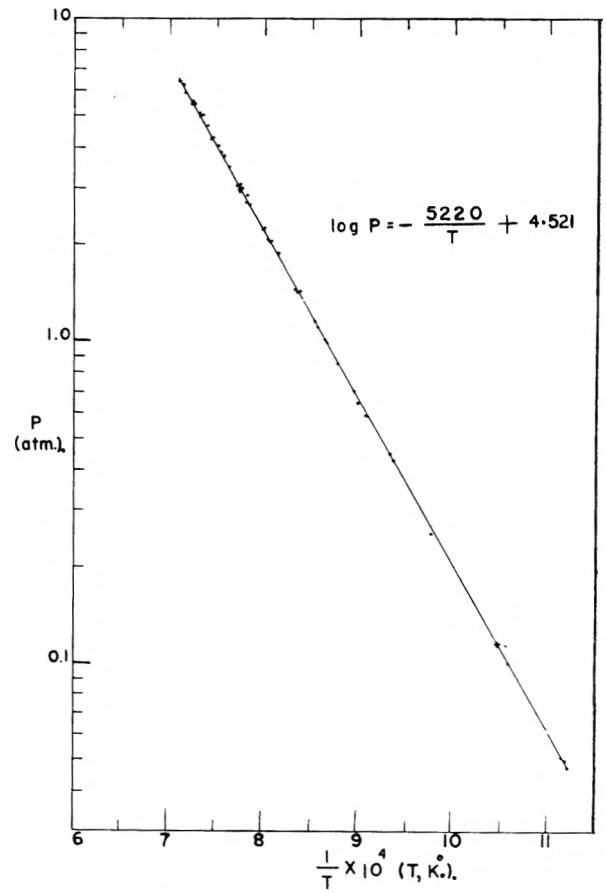

Fig. 1.—Vapor pressure of sodium.

TABLE II

CALCULATED TEMPERATURES FOR VARIOUS PRESSURES, DEGREES KELVIN

Pressure, mm.	Eq. 1, Rodebush[4]	Eq. 3, Kelley[5]	Eq. 4, Ditchburn[3]	Eq. 5, authors
1	715	712	713	705.2 ± 1.8
10	824	821	821	815.3 ± 2.2
100	973	973	969	966.2 ± 3.3
760	1156	1165	1154	1154.5 ± 4.7
1000	1187	1197	1180	1185.8 ± 5.2
10000	1521	1572	1525	1534.3 ± 8.5

The temperatures computed from equation 5 are for the 95% confidence intervals.

Table II shows that equation 1 agrees with equation 5 only in the range of 500 to 1000 mm. Equation 3 deviates considerably from equation 5 and tends to give higher temperatures than equation 5. Equation 4 on the other hand, agrees with equation 5 in the range between 100 and 1000 mm. and deviates more than the error limit of equation 5 elsewhere.

The above comparison suggests that, of the two three-term equations, 3 and 4 which are intended to cover a wide range of the vapor pressure, equation 4 is more dependable in predicting the vapor pressure of sodium in the range of 100 to 1000 mm. It is also concluded that none of the presently available vapor pressure equations for sodium including the authors' could be used safely to predict values above 5000 mm. Hence further experimental work on the vapor pressure of sodium above

the present range is necessary to complete the vapor pressure curve.

Acknowledgment.—The authors wish to acknowledge the advice and aid given by Dr. L. F. Epstein, Knolls Atomic Power Laboratory, General Electric Company, Schenectady, New York, and the sponsorship by the United States Atomic Energy Commission under contract AT(30-1) 1101.

TOTAL PRESSURE OVER CERTAIN BINARY LIQUID MIXTURES

BY JOSEPH A. NEFF[1] AND JAMES B. HICKMAN

Contribution from the Department of Chemistry, West Virginia University

Received July 22, 1954

Measurements of total pressure over binary liquid mixtures of perfluoroheptane with heptane and 3-methylheptane, titanium(IV) chloride with heptane, and tetrachloromethane with 3-methylheptane at two or more temperatures in the range 25–80° are reported. The data substantiate the conclusion that the solubility behavior of the non-regular solutions of hydrocarbons in other non-polar liquids is adequately represented by the Hildebrand equations, using an empirical solubility parameter for the hydrocarbon. The Hildebrand equations are used as a means of reducing the total pressure measurements to more usable form.

Introduction

Studies by Hildebrand[2,3] and others[4,5] on binary liquid mixtures of hydrocarbons with other non-polar substances have established that the criteria of regular solution formation are not met by such mixtures, and hence that the equations describing the behavior of regular solutions are not applicable to them. It has further been suggested[3] however, that for the group of binary non-polar mixtures containing a hydrocarbon and a non-hydrocarbon the regular solution equations can be made applicable by use of a suitable empirical solubility parameter for the hydrocarbon. This suggestion implies two consequences that have not been tested thoroughly by experiment: (1) that hydrocarbons should be better solvents for materials of high solubility parameter, and poorer solvents for materials of low solubility parameter, than their calculated solubility parameters indicate (only the latter has been well established), and (2) that the regular solution equations represent correctly the form of behavior of hydrocarbon–non-hydrocarbon mixtures, provided an empirical solubility parameter be used for the hydrocarbon.

It is here proposed to study these two conclusions on the basis of data from experimental determination of total pressure above binary liquid mixtures. This method of experimentation offers the advantages of simplicity of operation and avoidance of the possibilities of systematic error inherent in the determination of partial pressures. It is superior to the much simpler determination of critical solution temperatures in that it may be used with systems that remain homogeneous throughout the liquid range, and in that it can provide data for a wide range of temperatures and compositions. An advantage of total pressure measurement over determination of liquid–vapor equilibrium data is that total pressure is readily determined isothermally, providing information more susceptible to comparison with the predictions of the regular solution equations than are the isopiestic data of the liquid–vapor equilibrium method. Because of the limited nature of the questions asked in this research, concerning a restricted group of substances, the outstanding disadvantage of the total pressure method, absence of any wholly satisfactory method of reduction of the data[6] is largely avoided.

Experimental

Apparatus.—The apparatus used was essentially that described by Sanderson,[7] combining the essential features of his simplified high-vacuum apparatus-manometer, condensation traps and McLeod gage, illustrated in his Fig. 37 with his vapor pressure apparatus-air surge chamber, differential manometer, and sample chamber diagrammed in his Fig. 27. A Pirani hot-wire gage, calibrated against the McLeod gage, also was provided for rapid checking of the pressure during experiments, and as an aid in the detection of leaks. The sample was introduced into the system by distillation under vacuum, and degassed by distillation from one condensation trap to another, freezing and pumping. The thoroughness of degassing was indicated by constancy of pressure with time, and by the agreement of measured vapor pressures of pure substances with the best literature values. The liquid sample was constantly stirred during a determination by means of an iron bar sealed in glass, kept in motion by an external horseshoe magnet moved by a reciprocating stirrer.

Since the vapor pressure was determined by finding what external pressure had to be applied just to balance the pressure developed by the vapors above the liquid, and since the volume available for occupancy by the vapors of the liquid was small (less than 10 cm.^{3}), there was no appreciable change in composition of the liquid during an actual determination. A careful check was made to determine whether changes in composition might result from the degassing process. Although such changes were found, by analysis of samples before and after degassing, to amount to 2% or less, they were essentially eliminated by determining the composition of the sample at the end of each experiment, following a one-step distillation out of the system.

The temperature of the sample was measured by means of a copper–constantan thermocouple in a thermocouple well in the sample chamber. The thermocouple had been calibrated against a platinum resistance thermometer whose temperature–resistance characteristics had been determined by the U. S. National Bureau of Standards.

(1) Based in part on a dissertation submitted by Joseph A. Neff for the degree, Doctor of Philosophy, West Virginia University, May, 1954.

(2) J. H. Hildebrand, *J. Chem. Phys.*, **18**, 1337 (1950).

(3) J. H. Hildebrand, B. B. Fisher and H. A. Benesi, *J. Am. Chem. Soc.*, **72**, 4348 (1950).

(4) J. H. Simons and R. D. Dunlap, *J. Chem. Phys.*, **18**, 335 (1950).

(5) D. N. Campbell and J. B. Hickman, *J. Am. Chem. Soc.*, **75**, 2879 (1953).

(6) G. Scatchard in G. K. Rollefson (ed.), "Annual Review of Physical Chemistry," Vol. III, Annual Reviews, Inc., Stanford, Calif. 1952, p. 269.

(7) R. T. Sanderson, "Vacuum Manipulation of Volatile Compounds," John Wiley and Sons, Inc., New York, N. Y., 1948, pp. 78–105.

TABLE I

PURIFICATION AND PURITY MEASUREMENT FOR SUBSTANCES USED

Substance and source	Still efficiency, theo. plates	B.p., °C., cor. to 760 mm.	B.p., °C., 760 mm. lit.	F.p., °C.	Mole % impurity
Benzene, Eastman[a]	24	80.12[b,c]	80.0[c]	5.34	0.18
Tetrachloromethane, J. T. Baker	24	76.9[d]	76.7[e]	− 22.9	0.07
Heptane, Eastman	24	98.3[c]	98.428[c]	− 91.025	0.07
3-Methylheptane, synthesized	24	117.7[c]	118.9[c]	−122	2.0
Perfluoroheptane, Carbide and Carbon	100	81.5[f]	82.5[f]	− 76	3.6
Titanium(IV) chloride, National Lead	5	134.8[g]	135.8[g]	− 24.51	0.34

[a] All commercial chemicals best grade of the manufacturer. [b] Literature references for this column give source of dt/dp value used in correcting b.p. [c] F. D. Rossini, *et al.*, "Selected Values of Properties of Hydrocarbons," (Circular C461) U. S. Govt. Printing Office, Washington, D. C., 1943, pp. 483. [d] Ref. 10. [e] F. D. Rossini, *et al.*, "Selected Values of Chemical Thermodynamic Properties," (Circular C 500), U. S. Govt. Printing Office, Washington, D. C., 1952, pp. 588, 716. [f] R. D. Fowler, *et al.*, *Ind. Eng. Chem.*, **39**, 375 (1947). [g] L. L. Quill (ed.), "Chemistry and Metallurgy of Miscellaneous Materials," McGraw–Hill Book Co., New York, N. Y., 1950, pp. 193–275.

The sample chamber and intermediate differential manometer were thermostated in a large Dewar flask, the leveling of the mercury in the arms of the differential manometer being attained by matching a horizontal scratch on a previously leveled mirror contained in the Dewar flask. The manometer measuring the applied pressure was read by means of a cathetometer.

Materials.—Standard methods of preparation and purification, as summarized in Table I, were used for the substances employed.

Purities were determined by f.p. according to the methods of Rossini and co-workers,[8] the f.p. and purity determination for titanium(IV) chloride being carried out in a closed, magnetically stirred f.p. tube[9] into which the sample could be introduced by distillation under vacuum. The validity of results obtained by using this tube was indicated by obtaining identical purities within ±0.1 mole % for identical samples by use of the closed tube and the conventional Rossini apparatus (a non-hygroscopic sample being used for this test).

Analysis.—All mixtures except those involving titanium(IV) chloride or perfluoroheptane were analyzed by refractive index on the basis of refractive index–composition curves determined in the laboratory. Because of the hygroscopic nature of titanium(IV) chloride, mixtures containing it were analyzed by rapid hydrolysis in ice-water, followed by dilution to 500.0 ml. and titration of an aliquot with standardized sodium hydroxide, using brom thymol blue as an indicator. Analysis of known mixtures by this method gave results accurate to ±1.5% of the titanium(IV) chloride content.

Mixtures involving perfluoroheptane could not be analyzed by refractive index because of the low index of refraction of the fluorocarbon. The composition of these samples was determined by the Victor Meyer vapor density method, which was especially well suited to this determination because of the similar volatility and greatly differing molecular weights of the components. The error was ±1.0% in composition, as found by comparison with known samples of mixtures of the same materials.

Results and Discussion

The experimentally determined total pressure values are given in Fig. 1 (the significance of the dotted line in Fig. 1 is discussed below) and Tables II, III and IV. Total pressure data were also determined for the system tetrachloromethane–benzene, not given, as a check on apparatus and procedure. Results for this system were reproducible within ±1 mm. for different samples of the same composition, and deviated not more than ±3 mm. from the literature values.[10,11]

(8) A. R. Glasgow, Jr., A. J. Streiff and F. D. Rossini, *J. Research Natl. Bur. Standards*, **35**, 355 (1945), and references there cited.

(9) D. N. Campbell, J. A. Neff, R. F. Stewart and J. B. Hickman, *Proc. West Va. Acad. Sci.*, in press.

(10) F. A. H. Schreinemakers, *Z. physik. Chem.*, **47**, 445 (1904).

(11) C. P. Smyth and E. W. Engel, *J. Am. Chem. Soc.*, **51**, 2636 (1929).

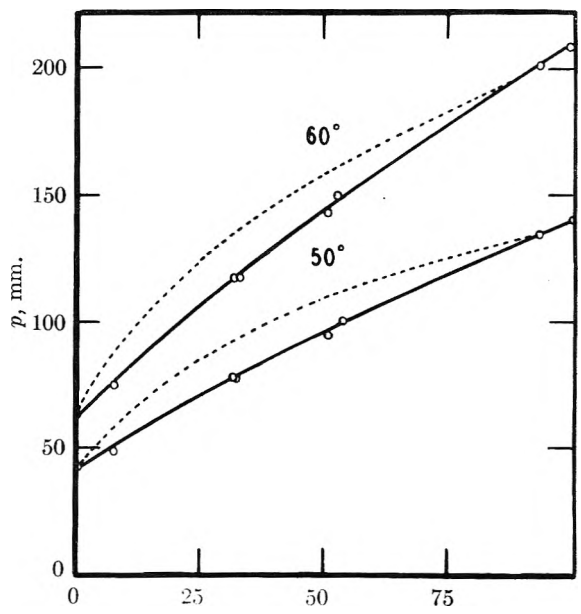

Fig. 1.—Total pressure in the system: titanium(IV) chloride–heptane (for significance of dotted lines, see text).

TABLE II

TOTAL PRESSURE, SYSTEM: PERFLUOROHEPTANE–3-METHYLHEPTANE

Perfluoroheptane, mole fraction	Pressure, cm. at 60°	65°	70°	80°
0.00	10.2	12.5	15.3	22.1
.0912	31.1	37.3	43.1	56.0
.314	38.2	45.5	53.8	73.8
.722	38.1	45.5	54.6	76.0
.755	38.6	45.9	55.1	76.8
.914	38.2	45.6	54.6	76.2
1.000	34.3	41.1	49.5	69.6

TABLE III

TOTAL PRESSURE, SYSTEM: PERFLUOROHEPTANE–*n*-HEPTANE

Perfluoroheptane, mole fraction	Pressure, cm. at 50°	55°	60°
0.000	14.1	17.3	21.0
.128	31.9	37.9	44.9
.394	32.3	38.8	46.3
.732	32.8	39.4	47.3
.856	31.8	38.0	45.5
1.000	23.7	28.9	34.9

TABLE IV

TOTAL PRESSURE, SYSTEM: TETRACHLOROMETHANE–3-METHYLHEPTANE

Tetrachloromethane, mole fraction	Pressure, cm. at 25°	35°	50°	60°
0.000	1.95	3.29	6.68	10.2
.330	5.14	8.12	14.7	21.3
.511	7.13	11.7	19.6	28.2
.742	9.39	14.2	25.1	35.7
.930	11.4	17.1	30.1	42.7
1.000	11.4	17.6	31.7	45.1

The dotted lines in Fig. 1 represent the total pressure for the system titanium(IV) chloride–heptane calculated by the regular-solution relationship

$$P_T = p_1^0 n_1 \exp [\Phi_2^2 v_1(\delta_1 - \delta_2)^2/RT] + p_2^0 n_2 \exp [\Phi_1^2 v_2(\delta_1 - \delta_2)^2/RT] \quad (1)$$

in which P_T is the total pressure, p^0_1 and p^0_2 the respective vapor pressures of the two components in the pure state at the temperature of investigation, n_1 and n_2 the mole fractions of the two components, Φ_1 and Φ_2 the respective volume fractions, *e.g.*, Φ_1 equals $n_1v_1/(n_1v_1 + n_2v_2)$ (v_1 and v_2 being the respective molar volumes of the pure components.) δ_1 and δ_2 are the calculated solubility parameters of the pure components, $\delta = (\Delta E_v/v)^{0.5}$, the values of ΔE_v (increase in internal energy of vaporization upon vaporization of one mole) and v being calculated for the temperature, T, at which the computation was being made.

Equation 1 follows directly from the Hildebrand equation

$$RT \ln \gamma_1 = \Phi_2^2 v_1(\delta_1 - \delta_2)^2 \quad (2)$$

and the definition of the activity coefficient, γ, as approximately equal to p/p^0n.

It will readily be observed in Fig. 1 that the actual total pressure of the system is less than that computed by equation 1 by an amount well exceeding the experimental error (the use of ΔE_v and v at the temperature of investigation rather than at 25° is a refinement probably unnecessary in view of the stated approximations involved in derivation of the Hildebrand equations, but this was done to minimize any deliberate exaggeration of the difference between the two curves). This provides experimental verification of the implication of Hildebrand's[3] work that the hydrocarbons are better solvents for materials of solubility parameter higher than their own, than would be inferred from the calculated solubility parameters.

Table IV reports total pressure data for the system 3-methylheptane–tetrachloromethane, likewise illustrating an entirely similar instance of behavior more nearly ideal than predicted. However, it does not constitute as sensitive a test as to the solvent power of the hydrocarbon because of the fact that the two parameters concerned have so nearly the same value.

Tables II and III present data showing the well-established large positive deviations from regular solution behavior for mixtures of hydrocarbons and fluorocarbons. Such deviations indicate that hydrocarbons are poorer solvents (than would be expected from the Hildebrand equations) for substances with solubility parameters lower than their own.

Analysis of Total Pressure Data.—In order to reduce the total pressure data to a form more readily available for comparison purposes, the following equation could be solved for x, the solubility parameter difference, $(\delta_1 - \delta_2)$

$$P_{T_e} = p_1^0(v_2/v_1 + v_2) \exp [0.25v_1x^2/RT] + p_2^0(v_1/v_1 + v_2) \exp [0.25v_2x^2/RT] \quad (3)$$

P_{T_e} being the measured total pressure when the volume fractions of the two components are equal (for which $n_1 = v_2/(v_1 + v_2)$, *etc.*), x being identical for the two right-hand terms of equation 3.

Use of equation 3 implies that solutions of hydrocarbons follow the regular solution equations provided that an empirical parameter difference be used. This is suggested, but not proved, by the fact that solutions of a hydrocarbon with a substance of high parameter are more nearly ideal, solutions of a hydrocarbon with a substance of low solubility parameter more highly deviating from ideality, than the regular solution equations predict.

A closer examination of the suitability of the form of the regular solution equations, using an empirical solubility parameter difference, has been made by analysis of the published experimental data of Simons and Dunlap[4] for the system pentane–perfluoropentane. This system provides a sensitive test for the applicability of equation 3, since the apparent parameter difference between the components is large—if it were small, the spread between the prediction of the regular solution equations, the actual behavior of the system, and ideality would be so small that no firm judgment could be made.

As a test of equation 3, the values of p/p^0n were calculated directly from Simons and Dunlap's experimental values of pressure of the pure substances and mixtures, and compared with values computed using equation 3 as follows (use of the method of Schultze[12] as a means of obtaining partial pressures proved entirely inadequate for these data): x was calculated at the composition corresponding to equality of volume fractions of the components according to equation 3, and the value of x inserted in equation 2, rewritten for ease in computation as

$$p_1/p_1^0n_1 = \exp [\Phi_2^2 v_1 x^2/RT] \quad (4)$$

Table V compares the values obtained.

TABLE V

COMPARISON OF VALUES[a] OF p/p^0n OBTAINED BY DIRECT COMPUTATION AND BY EQUATION 3

Temp., °K.	p/p^0n, C_5F_{12} Direct[b]	Eq. 3	p/p^0n, C_5H_{12} Direct[b]	Eq. 3
292.9	1.95	1.89	1.48	1.51
288.2	1.91	1.90	1.59	1.52
283.1	1.91	1.93	1.55	1.54
278.6	1.98	1.95	1.49	1.55
262.4	2.03	1.98	1.53	1.57

[a] For the composition, n C_5F_{12} = 0.393, at which $\Phi_1 = \Phi_2$. [b] From the data of ref. 4.

Evidence having been offered as to the correctness of the two implications inherent in the application of the regular solution equations (using an

(12) W. Schultze, *Z. physik. Chem.*, **198**, 314 (1951).

empirical parameter) to the non-regular mixtures of a hydrocarbon and a non-hydrocarbon, some derived results of experimental determinations are given in Table VI.

TABLE VI

COMPARISON OF VALUES OF $(\delta_1 - \delta_2)$, *etc.*, FROM COMPONENTS AND SOLUTIONS PROPERTIES

1 System	2 Temp., °K.	3 $(\delta_1 - \delta_2)$ from properties of Pure components	4 $(\delta_1 - \delta_2)$ from properties of Solutions[a]	5 $\delta_{apparent}$, Hydrocarbon, $(\Delta E_v/v)^{0.5} + \lvert 4 - 3 \rvert$
$TiCl_4$–C_7H_{16}	323.2	1.901	1.110	7.89
	333.2	1.798	1.098	7.54
CCl_4–C_9H_{18}	323.2	1.271	1.000	8.24
	333.2	1.218	1.000	8.11
C_7F_{16}–C_7H_{16}	333.2	1.56	2.65	7.75
C_7F_{16}–C_8H_{18}	333.2	1.73	2.77	8.05

[a] Calculated by equation 3.

In Table VI, column 5 represents an arbitrary and empirical solubility parameter for the hydrocarbon—ascribing all the effect of deviation to the alteration of the parameter of the hydrocarbon. It is considered significant that essentially the same numerical value of the parameter is obtained for each hydrocarbon, whether it is derived from calculations based on the behavior of mixtures with substances of higher, or of lower parameter.

Acknowledgments.—The director of this work (J. B. H.) gratefully acknowledges the assistance of a grant from the National Science Foundation, a part of the time made available by which was spent on this work; the authors acknowledge the assistance of the Atomic Energy Commission (as represented by Carbide and Carbon Chemicals Co.), the Minnesota Mining and Manufacturing Co., and the National Lead Co. in making samples of materials available free or at special prices.

TRACER ELECTROPHORESIS. II. THE MOBILITY OF THE MICELLE OF SODIUM LAURYL SULFATE AND ITS INTERPRETATION IN TERMS OF ZETA POTENTIAL AND CHARGE[1]

BY D. STIGTER[2] AND K. J. MYSELS

Contribution from the Department of Chemistry, University of Southern California

Received July 23, 1954

Measurements of electrophoretic mobility of micelles of sodium lauryl sulfate in water and salt solution at finite concentration of micelles are extrapolated to infinite dilution of micelles. Corresponding zeta potentials and charges at the shear surface of the micelle are calculated according to several theories including new modifications of Booth's approach. The great effect of the curvature of the double layer and of relaxation effects is thus established for these systems which are far from ideal even at the CMC. A comparison of the zeta potential with that calculated from the charge of the lauryl sulfate ions forming a smooth micelle with a diffuse double layer leads to a large discrepancy. A "roughness" of the surface of the micelle is therefore suggested. The calculations involved required the computation of charge–potential and of potential–distance relations for double curved layers at high potential. These general problems are dealt with in appendixes.

The size, charge and shape of a micelle, besides their intrinsic interest, provide experimental tests for any theory of association colloids, yet they are still a matter of uncertainty. In the present paper we shall present accurate measurements of the electrophoretic mobility of micelles of pure sodium lauryl sulfate (NaLS) obtained by the tagging technique suggested by Hoyer.[3] This mobility is obviously related to the charge, size and shape of the micelle and to the composition of the solution. These relations are not yet fully elucidated but it is shown that they lead already to a reasonably accurate estimate of the ζ potential and of the charge of the micelle. The ζ potential is quite high: 65–100 mv. and the charge corresponds to 25–30% ionization, which is not readily explainable by the conventional picture of a smooth micelle surface. Since the experimental accuracy greatly exceeds that of the interpretation, the present data should be capable of yielding more accurate estimates of charge as the theories are developed further.

Experimental

Methods and Materials.—The open tube method of measuring electrophoretic mobilities[4] and the sodium lauryl sulfate[5] and orange OT tracer[5] used have all been described previously. Oil red N-1700 obtained from the American Cyanamid Co. was purified by solution in acetone and precipitation with water repeated twice and followed by double recrystallization from ethanol–benzene.

Validity of the Method.—Three questions may be raised concerning the validity of our measurements. Is the mobility of the tracer accurate? Does introduction of the tracer dye modify the micelle? Does the mobility of the tracer equal that of the micelle? The first question has already been discussed in the first paper of this series.[4] The second question, about the disturbing effect of the dye, has been partially answered previously[6] but we can add the following: (a) Dr. H. W. Hoyer has found[7] that two different dyes, Sudan IV and Nile black, give the same mobilities (3.52 and 3.51 $\times$ 10^{-4} cm.^{2} v.$^{-1}$ sec.$^{-1}$, respectively) for the micelle of 5% potassium laurate solutions and we have found that orange OT and oil red N-1700 in 3.5% solutions of sodium lauryl sulfate give the same mobilities (3.70, 3.75 and 3.74, 3.73 $\times$ 10^{-4} cm.^{2} v.$^{-1}$ sec.$^{-1}$, respectively). It would be quite a coincidence if the disturbing effect of different dyes were significant and yet the same. (b) The fact that orange OT in saturated solution does not affect measurably the critical micelle concentration of sodium

(1) Presented in part at the J. W. McBain Memorial Symposium of the Division of Colloid Chemistry at the American Chemical Society meeting, Chicago, September, 1953.

(2) Bristol Myers Company Fellow, 1952–1953. Present address, Shell Research Laboratories, Amsterdam, The Netherlands.

(3) H. W. Hoyer and K. J. Mysels, THIS JOURNAL, **54**, 966 (1950).

(4) H. W. Hoyer, K. J. Mysels and D. Stigter, *ibid.*, **58**, 385 (1954).

(5) R. J. Williams, J. N. Phillips and K. J. Mysels, *Trans. Faraday Soc.*, submitted.

(6) K. J. Mysels and D. Stigter, THIS JOURNAL, **57**, 104 (1953).

(7) Ph.D. Dissertation, 1951, University of Southern California.

lauryl sulfate[5] suggests strongly that its effect on other micellar properties should be negligible.

There remains the question of identity of mobility of dye and micelle or in other words, whether the dye moves only by "riding" in a micelle. This is to be anticipated qualitatively because of the low mobility of the dye and its virtual insolubility in water.

Quantitatively, we may assume that in a given soap solution a constant fraction K of the total dye concentration C is dissolved in water and the remainder $(1 - K)C$ is solubilized by the micelles. The total transport of dye J is the sum of the transport j_w in water and that j_m in the micelle with corresponding mobilities U, u_w and u_m. Hence

$$j_w = Ku_wC \text{ and } j_m = (1 - K)u_mC$$

then

$$J = UC = [Ku_w + (1 - K)u_m]C$$

or

$$U = u_m\left[1 - K\left(1 - \frac{u_w}{u_m}\right)\right]$$

For a non-ionic dye the ratio u_w/u_m vanishes and for any water insoluble, easily solubilized dye K must be negligible.

Colorimetric measurements on orange OT solution[5] show that even in our most dilute solutions K does not exceed 1.5×10^{-3} so that any difference between the mobility of this tracer and of the micelle is well within experimental error.

Oil red N-1700 is more soluble in water and less easily solubilized by micelles so that K in this case is larger. We found that the mobility of this dye in dilute (0.45%) solution of NaLS was lower by $5 \pm 2\%$ than that of orange OT while in more concentrated (3.5% NaLS) solution, where K is much smaller, the difference of mobilities was negligible as pointed out above. This confirms qualitatively the above reasoning, although the lack of precision does not permit quantitative proof.

Results.—The results of our measurements are shown in Fig. 1. Each open circle represents an individual measurement. Only measurements in which a source of error, such as a leak, was clearly apparent are omitted.

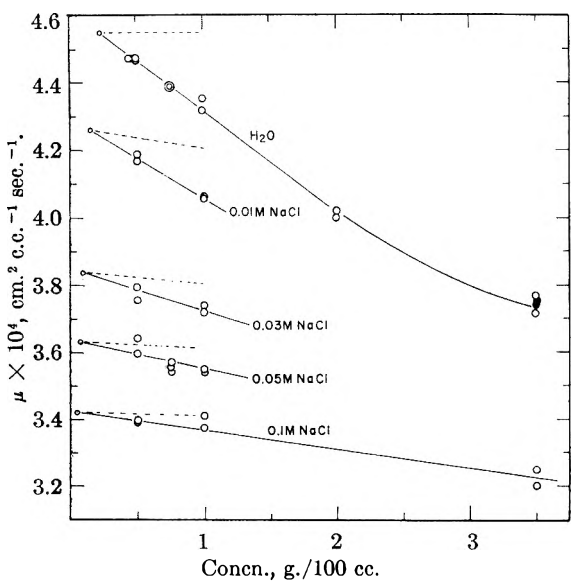

Fig. 1.—Electrophoretic mobility at 25° of sodium lauryl sulfate micelles in water and salt solution: ○, orange OT tracer: ●, oil red N 1700 tracer; o, extrapolated values at the CMC.

Interpretation

Any interpretation of the experimental results is bound to involve a model of the system. Our considerations are based on a spherical micelle (which is the only one susceptible of exact calculations) surrounded by an electrical diffuse double layer which neutralizes its charge and whose average thickness depends on the effective ionic strength of the solution, *i.e.*, the ionic strength prevailing outside of these double layers. Both sodium chloride, when present, and any unassociated NaLS contribute to this effective ionic strength.

Several theories of electrophoretic behavior of colloidal ions in the presence of small ions are known and we shall discuss them in some detail later. None of them takes into account the interaction of the colloidal ions with each other. These theories can therefore be applied only at "infinite dilution of micelles," yet as shown by the slope of lines of Fig. 1 this interaction has a marked effect. Infinite dilution of micelles may be assumed at the critical micelle concentration (or CMC) if properly defined.[5] Therefore, mobility values at the CMC are needed and these can be obtained only by extrapolation.

Extrapolation.—Extrapolation requires a theory of micellar interaction. An outline of such a theory has been proposed elsewhere,[8] and the present data extrapolated according to it. We assume that the repulsion of electric double layers prevents any direct interaction of micelles except where the volume occupied by the double layers is so high that they must overlap. This is the case in water alone above about 2% concentration and explains the curvature found in this region. Otherwise the true mobility of the micelle, with reference to the solvent and at constant salt concentration in the bulk of the solution, remains the same. However, Cl^- ions are mostly excluded from the solution within the double layer so that as the concentration of NaLS increases the salt concentration in the bulk of the solution increases and the mobility of the micelle correspondingly decreases. The slopes thus calculated are shown by the dotted lines in Fig 1. The remaining large part of the slope is attributed to a linear effect of back flow of solution entrained by the double layers as suggested by Enoksson[9] for sedimentation rate. This frame-of-reference effect is interpolated for intermediate concentrations from values obtained for the well-defined slopes at 0, 0.01 and 0.1 M NaCl. Finally, these slopes are fitted to the points for each concentration.

The average deviation of experimental points from the lines is 0.35% which is only slightly more than the error due to colorimetric dye determinations. The extrapolated mobilities are given closely by the relation $\log_{10} u = 3.582 - 0.115 \log_{10} C$, where C is the total molarity of Na^+ ions at the CMC. It may be noted that any reasonable extrapolation gives results within about 1.5% for the mobilities at the CMC.[10]

The ζ Potential.—This potential between the shear surface of the micelle and the bulk of the solution is related to the mobility at the CMC u, the "thickness" of the double layer $1/\kappa$, and

(8) D. Stigter, *Rec. trav. chim.*, **73**, 605 (1954); Thesis, Utrecht 1954. Due to the use of less accurate values of parameters the ζ potentials quoted are slightly too low.

(9) B. Enoksson, *Nature*, **161**, 934 (1948).

(10) The CMC values used are from the best line of reference 5.

the radius a of the micelle. For the radius a of the micelle we take the results of molecular weight determination by light scattering[11] assuming a density of 1.14 and a monomolecular hydration layer 1.5 Å. thick. This agrees with values obtained from self diffusion measurements[12] within the accuracy of the latter. The ionic strength determining $1/\kappa$ is taken as due to the total NaLS present at the CMC plus any NaCl added. Other constants used are $\lambda_{Na+} = 45$, $\lambda_{C_{12}-} = 70$, $\lambda_{LS-} = 18$ for ionic mobilities; $D = 78.5$ for the dielectric constant; and $\eta = 0.894$ centipoise for the viscosity of the solvent.

The relation between mobility and zeta potential can be always expressed as a power series in ζ

$$u = C_1\zeta + C_2\zeta^2 + C_3\zeta^3 + C_4\zeta^4 \ldots \qquad (1)$$

Theories of electrophoretic mobility deal with the values of the coefficients C_i.

The first approximation was given by Smoluchowski,[13] who set $C_1 = D/4\pi\eta$ and omitted the higher terms. This is valid for a double layer which is flat or thin compared to the radius of the particle, *i.e.*, $\kappa a \gg 1$. Henry[14] took into account the commensurate dimensions of the particle and its double layer and obtained C_1 as a function of κa varying between Smoluchowski's value and $D/6\pi\eta$ while the higher terms are again omitted.

Henry's formula is valid if deformation of the double layer by the electrophoretic motion is negligible. To take this deformation or relaxation effect into account Overbeek[15] calculated the two next terms, C_2 and C_3, for the general case. Later Booth[16] investigated the case of symmetrical electrolytes where $C_2 = 0$ and obtained expressions for C_3 and C_4. In both these treatments C_1 has the value calculated by Henry and the higher C's are function of κa and of the mobilities of the ions present. The C_3 term is common to both treatments and despite independent derivation and different form, its value is the same within the computational error of about 3%.

Normally u is the experimentally accessible quantity and ζ the calculated one. The application of Overbeek's and especially Booth's expression is quite awkward as it involves the solution of third and fourth degree equations, respectively. A great simplification may be obtained by inverting series (1). For the case at hand of a symmetrical salt where $C_2 = 0$ we obtain

$$\zeta = \frac{u}{C_1} - \frac{C_3}{C_1}\left(\frac{u}{C_1}\right)^3\left[1 - \left(\frac{C_3}{C_1}\right)^3\left(\frac{u}{C_1}\right)^6 - \left(\frac{C_4}{C_1}\right)^3\left(\frac{u}{C_1}\right)^9 \cdots\right] - \frac{C_4}{C_1}\left(\frac{u}{C_1}\right)^4\left[1 - \left(\frac{C_3}{C_1}\right)^4\left(\frac{u}{C_1}\right)^8 - \left(\frac{C_4}{C_1}\right)^4\left(\frac{u}{C_1}\right)^{12} \cdots\right] \cdots \qquad (2)$$

The series in square brackets converge very rapidly for the present data and may be set equal to unity without introducing a significant error. Then, with Booth's notation for the coefficients C, and introducing dimensionless units, (2) becomes

$$\Phi_0 = \frac{u'}{X_1^*} - \frac{X_3^* + Y_3^* + q_3^* Z_3^*}{X_1^*}\left(\frac{u'}{X_1^*}\right)^3 - \frac{q_4^* Z_4^*}{X_1^*}\left(\frac{u'}{X_1^*}\right)^4 \cdots \qquad (3)$$

where $\Phi_0 = e\zeta/kT$ ($\zeta = 25.7$ mvolts for $\Phi_0 = 1$ at 25°) and $u' = (6\pi\eta e/DkT)u$ ($u' = 0.75_2$ for $u = 10^{-4}$ cm.^{2} volt^{-1} sec.$^{-1}$ at 25° in water). The factors X^*, Y^* and Z^* depend on κa only[14] while q^* is related to the ionic mobilities.[17]

Figure 2 shows ζ values computed from the extrapolated values of Fig. 1 using equation 3 when successive terms are taken into account and also the results obtained with Smoluchowski's expression. Their comparison shows clearly that in our systems, taking into account the thickness of the double layer increases the ζ value by some 50% and introduction of relaxation effects raises it by another 15–20%.

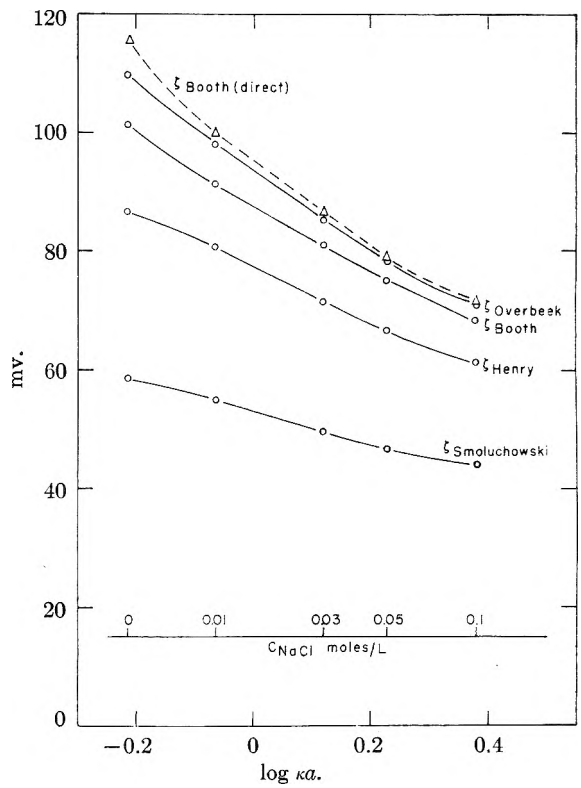

Fig. 2.—Zeta potentials of micelles of sodium lauryl sulfate at the CMC in water and salt solutions as calculated by several theories.

We have also used the original Booth series. The results, shown by the broken line in Fig. 2, are some 10% higher than those of the inverted series. This difference is not surprising since only an infinite series is identical with its inverted form. It is very difficult to estimate the error in ζ when the original Booth equation is to be solved for ζ. On the other hand, the error introduced by omission of higher terms in the inverted series is expected to be of the order of the last term accounted for, *i.e.*, $\zeta_{Booth} - \zeta_{Overbeek}$, provided that the

(11) J. N. Phillips and K. J. Mysels, THIS JOURNAL, submitted.

(12) D. Stigter, R. J. Williams and K. J. Mysels, *ibid.*, submitted.

(13) M. Smoluchowski, *Z. physik. Chem.*, **93**, 129 (1918).

(14) D. C. Henry, *Proc. Roy. Soc.* (*London*), **A133**, 106 (1931).

(15) J. Th. G. Overbeek, *Koll. Beih.*, **54**, 316 (1943); Thesis, Utrecht, 1941.

(16) F. Booth, *Proc. Roy. Soc.* (*London*), **A203**, 514 (1950); on p. 530, line 17, $X_1^*(b)$ should read $2/3X_1^*(b)$.

(17) Numerical values of $q^*/6$ are given in reference 15, page 316, table 3.

series converges somewhat regularly, which seems to be the case here. The inverted series should therefore give quite reliable results.

We have also investigated the effect of changing q^* and κa on ζ_{Booth}. A 10% change of q^* changes ζ_{Booth} by about 0.7%. This shows that our assumption of constant λ values does not introduce any significant error. A 10% change of κa shifts ζ_{Booth} by only 0.1%. Therefore, our computation of κ cannot introduce any significant error. Furthermore, moderately large variation in a, *i.e.*, in the radius of curvature of the micelle surface, is immaterial. Hence, the spherical model of the micelle can be replaced by an ellipsoidal one without changing the calculated ζ potential significantly.

The Micellar Charge by Booth's Method.—The mobility can also be expanded in terms of the charge Qe of the particle. Booth has computed the coefficients of such a series up to the $(Qe)^4$ term in the case of symmetrical electrolytes.

This series is similar to that of u in ζ, equation 1. However, the numerical solution is more difficult. We have inverted it and obtained a series of the same form as (2) with stars omitted from X^*, Y^* and Z^*, and with Φ_0 replaced by

$$R = Qe^2/aDkT \qquad (4)$$

(for $R = 1$ and a in cm., $Q = 0.1401a \times 10^8$ at 25° in water). This inverted series can be used readily in calculations. Figure 3 shows the values it yields upon taking successively into account the first term (Q_{Henry}), the second (Q_{Overbeek}) and the third (Q_{Booth}).

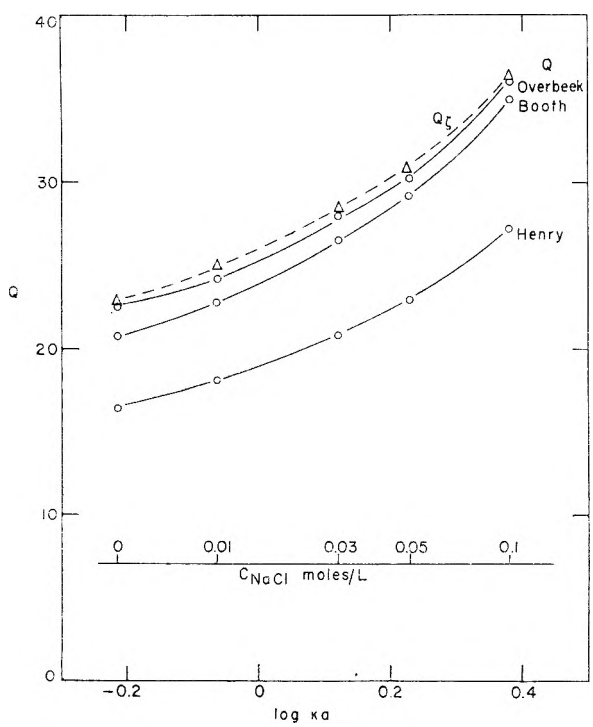

Fig. 3.—Micellar charge of sodium lauryl sulfate at the CMC in water and salt solutions as calculated by several theories.

Comparison of Figs. 2 and 3 shows that the convergence of the two series giving ζ and Q respectively, in terms of u is different. It is therefore of interest to compare them more closely.

The Micellar Charge from ζ Potential.—For low potentials the relation between the charge Q and the ζ potential is given by

$$R = (1 + \kappa a)\Phi_0 \qquad (5)$$

which connects the first, or Henry, terms of the two series. For higher potentials, when nonlinear terms become important, a correction factor must be introduced. Appendix I gives a method of estimating this correction factor. The results thus obtained from ζ_{Booth} are also shown in Fig. 3 as Q_ζ. They are some 10% higher than Q_{Booth} and even somewhat higher than Q_{Overbeek}.

The average ζ potential and the total particle charge are unaffected by the electrophoretic motion under the assumptions of the Booth theory. Hence the assumption of an undistorted spherical double layer in the calculation of Q_ζ, cannot cause the difference between Q_{Booth} and Q_ζ. The discrepancy must therefore lie in the neglected higher terms of the series.

The series for ζ converges faster than the one for Q. It appears therefore that the error produced by neglecting higher terms is lesser in calculation of ζ from u than Q from u. Since the calculation of Q from ζ involves few inaccuracies we feel that Q_ζ should be closer to the truth than Q_{Booth}.

As already mentioned, ζ is not sensitive to changes in κa, but this is no longer true for Q which changes by about 1% when κ changes by 1% or a by 0.5%.

Comparison with Other Calculations of Charge.—When ion atmosphere effects are negligible, the mobility of an ion is equal to the force exerted by its charge in unit field divided by its friction factor. The latter may be calculated either from Stokes law or by multiplication of the friction factor of the monomeric ion by the cube root of the degree of association. These two calculations give results within 20% of each other but the values of the charge thus calculated for our case decrease (from 10.4 and 8.7 to 8.7 and 7.3, respectively) instead of increasing as the concentration of NaCl increases and amount to only 50 to 25% of Q_ζ. This emphasizes the danger of considering micelles as ideal electrolytes even under conditions of infinite dilution with respect to micelles.

From the slope of light scattering plots one can compute a charge p which is an effective thermodynamic charge.[18] For our case the charge p is essentially constant at about 14.[11] The ratio of Q_ζ and p gives an indication of the activity coefficients to be expected in these solutions.

The Degree of Ionization.—The micellar charge can be also expressed as a degree of ionization, $\alpha = Q/n$, where n is the number of anions in the micelle. α is slightly less sensitive to errors in a than Q since a is related directly to n^3.

Summary of Results.—Table I summarizes the properties of micelles of sodium lauryl sulfate at the CMC as they emerge from the present discussion. It may be noted that while both the size and charge

(18) J. T. Edsall, H. Edelhoch, R. Lontie and P. R. Morrison, *J. Am. Chem. Soc.*, **72**, 4641 (1950); K. J. Mysels, THIS JOURNAL, **58**, 303 (1954).

TABLE I

THE CALCULATION OF ZETA POTENTIAL AND CHARGE OF MICELLES OF SODIUM LAURYL SULFATE AT 25°

m_{NaCl}	CMC,[a] mmoles/l.	n[b]	$\mu_c \times 10^4$, cm.^{2} v.$^{-1}$ sec.$^{-1}$	a,[c] cm. $\times 10^{-8}$	κa	ζ_{Booth}, mv.	Q_ζ	α[d]
0	8.12	80	4.55	21.5	0.61	101.2	22.9	0.287
.01	5.29	89	4.26	22.1	0.86	92.3	25.1	281
.03	3.13	995	3.84	23.0	1.32	80.9	28.5	285
.05	2.27	1045	3.63	23.4	1.69	75.0	30.9	295
.1	1.46	112	3.42	24.0	2.40	68.3	36.3	324

[a] Best line of reference 5. [b] Degree of association, reference 11. [c] Hydrated radius from n, with density 1.14 and 1.5 Å. hydration layer. [d] Degree of ionization = Q_ζ/n.

increase upon the addition of salt, the degree of ionization remains constant within the uncertainty of the determination.

Structural Consequences.—In this section we shall assume that the polar heads of the anions are distributed uniformly over the spherical surface of the micelle. This is equivalent to assuming an essentially liquid interior of the micelle. However, a more highly organized micelle, in which the polar heads are closer together, would only make the argument more cogent.

The n charges of all the anions, or the native charge of the micelle, distributed uniformly over the surface of the unhydrated micelle (radius = a − 1.5 A.) give rise at this surface to a potential ψ°. The first approximation ψ°_{coul} is calculated simply from Coulomb's law, the second ψ°_{DH} uses the first (Debye–Hückel) approximation of the diffuse double layer, and ψ°_{Gouy} uses the treatment presented in Appendix II for estimating correctly the effect of this double layer. The results summarized in Table II show that the diffuse double layer reduces the coulombic potential to a small fraction and that the Debye–Hückel approximation is inadequate under the high charge conditions prevailing here.

TABLE II

POTENTIALS AT THE SURFACE OF THE UNHYDRATED MICELLE

m_{NaCl}	ψ°_{coul}, mv.	ψ°_{DH}, mv.	ψ°_{Gouy}, mv.	ζ_{Booth}, mv.	Δ, Å.
0	720	450	190	101.2	7.4
.01	780	430	178	92.3	6.6
.03	830	370	161	80.9	5.6
.05	860	330	150	75.0	4.8
.1	900	280	136	68.3	4.0

The ζ potential is, as would be expected, lower than ψ° since it is measured at the surface of the hydrated micelle some 1.5 Å. further out. The surprising fact is, however, that it is so much (45–50%) lower.

If a diffuse double layer and dielectric constant of 80 are assumed, the empirical relation between potential and distance given by Hoskin[19] and discussed further in Appendix II shows that the potential drop from ψ°_{Gouy} to ζ_{Booth} should not occur until a distance Δ (shown in Table II) varying between 7.4 and 4.0 Å. from the surface of the unhydrated micelle. The discrepancy between the calculated and experimental values seems to be far beyond either experimental or computational errors.

Thus it appears that the sodium gegenions are concentrated at the surface of the micelle and within the surface of shear to a much greater extent than is predicted from the simple Gouy model. Introduction of finite ionic radii would only increase the discrepancy since the gegenions could not get as close to the micelle.

We are therefore faced with the necessity of introducing a new factor which would facilitate the adsorption of the gegenions on the surface of the micelle. Specific interactions, leading to partial dehydration and chemisorption, are unlikely in view of the small effect of the nature of gegenions on the critical micelle concentration.

The Rough Micelle.—A more plausible explanation lies in the fact that the surface of the micelle is not likely to be smooth, with polar heads partially buried in the hydrophobic body of the micelle. On the contrary, the heads may be expected to rise above the surface so as to expose their whole polar area to water. If they are distributed uniformly, each has about 60 Å.^{2} available, *i.e.*, some 2.5 times the area occupied in close packed monolayers. The smaller sodium ions should therefore be able to penetrate between the polar heads while remaining hydrated. This arrangement, of course, favors the adsorption of the gegenions by purely electrical forces in the high potential region around each polar head within the hydration layer of the micelle.

Thus the roughness of the micelle may explain its relatively low degree of ionization.

Acknowledgment.—We are indebted to Dr. C. I. Dulin for determining the K value of oil red, to the Bristol Myers Co. for its generous support through most of this work, and to the Office of Naval Research for providing through Project ONR-356-254 the materials and equipment used in this study. One of us (D. Stigter) had the invaluable benefit of many stimulating discussions with Prof. J. Th. G. Overbeek while developing the theoretical part of this work.

Appendix I

The Potential–Charge Relation.—For high potentials relation (5) must be replaced by

$$R = \beta(1 + \kappa a)\Phi_0 \qquad (6)$$

The correction factor β can be expanded in even powers of Φ_0

$$\beta = 1 + A_2\Phi_0^2 + A_4\Phi_0^4 + \ldots \qquad (7)$$

Hoskin[19] found that this series converges very rapidly by comparing it with results obtained using an electronic computer. The coefficients A_2 and A_4, given in equations (4,2) of his paper, are complicated functions of κa.

(19) N. E. Hoskin, *Trans. Faraday Soc.*, **49**, 1471 (1953).

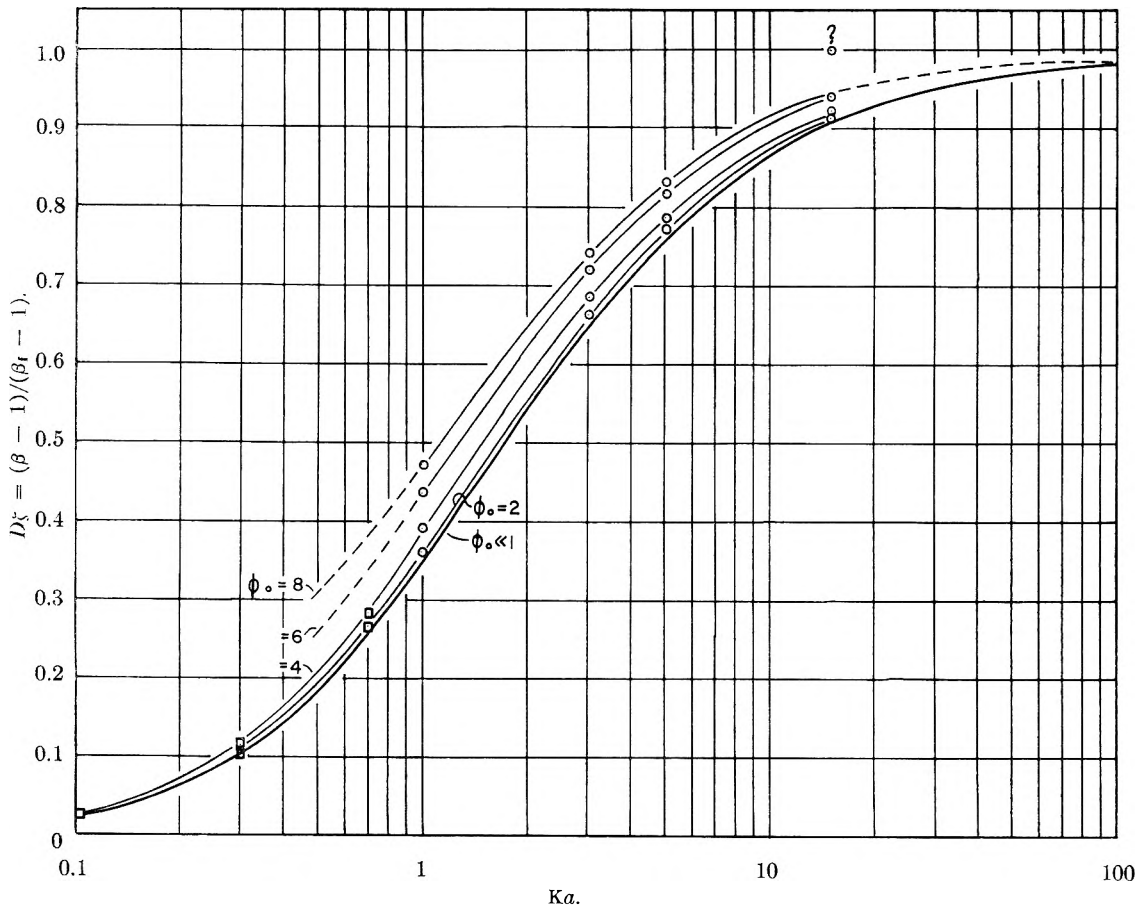

Fig. 4.—Interpolation function for the charge–potential relation. Circles based on Haskin's computation, squares on series (7). Lowest line $D_Q = A_2/24$.

From the known explicit expression of Verwey and Overbeek[20] for the surface charge of a flat double layer, one obtains for the limit β_f of β as κa becomes infinite

$$\beta_f = \frac{2}{\Phi_0} \sinh \frac{\Phi_0}{2} \tag{8}$$

or, after expansion

$$\beta_f = 1 + \frac{\Phi_0^2}{24} + \ldots \tag{9}$$

It is advantageous to introduce the function

$$D_Q(\Phi_0, \kappa a) = \frac{\beta(\Phi_0, \kappa a) - 1}{\beta_f(\Phi_0) - 1} \tag{10}$$

For any Φ_0 this function compares the deviation of the Debye–Hückel approximation from the real value with its deviation from the Verwey and Overbeek value for a flat surface. For $\Phi_0 \ll 1$ the expression for D_Q reads, in view of equations 7 and 9, $D_Q = A_2/24$. In Fig. 4, D_Q is plotted *versus* log κa. The open circles have been derived from Hoskin's β-values (electronic computer) and equation 3. The squares have been calculated with series (7) and equation (8).

Although the latter values for $\Phi_0 = 4$ might be slightly too low because terms higher than Φ_0^4 were omitted in series (7), the points indicate that all curves follow quite closely the one for $\Phi_0 \ll 1$.

(20) E. J. W. Verwey and J. Th. G. Overbeek, "Theory of Stability of Lyophobic Colloids," Elsevier Publishing Co., New York, N. Y., 1948, pp. 25–26.

As Φ_0 increases the effective thickness of the double layer decreases, the system resembles more a flat double layer and the curves shift toward $D_Q = 1$.

If Φ_0 is finite, κa tends to zero as a approaches this limit. Under these conditions, the average potential within the double layer also tends to zero so that the Debye–Hückel approximation becomes valid.[21] Therefore, $D_Q = 0$ for $\kappa a = 0$. On the other hand, according to its definition by (10), $D_Q = 1$ for $\kappa a = \infty$.

The curve for $\Phi_0 \ll 1$ and the points in Fig. 4 permit rather precise estimates of D_Q for any values of Φ_0 and κa and the relevant value of β can then be obtained directly with the help of equations 10 and 8.

Appendix II

The Potential Distance Relation.—The empirical equation given by equations (4,3) of Hoskin[19] reads in our notation

$$\Phi = \Phi_0 \frac{b}{x} e^{b-x} \left[\frac{1}{\gamma} + \left(1 - \frac{1}{\gamma}\right) e^{2(b-x)} \right] \tag{11}$$

with $b = \kappa a$ and $x = \kappa r$, $r - a$ is the distance from the surface of the spherical particle.

The expression in brackets is a correction to the Debye–Hückel approximation represented by the preceding factor. For large values of $b - x$, *i.e.*, far from the surface, the correction factor is a constant and equals $1/\gamma$.

(21) *Cf.* G. S. Hartley, *Trans. Faraday Soc.*, **35**, 31 (1935).

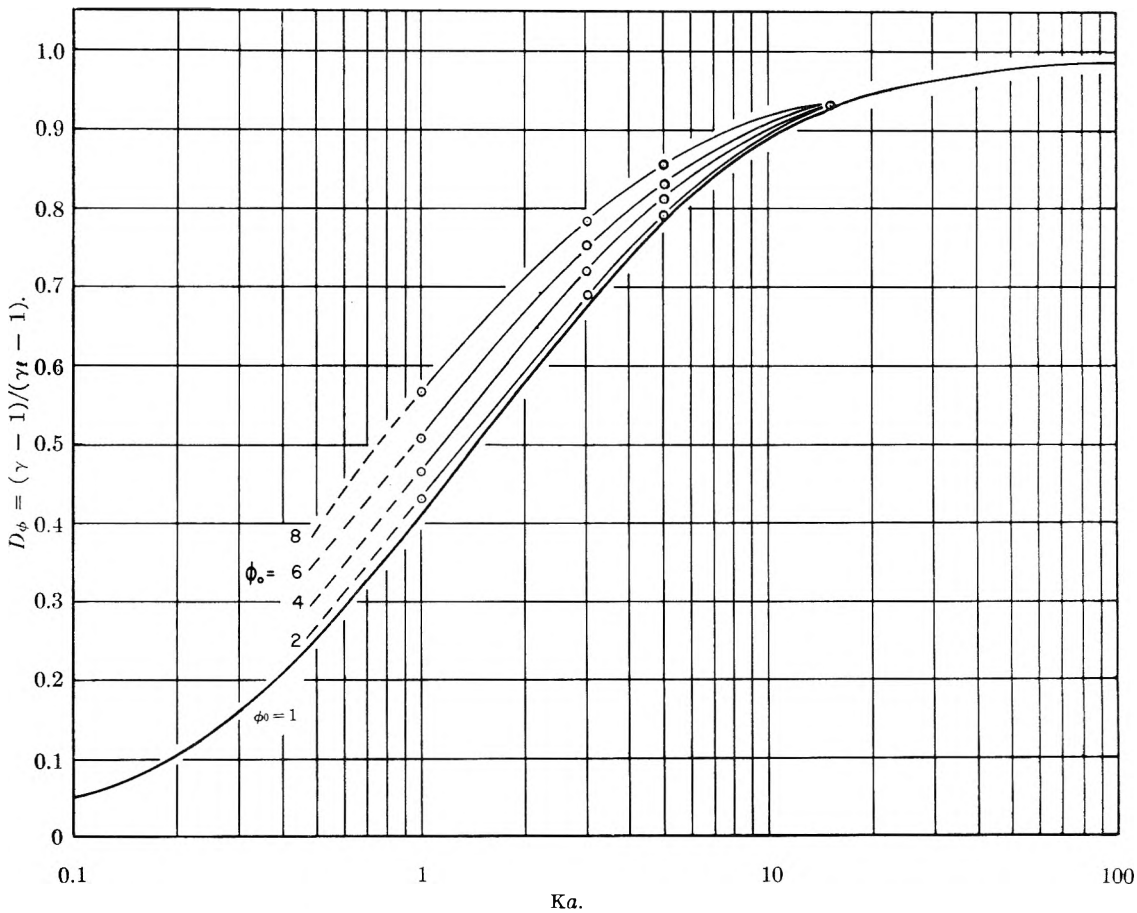

Fig. 5.—Interpolation function for the potential–distance relation, lowest line from equation (13).

The factor γ is a function of Φ_0 and of κa and can be estimated by a procedure analogous to that described in Appendix I.

In the limiting case of $\kappa a = \infty$, γ can be computed by Verwey and Overbeek's explicit potential–distance relation in a flat double layer.[21] Some values are as follows

Φ_0	0	1	2	3	4	5	6	8
γ_f	1	1.019	1.079	1.178	1.309	1.474	1.656	2.08

It is convenient to define the interpolation function

$$D\Phi(\Phi_0, \kappa a) = \frac{\gamma(\Phi_0, \kappa a) - 1}{\gamma_f(\Phi_0) - 1} \qquad (12)$$

which again compares the deviations of the Debye–Hückel approximation for any Φ_0 from the true value for κa and for the flat double layer.

For $\Phi_0 \ll 1$ the value of D_Φ can be computed by the expression

$\Phi_0 \ll 1$

$$D_\Phi = 8b^2[2e^{4b}E(4b) - e^{2b}E(2b)]$$

$$\text{with } E(u) = \int_u^\infty \frac{e^{-u}}{u}\,du \qquad (13)$$

which is derived from the series given by Gronwall, LaMer and Sandved[22] to express Φ in powers of the particle charge. The lower curve of Fig. 5 shows the values thus computed. The points for higher Φ_0 values have been computed with Hoskin[18] values of C_∞ ($= 1/\gamma$) and Table IV.

For all values of Φ_0, $D_\Phi \to 0$ for $\kappa a \to 0$ and $D \to 1$ for $\kappa a \to \infty$. D_Φ is similar to D_Q and the dotted lines have been drawn accordingly. In fact both functions may be regarded as measures of the effect of divergence of the electric field in the double layer around the spherical particle. This may explain the position of the transition range in the neighborhood of $\kappa a = 1$.

Equation 12 with Fig. 5, and the table of γ_f values, permits a precise estimate of γ for any system of given Φ_0 and κa. The potential at any point is then given rapidly by equation 11.

(22) T. H. Gronwall, V. K. LaMer and R. Sandved, *Physik. Z.*, **28**, 358 (1928).

QUATERNARY LIQUID SYSTEMS WITH THREE LIQUID PHASES

BY GEORGE M. HARTWIG, GEORGE C. HOOD AND RUSSEL L. MAYCOCK

Shell Development Company, Emeryville, California

Received July 26, 1954

Liquid phase equilibrium data are presented for the systems acetonitrile–water–benzene–heptane at 25° and sulfolane–water–benzene–heptane at 25°. A detailed discussion of the phase behavior of three liquid phase regions is given using the acetonitrile system as an example.

Introduction

Relatively few data exist for systems comprised of four liquid components. A summary published in 1949 lists only fifteen different systems which have been investigated.[1] More recently data concerning four quaternary liquid systems with two immiscible liquid pairs have been published.[2] This paper presents data on two new systems (benzene–heptane–sulfolane–water and benzene–heptane–acetonitrile–water) and gives an interpretation of the phase behavior in the regions containing three liquid phases.

Experimental

The materials used in this investigation were purified as follows.

Benzene.—Solvent grade material was purified by azeotropic distillation. Acetone was used as the entraining agent to remove impurities like cyclohexane. The benzene was then distilled through a 20-plate Oldershaw column at a reflux ratio of 10 in order to obtain a heart cut. The refractive index of the heart cut was $n^{20}D$ 1.5013.

Heptane.—Solvent grade material was purified by passage through a silica gel bed in order to remove aromatics. The heptane was then distilled through a 20-plate Oldershaw column at a reflux ratio of 10 in order to obtain a heart cut. The refractive index of the heart cut was $n^{20}D$ 1.3864.

Sulfolane.[3]—Material synthesized by the Shell Development Company was purified by a vacuum flash distillation. The purity of a heart cut was established by the m.p., namely, 27.4 ± 0.1°.

Acetonitrile.—Eastman Kodak Company material was used without further purification, $n^{20}D$ 1.3446.

The equilibrium liquid phase compositions of various gross starting mixtures were determined by the following procedure. The starting mixture which always contained a hydrocarbon to non-hydrocarbon ratio of 1 was placed in a pressure vessel constructed of heavy walled glass tubing sealed to a half inch glass industrial joint. A stainless steel fitting, containing the sampling lines and valves, was attached to the industrial joint and sealed with a Teflon gasket. Teflon O rings were used for valve seats and as valve packing. Small bore tubing was used for the sampling lines to minimize holdup. The pressure vessel was shaken in a thermostated bath of silicone oil by an air driven piston. After vigorous shaking for a half hour equilibrium was presumed to have been attained. This was checked on occasion by shaking samples ten minutes longer and analyzing. No differences from the half hour results were detected. The phases were allowed to separate for an hour or longer before sampling. When the phase separation was complete, samples of the phases were forced out of the pressure vessel by nitrogen pressure. The first few ml. of liquid were discarded and then samples for analysis were withdrawn.

Analysis of the phases was accomplished by first separating the hydrocarbons from the non-hydrocarbons. The samples containing acetonitrile were processed by water washing. A weighed portion of one of the equilibrium phases was mixed with about seven times its volume of water in a Babcock bottle, weighed and centrifuged. The hydrocarbon collected in the neck of the bottle; a small portion of the hydrocarbon layer was removed for refractive index analysis. The remaining hydrocarbon was removed by withdrawing it with a hypodermic syringe, being careful not to approach the interface too closely.

Isopentane was added to the thin layer of hydrocarbon remaining, and the mixture removed in the same way. This procedure was repeated until no visible hydrocarbon remained after evaporation of the isopentane. The bottle and its contents were then weighed, the loss in weight being considered to represent the original hydrocarbon content.

The samples containing sulfolane were processed by distillation. A weighed portion of one of the phases together with a small amount of water was distilled in a micro Podbielniak column. This column was 8 mm. in diameter, 12 inches long, and had a holdup of only 0.2 g. A reflux ratio of 2/1 was used. All of the hydrocarbon and a small amount of water were distilled into a Babcock bottle. Water was added to fill the bottle, and the remaining steps were the same as described above for the water washing method.

The relative amounts of benzene and heptane in the hydrocarbon mixtures withdrawn from the Babcock bottles were obtained from refractive index measurements; a formula of the type

$$w = \frac{b - n}{(b - n) + k(n - a)}$$

where

w = wt. fraction heptane
n = refractive index of mixture at 20°
a = refractive index of pure heptane
b = refractive index of pure benzene
k = a constant

was found to correlate the refractive index with the weight fraction of heptane in a mixture. The value of k was determined by measuring the refractive indices of several weighed mixtures of benzene and heptane. An average value of k = 1.53 was found for nine experiments with benzene–heptane mixtures. Using this value of k the composition of the original mixture could be calculated from the refractive indices to an accuracy of ±0.002 weight fraction.

The amount of water in the samples was obtained by analysis of separate samples using the standard Fisher method.

The amount of acetonitrile or sulfolane in the samples was calculated by difference, knowing the hydrocarbon and water content of the samples.

The data obtained are given in Tables I and II.

Results

As shown by the data the systems acetonitrile–water–benzene–heptane at 25° and sulfolane–water–benzene–heptane at 25° possess regions where three liquid phases coexist. At 100° the system sulfolane–water–benzene–heptane no longer possesses a three liquid phase region. The phase behavior of these types of quaternary systems will be discussed using the system acetonitrile–water–benzene–heptane as an example.

A simplified, out of actual scale, schematic diagram of this system is shown as Fig. 1. This figure shows only the ternary relationships on each of the faces of the tetrahedron. Two of the faces have binodal curves a,b,c and g,h,f with plait points

(1) J. C. Smith, *Ind. Eng. Chem.*, **41**, 2932 (1949); **42**, 1438 (1950).
(2) Y. C. Charg and R. W. Moulton, *ibid.*, **45**, 2350 (1953).
(3) The structural formula for sulfolane is

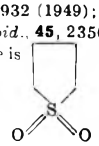

TABLE I

ACETONITRILE–WATER–BENZENE–HEPTANE

Temp. = 25°, non-hydrocarbon/hydrocarbon = 1 for quaternary mixtures, A = acetonitrile, W = water, B = benzene, H = heptane. All compositions are weight per cent.

Components	Starting mixture	Top phase	Bottom phase	Starting mixture	Top phase	Bottom phase	Starting mixture	Top phase	Bottom phase	Middle phase	Starting mixture	Top phase	Bottom phase	Middle phase
B	7.0	5.3	6.2	21.6	18.0	21.0	7.0	9.7	0	3.2	15.6	19.8	0	14.6
H	43.0	91.2	10.6	28.4	73.9	18.1	43.0	87.0	0	2.0	34.4	74.6	0	8.2
A	50.0	3.5	83.2	50.0	8.1	60.9	35.0	3.3	41.5	65.2	27.5	5.6	29.2	67.8
W	0	0	0	0	0	0	15.0	0	58.5	29.6	22.5	0	70.8	9.4
B	7.0	8.8	5.8	25.0	34.8	0	7.0	10.6	0	3.9	21.6	21.6	0	17.7
H	43.0	87.8	5.0	0	0	0	43.0	86.1	0	2.4	28.4	70.4	0	8.1
A	44.9	3.4	79.6	50.0	58.6	18.7	27.5	3.3	40.0	76.1	44.9	8.0	26.9	66.9
W	5.1	0	9.6	25.0	6.6	81.3	22.5	0	60.0	17.6	5.1	0	73.1	7.3
B	7.0	8.6	3.8	16.0	19.2	0	30.4	34.0	0	31.9	21.6	24.1	0	19.3
H	43.0	88.3	2.7	0	0	0	19.6	51.1	0	19.1	28.4	68.5	0	9.5
A	40.0	3.1	74.5	69.0	67.4	26.7	39.6	14.9	19.0	47.0	40.0	7.4	26.8	64.3
W	10.0	0	19.0	15.0	13.4	73.3	10.4	0	81.0	2.0	10.0	0	73.2	6.9
B	15.6	10.6	12.9	30.4	31.7	29.3	15.6	15.9	0	10.3	21.6	25.1	0	22.1
H	34.4	84.3	13.1	19.6	56.7	17.6	34.4	79.2	0	5.3	28.4	66.0	0	11.1
A	50.0	5.1	74.0	47.0	11.4	49.7	42.5	4.9	32.7	71.9	35.0	8.9	25.6	60.7
W	0	0	0	3.0	0.2	3.4	7.5	0	67.3	12.5	15.0	0	74.4	6.1
B	30.0	51.0	0	30.5	39.7	0	15.6	16.7	0	10.9	21.6	28.9	0	29.7
H	0	0	0	19.5	28.0	0	34.4	78.6	0	5.7	28.4	62.2	0	14.3
A	40.0	45.2	20.2	26.9	29.9	22.2	40.0	4.7	32.0	71.2	27.5	8.9	25.4	51.3
W	30.0	3.8	79.8	23.1	1.6	77.8	10.0	0	68.0	12.2	22.5	0	74.6	4.7
B	15.6	14.8	11.1	41.9	54.4	0	15.6	17.7	0	12.2	30.5	34.8	0	27.5
H	34.4	80.6	6.3	8.1	14.6	0	34.4	77.2	0	6.9	19.5	64.7	0	16.3
A	44.9	4.6	73.8	26.9	29.7	17.6	35.0	5.1	32.8	69.1	44.6	0	22.5	51.2
W	5.1	0	8.8	23.1	1.3	82.4	15.0	0	67.2	11.8	5.4	0.5	77.5	5.0

TABLE II

SULFOLANE–WATER–BENZENE–HEPTANE

Temp. = 25°, non-hydrocarbon/hydrocarbon = 1 for quaternary mixtures, S = sulfolane, W = water, B = benzene, H = heptane. All compositions are weight per cent.

Components	Starting mixture	Top phase	Bottom phase	Starting mixture	Top phase	Bottom phase	Starting mixture	Top phase	Bottom phase	Starting mixture	Top phase	Middle phase	Bottom phase
B	41.9	51.1	39.0	...	53.9	0.8	14.9	21.3	8.2	22.9	35.8	...	11.0
H	8.1	38.6	5.3	...	10.3	0.02	35.1	77.8	0.7	27.1	62.5	...	0.6
S	50.0	10.3	55.7	...	34.4	62.5	47.4	0.9	86.4	44.9	1.7	...	79.5
W	0	0	0	...	1.4	36.7	2.6	0.02	4.7	5.1	0.04	...	8.9
B	37.5	48.4	33.6	...	60.0	13.2	7.5	10.8	2.8	14.9	22.6	...	6.5
H	12.5	45.8	4.2	...	29.9	0.4	42.5	88.8	0.4	35.1	76.7	...	0.4
S	50.0	5.8	62.2	...	9.9	70.9	47.4	0.4	91.8	44.9	0.7	...	83.7
W	0	0	0	...	0.2	15.5	2.6	0.01	5.0	5.1	0.002	...	9.4
B	23.9	30.8	21.1	42.6	60.4	37.3	...	89.4	0	7.5	11.1	...	2.5
H	23.5	67.5	1.9	7.4	25.3	3.5	...	0	0	42.5	88.6	...	0.4
S	52.6	1.7	77.0	47.4	14.1	56.0	...	7.8	14.6	44.9	0.3	...	87.4
W	0	0	0	2.6	0.2	3.2	...	2.8	85.4	5.1	0.01	...	9.7
B	11.1	17.8	9.9	37.8	55.8	28.9	...	77.3	0	...	63.1	...	0
H	28.8	81.4	1.2	12.2	36.3	2.3	...	0	0	...	0	...	0
S	60.1	0.8	88.9	47.4	7.7	65.2	...	22.1	24.9	...	36.8	...	35.0
W	0	0	0	2.6	0.2	3.6	...	0.6	75.1	...	0.1	...	65.0
B	9.2	13.6	6.7	30.4	44.4	20.1	37.8	60.2	22.7	...	28.7	...	2.6
H	22.0	85.9	1.0	19.6	52.1	1.3	12.2	29.8	1.1	...	0	...	0
S	68.8	0.5	92.3	47.4	3.4	74.5	44.9	9.8	68.9	...	64.2	...	61.7
W	0	0	0	2.6	0.1	4.1	5.1	0.2	8.1	...	7.1	...	35.7
B	6.2	8.2	3.9	22.9	33.9	14.3	30.4	49.2	15.7	42.6	62.5	38.7	0
H	34.4	91.6	0.6	27.1	65.5	1.0	19.6	47.1	1.4	7.4	19.3	3.7	0
S	59.5	0.2	95.5	47.4	0.6	80.3	44.9	3.6	74.4	44.9	18.0	54.4	65.9
W	0	0	0	2.6	0.03	4.4	5.1	0.1	8.5	5.1	0.2	3.2	34.1

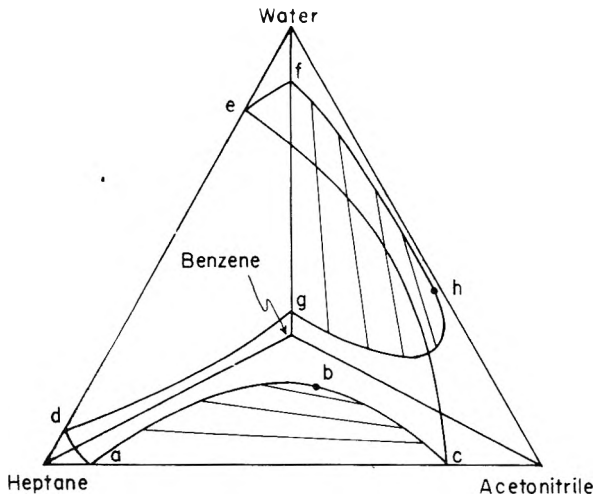

Fig. 1.—Quaternary system acetonitrile–water–benzene–heptane.

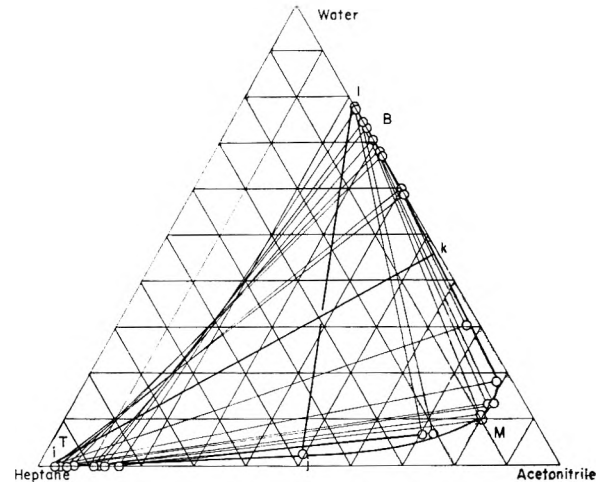

Fig. 2.—Projection of three-phase region on acetonitrile–water–heptane face.

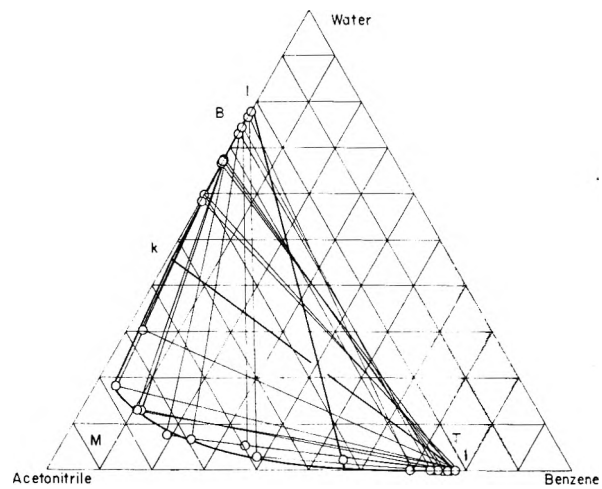

Fig. 3.—Projection of three-phase region on acetonitrile–water–benzene face.

while the other two faces have ternary relationships shown by a,c,e,d and d,e,f,g. The four ternary areas enter the tetrahedron as quaternary two-liquid volumes. Critical solution curves on the surfaces of two of these volumes originate at points b and h. These two curves do not meet, however, since different pairs of liquids are involved on each curve. The intersections of these volumes as they enter the tetrahedron develop a three-liquid phase region.

The shape of the three-liquid phase region is shown by Figs. 2 and 3. Figure 2 is a projection of the three-liquid phase region on the tetrahedron face acetonitrile–water–heptane while Fig. 3 is a projection on the face acetonitrile–water–benzene. The points on these figures may be obtained from the data given in the second half of Table I. Not all of the data given in Table I are plotted in order to avoid an unnecessarily complicated diagram.

The boundaries of the three-phase region are generated by an infinite set of the tie line triangles plotted on Figures 2 and 3. A gross composition point and the three equilibrium liquid phases into which it breaks all lie in a plane. The compositions of the three equilibrium liquid phases correspond to the three intersections of the plane with the single edge of the three-liquid phase region.

Any three-liquid phase region in this type of quaternary system is characterized by three three-dimensional curves, one for each of the liquids involved. For the system under consideration the three-liquid phase region involves two consolute points; therefore, the three curves form one continuous curve of three sections. Thus, geometrically, the three-liquid phase region is contained within a ruled surface having a single edge. The three phases involved are labeled B, M and T corresponding to the bottom, middle and top phases from the point of view of density. The B phase extends from l to k, the M phase from k to j, and the T phase from i to j. Phases B and M are consolute at k while in equilibrium with phase T of composition i. Phases M and T are consolute at j while in equilibrium with phase B of composition l.

The three-liquid phase region in the system sulfolane–water–benzene–heptane at 25° behaves in a similar fashion except that the three-phase region is considerably smaller.

Acknowledgment.—The authors wish to thank H. Y. Brecheisen and A. F. Johnson for their help with the experimental work and the Shell Development Company for permission to publish this manuscript.

INFRARED ABSORPTION SPECTRA OF CIS-TRANS ISOMERS OF COÖRDINATION COMPOUNDS OF COBALT(III)

BY PAUL E. MERRITT[1] AND STEPHEN E. WIBERLEY

Contribution from the Walker Laboratory of Rensselaer Polytechnic Institute, Troy, N. Y.

Received July 26, 1954

The infrared absorption spectra of several *cis-trans* pairs of coördination compounds of cobalt show specific differences between the *cis* and *trans* isomers. In the case of the ethylenediamine-containing complexes a shift occurred in the 6.2–6.4 μ region of the spectrum with the *trans* isomer having a maximum peak at a wave length of 0.04–0.08 μ shorter than the *cis* isomer. In the case of the *cis* and *trans* isomers of the cobalt complexes containing the tetraammine group a shift occurred in the absorption band in the 12 μ region with the *cis* isomer showing an absorption maximum at a wave length about 0.1–0.2 μ shorter than the *trans* isomer. All the compounds had an absorption maximum in the 6.1–6.5 μ region. This band has been assigned to the (N–H) bending frequency in agreement with the assignment of Richards and Thompson.

Introduction

A fundamental idea in inorganic chemistry is that coördination compounds, although numerous and of different types, have only a small number of stereochemical configurations. Recently an extremely interesting and important method for the study of the absorption spectra of compounds in the solid state was introduced by Stimson and O'Donnell[2] and by Scheidt.[3] The introduction of this method has given great impetus to structural studies of inorganic complex coördination compounds. Although many infrared spectra of inorganic compounds have been reported,[4,5] very little infrared work has been done to study the structure of these coördination compounds.

A completely satisfactory method has not been developed for distinguishing between *cis* and *trans* isomers of metal coördination compounds of the types Ma_2b_2, Ma_2bc, $M(AA)_2b_2$ and $M(AA)_2bc$, where a,b,c are monodentate groups, AA is a bidentate group and M is a metal. Previous workers have applied physical methods to aid in the determination of structural configurations. Holtzclaw and Sheetz[6] did a polarographic study of a series of cobalt complexes. Basolo[7] has studied the ultraviolet region for differences in the absorption spectra of *cis* and *trans* isomers of certain coördination compounds in solution. Curran, *et al.*,[8] have conducted infrared absorption studies which have been concerned with the effect of the charge of the metallic ion on the nitrogen to metal coördinate bond of complex compounds. Sen[9] has studied the absorption spectra of inorganic complexes of glycine, and discussed their possible configurations.

This study was concerned with the application of infrared absorption to aid in the differentiation between *cis* and *trans* isomers of a group of cobalt-containing complexes.

(1) Department of Chemistry, St. Lawrence University, Canton, New York.

(2) M. M. Stimson and M. J. O'Donnell, *J. Am. Chem. Soc.*, **74**, 1805 (1952).

(3) U. Scheidt, *Z. Naturforsch.*, **76**, 270 (1952).

(4) J. M. Hunt, M. P. Wisherd and L. C. Bonham, *Anal. Chem.*, **22**, 1478 (1950).

(5) F. A. Miller and C. H. Wilkins, *ibid.*, **24**, 1253 (1952).

(6) H. F. Holtzclaw, Jr., and D. P. Sheetz, *J. Am. Chem. Soc.*, **75**, 3053 (1953).

(7) F. Basolo, *ibid.*, **72**, 4393 (1950).

(8) C. Curran, D. N. Sen, S. Mizushima, and J. V. Quagliano, Paper 62, Pittsburgh Conference on Anal. Chem. and App. Spec., March, 1954.

(9) D. N. Sen, "Infrared Studies of Some Coördination Compounds," Ph.D. Thesis, University of Notre Dame, 1953.

Experimental

Determination of Infrared Spectra.—Infrared absorption spectra were obtained with a Perkin–Elmer Model 21 double beam recording instrument and a Perkin–Elmer Model 12B. A rock-salt prism was used in both instruments except in the case of the Model 12B where a lithium fluoride prism was used for the 2 to 4 μ region in order to obtain better dispersion. The compounds were studied using the solid potassium bromide technique. About 1.5 mg. of compound was intimately ground with about 98.5 mg. of dry potassium bromide that had been screened to 200 mesh particle size. The mixture was placed in a die constructed in this Laboratory and a rectangular sample was pressed. This sample was placed in a suitable holder and then placed in the infrared beam.

Preparation of Compounds

1 and 2.—*cis* and *trans*-dichlorobis-(ethylenediammine)-cobalt (III) chloride were prepared according to the method of Bailar.[10] *Anal.* Calcd. for $(Co(en)_2Cl_2)Cl$: Co, 20.7; Cl, 37.3. Found: Co, 20.4; Cl, 37.3.

3 and 4.—*cis*- and *trans*-dinitrobis-(ethylenediamine)-cobalt (III) nitrate were prepared according to the method of Holtzclaw, Sheetz and McCarty.[11] *Anal.* Calcd. for $(Co(en)_2(NO_2)_2)NO_3$: Co, 17.7; N, 29.1. Found: Co, 17.9; N, 29.0.

5.—Tris-(ethylenediamine)-cobalt(III) chloride was prepared by the method of Work.[12] *Anal.* Calcd. for $(Co(en)_3)Cl_3$: Co, 17.1; Cl, 30.6. Found: Co, 17.2; Cl, 30.7.

6.—Carbonatobis-(ethylenediamine)-cobalt(III) chloride was prepared by the method of Werner and Rapiport.[13] *Anal.* Calcd. for $(Co(en)_2CO_3)Cl.H_2O$; Co, 21.5; Cl, 12.9. Found: Co, 21.5; Cl, 13.1.

7.—*cis*-Chloroisothiocyantobis-(ethylenediamine)-ecbalt-(III) thiocyanate was prepared by the method of Werner and Schmidt as given by Jacobsen.[14] *Anal.* Calcd. for $(Co(en)_2(NCS)Cl)SCN$: Co, 17.8; N, 25.4. Found: Co, 17.5; N, 25.2.

8.—*cis*-Chloroisothiocyanatobis-(ethylenediamine)-cobalt(III) chloride was obtained as a by-product of the preparation of *cis*-chloroisothiocyanatobis-(ethylenediamine)-cobalt(III) thiocyanate. It was recrystallized from hot water and air dried. *Anal.* Calcd. for $(Co(en)_2(NCS)Cl)Cl$: Co, 19.22; N, 22.9. Found: Co, 19.0; N, 22.8.

9.—*trans*-Chloroisothiocyanatobis-(ethylenediamine)-cobalt(III) perchlorate was prepared by the method of Werner.[15] *Anal.* Calcd. for $(Co(en)_2(NCS)Cl)ClO_4$: Co, 15.9; N, 18.8. Found: Co, 16.2; N, 18.6.

10.—*cis*-Bromoaquobis-(ethylenediamine)-cobalt(III) bromide was prepared by the method of Werner and Schmidt.[16] *Anal.* Calcd. for $(Co(en)_2(H_2O)Br)Br_2$: Co, 13.6; N, 12.9. Found: Co, 13.7; N, 13.0.

(10) J. C. Bailar, Jr., "Inorganic Syntheses," Vol. II, John Wiley and Sons, Inc., New York, N. Y., 1946, p. 222.

(11) H. Holtzclaw, D. P. Sheetz and B. McCarty, *ibid.*, Vol. IV, 1953, p. 176.

(12) J. B. Work, *ibid.*, Vol. II, p. 221.

(13) A. Werner and J. Rapiport, *Ann.*, **386**, 72 (1912).

(14) C. A. Jacobsen, "Encyclopedia of Chemical Reactions," Vol. III, Reinhold Publ. Corp., New York, N. Y., 1949, p. 153.

(15) *Ibid.*, p. 154.

(16) A. Werner and R. Schmidt, *Ann.*, **386**, 136 (1912).

11.—*trans* - Hydroxoaquobis - (ethylenediamine) - cobalt (III) bromide was prepared by the method of Werner and Lange.[17] *Anal.* Calcd. for $(Co(en)_2(H_2O)(OH))Br_2$: Co, 15.77; N, 15.0. Found: Co, 15.5; N, 14.8.

12 and 13.—*cis*- and *trans*-dinitrotetraamminecobalt (III) bromide were prepared by the method of Biltz and Biltz.[18] *Anal.* Calcd. for $(Co(NH_3)_4(NO_2)_2NO_3$: Co, 21.1; N, 35.0. Found: Co, 21.3; N, 34.9.

14 and 15.—*cis*- and *trans*-dinitrotetraamminecobalt(III) chloride were prepared by the method of Biltz and Biltz.[18] *Anal.* Calcd. for $(Co(NH_3)_4(NO_2)_2)Cl$: Co, 23.2; Cl, 13.8. Found: Co, 23.0; Cl, 13.6.

16 and 17.—*cis*- and *trans*-dichlorotetraamminecobalt-(III) chloride; the *cis* salt was prepared by taking two grams of carbonatotetraamminecobalt(III) nitrate and dissolving in concentrated hydrochloric acid. The purple precipitate was filtered, washed with water and air-dried. *Anal.* Calcd. for $(Co(NH_3)_4Cl_2)Cl$: Co, 25.3; Cl, 45.6. Found: Co, 25.5; Cl, 45.4%. One gram of the *cis* compound was added to a small amount of water and heated over an open flame. The mixture changed to a green color on heating. The mixture was filtered hot and the solid obtained contained some of the purple compound which could not be removed. *Anal.* Calcd. for $(Co(NH_3)_4Cl_2)$-Cl: Co, 25.3; Cl, 45.6. Found: Co, 25.5; Cl, 45.4.

18.—Carbonatotetraamminecobalt(III) nitrate was prepared by the method described by Walton.[19] *Anal.* Calcd. for $(Co(NH_3)_4CO_3)NO_3 \cdot {}^1/_2H_2O$: Co, 22.8; N, 27.1. Found: Co, 22.8; N, 27.1.

19.—Hexaamminecobalt(III) chloride was prepared by the method of Bjerrum and McReynolds.[20] *Anal.* Calcd. for $(Co(NH_3)_6)Cl_3$: Co, 22.0; Cl, 39.8. Found: Co, 21.8; Cl, 39.6.

Discussion and Results

A strong absorption band appeared in the 6.1–6.5 μ region in the spectrum of each of the nineteen compounds studied. The assignment of the group frequency with which this band is identified is quite controversial. Lenormant[21] and Randall, *et al.*,[22] have argued that this band is characteristic of the amido (C–N) stretching frequency. Richards and Thompson[23] and others have assigned it to the (N–H) bending frequency. The latter base their argument on the fact that primary amines absorb broadly in this region, with this band being certainly due to this deformation. In acetamide, the frequency and the structure of this band are unchanged with respect to the primary amines. The absence of this band from the spectra of N,N-disubstituted amides and the fact that one would expect to find (N–H) bending in this region of the spectra of N-monosubstituted amides, is the basis for the assignment of this band. Richards and Thompson also studied the Raman spectra of CH_3NH_2 and CH_3ND_2, and found that with the introduction of deuterium in place of the hydrogen, the (N–H) bending band was shifted to a lower frequency by a factor of 1.33–1.36. The (C–N) stretching band was shifted by a factor of 1.05.

The evidence for the assignment of this band to (C–N) stretching frequency centers about the substitution of halogen atoms upon the nitrogen and further deuteration experiments of N-monosubstituted amides. Lenormant[21] found that the 6.4 μ band in these deuterated amides was shifted to lower frequencies by a factor of 1.05. This indicated, on the basis of the work of Richards and Thompson, that the assignment was better attributed to (C–N) stretching frequency. Also, Lenormant observed that the 6.4 μ band was totally absent in the spectrum of N-bromoethanamide. In regard to this, Richards and Thompson noted that the substitution of an electrophilic group on the amido-nitrogen sometimes decreases the frequency of this band. A band did appear at ~6.0 μ. Further substantiation for the assignment of this band came from Randall, *et al.*,[22] who observed that this band was absent from the spectra of lactams. Based on the evidence presented by Lenormant, and further evidence from their study of N,N-disubstituted ethanamides, Letaw and Gropp[24] have assigned this band to the (C–N) stretching frequency.

From the observation of the spectra of the compounds used in this study, evidence can be obtained to support the assignment of Richards and Thompson. As was previously pointed out, a strong band appeared in each spectrum in this region. These data appear in Table I. In this table compounds that contain both the (C–N) and (N–H) groups are listed as well as some that contain only the (N–H) group. Since this band appeared in all compounds, the assignment of Richards and Thompson is more reasonable.

TABLE I

WAVE LENGTH OF ABSORPTION BAND MAXIMUM IN SIX AND 12 μ REGION

	Formula	6 μ Region Wave length, μ	12 μ Region Wave length, μ
1	*cis*-$[Co(en)_2Cl_2]Cl$	6.48	
2	*trans*-$[Co(en)_2Cl_2]Cl$	6.30	
3	*cis*-$[Co(en)_2(NO_2)_2]NO_3$	6.32	
4	*trans*-$[Co(en)_2(NO_2)_2]NO_3$	6.24	
5	*cis*-$[Co(en)_3]Cl_3$	6.44	
6	*cis*-$[Co(en)_2CO_3]Cl \cdot H_2O$	6.34	
7	*cis*$[Co(en)_2(NCS)Cl]SCN$	6.41	
8	*cis*-$[Co(en)_2(NCS)Cl]Cl$	6.40	
9	*trans*-$[Co(en)_2(NCS)Cl]ClO_4$	6.34	
10	*cis*-$[Co(en)_2(H_2O)Br]Br_2$	6.36	
11	*trans*-$[Co(en)_2(H_2O)(OH)]Br_2$	6.30	
12	*cis*-$[Co(NH_3)_4(NO_2)_2]NO_3$	6.26	12.22
13	*trans*-$[Co(NH_3)_4(NO_2)_2]NO_3$	6.22	12.27
14	*cis*-$[Co(NH_3)_4(NO_2)_2]Cl$	6.20–6.30 (b)	12.20
15	*trans*-$[Co(NH_3)_4(NO_2)_2]Cl$	6.24	12.30
16	*cis*-$[Co(NH_3)_4Cl_2]Cl$	6.28	11.88
17	*trans*-$[Co(NH_3)_4Cl_2]Cl$	6.24	12.06
18	$[Co(NH_3)_4CO_3]NO_3 \cdot {}^1/_2H_2O$	6.28	12.06
19	$[Co(NH_3)_6]Cl_3$	6.46	

Examination of the spectra of the groups of compounds (1–11) containing ethylenediamine as the inert constituent in the complex shows there is a

(17) A. Werner and K. Lange, *Ann.*, **386**, 97 (1912).

(18) H. Biltz and W. Biltz, "Laboratory Methods of Inorganic Chemistry," 2nd Ed. John Wiley and Sons, Inc., New York, N. Y., 1928, p. 179–181.

(19) H. F. Walton "Inorganic Preparations," Prentice–Hall, Inc., New York, N. Y., 1948.

(20) J. Bjerrum and J. P. McReynolds, "Inorganic Syntheses," Vol. II, John Wiley and Sons, Inc., New York, N. Y., p. 216.

(21) H. Lenormant, *Ann. chim.*, **5**, 459 (1950).

(22) H. M. Randall, R. G. Fowler, N. Fuson, and J. R. Dangl, "Infrared Determination of Organic Structures," D. Van Nostrand Co., Inc., New York, N. Y., 1949.

(23) R. E. Richards and H. W. Thompson, *J. Chem. Soc.*, 1248 (1947).

(24) H. Letaw and A. H. Gropp, *J. Chem. Phys.*, **21**, 1621 (1953).

shift in the absorption band in the (N–H) bending region between the *cis* and *trans* isomer of any one compound. The absorption maxima of all compounds of the *cis* series appeared at approximately the same wave length. The compounds of the *trans* series show absorption maxima 0.04 to 0.08 μ lower. For each pair of isomers as illustrated by a typical example shown in Fig. 1, the *trans* isomer has a maximum that appears at a lower wave length and at a higher frequency than the *cis* isomer. This fact can be used to differentiate between the *cis* and *trans* isomer of a given cobalt ethylenediamine-containing complex.

Although this band appeared at approximately the same wave length in the spectrum of both the *cis* and *trans* isomer that contained four ammonia molecules as the inert constituent of the complex, a shift did occur in the broad band that appeared in the 12 μ region. In the three cases studied the maximum of this absorption band of the *trans* series was at a longer wave length and a lower frequency than the *cis* isomer. The compounds of the *trans* series have an absorption maximum which is 0.1–0.2 μ higher than the compounds of the *cis* series. This shift can be used to differentiate between the *cis* and *trans* isomers of complex inorganic compounds containing cobalt and the tetrammine group.

Although the spectra of the *cis* and *trans* isomers of individual compounds show definite differences, the only regions showing consistent variation between the *cis* and *trans* isomer having similar groups within the complex were the 6 and 12 μ regions.

Acknowledgment.—The authors are indebted to Dr. John Campbell, Behr-Manning Corporation, Watervliet, N. Y., for the use of the Model 21 Perkin-Elmer Infrared Spectrophotometer.

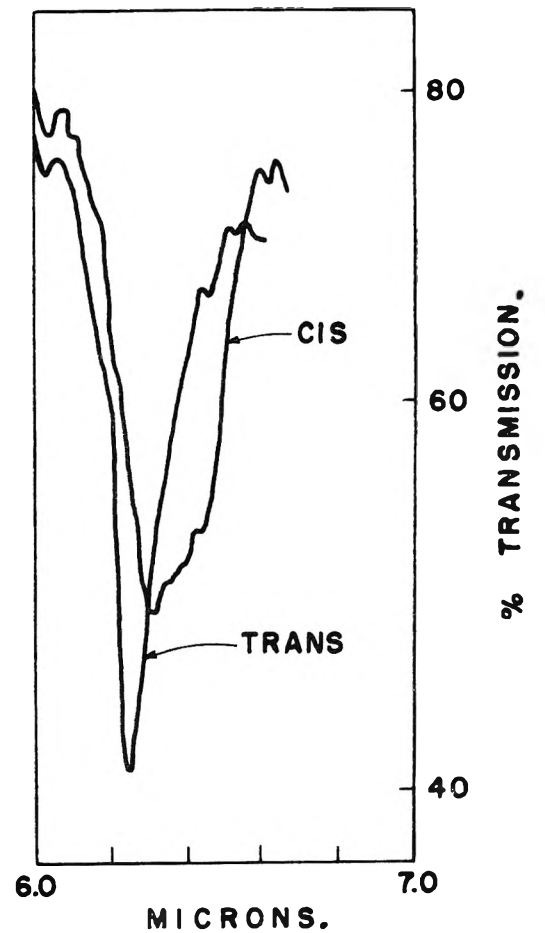

Fig. 1.—Typical shift of absorption maximum in 6 μ region using *cis*- and *trans*-dinitrobis-(ethylenediamine)-cobalt(III) nitrate as example.

THE INTERACTION OF GAS MOLECULES WITH CAPILLARY AND CRYSTAL LATTICE SURFACES[1,2]

BY W. A. STEELE[3,4] AND G. D. HALSEY, JR.

Department of Chemistry, University of Washington, Seattle, Washington

Received July 27, 1954

A theory of the interaction of gas molecules with a structureless plane has been modified to treat capillary spaces. The effect on the apparent area and energy of interaction is calculated. The interaction of a molecule with the surface of a simple cubic lattice of atoms has been computed and compared with the crude model. Experimental data on the interaction of helium, neon, argon, hydrogen, oxygen, nitrogen and methane with porous glass and saran charcoal are presented and discussed.

1. Introduction

The apparent volume V of a vessel containing a large surface area solid is given by the expression

$$V - V_{geo} = \int^{V_{geo}} \{\exp(-\epsilon/kT) - 1\} dV \quad (1.1)$$

where ϵ is the energy of interaction of the gas molecule with the solid, in the volume element dV. We have solved this problem previously[5] for the case of an isolated plane well composed of a structureless material with a hard-sphere repulsion for the gas atom. This analysis led to a value for the distance of closest approach, the energy of interaction at this distance and the surface area of the solid. We shall now consider some refined models: the problem of capillary spaces in a structureless solid, and that of the plane surface of a crystal of defi-

(1) Presented at the 126th national meeting of the American Chemical Society, New York, September 12–17, 1954. Partially supported by Contract AF19(604)-247 with the Air Force Cambridge Research Center.

(2) Presented in partial fulfillment of the requirements for the Ph.D. degree by W. A. S.

(3) National Science Foundation Pre-doctoral Fellow, 1953–1954.

(4) Pennsylvania State University, State College, Pa.

(5) W. A. Steele and G. D. Halsey, Jr., *J. Chem. Phys.*, **22**, 979 (1954).

nite lattice structure. We shall also present some data related to these cases.

2. Capillary Surfaces

Plane Parallel Walls.—We first consider two plane parallel walls, separated by a distance $2L$ between the planes passing through the centers of the surface layers of atoms making up the solid. We shall assume that each surface attracts the interacting molecule according to the inverse cube of the distance of the molecule from the surface, and that the hard-sphere distance of closest approach is D. Then, with the origin in the left-hand surface plane, the sum of the two interaction energies with both planes is

$$\epsilon(r) = -\epsilon^*[(D/r)^3 + (D/2L - r)^3] \qquad D < r < 2L - D \quad (2.1)$$
$$\epsilon(r) = +\infty \qquad D > r > 2L - D$$

where r is the distance of the molecule from the left-hand plane and ϵ^* is the energy of attraction at the distance of closest approach.

If this energy is substituted in eq. 1.1 the integrations parallel to the walls are trivial. They yield a factor equal to the area of one plane wall, or half the total area

$$V - V_{geo} = A/2 \int_0^{2L} (\exp\{\epsilon^*/kT[(D/r)^3 + (D/2L - r)^3]\} - 1)\, dr \quad (2.2)$$

Note that $V_{geo} = AL$. This expression can be further simplified by integrating over the range where ϵ is infinite, and then it can be expressed in the form

$$V_{ex}/AD = (V - AL + AD)/AD = \int_1^{L/D} (\exp\{\epsilon^*/kT[(D/r)^3 + (D/2L - r)^3]\} - 1)\, d(r/D) \quad (2.3)$$

By means of graphical integration, V_{ex}/AD was computed as a function of ϵ^*/kT, with L/D as a parameter. The results will be discussed together with those for cylindrical walls.

Cylindrical Walls.—We next consider the case of a surface consisting of cylindrical capillary holes of radius R. In this case, it is necessary to integrate the inverse sixth power law of London with appropriate boundary conditions, over all the solid. If the coördinate axis lies on the axis of the cylinder and furthermore, if the distance between the interacting particles in the plane perpendicular to the z axis is designated by ρ, then the distance between a gas atom and any point in the solid phase is $\sqrt{\rho^2 + z^2}$. Note that the origin for the new variable r' is located at the center of the cylinder. In the previous cases, the origin of r was in the surface of the solid. The expression for $\epsilon(r')$ then becomes

$$\epsilon(r') = -2N_0C \int_\pi^0 \int_\infty^s \int_{-\infty}^{+\infty} \frac{\rho\, dz\, d\rho\, d\theta}{(\rho^2 + z^2)^3} \qquad R - D > r' > -(R - D) \quad (2.4)$$
$$\epsilon(r') = +\infty \qquad R - D < r' < -(R - D)$$

where s is the distance in the ρ plane between the gas atom and the wall of the capillary, N_0 is the number of atoms per cc. in the solid, and C is a constant given by Kirkwood and Müller[6] which we have discussed in a previous paper[5]

$$C = 6mc^2 \left(\frac{\alpha_1\alpha_2}{\alpha_1/\chi_1 + \alpha_2/\chi_2}\right) \quad (2.5)$$

Here α and χ refer to the atomic polarizability and susceptibility, and mc^2 is the mass of the electron multiplied by the square of the velocity of light. Equation 2.4 can be integrated to give

$$\epsilon(r') = -(\pi N_0 C/4) \int_\pi^0 \frac{d\theta}{s^3} \qquad R - D > r' > -(R - D) \quad (2.6)$$

We apply the law of cosines to the triangle formed by s, R and r' and obtain

$$s = r' \cos\theta + \sqrt{R^2 - r'^2 \sin^2\theta}$$

Thus

$$\epsilon(r'/D) = -\pi N_0 C/4D^3 \int_\pi^0 \frac{d\theta}{(r'/D)\cos\theta + \sqrt{(R/D)^2 - (r'/D)^2 \sin^2\theta)^3}} \qquad R/D - 1 > r'/D > -(R/D - 1)$$
$$\epsilon(r') = +\infty \quad R/D - 1 < r'/D < -(R/D - 1) \quad (2.7)$$

This expression was integrated graphically to give $\epsilon/(r'/D)$ for a number of values of R/D.

In cylindrical coördinates, eq. 1.1 becomes

$$V - V_{geo} = \int^{V_{geo}} (\exp\{\epsilon(r'/D)/kT\} - 1) r'\, dr'\, d\theta\, dz \quad (2.8)$$

If we define A as the area of the surface passing through the nuclei of the atoms forming the walls of the cylinder, V_{geo} is then equal to AR. The integrations of eq. 2.6 with respect to z and θ are trivial and we obtain

$$V - V_{geo} = (A/R) \int_0^R (\exp\{\epsilon(r'/D)/kT\} - 1) r'\, dr' \quad (2.9)$$

We now integrate over the range of infinite ϵ

$$V - V_{geo} = A \int_0^{R-D} (\exp\{\epsilon(r'/D)/kT\} - 1) r'/R\, dr' - A(2RD - D^2)/2R \quad (2.10)$$

In dimensionless form

$$V_{ex}/AD = \int_0^{R/D-1} (\exp\{\epsilon(r'/D)/kT\} - 1)(r'/R)\, d(r'/D) + D/2R \quad (2.11)$$

This integral was evaluated graphically for those values of R/D for which $\epsilon(r'/D)$ had been computed.

Evaluation of Apparent Areas.—We will now compare these capillary models with the limiting case of a single plane wall. The shapes of the curves obtained when log V_{ex} is plotted against $1/T$ are only slightly changed when the walls get closer together. It will emerge that these curves are substantially straight lines over the experimentally important range. However, since the scale is shifted, the apparent area based on the limiting model with only one wall may be unequal to the real area of the capillary surface. We shall base this comparison on the straight-line portion of the plot. It will be convenient to make a formal analysis of the method of estimating area presented earlier.[5] The straight line portion can be written

$$\log V_{ex}/AD = Q_1(\epsilon^*/kT) + Q_2 \quad (2.12)$$

(6) A. Müller, *Proc. Roy. Soc. (London)*, *A***154**, 624 (1936).

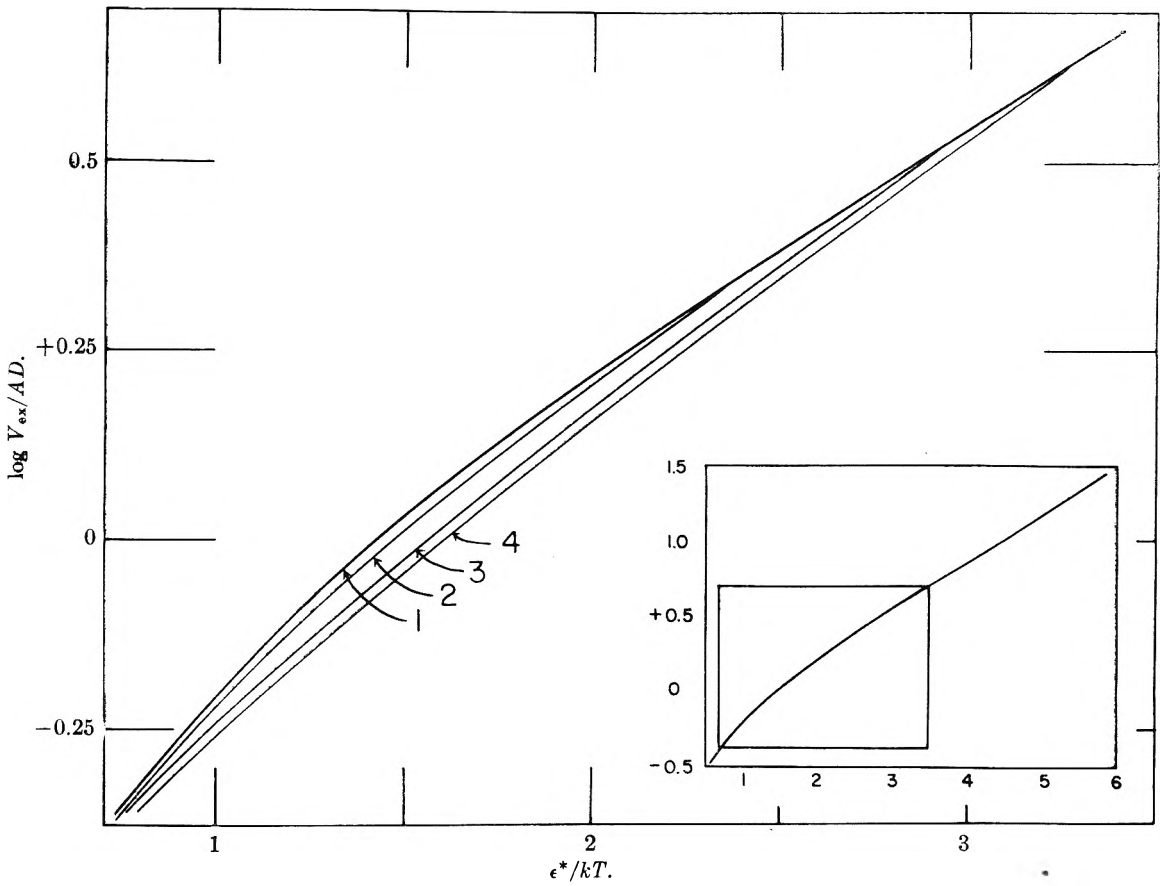

Fig. 1.—Curves of log (V_{ex}/AD) *versus* ϵ^*/kT. All models have the scales adjusted so that the linear portions of the curves coincide with the curve for the simple model. The inset shows the range of ϵ^*/kT for which the larger plot was made; all models coincide for $\epsilon^*/kT > 3.5$. Curve 1 is log (V_{ex}/AD) for the simple case, curve 2 is for a parallel-walled capillary with $L/D = 3$, curve 3 is for a cylindrical capillary with $R/D = 3$ and curve 4, a cylindrical capillary with $R/D = 2$.

where Q_1 and Q_2 are dimensionless constants, independent of particular values of A, D or ϵ^*.

If this is rearranged in terms of experimentally observed quantities

$$\log V_{ex} = Q_1\epsilon^*(1/kT) + Q_2 + \log AD \quad (2.13)$$

with a slope S given by

$$S = \mathrm{d}\,(\log V_{ex})/\mathrm{d}\,(1/kT) = Q_1\epsilon^* \quad (2.14)$$

and an intercept I given by

$$I = Q_2 + \log AD \quad (2.15)$$

Now, for the simple model[5]

$$\epsilon^* = \pi CN_0/6D^3$$

so

$$S = Q_1\pi CN_0/6D^3$$

and solving for D

$$D = (\pi Q_1 CN_0/6S)^{1/3} \quad (2.16)$$

Then

$$I = Q_2 + \log A + {}^1/_3 \log (\pi Q_1 CN_0/6S) \quad (2.17)$$

or solving for the logarithm of the area

$$\log A = I - Q_2 - {}^1/_3 \log (\pi Q_1 CN_0/6S) \quad (2.18)$$

For the purpose of comparing theoretical models, it is desirable to eliminate such parameters as C, N_0 and D. For that purpose a reduced temperature τ is defined as

$$1/\tau = \epsilon^*/kT = 1/kT(\pi CN_0/6D^3) \quad (2.19)$$

Then the straight-line portion of the capillary case is written

$$\log (V'_{ex}/A'D) = Q_1'(1/\tau) + Q_2' \quad (2.20)$$

We now set A' equal to unity to calculate the "apparent area" if a capillary solid is treated according to the single-plane model. Then

$$\log V'_{ex} = Q_1'(1/\tau) + Q_2' + \log D \quad (2.21)$$

whence

$$S = \mathrm{d} \log V_{ex}/\mathrm{d}\,(1/kT) = Q_1'(\pi CN_0/6D^3)$$

and

$$I = Q_2' + \log D$$

Substitution of these quantities in eq. 2.18 yields the apparent area

$$\log A_{app} = Q_2' - Q_2 - {}^1/_3 \log Q_1/Q_1' \quad (2.22)$$

Note that the Q's are scale factors multiplying V_{ex} and T; hence as long as two curves relating V_{ex} and T can be adjusted to coincidence, eq. 2.22 will hold; it is not necessary that the particular straight line function found here hold. In Fig. 1, the curves of V_{ex} *versus* $1/T$ are shown for a number of models. The scales have been adjusted so the linear portions of the curves coincide. It is clear that even in the region of non-linearity, the curves do not deviate significantly from each other.

A plot of the apparent area as a function of capillary size is shown in Fig. 2. The change in the apparent energy of interaction (given by Q_1'/Q_1) is

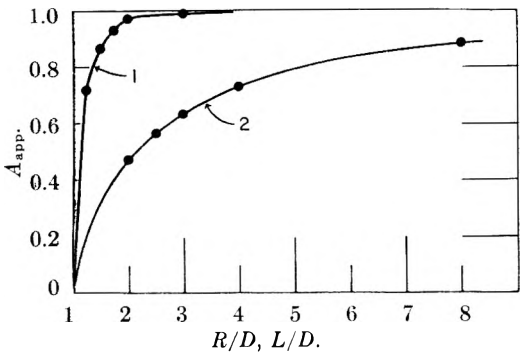

Fig. 2.—The apparent areas of a parallel-planar-walled capillary (curve 1) and a cylindrical capillary (curve 2) as a function of capillary size.

shown in Fig. 3. The apparent energy of interaction relative to the limiting case increases as the size of the cavity becomes smaller and the apparent area of the solid decreases to zero as the size of the cavity decreases to $R = D = L$. Both of these effects are in accord with what one might expect. Note that the effect of the size of the capillary on the apparent area persists to a greater relative distance for a cylindrical capillary than for one with parallel walls. It is apparent that the effect would be even more long range in the case of capillaries consisting of spherical cavities.

3. Interaction with a Simple Crystal Lattice

The Summation of Atom–Lattice Interactions.—We now consider the interaction energy between an atom in the gas and an array of atoms located on lattice points within the crystal face. We consider here the 100 face of a simple cubic lattice made up of atoms of one kind. We shall use the familiar Lennard-Jones potential function,[7] with inverse twelfth power repulsion, for the pair interaction. It can be written

$$\epsilon = 2\epsilon^* \left((r^*/r)^6 - \frac{1}{2}(r^*/r)^{12} \right) \qquad (3.1)$$

At a distance $r = r^*$ the energy ϵ has a minimum (negative) value ϵ^*. We shall choose ϵ^* such that the attractive term is in agreement with the Kirkwood-Müller formulation of the London force between unlike atoms.[5] We leave r^* as a parameter. Then

$$\epsilon_{1,2} = C(-(1/r_{1,2})^6 + (r^{*6}/2r_{1,2}^{12})) \qquad (3.2)$$

where C is the Kirkwood-Müller constant for unlike atoms.

The total energy of interaction between the solid and a gas atom at a given point over the lattice (denoted by 1) is then given by the sum of terms of the form 3.2 over all the atoms in the solid

$$\epsilon(1) = C\left(-\sum_i (1/r_{1,i})^1 + \sum_i (r^{*6}/2r_{1,i}^{12}) \right) \qquad (3.4)$$

It is convenient to express these distances in terms of the lattice parameter a. The energy ϵ will be a function of the perpendicular distance z from a lattice point in the surface, or of the reduced distance $\rho = z/a$. It will also be a function of the coördinate system x, y (with the origin at a lattice point and directions along the edges of the unit cell) in the plane of the surface, with unit vector equal to $1/a$. We define $\rho^* = z^*/a$ and also the functions

$$S_6 = \sum_i (a/r_{1,i})^6 \qquad (3.5)$$

$$S_{12} = \sum_i (a/r_{1,i})^{12} \qquad (3.5)$$

With these substitutions, eq. 3.4 can be expressed in the more general form

$$\epsilon(\rho, x/a, y/a) = (C/a^6)\left(-S_6 + \frac{1}{2}\rho^{*6} S_{12} \right) \qquad (3.7)$$

where x/a, y/a specify the position of the 1'th atom relative to the lattice. This energy must then be inserted into the integral for the apparent volume, and integrated over the unit cell in x and y, and to infinity in z, to obtain the volume per unit cell. It is then multiplied by A/a^2, the number of unit cells in area A, to obtain the total volume

$$V - V_{geo} = Aa \int_0^\infty \int_0^1 \int_0^1 (\exp\{\epsilon(\rho, x/a, y/a)/kT\} - 1) \mathrm{d}(x/a)\, \mathrm{d}(y/a)\, \mathrm{d}\rho \qquad (3.8)$$

The Approximate Calculation of ϵ and V.—The summation of $S_6(\rho)$ has been performed by Orr[8] for three cases:

$S_6(\rho, 0, 0)$—the gas atom directly over a lattice point.

$S_6(\rho, 0, 1/2) = S_6(\rho, 1/2, 0)$—the gas atom lying above the mid-point of the edge of a lattice cell.

$S_6(\rho, 1/2, 1/2)$—the gas atom over the center of a lattice cell. He also gives an analytical expres-

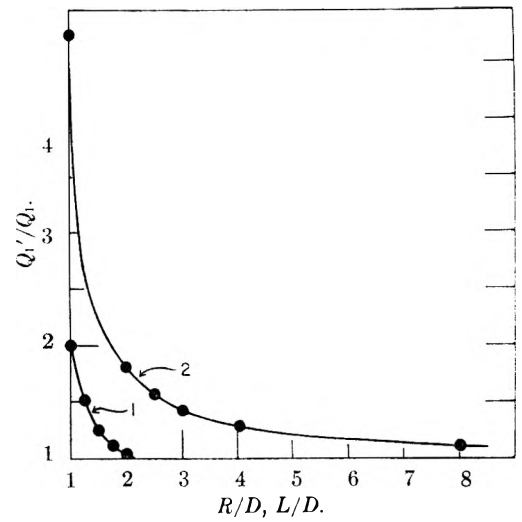

Fig. 3.—The apparent energy of interaction (given by Q_1'/Q_1) for capillaries. Curve 1 gives Q_1'/Q_1 for cylindrical capillaries and curve 2, for parallel planar walled capillaries.

TABLE I

ρ	$S_{12}(\rho, 0, 0)$	$S_{12}(\rho, 0, 1/2)$	$S_{12}(\rho, 1/2, 1/2)$
0	256.40	8194	∞
.5	22.456	128.38	4097.1
.6		39.046	459.44
.7	4.258	12.353	72.256
.8	1.827	4.147	14.771
.9	0.7992	1.467	3.663
1.0	.3564	0.5583	1.071
1.2	.0775	.0979	0.1337
1.5	.0101	.0108	.0122

(7) R. H. Fowler and E. A. Guggenheim, "Statistical Thermodynamics," Cambridge University Press, Cambridge, 1939, p. 280.

(8) W. J. C. Orr, *Trans. Faraday Soc.*, **35**, 1247 (1939).

sion for interpolation between the calculated values of $S_6(\rho)$. The sum $S_{12}(\rho)$ has been computed for the same values of x and y and the values are given in Table I. Interpolation formulas similar to those of Orr were used to find $S_{12}(\rho)$ for intermediate values of ρ.

The problem of evaluating eq. 3.8 by means of a suitable approximation now arises. It was found that the most suitable method was to linearize the expressions obtained when the integration with respect to ρ was performed. If we choose functions of x and y such that the expression of $V - V_{geo}$ is correct at the points (0, 0), (0, 1/2), and (1/2, 1/2) we obtain a useful linearization. The complete approximation for $V - V_{geo}$ is given by

$$V - V_{geo} = 4Aa\int_0^{1/2}\int_0^{1/2}(1 - x/a)(1 - y/a)\,d(x/a)\,d(y/a)\int_0^{\infty}(\exp\{\epsilon(\rho, 0, 0)/kT\} - 1)\,d\rho + 4Aa\int_0^{1/2}\int_0^{1/2}(x/a + y/a - 2xy/a^2)d(x/a)\,d(y/a)\int_0^{\infty}(\exp\{\epsilon(\rho, 0, 1/2)/kT\} - 1)d\rho + 4Aa\int_0^{1/2}\int_0^{1/2}xy/a^2\,d(x/a)\,d(y/a)\int_0^{\infty}(\exp\{\epsilon(\rho, 1/2, 1/2)/kT\} - 1)\,d\rho \quad (3.9)$$

When the integrations with respect to x and y are performed, we obtain

$$V - V_{geo} = (Aa/4)\int_0^{\infty}(\exp\{\epsilon(\rho, 0, 0)/kT - 1)d\rho + (Aa/2)\int_0^{\infty}(\exp\{\epsilon(\rho, 1/2, 0)/kT - 1)d\rho + (Aa/4)\int_0^{\infty}(\exp\{\epsilon(\rho, 1/2, 1/2)/kT - 1)d\rho \quad (3.10)$$

It is now clear that the approximation is equivalent to the assumption that the surface is sufficiently characterized by considering it to be composed of three patches having the computed value of $\epsilon(\rho)$ for the three lattice positions. Note that physically, each unit cell of the surface has every possible energy above it, and that this pattern repeats with the periodicity of the lattice. However, because only one gas atom is integrated through the gas volume, the relative position of volume elements of different energies is not significant. If two gas atoms were interacting with the surface and with each other, the correlation between the energy of adjacent volume elements would be important. The accuracy of the result here depends only on one factor: the jump in energy occasioned upon going from a patch with a given energy to the patch with the energy of nearest value to it. Clearly, if the number of lattice positions considered, and thus the number of patches considered is increased indefinitely, the approximation becomes exact. We have limited our calculation to three patches because Orr's tables existed for the corresponding three positions. For that reason, the numerical evaluation of eq. 3.10 was carried out for several values of ρ^* greater than unity. Below unity, the energy differences between the three positions became very large.

Computation and Comparison with the Crude Model.—For purposes of computation, it is desirable to express ϵ in dimensionless units. For this reason, $1/kT$ is replaced by the reduced temperature function related to the interaction energy ϵ^* of the crude model (eq. 2.19). Since $N_0 = 1/a^3$, the energy for the present model over kT becomes

$$\epsilon(\rho)/kT = (D/a)^3(6/\pi\tau)(-S_6 + 1/2\rho^{*6}S_{12}) \quad (3.11)$$

With the ratio D/a set equal to unity, this form of ϵ^* was used in eq. 1.1 to evaluate graphically $(V - V_{geo})/Aa$ as a function of $1/\tau$, according to eq. 3.8. This procedure is equivalent to computing $V - V_{geo}$ as a function of $1/\tau(D/a)^3$ if this ratio deviates from unity. The plot of $\log(V - V_{geo})$ *versus* $1/\tau$ is a straight line for this model, and is virtually indistinguishable from the same plot for the crude model. However, as in the case of the capillaries, the apparent area deviates from unity. In straight line form, with A set equal to unity

$$\log(V' - V_{geo}) = Q_1'(1/\tau)(D/a)^3 + Q_2' + \log a \quad (3.12)$$

When substituted into eq. 2.18, the formula (eq. 2.22) obtained previously for apparent area emerges.

The apparent area is plotted as a function of ρ^* in Fig. 4. The limiting value of the apparent area at

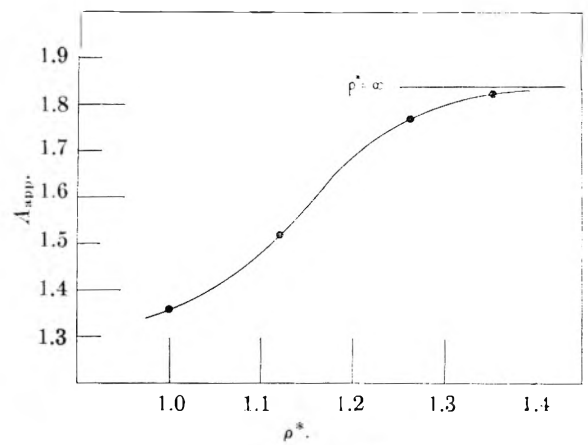

Fig. 4.—The apparent area of a lattice solid as a function of the reduced lattice spacing. $\rho^* = \infty$ corresponds to a structureless solid ($a = 0$).

$\rho^* = \infty$ was calculated by letting the lattice spacing a approach zero. This gives the case of the structureless surface, and the interaction energy is equal to the integral of the Lennard-Jones potential function (eq. 3.2) over the entire solid phase. When this integration is performed, we obtain

$$\epsilon = (\pi N_0 C/6r^{*3})(-(r^*/r)^3 + r^{*6}/4(r^*/r)^9) \quad (3.13)$$

where r^* is now the distance at which the ϵ specified in eq. 3.13 is at a minimum (the actual value for r^* for a given surface will vary according to the form chosen for ϵ). Equation 1.1 was evaluated using eq. 3.13, and the apparent area was obtained from eq. 2.18. The accuracy of the $V - V_{geo}$ values obtained in this case was checked by integrating 1.1 in series form (an analogous derivation to that given by Lennard-Jones[9] for two gas atoms having spherical symmetry). However, the series ob-

(9) J. E. Jones, *Proc. Roy. Soc. (London)*, **A106**, 463 (1924).

tained did not converge sufficiently fast for this solution to be of general use.

At first glance, the curve given in Fig. 4 appears odd. However, the reason for this is that there are two partially compensating effects entering in this case. A gas atom which is small in comparison to the size of the atoms in the solid will interact with only one atom at a time: therefore, the interaction potential will reduce to the inverse sixth power attraction and inverse twelfth power repulsion in the limit of ρ^* small. At the limiting value of $\rho^* = \infty$, the energy of eq. 3.13 which gives an accurate description of the interaction is somewhat smaller than that of the crude model with hard sphere repulsion. This is due to the rounding off of the energy *versus* distance curve when the r^{-9} repulsion is introduced. However, the area under the curve given by $\exp \epsilon(\rho)/kT - 1$ for equal $1/\tau$ is much larger for the refined model. These relationships are reflected in a large positive value of $Q_2' - Q_2$ and a Q_1'/Q_1 ratio of less than one. When these values are substituted in eq. 2.18, the apparent area is thus greater than one, and the value given in Fig. 4 emerges. The other values of ρ^* given here have potential functions intermediate between the $r^{-3} - r^{-9}$ and the $r^{-6} - r^{-12}$. As the exponents of r increase, the energy also increases, and thus the Q_1'/Q_1 increases. (See Fig. 5 for a plot of Q_1'/Q_1 as a function of ρ^*.) However, the curve of $\exp \epsilon(\rho)/kT - 1$ becomes sharper and the value of the integral at constant $1/\tau$ becomes smaller; this results in a decrease in $Q_2' - Q_2$. These two effects tend to balance each other, with the decrease in $Q_2' - Q_2$ being the dominant term down to $\rho^* = 1.0$. At values of $\rho^* < 1.0$, the approximation of eq. 3.9 breaks down. However, it is clear that as the gas atom gets smaller, the potential function will soon reach its limiting form. At this point, $Q_2' - Q_2$ becomes essentially constant; however, Q_1'/Q_1 increases rapidly as the atoms are allowed to approach each other more closely. This means that the apparent area will go through a minimum (at about $\rho^* = 0.6$ to 0.8) and then increase without limit, as the small gas atoms penetrate the lattice.

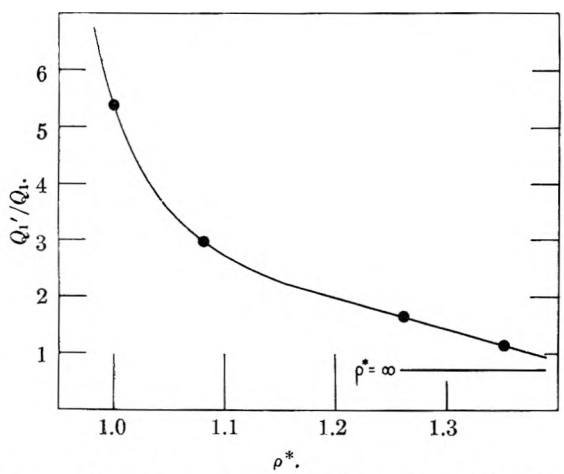

Fig. 5.—The apparent energy of interaction Q_1'/Q_1 for a lattice solid as a function of lattice spacing.

4. Experimental

The apparatus and procedure have been described in the previous paper.[5] Essentially, we have measured V, the apparent gas space volume in a bulb filled with high surface area powder as a function of temperature in the range where this volume is independent of pressure.

In the present work, precautions were taken to avoid small errors caused by the diffusion of helium through glass at high temperatures. A double walled bulb was used, with the outer compartment filled with helium to approximately the same pressure as the helium inside. Also, the time allowed for helium sample contact was kept to a minimum by starting new isosteres at shorter time intervals. As soon as the helium readings started to show a drift when one returned to the original temperature, a new isostere was started. The other gases used gave no trouble, with the exception of hydrogen. However, all the hydrogen determinations were made at room temperature or less. In this range, the drift was not appreciable for any of the gases.

The samples used in this work were the porous glass used in the previous work and a sample of high area saran sent to us by Professor Nelson Smith of Pomona College. This material, designated S-85, was saran which had been carbonized at 400°, ground and further heated at 600°, activated with steam at 900° to an 85% weight loss and cooled to room temperature in an atmosphere of nitrogen. All gases employed were reagent grades in glass flasks from Air Reduction Sales Co. except hydrogen and methane. The hydrogen was tank material which had been passed over platinized asbestos at 300° and then through a liquid air trap. Total impurities were mass spectrometrically determined to be less than 0.1%. The methane was from a tank and had been passed through a liquid air trap. Total impurities (mainly nitrogen) were less than 0.2%.

The data were fitted to the crude model of the previous paper. The notation and fitting technique are described there. A plot of $\log V_{ex}/AD$ *versus* ϵ^*/kT for several gases over porous glass is shown in Fig. 6. The values of V_{ex} for neon over glass were redetermined at an interval of six months after the original measurements which were reported previously.[5] The two sets of measurements did not differ appreciably (the new measurements are reported here). The calculated areas agreed within 5%. A similar plot of V_{ex}/AD *versus* ϵ^*/kT for some gases over saran charcoal (S-85) is given in Fig. 7.

In Table II, the values of ϵ^*, the energy at contact, D, the distance of closest approach, $V_{geo} - AD$, and the area A (all calculated from the crude model) are given. The values of the polarizabilities and susceptibilities for hydrogen, oxygen, nitrogen and methane are given in Table III. All other values were taken from Table II of the previous paper.

5. Discussion

The Absolute Area.—All the apparent areas calculated in Section 3 for refined models are greater than unity. That is, if experimental data were fitted directly to the refined models, the area that would emerge would be less than those calculated on the basis of the crude model. Thus, the refinements largely destroy the near agreement with the B.E.T. area shown by the crude model. Actually, for the high surface area capillary solids we have studied, the absolute area is in doubt, but we can point out a possible explanation to restore agreement.

In computing $V - V_{geo}$ by taking a weighted average of three positions over the lattice, one essentially combines three different types of surface, which is equivalent to introducing heterogeneity of a sort. The apparent area of a unit area for each lattice position can be computed and the resultant three values compared with the apparent area of the weighted average. In the cases computed the following generalization emerges: the weighted average of the apparent area of the single

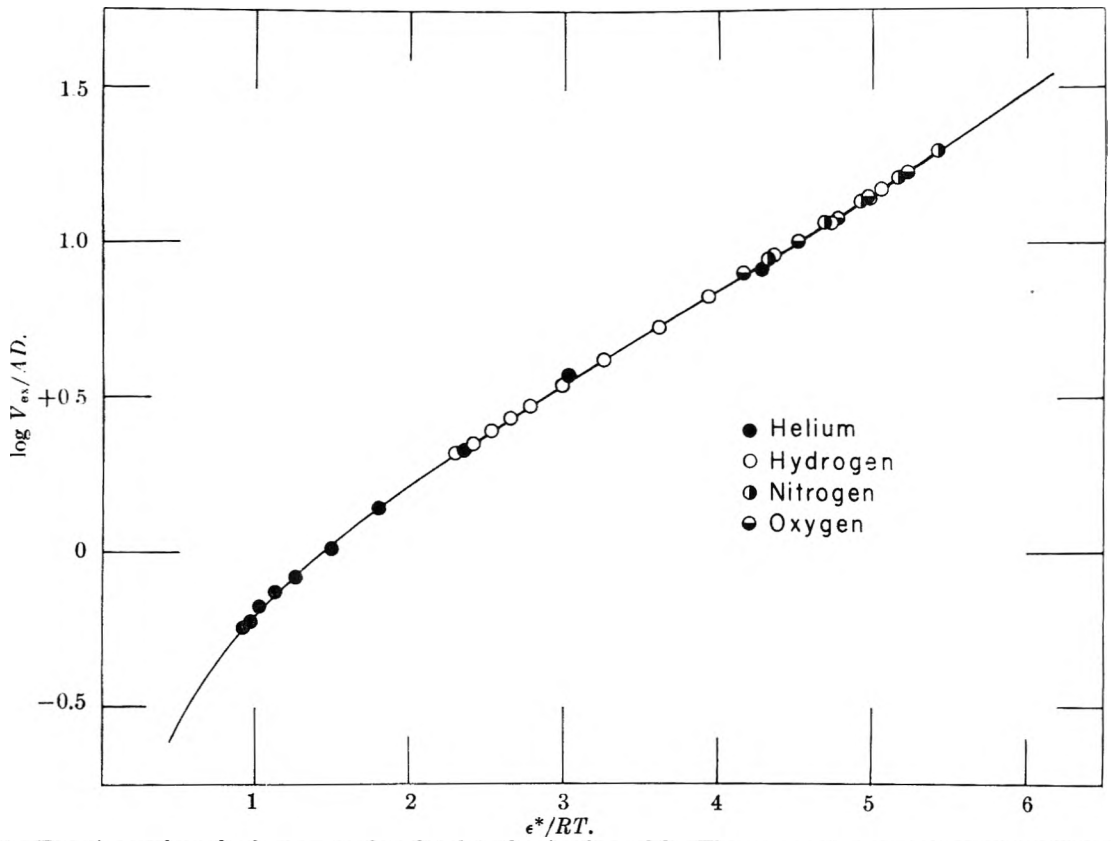

Fig. 6.—Experimental results for porous glass fitted to the simple model. The neon and argon data are omitted from this figure (see Fig. 5 of ref. 5).

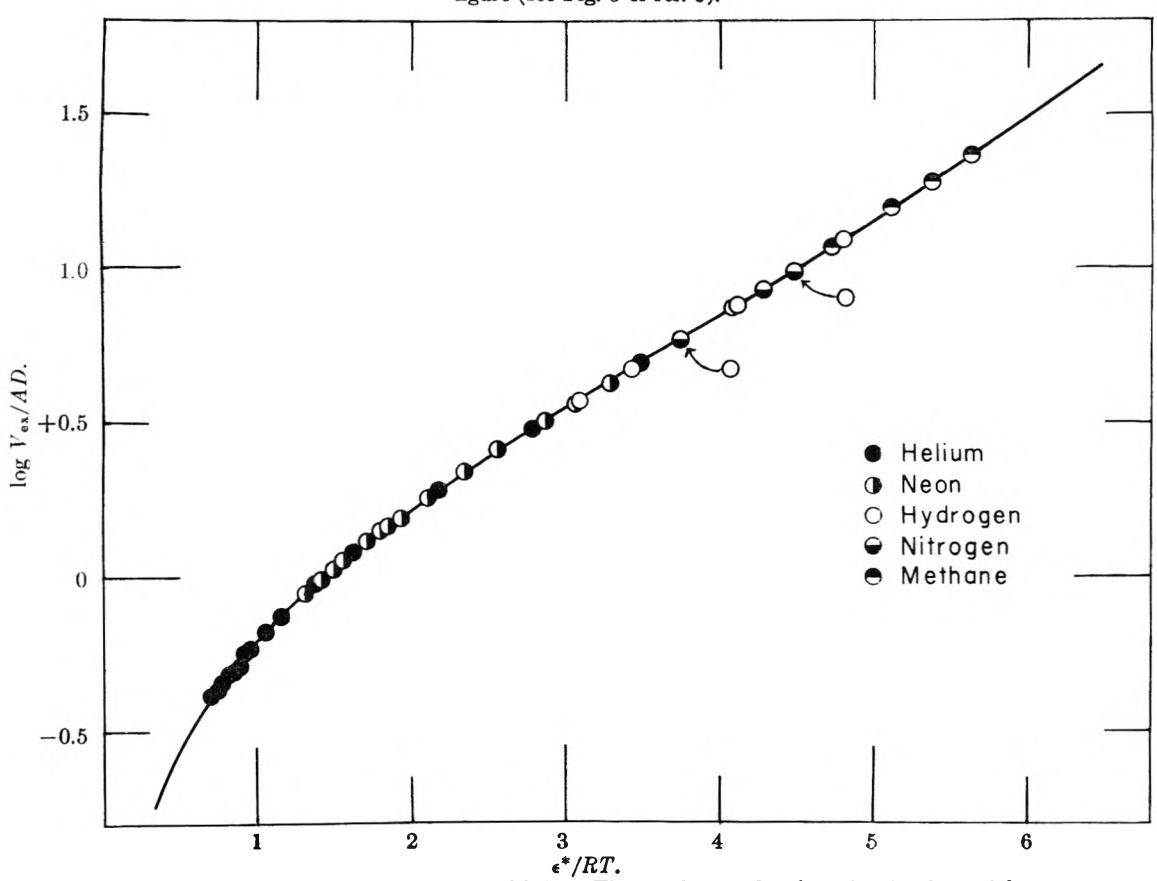

Fig. 7.—Fitted experimental results for saran charcoal S-85. The results are fitted to the simple model (see eq. 10 of the previous paper). The argon data are omitted from this figure for the sake of clarity.

TABLE II

Solid	Gas	D (Å.)	A (m.²/g.)	V_{geo} (m./g.)	ϵ^* (kcal.)	B.E.T. (m.²/g.)
Porous glass	Helium	1.87	118	0.8780	0.68	
	Hydrogen	1.86	123	.8780	1.97	
	Neon	1.93	106	.8740	1.54	
	Argon[a]	2.20	71	.8780	3.78	
	Oxygen	1.89	64	.8780	4.09	
	Nitrogen	1.99	49	.8780	4.26	117
Saran charcoal	Helium	2.47	1145	4.821	0.63	
	Hydrogen	2.30	1575	4.821	1.87	
	Neon	2.55	1135	4.821	1.28	
	Argon	2.90	1030	4.821	3.66	
	Nitrogen	2.59	1170	4.821	3.70	2079
	Methane	3.30	980	4.821	4.64	

[a] Taken from the previous paper.[5]

TABLE III

Gas	Atomic susceptibility $\times 10^{29}$	Atomic polarizability $\times 10^{24}$
Hydrogen	0.664[a]	0.81[b]
Oxygen	1.52[a]	1.57[c]
Nitrogen	1.98[a]	1.74[b]
Methane	6.64[a]	2.58[d]

[a] H. Margenau, *J. Chem. Phys.*, 6, 896 (1936). [b] G. G. Havens, *Phys. Rev.*, 43, 992 (1933). [c] E. C. Stoner, "Magnetism," Methuen and Co., Ltd., London, 1948, p. 38. [d] "International Critical Tables, Vol. VI, McGraw-Hill Book Co., Inc., New York, N. Y., 1926, p. 361.

types is greater than the apparent area of the previously averaged volumes. For example, for the model with $\rho^* = 1.00$, the apparent areas, obtained for the three types of energy curves taken separately are

$$\epsilon(\rho, 0, 0) - A_{app} = 2.29$$
$$\epsilon(\rho, 0, 1/2) - A_{app} = 1.86$$
$$\epsilon(\rho, 1/2, 1/2) - A_{app} = 1.82$$

The weighted average of these apparent areas is 1.96. However, the apparent area obtained when a weighted average of the $V - V_{geo}$ is used is 1.52. It is possible that any type of heterogeneity reduces the apparent area. It is clear that such an effect would act to compensate the over-estimation of area inherent in the crude model.

The Drift in Area with Molecular Size and Type.—The results for the rare gases on porous glass show a drift to smaller area as the molecular size and value of D increase. This effect is in qualitative agreement with the results calculated for capillary spaces in section 2. However, the capillaries in this solid are presumably more or less cylindrical with a diameter in the range of 60 ångströms.[10] From Table II, one finds that all the D's are near 2 Å. Thus R/D is about 15. This value is out of the range where the capillary size has much effect (Fig. 2). It appears then that a fraction of the area is in much smaller capillaries, or that some of the area is even totally inaccessible to the larger molecules. Note the slight reduction in V_{geo} on going from helium to neon. For the heavier gases, the fit is insensitive to the choice of V_{geo},[5] and so no further information about the accessibility can be obtained in this way. The three diatomic gases behave in a roughly similar manner. The hydrogen area is larger than the helium area, which at least suggests some partial "chemical" character to the adsorption. Also, nitrogen is adsorbed somewhat more strongly than oxygen; this effect is frequently encountered with these gases.[11] The calculations in section 3 suggest a drift in the opposite direction with molecular size, for atoms larger than the crystal lattice. Such an increase in area with increase in D was observed previously with alumina on going from argon to krypton. Preliminary data for neon on alumina confirm this drift.

The Area of the Saran Charcoal.—One reason for studying the saran sample was the phenomenal B.E.T. surface area, which is difficult to take seriously. Our method, with a number of gases, gives a consistent area of about 1000 m.²/g., which is more reasonable. With the exception of the hydrogen area, which is suspect because of the specific interaction possible, there is only a slight drift to lower areas as the size of the gas molecule increases. If the carbon is graphitic in structure, some further refinements can be introduced. Crowell and Young[12] have shown that the energy of attraction for argon on graphite does not vary appreciably for motion parallel to the basal plane. At first sight it would appear that the appropriate model for this situation would be the treatment of Section 3 with $\rho^* = \infty$. At this limit, there is no variation in energy with motion parallel to the basal plane. The area would then be reduced by the factor 1.84 to 560 m.²/g. This model is not correct, however, because it smooths the potential by averaging the energy over the three dimensions of the lattice cell. Thus the original Lennard-Jones 6–12 is reduced in power by three to 3–9 by the triple integration. The layer structure of graphite suggests a more valid approximation. The large distance between basal planes, compared to the short bond distance within the plane, makes the contribution of the first layer of atoms very important at short distances from the surface. Contributions from the underlying planes only become relatively important when the total energy is very small anyway. (In addition, it is likely that in the high surface saran charcoal, the solid is only a few layers thick.) Therefore, it is more nearly correct to integrate over the positions of the atoms in the surface plane, only.

(10) P. H. Emmett, private communication.

(11) J. R. Arnold, *J. Am. Chem. Soc.*, **71**, 104 (1949).

(12) A. D. Crowell and D. M. Young, *Trans. Faraday Soc.*, **49**, 1080 (1953).

In this case a 4–10 potential law results. This law has been introduced into the expression for V, and the apparent area calculated.[13] An area for the saran of 700 m.²/g. results. Crowell[14] has suggested that his calculations can be extended to our case and it will be of interest to see the area that his exact summation will yield.

In the absence of exact information concerning the structure of the charcoal, it is of interest to compare the present measurements with our earlier results[5] on a saran charcoal of lower area. There the B.E.T. and our areas were in substantial agreement with a value of 800 m.²/g.

(13) W. A. Steele, Thesis, University of Washington, 1954.
(14) A. D. Crowell, private communication.

The higher surface material is prepared by "burning out" the lower surface material. If such a procedure increases the capillary size, and at the same time destroys some of the capillaries, the various areas can be reconciled. If the nitrogen at "point B" in the B.E.T. measurements fills the pores rather than just forming the monolayer, it is clear that the volume so accommodated (and thus the B.E.T. area) will rise as the pores get larger. However, the area measured by our method is not influenced by condensation of gas, and so does not rise to the same extent. It would appear then that, on the basis of the arguments presented here, the apparent B.E.T. area of the higher surface area saran is unreasonably large.

LOW TEMPERATURE REDUCTION OF IRON OXIDES[1]

BY A. D. FRANKLIN AND R. B. CAMPBELL

Franklin Institute Laboratories for Research and Development, Philadelphia, Pa.

Received July 30, 1954

Comparison of the diameters of iron oxide crystallites before reduction with those of the iron particles produced at temperatures less than about 200° indicates that each oxide crystallite produces one iron particle. At higher temperatures, sintering occurs. These results suggest that for low temperature reduction, nucleation of the new phase is much slower than growth.

Introduction

The recent development of single-domain ferromagnetic particles[2–7] has focussed attention upon the low temperature reduction of metal oxides to produce metallic particles. In the literature on this type of reaction[7–12] there appears to be little discussion of the essential factors controlling the particle size of the final metal particles. It is well known that finer particles are produced at lower reduction temperatures, but the question of the relation between the geometric properties of the initial oxide and of the final metal remains unexplored. This paper presents the results of a study of the particle and crystallite sizes of some iron oxides and of the iron powder produced by reduction of these oxides at temperatures between 125 and 450°.

Experimental

Ferrous formate was prepared by dissolving General Aniline and Film Corporation Type "L" carbonyl iron in Merck Reagent formic acid. Excess formic acid was added to bring the pH of the solution to 2–3 to minimize oxidation of the ferrous ion, and the ferrous formate precipitated by evacuation of the solution. The hydrated ferrous formate crystals possessed diameters of the order of several microns. This ferrous formate was dehydrated below 150°, and then thermally decomposed at temperatures from 220 to 255° *in vacuo*.

Chemical analysis of the resulting oxides showed them to be principally FeO, containing less than 2% carbon by weight, and small, variable amounts of ferric ion. Their X-ray diffraction patterns indicated a spinel structure, in agreement with Lihl's[13] results on similar material. However, other evidence to be reported in a subsequent paper indicated that this FeO was really an intimate mixture of Fe and Fe_3O_4. The distribution and particle size of the Fe was such that the corresponding X-ray diffraction lines were scarcely observable in the pattern of the mixture. When data was taken from the spinel part of this pattern, it applied only to the Fe_3O_4 phase. It seems reasonable also to suppose that the Fe phase initially present made only a negligible contribution to the diffraction pattern observed after reduction. Three other iron oxide specimens were used. Fe_3O_4 and γ-Fe_2O_3 powders of the type used for magnetic recording tapes were included. The α-Fe_2O_3 specimen was Baker C.P. ferric oxide.

Reduction of the oxides at temperatures as low as 125° was accomplished by mixing with excess CaH_2 powder (Metal Hydrides, Inc.) and heating at the desired temperature in a low (2–5 cm.) pressure of hydrogen. Reduction with CaH_2 has been reported[14] to involve a two-step reaction

$$2FeO + 2H_2 \rightleftharpoons 2Fe + 2H_2O$$

$$CaH_2 + 2H_2O \rightleftharpoons Ca(OH)_2 + 2H_2 \quad (1)$$

$$Ca(OH)_2 + CaH_2 \rightleftharpoons 2CaO + 2H_2 \quad (2)$$

Preliminary experiments showed that under these conditions reaction 2 proceeded to completion. For each FeO molecule reduced, one excess molecule of H_2 was produced. Since the reaction velocity increased strongly with increasing H_2 pressure, the excess H_2 was removed from the reaction through a by-pass manometer, which allowed the hydrogen pressure in the reaction chamber to remain constant. The excess H_2 was pumped into a system of known volume, and the system pressure followed as a measure of the extent of reduction. The extent of reduction of the final product was also determined independently by dissolving a small sample in dilute H_2SO_4 and collecting the H_2 produced over mercury as a measure of the free metal present. The two methods showed reasonably good agreement.

(1) Supported by the Office of Naval Research.
(2) L. Neel, *Compt. rend.*, **224**, 1488 (1947).
(3) C. Kittel, *Phys. Rev.*, **70**, 965 (1946).
(4) F. Bertaut, *Compt. rend.*, **229**, 417 (1942); Thesis, University of Grenoble (1953).
(5) C. Guillaud, Thesis, University of Strasbourg (1943).
(6) W. C. Elmore, *Phys. Rev.*, **54**, 1092 (1938).
(7) F. Lihl, *Acta Phys. Austriaca*, **4**, 360 (1951).
(8) F. Lihl, *Metall.*, **5**, 183 (1951).
(9) N. I. Ananthanarayanan and J. F. Libsch, *J. Metals*, **5**, *Trans.*, 79 (1953).
(10) J. Robin and J. Benard, *Compt. rend.*, **232**, 1830 (1951).
(11) V. A. Roiter, V. A. Yuza and A. N. Kuznetsov, *Zhur. Fiz. Khim.*, **25**, 960 (1951).
(12) F. Olmer, *Rev. Met.*, **38**, 129 (1941).
(13) F. Lihl, *Monatsh.*, **81**, 632 (1950).
(14) H. Flood, *Kgl. Norske Videnskab. Selskab. Forh.*, **7**, 66 (1935).

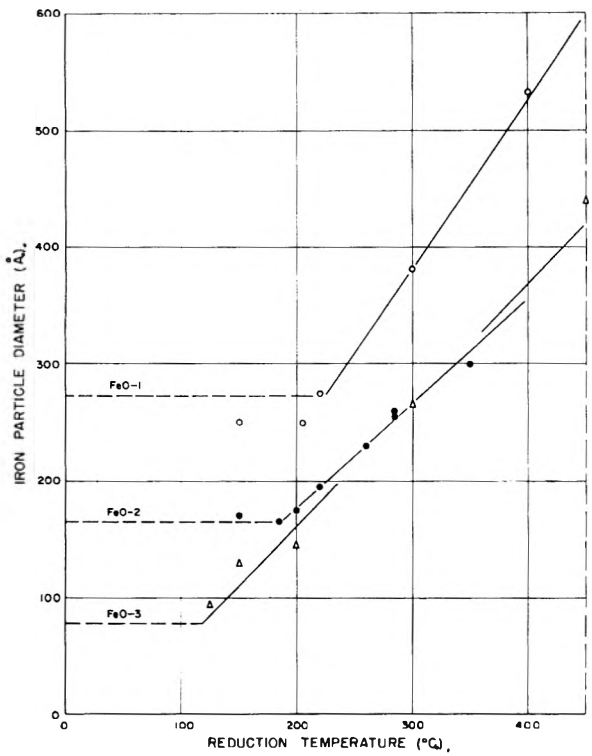

Fig. 1.—Effect of reduction temperature on diameter of iron particles.

Particle sizes were determined with the electron microscope. Crystallite sizes were determined from the broadening of X-ray diffraction lines, using a G. E. XRD-3 spectrometer and Fe K_α radiation. The observed broadening was corrected for the effect of the α_1-α_2 doublet using Jones'[15] method, and for instrumental broadening using Warren's[16] approximations. The instrumental broadening was determined at several values of 2θ from an annealed Armco iron specimen and from annealed zinc and tin. Crystallite diameters were determined using the (110) line for iron, the (311) line for the spinel oxides, and the (211) line for α-Fe_2O_3. The particles in some of the oxides appeared to be polycrystalline. The iron particles were single-crystal, as indicated by rough agreement between electron microscope and X-ray sizes.

Estimation of the crystallite diameter by the method used here involves considerable uncertainty. Aside from measurement errors, the chief source of uncertainty lies in the choice of the constant K in the Scherrer equation[17] used to relate line breadth and crystallite diameter

$$d = K\lambda/\beta \cos\theta$$

where d is the crystallite diameter, λ is the X-ray wave length, β is part of the breadth of the diffraction line due to crystallite size, and θ is the Bragg angle. The value of K depends upon the crystallite shape and structure. Since there is a change in structure upon reducing the oxide to iron (especially in the case of α-Fe_2O_3, where a drastic change in symmetry from rhombohedral to body-centered cubic occurs), the appropriate value may be different before and after reduction. Even for relatively simple shapes and structures, however, the value of K is in doubt by about 20%.[18] In this work, a value of 0.94 was chosen for all materials. This uncertainty in the crystallite diameters must be considered in the interpretation of the data.

Results

Table I lists all of the data for the FeO reduction. In this table T_1 is the temperature of decomposition of the ferrous formate to the oxide, and d_1 the oxide crystallite diameter. T_2 is the temperature at which the oxide was reduced to iron, and d_2 the iron crystallite (and particle) diameter. The column headed % Free Iron gives the degree of reduction, determined by hydrogen evolution.

TABLE I

REDUCTION OF FeO PARTICLES

Oxide sample	T_1, °C.	d_1, Å.	T_2, °C.	d_2, Å.	Free iron, %
FeO-1	255	350	400	536	95
			300	382	75
			220	275	82
			205	250	92
			150	250	91
FeO-2	235	210	350 ± 10	300	80
			285	255	70
			285	260	68
			260	230	72
			220	195	80
			200	174	60
			185	165	68
			150	170	85
FeO-3	220	100	450	440	72
			300	265	86
			200	145	62
			150	130	70
			125	95	68

Table II, with the same notation, gives the data for the lowest temperatures of reduction for the FeO, and for three other oxides reduced at temperatures sufficiently low to avoid sintering.

TABLE II

OBSERVED AND COMPARISON OF CALCULATED LOWER LIMITING Fe PARTICLE DIAMETERS

Oxide sample	d_1, Å.	T_2, °C.	d_2, Å. (Obsd.)	d_2, Å. (Calcd.)	Oxide density, g./cm.³
FeO-1	350	200	250	273	4.8
FeO-2	210	200	170	164	4.8
FeO-3	100	125	95	78	4.8
Fe_3O_4	280	225	200	221	5.2
γ-Fe_2O_3	356	210	275	264	4.6
α-Fe_2O_3	430	210	330	331	5.2

The calculated values for d_2, the iron particle diameter given in the fourth column, were obtained from the oxide crystallite diameters, assuming that each oxide crystallite produces one iron particle without change of shape. The oxide densities listed in the fifth column were used in this calculation, together with a value of 7.9 g./cm.³ for metallic iron.

Discussion

In Fig. 1, the iron particle diameters listed in Table I are plotted for the three sizes of FeO crystallites as a function of reduction temperature. Each curve terminates at the lower left in a horizontal dotted line. This line represents the iron particle diameter expected if each oxide crystallite produced one iron particle. For low reduction temperatures, the observed iron particle diameters agree with these expected diameters. This result is confirmed by the data in Table II. The correspondence between oxide and iron diameters is repeated for the FeO, and is also shown for some

(15) F. W. Jones, *Proc. Roy. Soc.* (*London*), **166A**, 16 (1938).

(16) B. E. Warren, *J. Appl. Phys.*, **12**, 375 (1941).

(17) See for instance R. W. James, "The Optical Principles of the Diffraction of X-rays," G. Bell and Sons, London, 1948, p. 536.

(18) L. Alexander and H. P. Klug, *J. Appl. Phys.*, **21**, 137 (1950).

Fe_3O_4, γ-Fe_2O_3, and α-Fe_2O_3 specimens. For the latter three, the oxide particles were polycrystalline. Each particle contained several thousand crystallites. The iron particle diameter is clearly determined by the crystallite rather than particle diameter of the oxide.

In terms of nucleation-and-growth, it appears that only one nucleus is formed per oxide crystal. This in turn implies that nucleation may be slow, and that once a nucleus is formed, it grows rapidly until it has consumed the entire oxide crystallite.

The role of nucleation as the slow process is borne out by the kinetics of the reduction. Tatievskaya[19] and co-workers have shown that in the temperature region from 350 to 600° the reduction of α-FeO, Fe_3O_4 and α-Fe_2O_3 is autocatalytic. According to their data, and also to observations made during this work, the reaction velocity passes through a maximum as reduction proceeds. In the nucleation-growth picture, the slow initial portion corresponds to the period of nuclei formation, while the rapid reaction at maximum velocity corresponds to the particle growth.

(19) E. P. Tatievskaya, G. I. Chufarov and V. K. Antonov, *Zhur. Fiz. Khim.*, **24**, 385 (1950).

For higher reduction temperatures, an abrupt change in slope of the curves in Fig. 1 occurs. In the high temperature region, some form of sintering apparently takes place. This sintering occurs at surprisingly low temperatures, beginning in the neighborhood of 100° for the 100 Å. diameter FeO. This result is in conformity with observations on thin films. Wheeler[20] states that evaporated iron and nickel films sinter at temperatures as low as 25°.

Conclusions

The following conclusions are drawn from this work: 1. For reduction temperatures from 125 to 450°, iron oxides are reduced in such a fashion that each oxide crystallite produces one single-crystal iron particle. 2. Sintering of iron particles smaller than 300 Å. in diameter begins at temperatures as low as 200°. 3. In the reduction process, nucleation of the new phase is much slower than growth. This view also explains the general form of the kinetics of reduction.

(20) A. Wheeler, in the chapter "Chemisorption on Solid Surfaces," in "Structure and Properties of Solid Surfaces," University of Chicago, Chicago, Illinois, 1952, p. 459.

THE ADSORPTION OF WATER VAPOR ON GERMANIUM AND GERMANIUM DIOXIDE

By J. T. Law

Bell Telephone Laboratories, Inc., Murray Hill, N. J.

Received August 4, 1954

Isotherms have been measured for water adsorbed on germanium and germanium dioxide at temperatures close to 300°K. These are compared with published data for water on silicon dioxide. The isotherms are all of the multilayer type and from these have been calculated free energies, heats and entropies of adsorption at various coverages. By comparing the experimental entropy values with figures calculated from various models, it is shown that the first layer is localized but that succeeding layers are mobile and have effectively the same properties as liquid water.

Introduction

It is well known that germanium surfaces are very sensitive to the presence of water vapor and experiments have been reported as to the effect humidity has on germanium junction devices.[1] No one, however, has investigated the basic process which must underlie this deterioration, namely, adsorption of water vapor on the surface. The only attempt to correlate electrical changes with the amount of water adsorbed on the surface was made by Christensen[2] who measured gravimetrically the adsorption isotherm for water on germanium dioxide.

In this paper results will be presented for the adsorption of water vapor on germanium at pressures above 0.5 mm. and the correlation between these results and electrical measurements on germanium devices discussed.

Experimental

The adsorption of water vapor on a germanium filament at very low pressures has already been studied using a mass spectrometer.[3] It was found that on heating the germanium to 350° the water desorbed completely as a mixture of water and hydrogen presumably as a result of the reaction

$$Ge + xH_2O \rightleftharpoons GeO_x + xH_2$$

Therefore it should be possible to determine the adsorption isotherm by measuring the pressure change in a closed system on heating the germanium after adsorption. This would eliminate any dead space corrections which are required in the more usual type of constant volume adsorption apparatus. The accuracy of the pressure measurements was 10^{-2} mm. so that it was necessary that the pressure change on desorption was of the order of 1 mm. For this reason we had to use samples of crushed germanium with a surface area of about 300 cm.^{2}. The germanium dioxide available was already finely divided and had a surface area of several square meters per gram. The germanium dioxide powder was produced by Eagle Picher Co. and was high purity material of the "soluble" type. The germanium was originally a crystal of high resistivity n-type material, while the silicon was obtained from a low resistivity p-type crystal.

The apparatus used consisted of a water vapor source, an adsorption–desorption vessel (A-B), a differential manometer and a pumping system. The sample of crushed material was placed in the thermostated half (A) of a dumbbell shaped vessel. The other bulb (B) was made of quartz and attached to bulb A through a graded seal. Round B was wound a nichrome furnace, with a thermocouple embedded in the center.

The two bulbs were so arranged that the sample could be transferred from one bulb to the other by rotating the

(1) R. M. Ryder and W. R. Sittner, *Proc. I.R.E.*, **42**, 414 (1954).

(2) H. Christensen, *J. Applied Phys.*, to be published.

(3) J. T. Law and E. E. Francois, *Ann. N. Y. Acad. Sci.*, in press.

assembly about a standard taper joint. The advantage of winding the furnace directly onto the tube was that during a desorption measurement the temperature of only the germanium was changed and no desorption occurred from the glass walls of the apparatus.

A sample of distilled water was freed from gas by alternately freezing and melting under vacuum. The powdered solid was placed in B and degassed at 800° in a vacuum of 10^{-6} mm. for several hours. After cooling to 350° it was tipped into A and adsorption measurements started when it reached room temperature. Water vapor was admitted and left in contact with the solid for 30 minutes (no detectable change occurred if left for a further 18 hours). The sample was then tipped into the bulb B which had been maintained at 350°. The resulting increase in pressure was read by means of a travelling microscope on the wide arm (20 mm.) mercury manometer. The volume of the system had been determined by filling it with water so that the amount of gas desorbed could be determined. This however only gives the volume of gas desorbed from the whole sample and it is necessary to know its surface area before any useful figures can be calculated.

The surface area of the powder can be determined from the water isotherm at room temperature, by either the Hüttig[4] or the Brunauer, Emmett and Teller[5] (B.E.T.) method. A cross-sectional area for the water molecule of 10.6 Å.^{2} at 295°K. was assumed. The areas (in cm.^{2}/g.) obtained are listed in Table I where values are also quoted which were obtained from electron microscope pictures for germanium dioxide.

TABLE I

	Germanium, cm.^{2}/g.	Germanium dioxide, cm.^{2}/g.
B.E.T.	220	2.9×10^4
Hüttig	...	3.5×10^4
Electron microscope	...	$3.5\text{–}5.0 \times 10^4$

From these data the volume (V_m) required to form a statistical monolayer could be calculated and the adsorption results are presented in terms of V_{Ads}/V_m.

Results

Germanium.—The isotherms obtained for water on germanium at 16 and 30° are shown in Fig. 1.

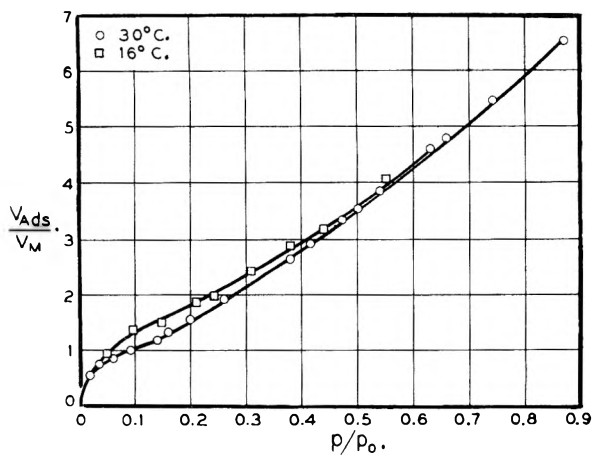

Fig. 1.—Variation of volume of water adsorbed on germanium with p/p_0.

In Fig. 1 the amount adsorbed is plotted against p/p_0. The numbers on the ordinate represent layers in that the value V_m from the B.E.T. calculation was set equal to one. Thus it can be seen that the monolayer is filled at less than $0.1p_0$ and that multilayer adsorption then commences. Near the saturation vapor pressure something like 8–10 layers are adsorbed. In Fig. 1 it can be seen that the curves for the two temperatures coincide above $0.5p_0$. This indicates that the heat of adsorption in this region is identical with the heat of condensation of water vapor, as would be expected in the high multilayer region.

Germanium Dioxide.—The adsorption isotherms on GeO_2 are shown in Figs. 2 and 3. Here again the monolayer is complete at quite low pressures and multilayer adsorption is found at higher pressures. At pressures above $0.3p_0$ the amount adsorbed is about half that found for germanium so that the surfaces clearly behave quite differently. The results obtained by H. Christensen[2] are also shown in Fig. 2 and seem to indicate that his surface was not completely degassed before the measurements. If it is assumed that a monolayer was already present on his surface his results are not too unlike those found in the present work.

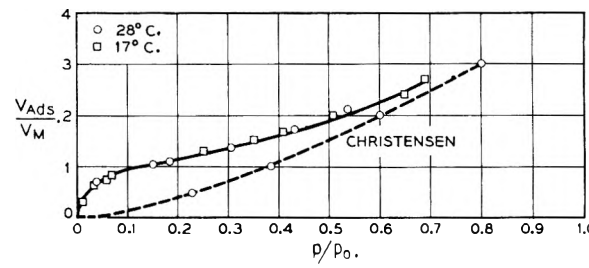

Fig. 2.—Variation of volume of water adsorbed on germanium dioxide with p/p_0.

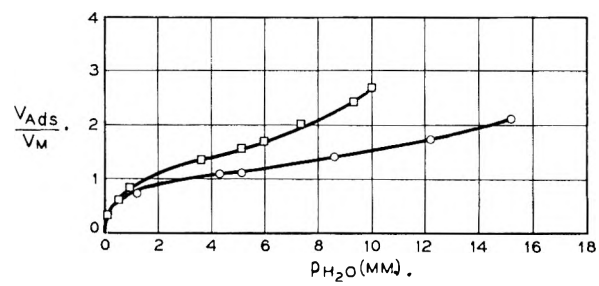

Fig. 3.—Variation of volume of water adsorbed on germanium dioxide with pressure.

Silicon.—Attempts were made to measure the isotherm for water adsorbed on silicon but the results obtained were identical with those described below for silica. For this reason it is felt that the surface was covered with a heavy oxide film. The sample was heated to 1320°K. in an effort to remove it but no marked improvement was obtained. This is not too surprising as the heating was done in a quartz tube where the following equilibrium must exist.

$$SiO_2 + Si \rightleftarrows 2SiO$$

Silicon Dioxide (Silica).—The isotherm for silica that was taken from Livingston's[6] thesis appears to be practically identical with the one obtained for GeO_2 in the present work. It is shown in Fig. 4 together with the corresponding isotherms for germanium and germanium dioxide for comparison.

(4) G. F. Hüttig, *Monatsh.*, **78**, 177 (1948).

(5) K. Brunauer, P. H. Emmett and E. Teller, *J. Am. Chem. Soc.*, **59**, 1533 (1937).

(6) H. K. Livingston, "Adsorption and Free Surface Energy of Solids," Ph.D. Dissertation, University of Chicago, 1941.

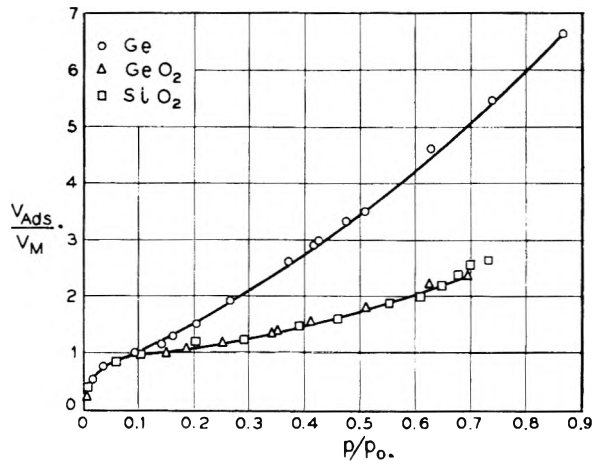

Fig. 4.—Comparison of adsorption isotherms for water on germanium, germanium dioxide and silicon dioxide.

Thermodynamics of Adsorption.—We will now confine our attention to germanium and germanium dioxide as these were the two materials most studied. In each case a multilayer isotherm was obtained which was reversible, *i.e.*, the adsorbed water could be removed by pumping. This was true until the monolayer region was reached when further water could only be desorbed by heating, thus indicating some form of chemisorption. The temperature required for desorption was not investigated carefully but is known to lie somewhere below 350°. During desorption the germanium surface was oxidized as a result of the reaction

$$Ge + xH_2O \rightleftharpoons GeO_x + xH_2$$

and if it was not cleaned by heating *in vacuo* before the next measurement lower values of the amount adsorbed were obtained. This indicates that if a germanium surface is sufficiently heavily oxidized it will behave much like GeO_2 and adsorb less water at a given pressure than a clean surface. From two or more isotherms at different temperatures it is possible to calculate heats, free energies and entropies of adsorption and so determine the degree of mobility of the adsorbed molecules. This is done by comparing the experimental figures with values calculated for different models, namely, fixed and mobile adsorption.

According to the mobile adsorption model, the adsorbed molecules behave as a two-dimensional gas, moving freely over the surface. Recently Kemball,[7] Everett[8] and deBoer[9] have studied the adsorption of various gases in this manner, their approach differing mainly in the choice of a standard state for the adsorbed species.

The differential heats of adsorption were evaluated using the Clausius–Clapeyron equation

$$\left(\frac{\partial \ln p}{\partial T}\right)_V = \frac{\overline{\Delta H}}{RT^2}$$

where V refers to the volume of vapor adsorbed, p the equilibrium pressure and $\overline{\Delta H}$ is the differential heat of adsorption.

(7) C. Kemball, "Advances in Catalysis," Vol. II, Academic Press, Inc., New York, N. Y., 1950, p. 233.

(8) D. H. Everett, *Trans. Faraday Soc.*, **46**, 453, 942 (1950).

(9) J. H. deBoer, *Koninkl, Nederland Akad. Wetenschap. Proc.*, **55**, 451 (1952).

The difference in free energy between the three-dimensional gas standard at temperature T and the adsorbed molecules in equilibrium with p was given by

$$\Delta G = RT \ln p/p_0'$$

The differential entropies were then calculated using

$$T\overline{\Delta S} = \overline{\Delta H} - \Delta G$$

The standard state in the gas phase (p'_0) was taken as 760 mm.

To facilitate the calculation of $\overline{\Delta H}$, V was plotted against log p, as shown in Fig. 6 for germanium.

$$\Delta H = 2.3RT^2 \frac{\Delta \log_{10} p}{T_2 - T_1}$$

The values obtained for $\overline{\Delta H}$ and $\overline{\Delta S}$ at 295°K. are shown in Fig. 5. Although they are not included in this figure, heats of adsorption were calculated from all possible pairs of curves in Fig. 6. The values at a given coverage never differed by more than 1 kcal./mole so that the average values shown were reproducible within ±0.5 kcal./mole.

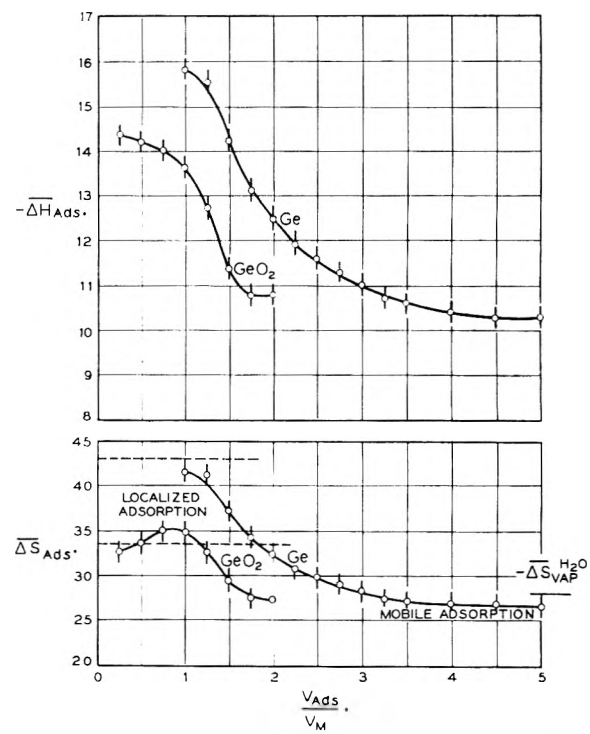

Fig. 5.—Variation of the heat and entropy of adsorption of water on germanium and germanium dioxide.

Accurate values of the entropy of water have been available for some time. Gordon,[10] neglecting the nuclear spin contribution, gave a figure of 45.1 e.u. at 298°K. and 1 atmosphere. Gordon's value was confirmed by Giauque and Archibald[11] using the reaction

$$Mg(OH)_2 \rightleftharpoons MgO + H_2O$$

The contributions of the vibrations to the entropy and the effect of the vibrations on the

(10) A. R. Gordon, *J. Chem. Phys.*, **2**, 65 (1934).

(11) W. F. Giauque and R. C. Archibald, *J. Am. Chem. Soc.*, **59**, 561 (1937).

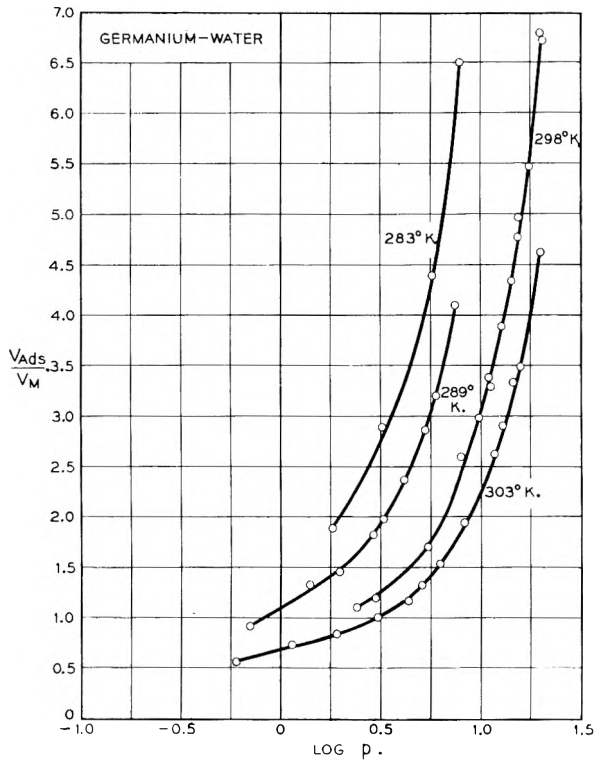

Fig. 6.—Variation of volume of water adsorbed on germanium with log p at various temperatures.

moments of inertia are small at room temperature and may be ignored. Using the moments of inertia given by Gordon[10] the sum of the translational and rotational entropy is found to be 45 e.u. compared with the accurate value of 45.1 e.u.

The rotational entropy was calculated from

$$S_R = 3/2R + R \ln \frac{8\pi^2}{\sigma h^3} (8\pi^3 ABC)^{1/2} (kT)^{3/2}$$

where A,B,C, are the principal moments of inertia and σ is the symmetry number. For water S_R = 10.5 e.u. at 295°K.

The translational contribution was obtained from the familiar Sackur–Tetrode equation and was found to be 34.5 e.u. at 295°K. From the total entropy in the gas phase and the experimental values of $\overline{\Delta S}_{Ads}$, the entropy values for the adsorbed molecules S_{Ads} were obtained. In Fig. 5 the experimental values of the heat and entropy of adsorption are plotted against the surface coverage. A striking feature about the differential entropies is the parallelism between the heat and entropy curves which is in agreement with the behavior noted by Everett.[8]

The general form of the entropy curve in Fig. 5 is that which has been described by Hill, *et al.*,[12] on the basis of the B.E.T. model. The maximum that occurs in the entropy curve for GeO_2 at $V = 0.75$ is indicative[12] of strong binding to the surface because of the small number of possible configurations of the system in the region of the monolayer. The initial increase in $\overline{\Delta S}_{Ads}$ has been shown[13] to be mostly due to the change in configurational entropy with concentration. The decrease in $\overline{\Delta S}_{Ads}$ for water on both germanium and germanium dioxide after the monolayer has been passed, reflects the building up of multilayers. In order to obtain more information about the freedom of the adsorbed molecules it is possible to compare the results with the calculated loss of entropy for water undergoing non-localized adsorption.

The experimentally determined entropies were differential quantities so that we need to obtain the differential entropy of a two-dimensional gas on the surface. The molecular partition function for an ideal two-dimensional gas is given by

$$Q = 2\pi mkTa/h^2$$

where a is the area available per molecule. We will define this area by

$$a = a_0(N_0 - N_s/N_s)$$

where a_0 is the cross-sectional area of the molecule, N_0 the number of molecules required to saturate a given area of adsorbent and N_s the number actually adsorbed at any stage.

Using the normal expressions for entropy in terms of partition functions and assuming a_0 is independent of temperature we obtain

$$N\bar{S}_s = R \ln \left[\left(\frac{2\pi mkTa_0 e}{h^2} \right) \left(\frac{N_0 - N_s}{N_s} \right) + 1 \right]$$

Using a_0 = 10.6 Å.^{2} for water, this gives the differential two-dimensional translational entropy per mole on a half covered surface as 10.6 e.u. at 295°K. On adsorption the third degree of translational freedom will be replaced by a weak vibration with which there will be associated an entropy of approximately 4 e.u.[7] If we assume that the rotational entropy of the water molecules is unimpaired by adsorption (which will almost certainly be true in the case of germanium when six layers are adsorbed) the differential entropy of adsorption will be

$$-\overline{\Delta S} = S^3_{Trans} - S^2_{Trans} - S_{Vibn}$$
$$= 34.5 - 10.6 - 4 = 20 \text{ e.u.}$$

which may be compared with the experimental value of 27.5 ± 2 e.u. The discrepancy between the calculated value of 20 and the experimental value of 27.5 e.u. is sufficiently great that the postulated model must be incorrect. The obvious reason is that we have assumed that in the multilayer region water behaves as a perfect two-dimensional gas. From what is known about the tendency of water to associate this is almost certainly not true. Any restriction resulting from association of the molecules will lead to an increase in the calculated value of $\overline{\Delta S}$. As a first approximation we are justified in taking the value of ΔS_{Vap} and comparing it with the observed entropy of adsorption. Wagman, *et al.*,[14] obtained a value of ΔS_{Vap} = 28.4 cal./mole and it seems reasonable to say that for a mobile layer of water molecules $-\overline{\Delta S}_{Ads}$ will lie between 20 and 28.4 e.u. and probably much nearer the latter figure in agreement with the experimental value of 27.5 e.u. This agreement suggests that in the multilayer region on both germanium and germanium dioxide the water molecules are undergoing non-localized adsorption.

(12) T. L. Hill, P. H. Emmett and L. G. Joyner, *J. Am. Chem. Soc.*, **73**, 5102 (1951).

(13) L. E. Drain and J. A. Morrison, *Trans. Faraday Soc.*, **48**, 316 (1952).

(14) D. D. Wagman, J. E. Kilpatrick, W. J. Taylor, K. S. Pitzer and F. D. Rossini, *J. Research Natl. Bur. Standards*, **34**, 143 (1945).

Let us now consider the monolayer region where the adsorption may be localized. If all translational freedom is restricted there will remain the differential molar localisation entropy which is given by

$$N\bar{s}_a = R \ln \left(\frac{1-\theta}{\theta}\right)$$

(where θ is the fraction of the surface covered) and the entropies associated with the two vibrations in the plane of the surface. The free rotation of the water molecules will probably be replaced by a restricted rotation about the germanium–oxygen bond: Surface Ge–O$\overset{H}{\underset{H}{}}$. At half coverage the configurational entropy term is zero so we have

$$-\overline{\Delta S} = S^3_{\text{Rotn}} + S^3_{\text{Trans}} - S^2_{\text{Vibn}} - S^2_{\text{Rotn}}$$
$$= 45.0 - 5 - 2 = 38 \pm 5 \text{ e.u.}$$

assuming reasonable values for S^2_{Vibn} and S^2_{Rotn}. This value is close enough to the experimentally determined values of 41.6 for germanium and 34.9 for germanium dioxide that we are justified in saying that the monolayer region consists of localized adsorption.

Comparison of Adsorption Results and Electrical Deterioration of Germanium Units.—It has been shown[1] that the reverse current of a germanium p–n junction begins to increase rapidly when the unit is exposed to humidities of 40% or higher. By a comparison of Figs. 4 and 5 of the present work, it may be seen that this corresponds to the formation of a third layer in which the water molecules are quite mobile. It is quite striking that the electrical properties are not appreciably affected by the first localized layer or by the second transitional layer but that as soon as the water molecules have a high mobility the reverse current increases rapidly. This seems to indicate that a process of ionic conduction in the adsorbed film is either the cause of the high conductivity or an intermediate step in its occurrence. The electrical measurements like the adsorption isotherm are reversible upon removal of the water vapor even though the monolayer region must be unaffected by this treatment.

Acknowledgment.—The author wishes to thank J. A. Burton for many helpful discussions.

THE SIZE OF INTERSTITIAL SOLUTE ATOMS IN CLOSE-PACKED METALS

BY KENNETH A. MOON

Ordnance Materials Research Office, Watertown Arsenal, Watertown 72, Mass.

Received August 4, 1954

An improved method has been developed for calculating the size of octahedral solute atoms in primary close-packed metallic interstitial solutions from observed X-ray lattice expansion data. Values of the solute–metal bond length have been calculated by this method for the eight solutions for which X-ray data are available. Comparison of these values with bond lengths predicted by the method of Pauling shows that the solute atoms are bound to the lattice by slightly strained covalent bonds. The partial molar volume of the solute is in some cases much larger than would be expected from the degree of misfit alone. It has been shown that such discrepancies can be attributed to the transfer of electrons from the lattice to the solute–metal bonds.

Progress in understanding the properties of interstitial metallic solutions will require more precise and reliable information than is presently available concerning the size of interstitial solute atoms, and how the size is related to the electronic properties of the metal atoms and solute atoms. Some attempts to calculate the size of the solute atoms from the observed X-ray lattice expansion have appeared in the literature,[1–3] but the treatment has been tentative. The approach used by Speiser, Spretnak and Taylor[3] seems especially promising, but Speiser, *et al.*, made no attempt to justify their basic assumption, and made a number of unnecessary simplifications which introduced significant errors. The present paper will attempt to place the calculation of solute atom size from X-ray lattice expansion measurements upon a more secure foundation. The values of solute atom size so obtained will then be compared with theoretical values calculated on the basis of Pauling's ideas concerning the binding of atoms in crystals.

Measurements of X-Ray Lattice Expansion Due to Interstitial Solutes.—Figures 1 to 6 and Table I show the effect of solute concentration upon the lattice volume for all the close-packed dilute primary metallic interstitial solutions for which X-ray data could be found in the literature,[4] except the (Pd,H)f.c.c. system. The concentration m is in terms of atoms solute per metal atom, and the lattice volume v is in cubic ångström units per metal atom.

Figures 1 to 6 indicate that Vegard's law is valid in these systems as a limiting law in dilute solutions. The significance of this has been discussed by

(1) K. H. Jack, *Proc. Roy. Soc. (London)*, **208A**, 200 (1951).

(2) A. U. Seybolt and H. T. Sumsion, *Trans. Am. Inst. Mining Met. Engrs.*, **197**, 293 (1953).

(3) R. Speiser, J. W. Spretnak and W. J. Taylor, *Trans. Am. Soc. Metals*, **46**, 1168 (1954).

(4) Figure 1: open circles, I. Cadoff and J. P. Nielsen, *Trans. Am. Inst. Mining Met. Engrs.*, **197**, 248 (1953); full circles: P. Ehrlich, *Z. anorg. allgem. Chem.*, **259**, 1 (1949). Figure 2: open circles, A. E. Palty, H. Margolin and J. P. Nielsen, *Trans. Am. Soc. Metals*, **46**, 312 (1954); semicircles, H. T. Clark, *Trans. Am. Inst. Mining Met. Engrs.*, **185**, 588 (1949); full circles, P. Ehrlich, above (1949). Figure 3: open circles, I. Cadoff, A. E. Palty, New York University, Contract No. DA-30-069-ORD-76, Final Report to Watertown Arsenal, Oct. 31, 1952; vertical semicircles, H. T. Clark, above (1949); horiz. semicircles, E. S. Bumps, H. D. Kessler and M. Hansen, *Trans. Am. Soc. Metals*, **45**, 1008 (1953); full circles, P. Ehrlich, *Z. anorg. allgem. Chem.*, **247**, 53 (1941). Figure 4: open circles, K. Honda and Z. Nishiyama, *Science Repts. Tôhoku Univ.*, **21**, 299 (1932); full circles, E. Öhman, *J. Iron Steel Inst. (London)*, **123**, 445 (1931). Figure 5: open circles, K. H. Jack, ref. 1 (1951); full circles, V. G. Paranjpe, M. Cohen, M. B. Bever and C. F. Floe, *Trans. Am. Inst. Mining Met. Engrs.*, **188**, 261 (1950). Figure 6: open circles, R. M. Treco, *ibid.*, **196**, 344 (1953); full circles, J. D. Fast, *Chem. Weekblad.*, **37**, 342 (1940). Table I, (Zr, B): R. Kiessling, *Acta Chem. Scand.*, **3**, 90 (1949); (Zr, N): J. D. Fast, above.

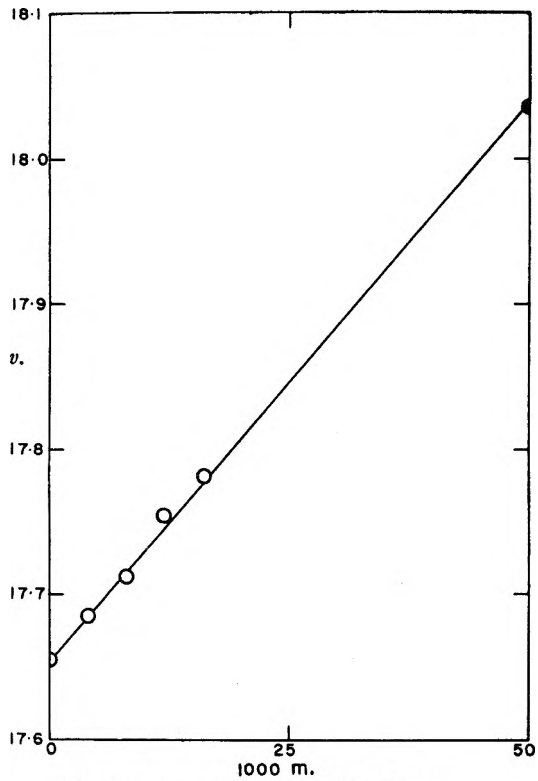

Fig. 1.—Lattice volume of (Ti, C)h.c.p.

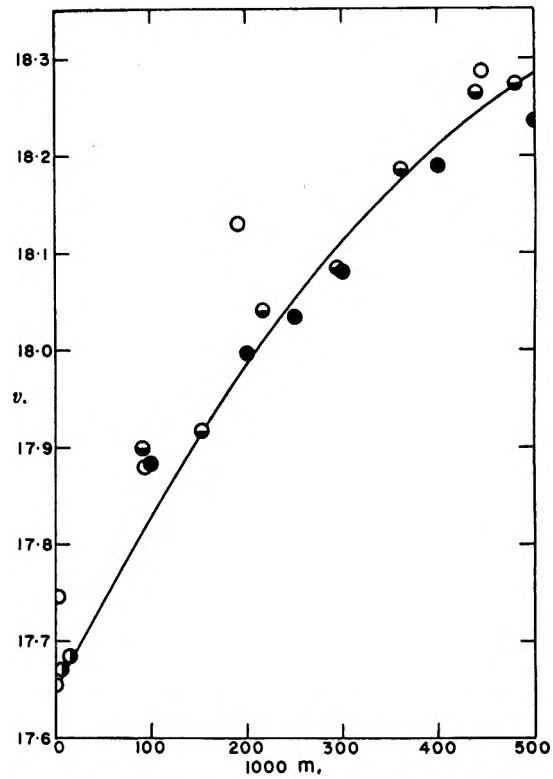

Fig. 3.—Lattice volume of (Ti, O)h.c.p.

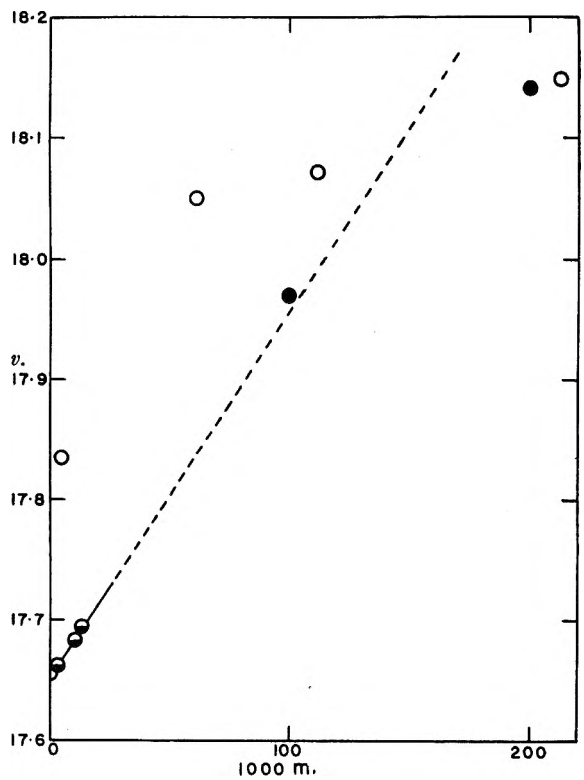

Fig. 2.—Lattice volume of (Ti, N)h.c.p.

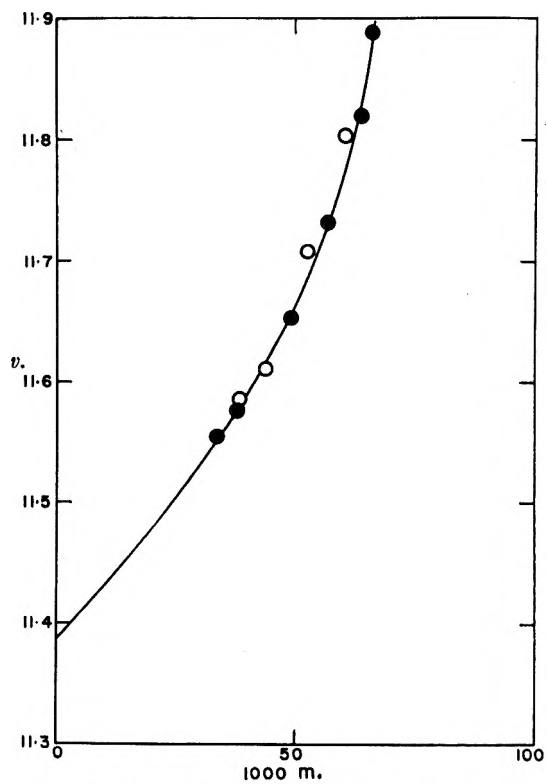

Fig. 4.—Lattice volume of (Fe, C)f.c.c.

Darken and Gurry,[5] and a general theoretical treatment which is pertinent to these systems has been given by Eshelby.[6] The partial molar volume of the solute in infinitely dilute solution, $E = (\partial v/\partial m)_{m=0}$, has been estimated from Figs. 1 to 6 and is listed in Table I. For the systems (Zr,B)h.c.p. and (Zr,N)h.c.p. there were X-ray measurements for only one or two values of m, so the values of E

(5) L. S. Darken and R. W. Gurry, "Physical Chemistry of Metals," McGraw-Hill Book Co. Inc., New York, N. Y., 1953.
(6) J. D. Eshelby, *J. Appl. Phys.*, **25**, 255 (1954).

TABLE I

LATTICE EXPANSION OF SOLVENT METALS AND CALCULATED SOLUTE-METAL BOND LENGTHS

All measurements are in ångström units. a_0 and c_0 are the lattice parameters of the pure metal, and v_0 is the corresponding lattice volume. The limits of error given for E and A represent only the estimated error in reading the slope of the curves in Figs. 1 to 6.

System	Ti, C	Fe, N	Zr, B	Zr, N	Fe, C	Ti, N	Zr, O	Ti, O
Structure	h.c.p.	f.c.c.	h.c.p.	h.c.p.	f.c.c.	h.c.p.	h.c.p.	h.c.p.
a_0	2.9506	3.571	3.2323	3.2323	3.571	2.9506	3.2323	2.9506
c_0	4.6833		5.1471	5.1471		4.6833	5.1471	4.6833
v_0	17.6552	11.3844	23.2856	23.2856	11.3844	17.6552	23.2856	17.6552
A_0	2.07	1.79	2.27	2.27	1.79	2.07	2.27	2.07
E	7.6 ± 0.7	6.4 ± 0.6	6.25	6.1	4.8 ± 0.7	3.0 ± 0.6	2.9 ± 0.9	1.8 ± 0.6
A (eq. 5)		1.90 ± 0.01			1.87 ± 0.01			
A (eq. 7)	2.15 ± 0.01	1.88 ± 0.01	2.33	2.32	1.86 ± 0.01	2.10 ± 0.01	2.29 ± 0.01	2.09 ± 0.01

given in Table I for these two systems are less reliable than for the others.

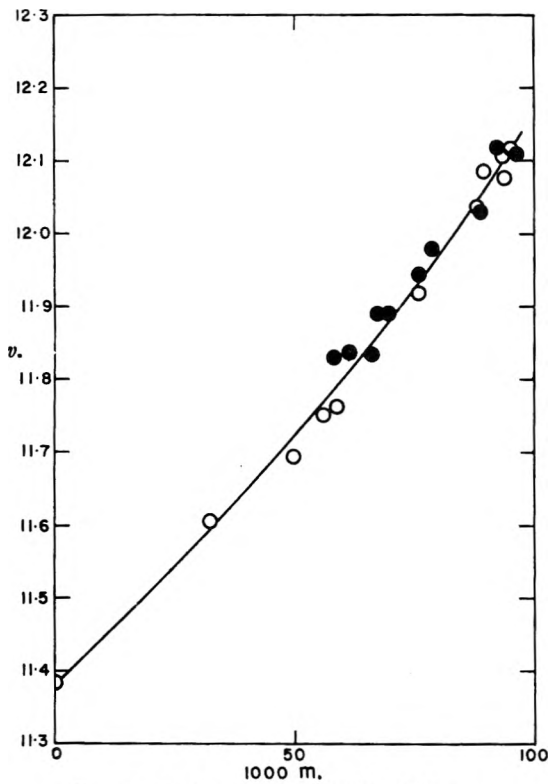

Fig. 5.—Lattice volume of (Fe, N)f.c.c.

Derivation of Equations Relating Solute Atom Size to X-Ray Lattice Expansion.—In addition to assuming that Vegard's law is a valid limiting law, we have to assume that the geometrical expansion of the lattice is equal to the expansion calculated from X-ray lattice parameter measurements. The latter assumption has been investigated theoretically by Eshelby,[6] who found it to be valid if the distribution of solute atoms is uniform throughout the crystal. On the basis of these assumptions, the geometrical expansion of a crystal containing N metal atoms and Nm solute atoms ($m \ll 1$) is

$$\Delta V = NmE \qquad (1)$$

The next step is to relate ΔV to the degree of misfit of the solute atom in the lattice. In general, it would seem that if one could determine by a detailed atomic calculation the expansion up to a certain distance r_0 (equal perhaps to several ångströms) from the solute atom, it would then be a satisfactory approximation to treat the expansion beyond r_0 on the model of a continuous elastic isotropic medium. It is the choice of r_0 and the detailed calculations for $r < r_0$ which present the difficulty.

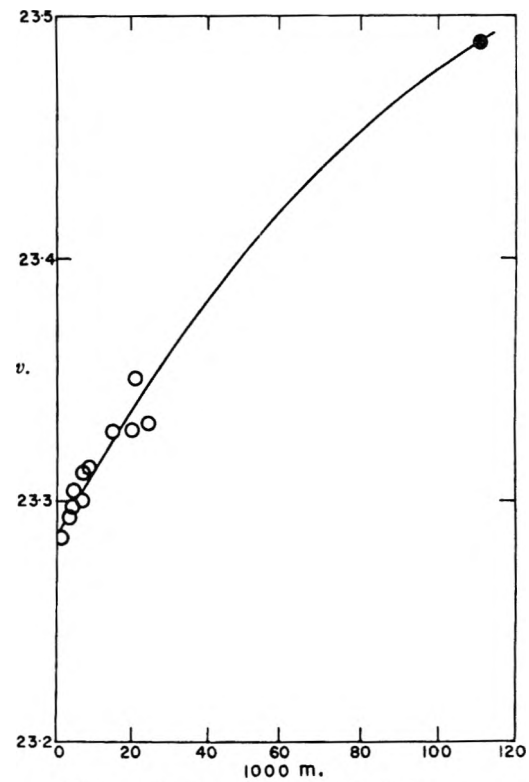

Fig. 6.—Lattice volume of (Zr, O)h.c.p.

The basic assumption of Speiser, *et al.*,[3] was to take r_0 as the distance A_0 from the empty octahedral interstitial site to the six nearest metal atoms, and to assume that this spherical segment of radius A_0 was expanded by introduction of a solute atom to radius A, where A is the desired solute–metal bond length.

Two serious objections can be raised to this assumption. First, the first coördination shell of metal atoms around the solute atom is not a good approximation to a sphere. Second, the calculated values of the expansion $A - A_0$ are in some cases so large that it is doubtful whether the lattice beyond $r = A_0$ can be treated as a continuous elastic isotropic medium. Accordingly, an attempt has been made for the face-centered cubic lattice to carry out

detailed calculations giving the outward displacement of the third nearest neighbors of the octahedral solute atom, given the outward displacement of the nearest neighbors. There are 24 metal atoms in the third coördination shell, and each is bonded to 3 atoms in the same shell, 2 in the second shell, and one in the first shell, making a total of 144 bonds among the 38 metal atoms within the third shell.

The approach used in calculating the expansion of the aggregate of 38 metal atoms was to assume that the metal atoms in the first shell are displaced radially outward a distance equal to $A - A_0$, and that the coördinates of the other 32 metal atoms are changed in such a way that the sum of the squares of the strains of metal–metal bonds is a minimum. Because of the symmetry of the lattice, only four coördinates need be considered: namely, the radial outward displacements $A - A_0$, $B - B_0$, and $C - C_0$ of the metal atoms in the first, second and third coördination shells, respectively, and the angle ϵ subtended at the solute atom by the bond joining a metal atom in the first shell to one in the third shell. Unfortunately, the mathematical complexity of the problem made it necessary to assume ϵ constant. With this assumption, the sum of the squares of the strains in the metal–metal bonds is

$$6a_0^2\{[\alpha - 1]^2 + [(\alpha^2 + 3\beta^2 - 2\alpha\beta)^{1/2} - 2^{1/2}]^2 + [(\alpha^2 + 5\gamma^2 - 4\alpha\gamma)^{1/2} - 2^{1/2}]^2 + 2[(5\gamma^2 - 6\beta\gamma + 3\beta^2)^{1/2} - 2^{1/2}]^2 + 3[\gamma - 1]^2\} \quad (2)$$

where $\alpha = A/A_0$, $\beta = B/B_0$, and $\gamma = C/C_0$, and a_0 is the lattice parameter of the pure metal. Equating derivatives to zero and solving by successive approximations gave the following results

α = 1.0	1.1	1.2	1.3	
β = 1.0	0.9980	0.9919	0.9819	(3)
γ = 1.0	1.0124	1.0238	1.0336	

The expansion of the crystal caused by introduction of Nm of these aggregates of 38 metal atoms and one solute atom with radius C into Nm spherical holes with radius C_0 is given[6] by

$$\Delta V = 4\pi Nm(C^3 - C_0^3)/3 \quad (4)$$

Combination of equations 1 and 4, and introduction of $\gamma = C/C_0$, gives

$$\gamma^3 = 1 + 3E/4\pi C_0^3 = 1 + 0.042705E/v_0 \quad (5)$$

where v_0 is the lattice volume per atom in the pure metal. Thus the desired solute–metal bond length A can be calculated from E by use of equation 5 and interpolation of the data in (3), together with the definition $A = A_0\alpha = 1/2a_0\alpha$. Values of A calculated in this way are given in Table I for carbon and nitrogen in iron.

It is believed that values of A calculated from (5) and (3) are fairly reliable. The error resulting from the assumption of constant ϵ is probably not serious because 11 of the bonds to a metal atom in the third coördination shell tend to hold ϵ constant while only one tends to increase ϵ. Moreover, this error in A is probably negative, whereas that due to the assumption, implicit in equation 4, that the aggregate of 38 metal atoms and one solute atom has the same compressibility as the lattice as a whole is probably positive. More serious error may result from the use of the parabolic interatomic potential function. Compared with a Morse potential function, a parabolic function makes stretched bonds seem too stiff and compressed bonds not stiff enough. Thus the parabolic law gives values of A higher than would be obtained if a Morse function were used. However, even the Morse function may not be suitable for this calculation, because the non-uniformity of the strains in the neighborhood of the solute atom may result in electron shifting effects which will tend to relax the strain energy.

Simplified Calculations.—The detailed calculations of the previous section show that the very severe lattice distortions are confined to the immediate neighborhood of the solute atom, and provide some justification of the basic assumption of Speiser, *et al.* The expansion of the crystal caused by introduction of Nm incompressible spheres of radius A into Nm holes of radius A_0 is given[5,6] by

$$\Delta V = (4/3)\pi Nm[3(1 - \mu)/(1 + \mu)](A^3 - A_0^3) \quad (6)$$

where μ is Poisson's ratio, which we will assume equal to 0.3. Combination with (1) gives

$$A^3 = A_0^3 + 3E[(1 + \mu)/3(1 - \mu)]/4\pi \quad (7)$$

This equation is not exactly representative of those given by Speiser, *et al.*, because they neglected the term in μ, made the approximation $A^3 - A_0^3 = 3A_0^2(A - A_0)$, neglected changes in a_0 when calculating E for hexagonal close-packed metals, and apparently accidentally used $A_0 = a_0/2$ for hexagonal close-packed metals instead of $(c_0^2/16 + a_0^2/3)^{1/2}$ or approximately $a_0/2^{1/2}$.

Table I includes values of A calculated with equation 7. For the two cubic solutions the agreement with A calculated by means of (5) and (3) is excellent, and the discrepancy is in such a direction that we might even prefer the results of the simple calculation. Because of the similarity between the cubic and hexagonal close-packed structures, equation 7 may be considered reliable also when applied to titanium and zirconium.

Calculation of Theoretical Values of the Solute Size.—Values of the solute–metal bond length A' which would be expected in absence of strain can be calculated by using Pauling's equation[7] relating bond length to valence and coördination number

$$A' = R_1 + R_2 - 0.6 \log n \quad (8)$$

where R_1 and R_2 are the appropriate single bond covalent radii of the metal and solute, respectively, and n is the bond number, half the number of shared electrons in the bond, which in this case is the valence of the solute atom divided by the coördination number 6.

The calculations are shown in Table II. Values of the single bond radii listed in the table are those given[8,9] by Pauling and co-workers. For oxygen and nitrogen the tetrahedral radii were used, except in the case of (Fe,N), where it was presumed that a value intermediate between the tetrahedral radius and the normal covalent radius should be used, since the presence of 4.6 electrons on the nitrogen atom (see below) would make its bonds intermediate in hybrid character between normal and tetrahedral. The valences of the metals are those given[7] by Pauling. The electronegativities x_1 and x_2 for metal

(7) L. Pauling, *Proc. Roy. Soc. (London)*, **196A**, 343 (1949).
(8) L. Pauling, *J. Am. Chem. Soc.*, **69**, 542 (1947).
(9) M. E. Jones and R. E. Marsh, *ibid.*, **76**, 1434 (1954).

TABLE II

ELECTRONIC PROPERTIES OF METAL AND SOLUTE ATOMS, AND CALCULATED VALUES OF SOLUTE-METAL BOND LENGTHS

All lengths are in ångströms.

System	Ti, C	Fe, N	Zr, B	Zr, N	Fe, C	Ti, N	Zr, O	Ti, O
R_1	1.33	1.17	1.46	1.46	1.17	1.33	1.46	1.33
R_2	0.77	0.72	0.77	0.70	0.77	0.70	0.66	0.66
Valence of pure metal	4	5.78	4	4	5.78	4	4	4
x_1	1.7	2.3	1.6	1.6	2.3	1.7	1.6	1.7
x_2	2.55	3.0	1.9	3.0	2.55	3.0	3.45	3.45
% ionic character	17	11	2	39	1	34	57	53
Valence of solute	3.4	3.4	2.9	3.6	4.0	3.7	3.8	3.9
$-0.6 \log n$	0.15	0.15	0.19	0.13	0.11	0.13	0.12	0.12
A'	2.25	2.04	2.42	2.29	2.05	2.16	2.26	2.11
$A' - A$	0.10	0.16	0.09	−0.04	0.19	0.06	−0.03	0.02

Table III

CORRECTION OF OBSERVED LATTICE EXPANSION FOR ELECTRONIC EFFECTS

System	Ti, C	Fe, N	Zr, B	Zr, N	Fe, C	Ti, N	Zr, O	Ti, O
No. of electrons lost to solute	2.8		2.8	2.2		2.4	1.6	1.8
Bond length in pure metal	2.923		3.206	3.206		2.923	3.206	2.923
E (electronic)	3.3	0	4.0	3.1	0	2.8	2.3	2.1
E (net)	4.3	6.4	2.25	3.0	4.8	0.2	0.6	−0.3
$1000(A' - A_0)^3$	5.8	15.6	3.4	0	17.5	0.7	0	0.1

and solute, respectively, are the commonly accepted values, except for titanium and iron, which were calculated with Gordy's equation[5] using the metal valence and single bond radius shown in Table II. From the electronegativity difference $x_2 - x_1$ one obtains[10] the percentage ionic character of the solute–metal bonds. According to Pauling's postulate[11] of the essential electrical neutrality of atoms, the ionic character of the bonds can be interpreted as the fractional electronic charge in the bonds, over and above one-half, which is contributed by the more electronegative atom. The valence of the solute is then readily calculated. For example, in the (Ti,N)h.c.p. system the $6n$ solute–metal bonds are 34% ionic, so that $2.08n$ excess electrons are contributed by the nitrogen atom to the bonds, leaving $5 - 2.08n$ as the valence of nitrogen. But by definition the valence is equal to $6n$, so that $n = 5/8.08 = 0.62$. Application of equation (8) then gives $A' = 2.16$.

Comparison of the values of A' in Table II with the corresponding values of A indicates that the solute–metal bonds in these solutions are slightly strained covalent (or metallic) bonds, as expected.

Lattice Expansion Due to Electronic Effects.—Neglecting differences in the stiffness of the various bonds, one might expect that the partial molar volume E of the solute should be approximately proportional to $(A' - A_0)$.[3] That this is far from true is evident from Fig. 7. Some of the discrepancy may be due to errors in E, A and A', but it seems probable that much of the discrepancy may arise as a result of lattice expansion due to electronic effects, as distinct from expansion due to mechanical stress. Certainly some of the electrons in the solute–metal bonds are contributed by the metal, and in titanium and zirconium these must come from the metal–metal bonds, with a resultant lattice expansion. In iron, which Pauling has called[12] a "buffer" element, the necessary electrons can at first be drawn from the reserve supply of non-bonding electrons. After this reserve supply has been exhausted, however, the metal–metal bonds must suffer, and this is probably the explanation of the fact apparent in Figs. 4 and 5 that the partial molal volume of the solute in iron increases with increasing concentration.

It is impossible to make reliable calculations of this effect, but a reasonable idea of the magnitude is given by the calculations in Table III. Again taking (Ti,N)h.c.p. as an example, one solute atom

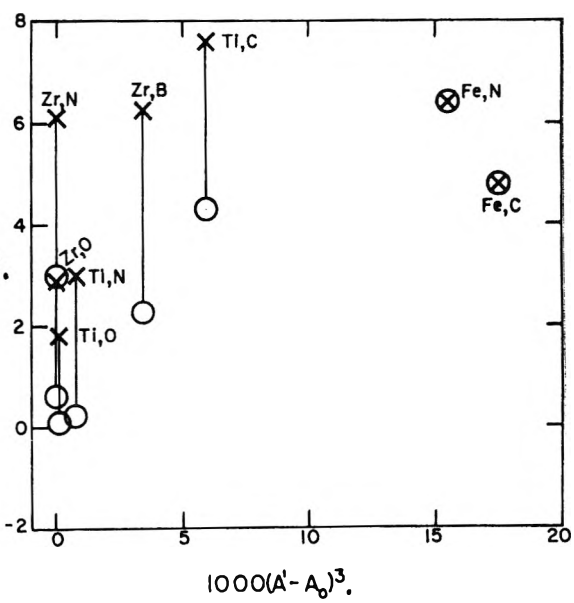

Fig. 7.—Correlation of lattice expansion with calculated degree of misfit of solute atoms in interstitial sites. Crosses are observed values of E; circles are net values after subtraction of the assumed correction due to electronic effects.

(10) L. Pauling, "The Nature of the Chemical Bond," 2nd ed., Cornell Univ. Press, Ithaca, N. Y., 1945, p. 70.

(11) L. Pauling, *J. Chem. Soc.*, 1461 (1948).

(12) L. Pauling, *Proc. Nat. Acad. Sci. U. S.*, **36**, 533 (1950).

draws $6n - 2.08n = 2.4$ electrons from the metal. It is probable that electronic shifts occur among the bonds in the rapidly varying stress field near the solute atom, stretched bonds losing electrons and compressed bonds gaining electrons, so that 2.4 may not be exactly the net loss of electrons from the lattice as a whole to the neighborhood of each solute atom, but we will assume that this is nearly correct, and that the loss is spread over the lattice as a whole. Thus if we add Ndm solute atoms to a crystal containing N metal atoms, the average metal valence will be decreased by $2.4Ndm/N$, and the bond number of the metal–metal bonds will decrease from 4/12 to $(4 - 2.4dm)/12$. From equation 8 we see that the resulting increase in bond length is

$$0.6 \log(1/3) - 0.6 \log[(4 - 2.4dm)/12]$$
$$= -0.6 \log(1 - 2.4dm/4) = (0.6)(2.4)(dm)/(2.3)(4)$$

if dm is small. By geometry the electronic contribution to the partial molar volume of the solute is

$$E(\text{el.}) = (3)(17.6552)(0.6)(2.4)/(2.923)(2.3)(4) = 2.8$$

where 17.6552 is v_0 and 2.923 is the metal–metal bond length in the pure metal. The net value of E which is to be attributed to mechanical strain is 0.2.

Figure 7 shows values of E(net) as a function of $(A' - A_0)^3$, and we see that despite the crudity of our calculations there has been a marked improvement in the correlation.

POLYMERIZATION AND DEPOLYMERIZATION PHENOMENA IN PHOSPHATE–METAPHOSPHATE SYSTEMS AT HIGHER TEMPERATURES. III. CONDENSATION REACTIONS OF DIVALENT METAL HYDROGEN PHOSPHATES[1,2]

BY R. K. OSTERHELD[3] AND R. P. LANGGUTH

Department of Chemistry, Cornell University, Ithaca, New York

Received August 4, 1954

The reactions taking place when barium dihydrogen orthophosphate is heated were studied with the use of thermal analyses, X-ray and chemical analyses, and weight loss data. The rate of thermal decomposition of this compound became appreciable about 243°, the ultimate product being barium tetrametaphosphate. At temperatures just above 243° an appreciable amount of barium dihydrogen pyrophosphate was found to be present during the course of the reaction as an unstable intermediate. Using similar methods the rate of thermal decomposition of lead dihydrogen orthophosphate was found to become appreciable about 195°, aggregation proceeding through an unstable intermediate to form lead tetrametaphosphate. Samples corresponding to various compositions in the lead pyrophosphate–lead metaphosphate system were prepared by heating appropriate mixtures of lead dihydrogen and monohydrogen orthophosphates to constant weight at 550°. A form of phase diagram constructed from thermal analyses of these samples clearly indicated the presence of a compound of the composition corresponding to lead tetraphosphate. Lead tetraphosphate melted incongruently at 700°. X-ray diffraction patterns of samples from the system supported the thermal evidence for the formation of lead tetraphosphate.

Relatively few studies have been made of the aggregation reactions occurring when solid divalent metal hydrogen phosphates are heated. The reactions occurring might be expected to be analogous to those in the classical method for preparation of tetrametaphosphate compounds,[4] which involves the heating of copper oxide, lead oxide or another heavy metal oxide with a slight excess of orthophosphoric acid, first to dryness, then to a temperature not to exceed 450°. In a program of investigating better defined systems studies were made of the thermal aggregation reactions of barium dihydrogen orthophosphate, of lead dihydrogen orthophosphate, and also of mixtures of lead dihydrogen and monohydrogen orthophosphates.

Experimental Procedures

The methods of investigation were essentially those described in earlier papers of this series.[5,6] Differential thermal analyses served to determine the temperatures at which reactions became appreciable in rate or changes in phase occurred during the heating of the various samples. The behavior of the samples at these temperatures was then studied by noting the weight loss occurring at each temperature and by chemical and X-ray analyses of initial, intermediate and final materials. Although X-ray diffraction patterns were obtained primarily for a qualitative determination of the crystalline phases present in a sample, a number are reported here in detail as they may be of interest to other workers.

To prepare barium dihydrogen orthophosphate, powdered barium hydroxide was added to a 50% solution of orthophosphoric acid until precipitation began. After discarding the precipitate slow evaporation of the filtrate on a steam-bath produced anhydrous crystals of barium dihydrogen orthophosphate. *Anal.* of product: Ba, 41.30; P present as PO_4^{-3}, 18.75 (calcd.: 41.44 and 18.69%, respectively). Lead monohydrogen orthophosphate precipitated when a hot solution of lead nitrate was added to a boiling solution of orthophosphoric acid. *Anal.* of the product: P present as PO_4^{-3}, 10.21% (calcd.: 10.22%). The lead monohydrogen orthophosphate was dissolved in warm concentrated orthophosphoric acid to obtain lead dihydrogen orthophosphate which precipitated on cooling. *Anal.* of product: Pb, 51.21%; P present as PO_4^{-3}, 15.54% (calcd.: 51.65 and 15.44%, respectively).

(1) (a) Abstracted from a thesis submitted by R. P. Langguth in partial fulfillment of the requirements for the degree of Master of Science, 1952, Cornell University. (b) Presented at the 125th American Chemical Society National Meeting, Kansas City, Missouri, March 31, 1954.

(2) A portion of this work was supported by the Office of Naval Research.

(3) Department of Chemistry, Montana State University, Missoula, Montana.

(4) F. Warschauer, *Z. anorg. Chem.*, **36**, 137–200 (1903).

(5) R. K. Osterheld and L. F. Audrieth, THIS JOURNAL, **56**, 38 (1952).

(6) L. F. Audrieth, J. R. Mills and L. E. Netherton, *ibid.*, **58**, 482 (1954).

Thermal Decomposition of Barium Dihydrogen Orthophosphate.—Differential thermal analysis of barium dihydrogen orthophosphate (Fig. 1A) showed that endothermic processes became appreciable in rate near 240°, at something over 300° (very weak break), and at 875°. Weight losses for samples of barium dihydrogen orthophosphate heated to constant weight at 245 and 270° (*i.e.*, above the first thermal analysis break) corresponded to the loss of 1.95 and 2.05 moles of water, respectively, per formula weight of barium dihydrogen orthophosphate. The reaction that became rapid near 240° must have produced a barium metaphosphate (eq. 1).

$$n\mathrm{Ba(H_2PO_4)_2} \longrightarrow [\mathrm{Ba(PO_3)_2}]_n + 2n\mathrm{H_2O} \quad (1)$$

The endothermic process that occurred just above 300° was very weak. Since (a) it appeared only in the first heating curve of the barium metaphosphate after its preparation, and (b) there was no detectable weight loss or change in X-ray diffraction pattern associated with the break, it was attributed to a small amount of impurity, perhaps previously unconverted dihydrogen pyrophosphate or the product of a side reaction. The endothermic break at 875° corresponded to the fusion of the barium metaphosphate. On slow cooling the melt appeared to recrystallize completely to give the original metaphosphate. The X-ray pattern was unchanged by fusion and recrystallization, and subsequent heating curves (Fig. 1B) showed only the break accompanying fusion.

The barium metaphosphate produced by the thermal decomposition of crystalline barium dihydrogen orthophosphate was identical with the barium metaphosphate produced by the Warschauer method following the directions of Andress, *et al.*[7] As can be seen in Fig. 1 the products had the same melting point, and they produced the same X-ray diffraction pattern (Table I). Since the Warschauer preparations employing barium or copper compounds have been shown to produce the cyclic tetrametaphosphate anion[7-9] we concluded the thermal decomposition of crystalline barium dihydrogen orthophosphate led to the formation of barium tetrametaphosphate. Furthermore, the X-ray pattern of the soluble product obtained from our barium metaphosphate by metathesis with sodium sulfate solution and dried at 80° contained the strong lines of the high temperature form of sodium tetrametaphosphate four-hydrate[10] and anhydrous sodium tetrametaphosphate plus some of the lines of sodium sulfate.

Samples for analysis were removed at intervals during the heating of a sample of barium dihydrogen orthophosphate at 245°. Each sample was extracted with 0.1 *N* nitric acid and the solution analyzed to determine the percentage of the total phosphorus in the sample present as orthophosphate,[11]

(7) K. R. Andress, W. Gehring and K. Fischer, *Z. anorg. Chem.*, **261**, 331 (1950).

(8) K. R. Andress and K. Fischer, *Acta Cryst.*, **3**, 399 (1950).

(9) C. Romers, J. A. A. Ketelaar and C. H. MacGillavry, *ibid.*, **4**, 114 (1951).

(10) R. N. Bell, L. F. Audrieth and O. F. Hill, *Ind. Eng. Chem.*, **44**, 568 (1952).

(11) L. T. Jones, *Ind. Eng. Chem., Anal. Ed.*, **14**, 536 (1942).

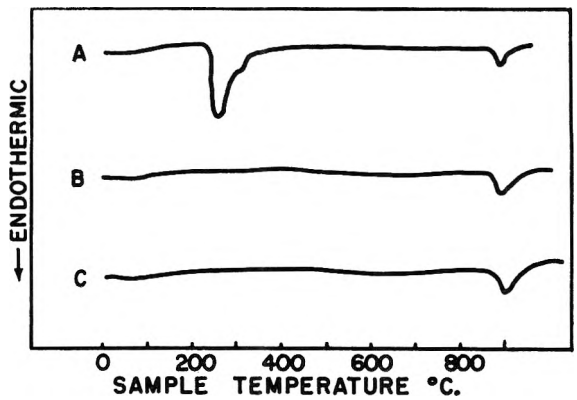

Fig. 1.—Differential thermal analyses: A, $Ba(H_2PO_4)_2$; B, previously fused $Ba(PO_3)_2$; C, Warschauer method $Ba_2(PO_3)_4$.

TABLE I

X-RAY DIFFRACTION DATA FOR BARIUM TETRAMETAPHOSPHATE

A. $Ba_2(PO_3)_4$ from $Ba(H_2PO_4)_2$		B. $Ba_2(PO_3)_4$ from Warschauer method	
d.	Int.	*d.*	Int.
5.16	W	5.20	W
4.24	M	4.25	M
3.76	VW	3.76	VW
3.39	VS	3.40	VS
3.18	M	3.18	M
3.00	VS	2.99	VS
2.70	VW	2.72	VW
2.56	VW	2.58	VW
2.52	W	2.53	W
2.36	VW	2.36	VW
2.25	VS	2.25	VS
2.15	W	2.16	W
2.07	W	2.07	W
2.01	W	2.01	W
1.86	W	1.88	W
1.70	W	1.71	W
1.64	W	1.65	W
1.60	W	1.62	W
1.55	W	1.56	W
1.52	W	1.52	W

pyrophosphate,[12] and triphosphate.[12] The tetrametaphosphate content was calculated from the weight of material insoluble in 0.1 *N* nitric acid. The results are presented in Fig. 2 and Table II. Pyrophosphate was an unstable intermediate in the reaction. No triphosphate was detected; with the Bell method of analysis this implied that higher polyphosphates were absent as well.

TABLE II

AGGREGATION OF $Ba(H_2PO_4)_2$ AT 245°

Time of heating, hr.	Moles of water lost[a]	% of total P as PO_4^{-3}	% of total P as $P_2O_7^{-4}$	% of total P as $P_4O_{12}^{-4}$
0.5	0.175	82.2	17.9	0.0
1.0	0.504	50.1	49.3	0.0
1.5	1.023	15.9	72.0	11.6
2.0	1.703	8.4	20.8	69.5
2.5	2.015	1.4	4.0	93.5
3.0	2.046	0.8	1.0	98.0

[a] Per formula weight of $Ba(H_2PO_4)_2$.

X-Ray diffraction patterns were obtained for the analytical samples. It is of interest that the X-

(12) R. N. Bell, *Anal. Chem.*, **19**, 97 (1947).

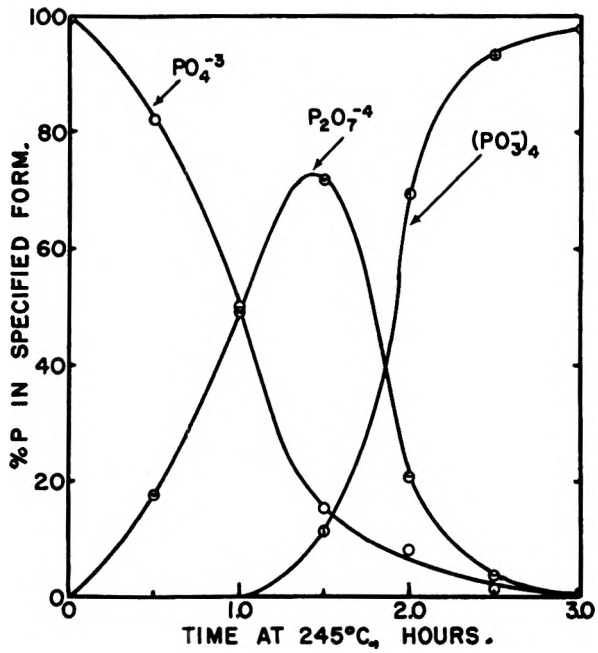

Fig. 2.—Thermal decomposition of $Ba(H_2PO_4)_2$.

ray pattern characteristic of barium dihydrogen orthophosphate persisted (except for minor shifting corresponding to a slight lattice contraction) through three half-hour heating periods at 245°; at that point the weight loss corresponded to about one mole of water per formula weight of barium dihydrogen orthophosphate, and the analytical data showed 84% of the dihydrogen orthophosphate groups had decomposed, about 72% having been converted to pyrophosphate and 12% to metaphosphate. Shortly after this point in the thermal decomposition the X-ray patterns of the analytical samples exhibited the lines characteristic of barium tetrametaphosphate. The lattice contraction noted above might have accompanied the replacement of pairs of dihydrogen orthophosphate ions by dihydrogen pyrophosphate ions, the temperature perhaps being insufficient to permit recrystallization. The X-ray pattern of a salt of a heavy metal ion is, of course, largely due to reflections from the metal ion planes in the crystal.

Thermal Decomposition of Lead Dihydrogen Orthophosphate.—The differential thermal analysis of lead dihydrogen orthophosphate (Fig. 3) indicated that increases in the rates of endothermic processes occurred near 208, 320 and 388°. At temperatures as low as 195° lead dihydrogen orthophosphate samples experienced losses in weight corresponding to the production of a lead metaphosphate (eq. 2).

$$n\mathrm{Pb(H_2PO_4)_2} \longrightarrow [\mathrm{Pb(PO_3)_2}]_n + 2n\mathrm{H_2O} \qquad (2)$$

Heating the lead metaphosphate to temperatures above the temperature of preparation caused nothing further to happen until the material fused near 667°. Thus, while the thermal analysis breaks at 320 and 388° probably corresponded to temperatures at which steps in the over-all process increased in rate, the entire process occurred rapidly enough near 200° to readily effect complete conversion to metaphosphate at that temperature. Consistent

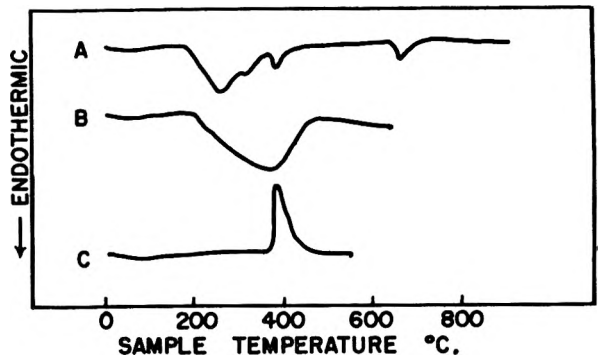

Fig 3.—Differential thermal analyses: A, $Pb(H_2PO_4)_2$; B, $Pb(H_2PO_4)_2$ minus 1.5 moles H_2O; C, $Pb(PO_3)_2$ ground glass.

with this is the observation (Fig. 3B, differential scale exaggerated) that a sample that had lost three-fourths of its water still underwent reaction over the entire temperature interval, starting at the lowest temperature. Moderately slow cooling of fused lead metaphosphate produced a clear, glassy material. The powdered glass crystallized when heated to 375° (Fig. 3C) to give a material having the same X-ray pattern as the original metaphosphate.

The X-ray pattern of the soluble product obtained from the lead metaphosphate by metathesis with sodium sulfide solution and dried at 120° was made up of the lines of anhydrous sodium tetrametaphosphate and the high temperature form of sodium tetrametaphosphate four-hydrate.[10] On this basis the lead metaphosphate formed in this system was lead tetrametaphosphate. The lead tetrametaphosphate produced by the thermal decomposition of lead dihydrogen orthophosphate had the same melting point and X-ray pattern (Table III, A and C) as the product of the analogous Warschauer preparation, the latter having been labeled tetrametaphosphate by Warschauer[4] on the basis of conductivity studies.

An investigation of the course of this aggregation reaction was hampered by inability to devise a satisfactory analytical scheme. However, by the time thermal decomposition had proceeded at 195° to the extent of a loss of one mole of water per formula weight of $Pb(H_2PO_4)_2$ a new set of lines had replaced those of lead dihydrogen orthophosphate in the X-ray diffraction patterns of samples withdrawn from the reaction mixture. This new X-ray diffraction pattern (Table IVA) was presumed to be that of lead dihydrogen pyrophosphate, which was postulated on this basis to be an unstable reaction intermediate. The X-ray pattern for a sample that had undergone loss of one and one-half moles of water per formula weight of original lead dihydrogen orthophosphate showed only the lines of the presumed dihydrogen pyrophosphate but at angles corresponding to slightly decreased interplanar spacings. The X-ray pattern for a sample that had lost two moles of water was the same as that of any of the lead tetrametaphosphate preparations.

The conclusion that the thermal decomposition of crystalline lead dihydrogen orthophosphate produces lead tetrametaphosphate is consistent with the work of Warschauer,[4] who reported the forma-

TABLE III

X-RAY DIFFRACTION DATA FOR LEAD METAPHOSPHATE

A. $Pb_2(PO_3)_4$ of this work		B. $[Pb(PO_3)_2]_n$ of Andress & Fischer[a]		C. $Pb_2(PO_3)_4$ from Warschauer method	
d.	Int.	*d.*	Int.	*d.*	Int.
7.20	M	7.25	M	7.20	M
5.83	S	5.75	M	5.83	S
4.34	M	4.23	M	4.36	M
3.89	VS	3.80	S	3.90	VS
		3.59	W		
3.25	W	3.28	M	3.25	W
3.14	W	3.16	M	3.14	W
2.95	W	2.95	M	2.97	W
2.66	M	2.60	S	2.67	M
2.56	VW	2.51	VW	2.56	VW
2.44	M			2.44	M
2.39	W	2.35	W	2.40	W
		2.25	VW		
		2.20	VW		
2.16	W	2.11	VW	2.17	W
2.09	W	2.05	VW	2.09	W
2.02	VS	1.97	VS	2.02	VS
		1.93	VW		
1.89	VW	1.84	W	1.89	VW
1.83	VW	1.80	M	1.85	VW
1.77	W			1.77	W
1.67	VW			1.67	VW
1.63	W			1.63	W
1.58	W			1.58	W
1.53	VW			1.53	VW
1.48	VW			1.48	VW
1.46	W			1.45	W

[a] Read from Fig. 2 of ref. 13.

TABLE IV

X-RAY DIFFRACTION DATA FOR SEVERAL LEAD PHOSPHATES

A. Presumed $PbH_2P_2O_7$		B. $Pb_2P_2O_7$		C. $Pb_3P_4O_{13}$	
d.	Int.	*d.*	Int.	*d.*	Int.
6.95	W	4.43	W	7.50	VW
5.40	M	4.03	VW	6.25	VW
4.87	M	3.70	VW	5.75	VW
4.00	M	3.42	M	4.96	W
3.67	S	3.32	M	4.60	M
3.50	W	3.14	S	3.80	VW
3.32	W	3.07	M	3.68	M
3.20	W	2.92	VW	3.50	S
3.16	S	2.68	VW	3.30	W
2.91	M	2.45	W	3.20	VS
2.77	S	2.34	VW	3.03	M
2.42	W	2.30	VW	2.97	M
2.37	W	2.20	M	2.72	M
2.28	W	2.12	W	2.49	W
2.24	W	2.03	W	2.34	W
2.20	M	1.93	W	2.27	W
2.14	W	1.90	W	2.17	W
2.07	VW	1.81	VW	2.13	M
2.02	W	1.75	W	2.03	W
1.94	S	1.68	W	1.98	W
1.86	W			1.93	M
1.82	M			1.86	W
1.76	W			1.83	W
1.70	W			1.78	W
				1.73	W
				1.67	W
				1.54	W
				1.48	W

tion of lead tetrametaphosphate when lead oxide was heated with a slight excess of phosphoric acid to a temperature not over 400° and the conversion of this material to another modification (apparently high molecular weight) when the material was heated above 400° to the point of forming a clear melt. It should be noted, however, that Andress and Fischer[13] have reported that a lead metaphosphate studied by them was a long-chain metaphosphate. Their lead metaphosphate was produced in a manner similar to ours, had the same X-ray pattern as ours (Table III, A and B), but melted about 50° lower. The sodium salt solution obtained by Andress and Fischer from their lead metaphosphate by metathesis with sodium sulfide solution was highly viscous, had considerable complexing ability, and would not yield a crystalline sodium metaphosphate. These properties were the main bases for assignment of a long-chain structure to their preparation. The sodium salt solution prepared in our studies was not viscous and readily yielded crystalline precipitates upon addition of acetone. The metathetical cycle used by Andress and Fischer to specifically demonstrate the thermal instability of lead tetrametaphosphate in the temperature range involved in these preparations serves equally well to demonstrate lead tetrametaphosphate is stable at the temperatures involved using their results, a different viewpoint, and considering the X-ray pattern assigned by them to the long-chain metaphosphate to be the pattern of the tetrametaphosphate.

Thermal Decomposition of Lead Dihydrogen–Monohydrogen Orthophosphate Mixtures.—The triphosphate is the only polyphosphate intermediate between the pyrophosphate and metaphosphate compositions that has been produced by heating sodium or potassium hydrogen phosphate mixtures. To evaluate the behavior of an analogous divalent metal system an investigation was undertaken of the materials obtained by heating lead dihydrogen–monohydrogen orthophosphate mixtures.

TABLE V

THE SYSTEM LEAD PYROPHOSPHATE–LEAD METAPHOSPHATE

Mole %[a]		$Pb_3P_4O_{13}$–$Pb_2(PO_3)_4$ Eutectic		$Pb_3P_4O_{13}$ Incongruent m.p.		Liquidus temp., °C.
$P_2O_7^{4-}$	PO_3^-	Temp., °C.	Strength	Temp., °C.	Strength	
0.0	100.0	..	..	..	..	667
5.0	95.0	645	*b*	..	..	663
10.0	90.0	645	*b*	..	..	652
15.0	85.0	645	*b*	..	..	648
20.0	80.0	645	8	..	..	675
25.0	75.0	645	4	..	..	695
30.0	70.0	645	2	703	10	700
33.3	66.7	..	0	700	17	733
40.0	60.0	..	..	700	11	770
45.0	55.0	..	..	700	8	780
50.0	50.0	..	..	700	6	790
55.0	45.0	..	..	700	5	794
60.0	40.0	..	..	701	3	798

[a] Molar compositions are calculated in terms of the species PO_3^- and $P_2O_7^{4-}$ and not in terms of their lead salts. [b] Rate control not in use.

(13) K. R. Andress and K. Fischer, *Z. anorg. allgem. Chem.*, **273**, 193 (1953).

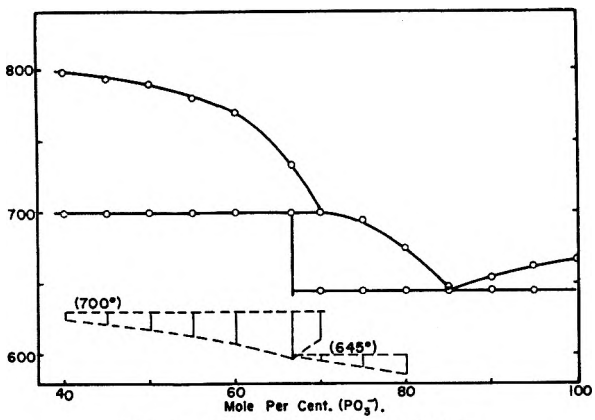

Fig. 4.—System $Pb_2P_2O_7$–$Pb_2(PO_3)_4$.

Reaction products were prepared by heating mixtures of lead dihydrogen and monohydrogen orthophosphates to constant weight at 550°, a temperature above the thermal decomposition temperatures of the individual reactants but below the temperature of appearance of any liquid phase. The products were ground thoroughly and reheated at 550° for 12 hours to ensure complete reaction.

The results of differential thermal analyses of the products appear in Table V and are plotted in Fig. 4. The plotting of the temperatures of the thermal analysis breaks in this way plus the magnitudes of the breaks at 700 and at 645° clearly indicated the presence of a compound of the composition 2 PO_3^-·1 $P_2O_7^{-4}$. This was the tetraphosphate composition: $P_4O_{13}^{-6}$. The X-ray pattern for a sample of the lead tetraphosphate composition (Table IVC) was distinct from those of lead tetrametaphosphate and lead pyrophosphate (Tables IIIA and IVB). Lead tetraphosphate melted incongruently at 700°.

STUDIES ON COÖRDINATION COMPOUNDS. XIII. FORMATION CONSTANTS OF BIVALENT METAL IONS WITH THE ACETYLACETONATE ION[1]

BY REED M. IZATT, W. CONARD FERNELIUS AND B. P. BLOCK

Contribution from The College of Chemistry and Physics, The Pennsylvania State University, State College, Pa.

Received August 6, 1954

Thermodynamic, stepwise equilibrium formation constants are given for the reaction in aqueous solution of the acetylacetonate ion with Mg^{2+}, Cd^{2+}, Mn^{2+}, Fe^{2+}, Co^{2+}, UO_2^{2+} and Cu^{2+}. An over-all molarity quotient is given for the reaction of Hg^{2+} with the acetylacetonate ion in a solution with ionic strength 0.50. Plots of $^1/_2$ (log K_{f_1} + log K_{f_2}) for all the above ions (except UO_2^{2-}) *vs.* (1) electronegativity of the metal ion, or (2) second ionization potential of the gaseous atom, show a linear relationship with two very notable exceptions, Hg^{2+} and Be^{2+}, which form more stable complexes in each case than would be expected from their electronegativity or second ionization potential values. The following order of stability was observed for the elements of Group II with acetylacetone: Mg < Cd < Zn < Be < Hg.

Introduction

The many reports in the literature on the relative stabilities of bivalent elements of the first transition series (Mn, Fe, Co, Ni, Cu and Zn) with a wide variety of ligands together with those involving relative stabilities of other bivalent ions have recently been summarized and discussed by Irving and Williams.[2] They conclude that, although the order of stability

$$Mn < Fe < Co < Ni < Cu > Zn \qquad (I)$$

holds for a wide variety of ligands, one cannot expect to be able to predict with certainty orders of stability when other bivalent ions are included with these because one cannot, with any degree of certainty, predict what the effect of changing both ionic radius and second ionization potential simultaneously will be on the stability of the chelate compound formed. In series (I) cited above the ionic radii vary only slightly, and so the effect on the chelate stability of the changing ionization potential readily may be seen.

The purpose of the present paper is to present the relationship of 1/2 (log K_{f_1} + log K_{f_2}) *vs.* X_M, and 2nd I_p where

K_{f_1} and K_{f_2} = 1st and 2nd thermodynamic formation constants of the metal ion, M^{++}, with the acetylacetonate ion, Ch^-

X_M = electronegativity of the M^{++} (values from Haissinsky)[3]

I_p = ionization potentials[4] of the gaseous atoms

Experimental

Perchlorates of Cu^{2+}, Co^{2+}, Mg^{2+}, Mn^{2+}, Cd^{2+} and Hg^{2+} were obtained from the G. F. Smith Chemical Co. $Be(NO_3)_2$ was obtained from the Brush Beryllium Co. Stock solutions of these metal ions (about 0.2 *M* in metal ion) were standardized by conventional means. C.P. UO_3, obtained from the Fisher Scientific Company, was dissolved in a known volume of excess 0.1164 *N* $HClO_4$. The UO_2^{2+} concentration was determined by precipitating with NH_4OH, igniting and weighing as U_3O_8. The $Fe(ClO_4)_2$ solution was prepared by dissolving a known weight of iron wire in a standard $HClO_4$ solution. The resulting solution gave a negative KSCN test for Fe^{+++}. The Fe^{++} determination was made immediately after preparing the standard Fe^{++} solution. It was necessary to use boiled distilled H_2O in preparing all solutions containing Fe^{++} to prevent oxidation during the course of the titration.

(1) From a portion of a thesis presented by Reed M. Izatt in partial fulfillment of the requirements for the degree of Doctor of Philosophy, August, 1954.

(2) H. Irving and R. J. P. Williams, *J. Chem. Soc.*, 3192 (1953).

(3) M. Haissinsky, *J. Phys. Radium*, [8] **7**, 7 (1946).

(4) G. Herzberg (English translation by J. W. T. Spinks), "Atomic Spectra and Atomic Structure," 2nd Ed., Dover Publications, New York, N. Y., 1944, pp. 200–201.

Unless otherwise noted solutions containing about 0.01 M metal ion and 0.05 M acetylacetone were titrated with 0.20 N NaOH. The pH of the solution was measured after each addition of base by means of a Beckman Model G pH meter equipped with saturated calomel and glass electrodes. The electrodes were checked against Beckman buffer solutions (pH 4.01 and 6.98) periodically. Several titrations were performed in the cases of Be^{2+}, Cu^{2+} and UO_2^{2+} at varying metal ion and ligand concentrations. An atmosphere of nitrogen was used in the Fe^{2+} titration.

The experimental results are tabulated in Tables I and II. Data on the Ni^{2+} and Zn^{2+} systems which appear in Figs. 2 and 3 are given in a previous paper of this series.[5]

TABLE I

FORMATION CONSTANTS (GIVEN AS THE LOGARITHMS) OF SEVERAL BIVALENT METAL IONS WITH THE ACETYLACETONATE ION (T = 30°)

M^{n+}	$[M^{n+}]$, M	log K_{f_1}	log K_{f_2}
Cu^{2+}	3.0×10^{-3}	8.22	6.73
	4.0×10^{-3}	8.23	6.69
Be^{2+}	4.0×10^{-3}	7.80	6.69
	1.0×10^{-2}	7.86	6.72
UO_2^{2+}	1.7×10^{-3}	7.74	6.43
	4.3×10^{-3}	7.76	6.40
	1.0×10^{-2}	7.68	6.32
Co^{2+}	1.0×10^{-2}	5.40	4.11
Fe^{2+}	3.8×10^{-3}	5.07	3.60
Mn^{2+}	1.0×10^{-2}	4.18	3.07
Cd^{2+}	1.0×10^{-2}	3.83	2.76
Mg^{2+}	1.0×10^{-2}	3.63	2.54

chelation and by hydrolysis. This difficulty may be overcome by making the determinations in a pH region in which hydrolysis is known to be negligible. In the present paper experimental conditions were so arranged that this condition was met.

Since the extent of metal hydroxide formation is pH dependent, it is possible by varying the metal ion and ligand concentrations to find a region in which hydrolysis is negligible. The measured thermodynamic formation constants for the reaction of a given metal ion and ligand should be the same within experimental error in any part of the pH region in which chelation occurs. It should, therefore, be possible to determine whether or not appreciable hydrolysis is occurring by observing the precision of thermodynamic formation constant values determined at varying pH values. The precision of the values for the reaction of Ni^{2+} and Zn^{2+} with Ch^- from $2\mu = 0.01$ to $2\mu = 0.49$[6] indicates that appreciable hydrolysis does not occur under the experimental conditions used. The assumption was made that no hydrolysis occurs in the cases of Co^{2+}, Fe^{2+}, Mg^{2+}, Mn^{2+} and Cd^{2+}. Since there was considerable doubt as to whether Be^{2+} and UO_2^{2+} hydrolyzed under the experimental conditions used, it was thought wise to make determinations at several metal ion concentrations. The agreement of these values was good in both cases indicating a negligible amount of hydrolysis. It has been established that UO_2^{2+} is the species of U^{6+} existing in solutions below pH ~3.0.[7]

It was known in the case where $[Be^{++}] = 1 \times 10^{-2}$ M that hydrolysis was negligible at the beginning of the titration because $pH_{(read)} = pH_{(calcd.\ from\ excess\ HClO_4\ added)} = 2.00$. It is probable that considerable coördination with Ch^- had occurred before any hydrolysis took place. The agreement of the two beryllium determinations is good as given in Table I. These values were calculated from values obtained in different pH regions [$\bar{n}$ and Ch^- values taken at

TABLE II

VALUES FOR LOG Q (FOR REACTION VII) AT VARYING $[Cl^-]$

$[Cl^-]$	0.50	0.40	0.30	0.20
A { Contribution of Hg^{2+}-chloro complexes as a function of $[Cl^-]$ given as the log	13.95	13.60	13.19	12.55
B { Molarity quotient values ($Q_{f_1}.Q_{f_2}$) for reactions (V) and (VI) given as the log	7.61	7.93	8.49	8.82
$\log Q = B + A$ or $\log Q = \log \left(\frac{[HgCh_2][Cl^-]^4}{[HgCl_4^=][Ch^-]^2} \right) + \log \left(\frac{[HgCl_4^=]}{[Hg^{++}][Cl^-]^4} \right)$	21.56	21.53	21.68	21.37
$\log Q = \log \left(\frac{[HgCh_2]}{[Hg^{++}][Ch^-]^2} \right)$				

Ionic strength constant at 0.50, temp. = 30°.

The differences in chemical properties of the bivalent metal ions utilized in this study necessitated a careful study of the experimental conditions in order to be fairly certain that the stepwise reactions in each case were

$$M^{++} + Ch^- \rightleftharpoons MCh^+ \qquad (II)$$

$$MCh^+ + Ch^- \rightleftharpoons MCh_2 \qquad (III)$$

where Ch^- = the acetylacetonate ion and all hydration is neglected. For comparative purposes it is desirable that a common starting material, *e.g.*, the hydrated metal ion, be employed. If, for example, chloride ion is present and some of the metal ion is present as the chloro complex, any constants calculated for the above reactions (II and III) which ignore the presence of these chloro complexes will be in error by a certain unknown amount. Van Uitert, *et al.*,[6] showed that for a given metal ion and chelating agent the measured formation constant increases as the anion present varies from Cl^- to NO_3^- to ClO_4^-.

An important error in a perchlorate solution may arise from the formation of metal hydroxide bonds. If this metal hydroxide formation is appreciable (above 3 or 4 parts per 100), there will be a certain error in the pH read inasmuch as this pH will then be a measure of protons liberated both by pH 2.12 and 3.60 for $[Be^{++}] = 1 \times 10^{-2}$ M and at pH 3.30 and 4.49 for $[Be^{++}] = 4 \times 10^{-3}$ M]. For these reasons it was felt that in the case of the Be^{++} determination hydrolysis was negligible.

Copper(II) perchlorate is hydrolyzed to some extent in aqueous solution. However, it was found in the present study that under the experimental conditions used hydrolysis of the Cu^{2+} was negligible. In order to obtain values for K_{f_1} and K_{f_2} in the case of Cu^{2+} the following method was employed. To a solution of $Cu(ClO_4)_2$, about 2×10^{-3} M in Cu^{2+}, a standard (4×10^{-3} M) acetylacetone–water solution was added. The pH of the solution was measured after each addition of the chelating agent. Since the pH of the original solution was 5.10 ($H^+ \cong 9 \times 10^{-6}$ M) and the pH when $\bar{n} \sim 1/2$ about 2.80 ($H^+ = 1.76 \times 10^{-3}$), the change in pH is almost a direct measure of the change in proton concentration due to chelation by the metal ion of Ch^-.

$$Cu^{2+} + HCh \longrightarrow CuCh^+ + H^+ \qquad (IV)$$

In the case of Cu^{2+} a green complex forms initially and, at $\bar{n}$ values near one, traces of a blue complex appear. At $H \sim 1.05$ ($Cu^{2+} = 1 \times 10^{-2}$ M) the blue complex precipitates. However, with $Cu^{2+} = 4 \times 10^{-3}$ M precipitation occurs at $\bar{n} \sim 1.30$, so by varying the experimental conditions K_{f_2} may be obtained. The pH of the solution was more than

(5) R. M. Izatt, C. G., Haas, Jr., B. P. Block and W. C. Fernelius, THIS JOURNAL, **55**, 1133 (1954).

(6) L. G. Van Uitert, W. C. Fernelius and B. E. Douglas, *J. Am. Chem. Soc.*, **75**, 2739 (1953).

(7) H. W. Crandall, *J. Chem. Phys.*, **17**, 602 (1949); also S. Ahrland, *Acta Chem. Scand.*, **3**, 374 (1949).

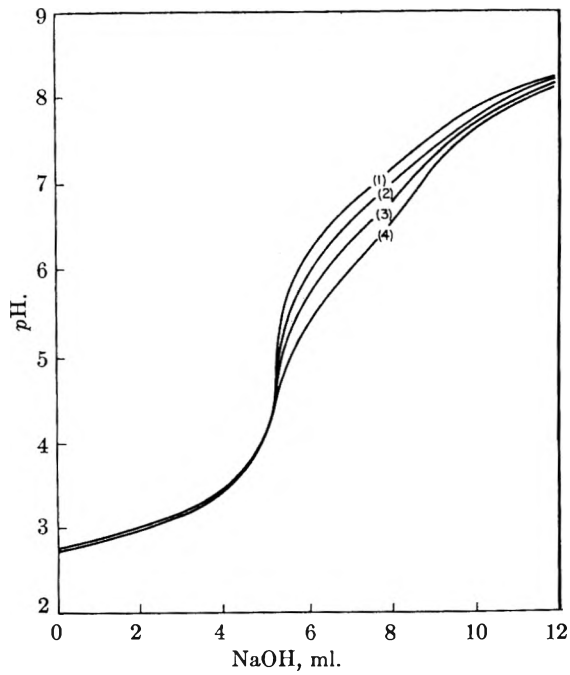

Fig. 1.—Titration curves of solutions containing 6.34 × 10^{-5} mole $Hg(ClO_4)_2$; 1.00 × 10^{-4} mole $HClO_4$ and varying amounts of NaCl and $NaClO_4$ to keep μ = 0.50: (1) = 0.50 *M* NaCl; (2) = 0.40 *M* NaCl; (3) = 0.30 *M* NaCl; (4) = 0.20 *M* NaCl; temp. = 30°; total volume at 0 ml. NaOH = 60.0 ml.

one *p*H unit below the initial *p*H (5.10) throughout the determination and so hydrolysis never became an important factor.

The determination of Hg^{2+} presented an interesting problem. If a solution of mercuric perchlorate and acetylacetone is titrated with NaOH, a precipitate forms after the addition of ~1/2 equivalent base per equivalent Hg^{2+} (2 × 10^{-2} *M*). If more dilute solutions of Hg^{2+} are used, hydrolysis of the Hg^{2+} becomes increasingly important.[8] Mercuric ion forms stable, soluble complexes with chloride ion, the formation molarity quotients of which have been determined by Sillen.[9] Mercuric ion may be kept in a chloride solution as the chloro complex and is stable toward hydrolysis to a fairly high *p*H (about 8),[6] depending on the $[Cl^-]$. The acetylacetonate ion will displace the chloride ions coördinated to the Hg^{2+}. If this reaction proceeds in a stepwise manner in a *p*H region in which hydrolysis of the Hg^{2+} is negligible, one would expect that an over-all Hg^{2+}–acetylacetonate ion formation quotient could be calculated using as a correcting factor the chloro complexity quotient values determined by Sillen at ionic strength = 0.50 and t = 25°. Four titrations were performed at constant ionic strength of 0.50 (maintained with $NaClO_4$) and varying $[Cl^-]$ of 0.50, 0.40, 0.30, and 0.20. The titration curves (*p*H *vs.* ml. NaOH soln.) are shown in Fig. 1. Formation molarity quotients were calculated assuming stepwise addition of two Ch^- ions as

$$HgCl_4^{=} + Ch^- \rightleftharpoons HgCl_2Ch^- + 2Cl^- \quad (V)$$

$$HgCl_2Ch^- + Ch^- \rightleftharpoons HgCh_2 + 2Cl^- \quad (VI)$$

No precipitation was observed to *p*H 8.20 and the solutions remained colorless throughout the titrations. One may now convert the over-all quotient for (V) and (VI) to the quotient for reaction (VII)

$$Hg^{2+} + 2Ch^- \rightleftharpoons HgCh_2 \quad (VII)$$

From a plot of $\frac{1}{2}\Sigma K_n[Cl^-]^n$ *vs.* $[Cl^-]$ one may determine the total contribution of the various Hg(II) chloro complexes at any given $[Cl^-]$. It is seen in Table II where Q_n are the chlorocomplexity quotients given by Sillen[6,7] and $[Cl^-]$ is the total Cl^- concentration, that the values obtained after this correction are in good agreement from 0.50 *M* Cl^- to 0.20 *M* Cl^-. This agreement is a good indication that the over-all reaction (VII) using these experimental conditions is independent of the chloride ion concentration.

Calculations.—The method used in calculating the formation constants and molarity quotients is described elsewhere.[5]

Discussion

In Figs. 2 and 3, the electronegativity, X_n, and the second ionization potential, 2nd Ip, respectively,

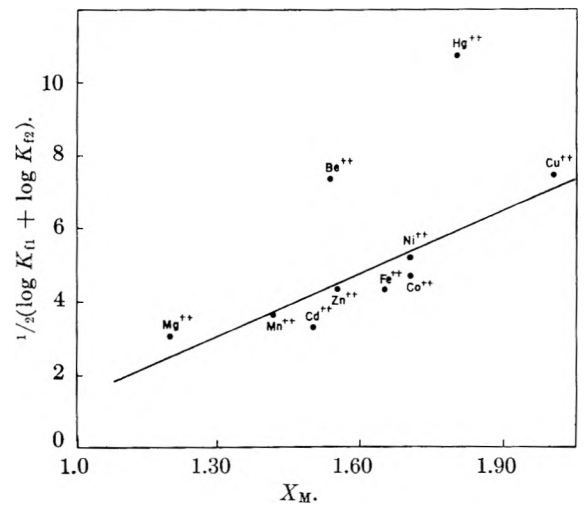

Fig. 2.—Plot of $\frac{1}{2}(\log K_{f1} + \log K_{f2})$ for several bivalent metal ions, $\frac{1}{2}(\log Q_{f1} + \log Q_{f2})$ in the case Hg^{2+}, with the acetylacetonate ion *vs.* the electronegativity, X_M, of the metal ion; temp. = 30°.

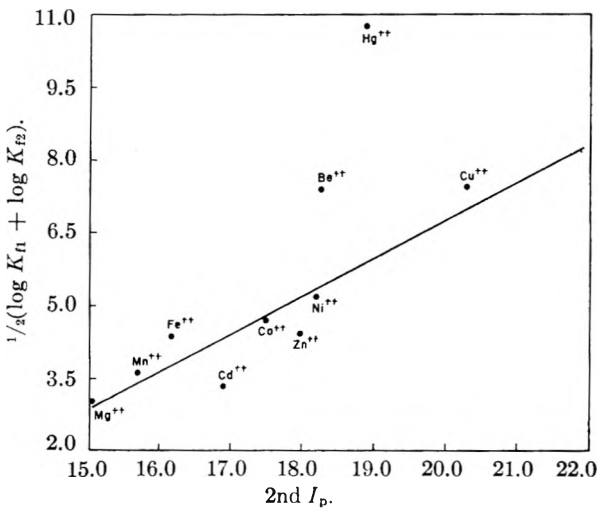

Fig. 3.—Plot of $\frac{1}{2}(\log K_{f1} + \log K_{f2})$ for several bivalent metal ions, $\frac{1}{2}(\log Q_{f1} + \log Q_{f2})$ in the case of Hg^{2+}, with the acetylacetonate ion *vs.* the 2nd ionization potential of the gaseous atom,[4] 2nd I_p; temp. = 30°.

are plotted against $1/2 \log K_{f1}K_{f2}$. With the exception of Be^{++} and Hg^{++}, the points fall on a straight line. From the work reported in this paper and that of Van Uitert[10] the order

$$Ba < Sr < Ca < Mg < Cd < Zn < Be < Hg \quad (VIII)$$

is applicable to acetylacetone and probably to other beta-diketones as well. The values obtained by

(8) J. J. Wylegała, Ph.D. Thesis, Pennsylvania State University, 1954.

(9) L. G. Sillen, *Acta Chem. Scand.*, **3**, 539 (1949).

(10) L. G. Van Uitert, Ph.D. Thesis, The Pennsylvania State University, 1952, pp. 199, 200, 205.

Van Uitert[10] in 75 volume % dioxane–water solution for dibenzoylmethane and for 2-thenoyl-2-furoylmethane give the order Mg < Cd < Zn < Be in each case. His data for Ch^- and several other beta-diketones follow the order Ba < Sr < Ca < Mg.

Two primary factors which affect the stability of the complexes formed by these ions are (1) ionic radii and (2) atomic number. From the ionic radii of these ions given by Goldschmidt,[11] one would expect the order of stability to decrease in the series Mg^{2+}, Ca^{2+}, Sr^{2+}, Ba^{2+} due to the regular increase in ionic radius. Such a decrease is observed with beta-diketones.[8] However, as will be pointed out shortly, the position of Mg^{2+} in such a series varies with different ligands.

It is not surprising that Be^{2+} with a very small radius and a 4+ nuclear charge which cannot be effectively screened by the two available electrons should form a very stable complex with two Ch^- which can share needed electrons to aid in screening the Be^{2+} nucleus. Beryllium acetylacetonate melts at 108° to a liquid which still has the composition of the solid and this liquid boils at 270° to give molecules of beryllium acetylacetonate in the vapor state.[12] One would not expect Mg^{2+} to form a compound of comparable stability to that of Be^{2+}. The ionic radius of Mg^{2+} is more than double that of Be^{2-}. The Mg^{2+} nucleus is much better screened than is that of Be^{2+}, and the repulsion forces between the electron cloud surrounding the Mg^{2+} and the electron clouds surrounding the oxygens in Ch^- are greater than is the case with Be^{2+}.

In Group IIB there is also a progressive increase in the radius but the relative changes in atomic number and radius are different. In the transition from Cd^{2+} to Hg^{2+} the nuclear charge is increased by 32 units whereas the radius increases by only 0.09 Å. In Hg^{2+} the electrons in the outer orbitals screen the nucleus less adequately than in Cd^{2+}. For this reason Hg^{2+} would be expected to form a stronger bond with any atom or ion which can supply electrons to better screen the Hg^{2+} nucleus. Hg^{2+} forms very stable complexes with Cl^-, Br^- and I^-, the stability increasing in the above order as would be expected. These Hg^{2+} complexes are especially stable compared to the corresponding complexes of Zn^{2+} and Cd^{2+} (Q_D for $HgI_4^= = 5.3 \times 10^{-31}$; Q_D for $CdI_4^= = 5 \times 10^{-7}$; Q_D for $ZnI_4^=$ < Q_D for $CdI_4^=$).[13]

The Zn^{2+} and Cd^{2+} chelates are observed to have about the same order of stability and one cannot predict with certainty which will be more stable with a particular ligand. With acetylacetone the order is Zn > Cd, but in a recent summary Irving[2] reports that salicylaldehyde complexes of Cd^{2+} are more stable than are those of Zn^2 by an appreciable amount. A possible explanation for this lack of predictability lies in the fact that two opposing effects are present. In going from Zn^{2+} to Cd^{2+} the ionic radius increases by 0.20 Å. This factor taken alone would cause Zn^{2+} to be the more stable. However, at the same time the nuclear charge has increased by 18 units in the case of Cd^{++}. This latter effect would result in a more stable Cd^{2+} complex. Apparently these two opposing effects are so balanced that compounds of similar stability result in most instances.

From the work reported in the literature it appears that whether Mg^{2+} is more or less stable than the corresponding Ca^{2+} chelate is dependent upon the type of ligand to which the Mg^{2+} is bound. As examples of the variability of Mg^{2+} the following may be cited. The aminoacid type compounds,[14,15] beta-diketones,[10] and dicarboxylic acids (malonic[16] and oxalic)[17] appear to follow the order Mg > Ca > Sr > Ba. However, the order Mg < Ca > Sr > Ba appears to be followed in compounds of the substituted amines, such as nitrilotriacetic acid,[18] 2-sulfoanilinediacetic acid,[19] ethylenediaminetetraacetic acid,[20] methyliminodiacetic acid,[21] and various hydroxy acids (as malic, *dl*-tartaric and glycolic).[22]

The position of Be^{2+} in the stability order given above (VIII) is fairly well substantiated for acetylacetone and other beta-diketones.[10] There appears to be uncertainty, however, over the coördinating ability of Be^{2+} with some other ligand types. Perkins[23,24] has reported the stabilities of a series of 26 amino acids with Hg^{2+}, Zn^{2+}, Cd^{2+} and Be^{2+}. Without exception he found the order of stability to be Cd < Zn < Be < Hg. Although the order given by Perkins is in agreement with that given in (II) above, he expresses some doubt[23] concerning the correctness of his Be^{++} values. Recent work in this laboratory on the coördination of Be^{2+} with ligands containing nitrogen as the coördinating atom indicates that Be^{2+} either does not form complexes with these ligands or that the complexes formed are very weak. Sen[25] has studied the behavior of Be^{2+} toward several amino acids and other nitrogen- and oxygen-containing ligands. He has found that the presence of amino acid and certain other ligand types causes no change in the *p*H at which beryllium hydroxide precipitates. His study included glycine, N-methylglycine, N-phenylglycine, β-alanine, picolinic acid, anthranilic acid, iminodiacetic acid, methyliminodiacetic acid, O-$(CH_2CH_2COOH)_2$ and O$(CH_2COOH)_2$. In addition, the potentiometric titration of Zn^{2+} and Cd^{2+} complexes with Be^{2+} indicates there is no competition between these ions and Be^{2+} for the amino acid ion. If Be^{++} forms amino acid complexes of

(11) V. M. Goldschmidt, *Geochemische Verteilungsgesetze der Elemente*, **8**, 69 (1926); *Ber.*, **60**, 1263 (1927).

(12) A. Combes, *Compt. rend.*, **119**, 1221 (1894).

(13) W. Latimer, "Oxidation Potentials," 2nd Edition, Prentice-Hall, Inc., New York, N. Y., 1952, pp. 168–82.

(14) C. P. Monk, *Trans. Faraday Soc.*, **47**, 297 (1951).

(15) R. F. Lumb and A. E. Martell, THIS JOURNAL, **57**, 690 (1953).

(16) D. I. Stock and C. W. Davies, *J. Chem. Soc.*, 1371 (1949).

(17) R. W. Money and C. W. Davies, *Trans. Faraday Soc.*, **28**, 609 (1952).

(18) G. Schwarzenbach, E. Kampitseh and R. Steiner, *Helv. Chim. Acta*, **28**, 828 (1945).

(19) G. Schwarzenbach, A. Willi and R. O. Bach, *ibid.*, **30**, 1303 (1947).

(20) G. Schwarzenbach and H. Ackermann, *ibid.*, **30**, 1798 (1947).

(21) G. Schwarzenbach, H. Ackermann and P. Ruckstuhl, *ibid.*, **32**, 1175 (1949).

(22) K. Cannan and A. Kibrick, *J. Am. Chem. Soc.*, **60**, 2314 (1938).

(23) D. J. Perkins, *Biochem. J.*, **51**, 487 (1952).

(24) D. J. Perkins, *ibid.*, **55**, [4] 649 (1953).

(25) D. Sen, unpublished results.

the stability reported by Perkins[23,24] exchange with Zn^{++} and Cd^{++} should readily occur. Bryant[26] found that there was no coördination between the Be^{2+} ion and 2-aminotropone in 50% H_2O–dioxane solution as evidenced by the formation of beryllium hydroxide at the same *p*H whether the 2-aminotropone was present or not.

(26) B. Bryant, *J. Am. Chem. Soc.*, **76**, 4864 (1954).

Acknowledgment.—The authors gratefully acknowledge financial support furnished for this work by the United States Atomic Energy Commission through Contract AT(30-1)-907.

TRANSFERENCE NUMBERS OF POTASSIUM ION IN SOLUTIONS OF POTASSIUM BROMIDE IN METHANOL AND POTASSIUM THIOCYANATE IN METHANOL AND IN ETHANOL AT 25°

BY JOE SMISKO[1] AND LYLE R. DAWSON

Contribution from the Department of Chemistry, University of Kentucky, Lexington, Ky.

Received August 9, 1954

Cation transference numbers have been determined at 25° by the autogenic boundary method in solutions of potassium bromide in methanol and potassium thiocyanate in methanol and in ethanol at concentrations ranging from 0.0015 to 0.01 *N*. Plots showing the concentration dependence of the Longsworth function are linear up to approximately 0.01 *N*. The results indicate that for these two potassium salts the tendency for the cation to solvate, relative to the anion, is greater in methanol than in ethanol or water.

Relatively few transference data in non-aqueous media can be found in the literature, and many of those which are available may be not highly accurate. Most of the published results have been obtained by the Hittorf method. The autogenic boundary method was used first by Franklin and Cady[2] in liquid ammonia. Recently Davies, Kay and Gordon[3] have determined values for sodium and potassium chlorides in methanol using the moving boundary method.

Numerous transference data are needed for developing the theory of electrolytes in non-aqueous media, especially for calculating ionic conductances and applying the limiting Onsager equation to unsymmetrical electrolytes. The present investigation was initiated in this Laboratory as a part of a program of study of the electrochemical and thermodynamic properties of some non-aqueous solutions.

Experimental

Apparatus.—A typical autogenic boundary cell was used. The anode was constructed from a pure cadmium rod which had been ground cone-shaped and sealed into position with Apiezon. A coat of shellac provided electrical insulation and protected the Apiezon from the bath liquid. A silver–silver chloride electrode was used for the cathode.

The graduated boundary tube, which was 11 cm. long, was made from 4 mm. Pyrex tubing having an internal diameter of approximately 2.5 mm. It was calibrated carefully before it was sealed to the cell. A similar boundary tube, 7.5 cm. long, was used with the ethanol solutions which have higher electrical resistances.

The cell was held in a thermostated kerosene-bath so that the boundary tube was between parallel plate glass wall sections about four inches apart. Light from a slit illuminated the boundary which was observed with a magnifying lens. Its motion was timed with a mechanical timer.

By the use of an efficient current regulator, variations of the current through the cell were limited to 0.05% for the methanol solutions and 0.10% for the ethanol solutions.

Salts.—Potassium bromide was prepared from hydrobromic acid and potassium carbonate by the method described by Jervis, Muir, Butler and Gordon.[4]

Reagent grade potassium thiocyanate was recrystallized twice and dried for four hours at 110° in an atmosphere of dry nitrogen. Then it was stored in the dark over magnesium perchlorate.

Solvents.—J. T. Baker Analyzed absolute methanol was refluxed over calcium oxide for 12 hours, then fractionated through a ten-plate column retaining only the middle portion. Silver nitrate was added to remove aldehydes, the mixture was refluxed for 12 hours, and finally distilled again retaining only the middle fraction. The specific conductance of the purified methanol ranged from 3 to 6 $\times 10^{-7}$ ohm^{-1} cm.$^{-1}$ at 25°. Less than 0.01% water was indicated by the Karl Fischer reagent.

Commercial absolute ethanol was refluxed with magnesium and iodine and fractionated. To the middle portion of the distillate was added a few grams of 2,4,6-trinitrobenzoic acid to remove traces of bases, and the mixture was refluxed and distilled. The specific conductance of the fraction retained ranged from 5 to 9 $\times 10^{-8}$ ohm^{-1} cm.$^{-1}$ at 25°. The Karl Fischer reagent showed approximately 0.003% water.

Procedure.—Prior to a determination, the equipment was allowed to operate for 30 minutes to ensure equilibration. The solution was introduced through a capillary tube which extended to the anode, care being exercised to prevent the entrapment of air; then the cathode cup was filled and the electrode was introduced. The filling operation required about 30 seconds. The current was adjusted so that a few minutes elapsed before the boundary reached the first mark on the tube, thus allowing ample time for the electrical equipment to reach a steady state. From 800 to 5000 seconds was required for the boundary to move through the graduated portion of the tube.

From 20 to 30 separate measurements, involving duplicate or triplicate determinations at each set of operating conditions, were made for each salt. Solute concentrations varied from 1.5 to 9.5 $\times 10^{-3}$ mole per liter. Currents used for the various solutions ranged from 0.04 to 0.42 ma.

Evidence of the reliability of the calibrations and the general experimental procedure was obtained by determining the transference number of potassium ion in a 0.02 *N* solution of potassium chloride in water. A value of 0.4897 was obtained which agrees quite well with 0.4901 reported by Longsworth.[5] Also the transference number of sodium ion in 0.005 *N* solution of sodium chloride in methanol was measured. A value of 0.4592 was obtained; Davies, Kay and Gordon[3] reported 0.4595.

(1) Based on a dissertation submitted by Joe Smisko in partial fulfillment of the requirements for the degree of Doctor of Philosophy.

(2) E. C. Franklin and H. P. Cady, *J. Am. Chem. Soc.*, **26**, 499 (1904).

(3) J. A. Davies, R. L. Kay and A. R. Gordon, *J. Chem. Phys.*, **19**, 749 (1951).

(4) R. E. Jervis, D. R. Muir, J. P. Butler and A. R. Gordon, *J. Am. Chem. Soc.*, **75**, 2855 (1953).

(5) L. G. Longsworth, *ibid.*, **54**, 2741 (1932).

The conductances of the solvent and of the solution were measured with a Jones bridge, which was manufactured by Leeds and Northrup Company, by the method described in earlier papers from this Laboratory.[5] Solvent corrections were derived from these data. Corrections due to volume changes were negligible.

Results and Discussion

Experimental conditions were arranged so as to provide comparisons of transference data at different current densities in order to ascertain mixing effects at the boundary. Readings made at several graduations gave evidence of the constancy of the transference number as the boundary moved up the tube.

A summary of the results is presented in Table I, where C is the concentration in moles per liter, I is the current in milliamperes, t_+ is the corrected transference number, and d is the mean absolute deviation of the measurements at the given concentration from the average value listed.

TABLE I

TRANSFERENCE DATA

$C \times 10^3$	No. of meas.	I	t_+	$d \times 10^4$
		KBr in Methanol		
3.890	9	0.05–0.12	0.4787	3
6.068	11	.07– .13	.4790	3
9.606	9	.12– .21	.4793	4
		KSCN in methanol		
2.3147	5	0.06–0.11	0.4533	3
2.3164	5	0.12	.4531	3
4.970	7	.13– .21	.4529	2
4.962	6	.12– .25	.4532	2
7.552	8	.15– .32	.4530	3
9.988	8	.23– .42	.4528	3
		KSCN in ethanol		
1.5094	8	0.04–0.10	0.4595	6
2.3106	7	.07– .13	.4587	4
2.3234	3	0 10	.4586	4
4.985	8	.12– .18	.4588	5
5.006	6	.10– .20	.4589	5
7.461	11	.20– .35	.4591	5

All boundaries for potassium bromide in methanol were rather faint. Below 0.004 N the boundary was not discernible and above 0.01 N the transference number varied with current density. This was attributed to heating effects since a greater current density was required to maintain a visible boundary.

With potassium thiocyanate in methanol, the boundaries were sharp and easily observed over the concentration range 0.002 to 0.01 N. Because of the high electrical resistance of the ethanol solutions of potassium thiocyanate, reliable transference data could not be obtained at concentrations above 0.0075 N. The lowest concentration used was 0.0015 N; in more dilute solutions the boundary was very indistinct.

Plots of the Longsworth[6] function

$$t_+^{0\prime} = [t_+\Lambda' + {}^1/_2A(C)^{1/2}]/[\Lambda' + A(C)^{1/2}]$$

are shown in Fig. 1. In this expression $\Lambda' = \Lambda_0 - (A + B\Lambda_0)(C)^{1/2}$, $A = 82.43/(DT)^{1/2}\eta$, $B = 8.203 \times 10^5/(DT)^{3/2}$. D is the dielectric constant[7] (methanol = 32.63, ethanol = 24.3), η is the viscosity[8] (methanol = 0.00546, ethanol = 0.0109), and C is the concentration in moles per liter. The values of A and B are 153.07 and 0.8549 for methanol at 25°; for ethanol at 25°, A = 88.84 and B = 1.330.

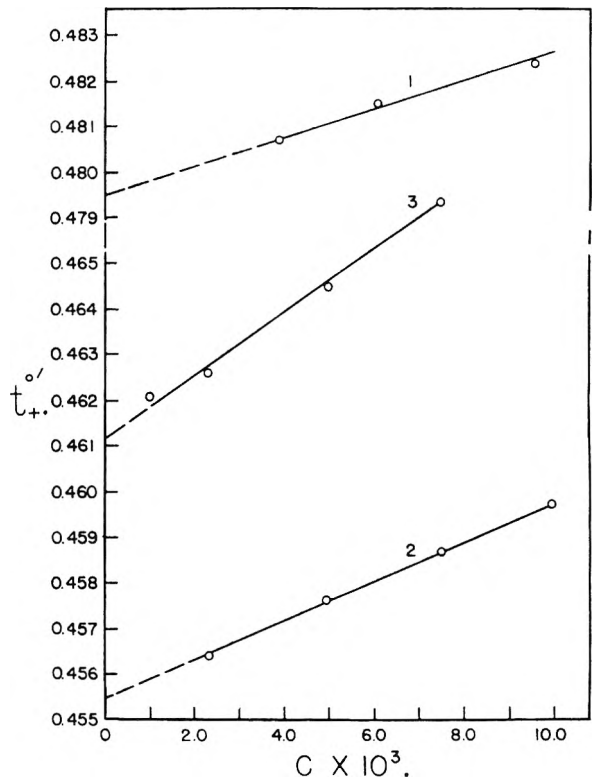

Fig. 1.—The concentration dependence of the Longsworth function for: 1, KBr in methanol; 2, KSCN in methanol; 3, KSCN in ethanol.

The Longsworth plots exhibit essentially linear relationships for the three solutions within the experimental concentration ranges. However, $t_+^{0\prime}$ for KSCN in ethanol at 0.01 N would be approximately 0.468, which is evidence that the plot becomes definitely curved above 0.007 N. By the method of least squares an equation of the form, $t_+^{0\prime} = t_+^0 + bC$ was obtained for each system. Values of the intercept and the constant, b, are shown in Table II. The precision of the limiting transference number is estimated to be within 0.25%. The data in Table III correspond to the plots in Fig. 1.

TABLE II

LIMITING TRANSFERENCE NUMBERS FOR THE POTASSIUM ION AT 25°

Salt	Solvent	b	t_+^0
KBr	Methanol	0.30	0.4795
KCNS	Methanol	.42	.4555
KCNS	Ethanol	.66	.4612

(6) L. R. Dawson and W. M. Keely, *J. Am. Chem. Soc.*, **73**, 3783 (1951).

(7) A. A. Maryott and E. R. Smith, National Bureau of Standards Circular 514, 1951.

(8) R. C. Miller and R. M. Fuoss, *J. Am. Chem. Soc.*, **75**, 3076 (1953).

TABLE III

TRANSFERENCE NUMBERS FOR THE CATION IN SOLUTIONS OF KBr AND KSCN

$C \times 10^3$	t_+, KBr in methanol	t_+, KSCN in methanol	t_+, KSCN in ethanol
0	(0.4795)	(0.4555)	(0.4612)
0.2	.4791	.4547	.4603
0.5	.4790	.4543	.4599
1.0	.4789	.4539	.4595
3.0	.4786	.4531	.4588
5.0	.4787	.4528	.4588
7.0	.4789	.4527	.4590
10.0	.4793	.4528	.4596

Using the conductance data reported by Gordon, *et al.*,[4] for KBr in methanol and Hartley and coworkers'[9] data for KSCN in methanol in conjunction with the limiting transference numbers reported herein, values of 52.11 and 52.24 ohm^{-1} $cm.^2$ for the limiting ionic conductances of the potassium ion were obtained for the KBr and KSCN solutions, respectively. Other investigators have reported λ_{0K^+} in methanol as follows: Hartley and Raikes,[10] 53.8, Gordon, *et al.*,[3] 52.40, and Evers and Knox,[11] 50.2. Using 52.2 ± 0.15 as the most probable value for the potassium ion, from our data we obtain the following anion conductances in methanol: $\lambda_{0Br^-} = 56.7$, $\lambda_{0CNS^-} = 62.2$.

Our transference numbers applied to Barak's and Hartley's[12] conductance data, after extrapolation to infinite dilution by the Shedlovsky method, yields 23.4 and 27.4 for the limiting ionic conductances of potassium and thiocyanate ions in ethanol at 25°. Barak and Hartley reported 22.0 for the potassium ion based on the transference number of the cation in hydrogen chloride (0.71 ± 0.01) as determined by the electromotive force method, in conjunction with a Λ_0 of 83.8. It is difficult to ascertain the reliability of their results because of the uncertainty in the limiting equivalent conductance of hydrochloric acid for which MacInnes[13] reports 81.8, obtaining this value from the data of Goldschmidt and Dahil,[14] while Bezman and Verhoek[15] report 84.25.

The ratio t_+^0/t_-^0 for KBr in methanol is 0.922; for KSCN it is 0.839 and 0.855 in methanol and ethanol, respectively. For KBr in water the ratio is 0.94[16]; for KSCN in water it is approximately 1.11.[17] From the foregoing results it is evident that the potassium ion moves slower in comparison to the thiocyanate ion in both methanol and ethanol than in water, the relative decrease in mobility being greater in methanol. In KBr solutions the cation moves slower in comparison to the anion than in water, although the relative decrease in mobility is not as great as in the KSCN solutions. Thus for these two potassium salts the tendency for the cation to solvate, relative to the anion, seems to be greatest in methanol and least in water.

(9) A. Unmack, D. M. Murray-Rust and H. Hartley, *Proc. Roy. Soc. (London)*, **A127**, 228 (1930).

(10) H. Hartley and H. R. Raikes, *Trans. Faraday Soc.*, **23**, 393 (1927).

(11) E. C. Evers and A. G. Knox, *J. Am. Chem. Soc.*, **73**, 1739 (1951).

(12) M. Barak and H. Hartley, *Z. physik. Chem.*, **A165**, 272 (1933).

(13) D. A. MacInnes, "The Principles of Electrochemistry," Reinhold Publ. Corp., New York, N. Y., 1939, p. 365.

(14) H. Goldschmidt and P. Dahil, *Z. physik. Chem.*, **A114**, 1 (1925).

(15) I. I. Bezman and F. H. Verhoek, *J. Am. Chem. Soc.*, **67**, 1330 (1945).

(16) H. S. Harned and B. B. Owen, "The Physical Chemistry of Electrolytic Solutions," Reinhold Publ. Corp., New York, N. Y., 1950.

(17) C. W. Davies, "The Conductivity of Solutions," Chapman and Hall, Ltd., London, 1933.

ION-EXCHANGE MEMBRANES. I. MEMBRANE POTENTIALS

BY W. F. GRAYDON AND R. J. STEWART

Department of Chemical Engineering, University of Toronto, Toronto, Canada

Received August 13, 1954

A method of preparing homogenous ion-exchange membranes of the polystyrenesulfonic acid type is described. Measurements are reported which show that these membranes may be prepared with high tensile strength and low electrical resistance. The membrane potentials characteristic of these membranes are good approximations to the ideal membrane potentials for cation transfer only. Deviations from the ideal membrane potential are discussed. It is concluded that water transfer is in many cases the major cause of these deviations. Approximate water transference numbers for various membranes are estimated.

Introduction

The primary requirement for an ideal cation-exchange membrane is that it be permeable to cations only and impermeable to anions and neutral molecules. Secondary requirements of considerable practical importance are chemical stability, mechanical strength and high cation mobility in the membrane. A number of methods have been described for the preparation of membranes to determine the extent to which these requirements may be met. The materials which have been studied include collodion,[1] clay,[2] granular ion-exchange resins in binder[3] and "homogenous" ion-exchange resins of the condensation polymer type.[4]

Because of the chemical stability of ion-exchange materials of the polystyrenesulfonic acid type and the inherent advantages of essentially homogeneous membranes attempts were made to prepare membranes of this type by adaptation of the methods used for bead polymers.[5] The product resulting from the sulfonation of polystyrene sheet was extremely fragile and no suitable membranes were obtained.

(1) H. P. Gregor and K. Sollner, THIS JOURNAL, **58**, 409 (1954).

(2) C. E. Marshall, *ibid.*, **52**, 1284 (1948).

(3) M. R. J. Wyllie, *ibid.*, **58**, 67 (1954).

(4) W. Juda, N. W. Rosenberg, J. A. Marinsky and A. A. Kasper, *J. Am. Chem. Soc.*, **74**, 3736 (1952).

(5) G. F. D'Alelio, U. S. Patent 2,366,007 (Dec. 26, 1945).

TABLE I

MONOMER CHARGE COMPOSITION

Membrane no.	Propyl ester, ml.	Styrene, ml.	Divinyl-benzene, ml.	Capacity, meq./g.	Moisture content, g. H_2O/g.	Thickness, mm.
1–6	0.6	2.1	0.36	1.13	0.339	0.343
1–4	0.6	2.2	.24	1.22	.386	.302
1–2	0.6	2.3	.12	1.40	.739	.513
2–6A	1.0	1.7	.36	2.10	.657	.363
2–6B	1.0	1.7	.36	1.75	.501	.432
2–4	1.0	1.8	.24	1.92	.725	.483
2–2	1.0	1.9	.12	1.96	1.24	.541
3–6A	1.4	1.3	.36	2.65	0.881	.541
3–6B	1.4	1.3	.36	2.56	0.823	.536
3–4	1.4	1.4	.24	2.72	1.25	.505
3–2	1.4	1.5	.12	2.94	2.14	.571

Capacity and moisture measurements are recorded on the basis of bone-dry leached hydrogen form of the resin. The first digit in the membrane number refers to the nominal capacity, the second the nominal percentage cross-linking as mole per cent. divinylbenzene.

The membranes described in this report were prepared by the copolymerization of the propyl ester of *p*-styrenesulfonic acid with styrene and divinylbenzene and subsequent hydrolysis of the polymer to produce polystyrenesulfonic acid. This method permitted the preparation of membranes of various capacities with the sulfonate groups distributed throughout the bulk of the membrane.

Experimental

Materials.—The styrene and divinylbenzene (50% solution) used in this work were supplied by the Dow Chemical Company. Both were washed with 10% caustic soda solution, dried and distilled. The propyl ester of *p*-styrenesulfonic acid was prepared by the method of Spinner, *et al.*[6] The sodium chloride was B.D.H. "Analar" reagent and was used without further purification.

Membrane Preparation.—Membranes were prepared by the bulk copolymerization of the propyl ester of *p*-styrenesulfonic acid, styrene and divinylbenzene. Each membrane was prepared by the polymerization of three ml. of liquid monomer in an 8-cm. Pyrex Petri dish. Forty mg. of benzoyl peroxide was used as catalyst. The monomer solution, of one of the compositions as shown in Table I, was sealed in a covered Petri dish with masking tape. The polymerization was allowed to proceed for 30 minutes at 110°. The glass dish with its adherent polymer membrane was placed in boiling 5% sodium hydroxide solution. When the membrane became detached from the glass, it was placed in a glass rod frame and the hydrolysis was continued by boiling in 5% caustic solution until maximum capacity had been obtained. Hydrolysis required from 30 hours to five days.

Membrane Moisture Content.—Samples of the membranes in the hydrogen form were shaken with portions of distilled water until no acid reaction to brom cresol green was obtained. The samples were surface dried and placed in a closed vessel maintained at 100% relative humidity at 25°. When constant weight had been attained the samples were oven dried for 16 hours at 110°.

Membrane Capacity.—Duplicate membrane samples in the leached hydrogen form, surface dried, were added to 50-ml. portions of 2 *N* sodium chloride solution and the solutions titrated with 0.1 *N* sodium hydroxide using brom cresol green.

Membrane Yield Strength.—Yield strengths were determined on surface dried, hydrogen form membrane samples 1 cm. in width by 4 cm. long. The test involved clamping the sample between a movable clamp and a fixed clamp, leaving 3 cm. exposed. The movable clamp was attached to a trolley to which weights had been added. On starting the machine the trolley track rotated from the horizontal toward the vertical position until the sample fractured. Samples which did not break near the middle were discarded. Three to five samples were tested for each type of membrane. The samples were tested using a Scott Tester, model 1P4 manufactured by Scott Testers Inc., Providence, R. I., U. S. A.

Membrane Thickness.—The thickness of the membranes used was measured on the surface dried membrane, one side of which had been in equilibrium with 0.1 *N* $NaNO_3$, the other with 0.1 *N* HCl. The average variation of the thickness was 0.7 thousandth of an inch from the average thickness. Membranes which gave a single thickness measurement which differed from the average thickness by more than 1.5 thousandths of an inch were discarded.

Potential Measurements.—All measurements were taken in a constant temperature room at 25 ± 0.1°. The cell used for the potential measurements was constructed of lucite. The design was similar to that of J. T. Clarke and co-workers.[7] This cell permitted the solutions on either side of the membrane to be changed rapidly without disturbing the membrane.

A circle of membrane 1.5 cm. in diameter was cut and placed between rubber gaskets in the cell. The two halves of the cell were bolted in place and the two silver–silver chloride electrodes were fitted. Each side of the cell was then filled with sodium chloride solution from the reservoirs. The solution concentrations used on each side of the membrane for each measurement are given in Table II.

All potential measurements were made with the solutions at rest in the cell. None were made with the solutions flowing. The solutions on the two sides were renewed until further renewal caused no change in the potential obtained. With membranes which gave nearly ideal potentials as for example the 1–6, 1–4, or 2–6 membranes, two or three renewals of solutions at 5-minute intervals were sufficient to establish the concentration gradient in the membrane. With these membranes the potential remained unchanged (±0.02 mv.) over a period of at least one hour without further renewal of solutions. The poorer membranes such as the 3–2 and 2–2 required numerous and more frequent solution renewals and the potentials obtained fell much more rapidly. The potential across the 2–2 membrane was stable within 0.2 mv. for about one minute only.

The potentials were measured using a Leeds and Northrup type K 2 potentiometer and a moving coil galvanometer of sensitivity 10^{-11} amp./cm., resistance 866 ohms.

In order to test for asymmetry of membranes or electrodes, all the potentials listed in Table II are averages of at least eight measurements. Duplicate readings were taken on each of the four possible combinations of membrane, solutions and electrodes. No evidence of membrane asymmetry such as Kressman reported for ion-exchange rods[8] has been observed. As a typical example of the four possible readings the 1–6 membrane gave 33.05, 33.08, 33.06 and 33.08 mv. in 0.1–0.05 *N* NaCl. Hence it is apparent that neither the electrode nor the membrane asymmetry could have been greater than ±0.02 mv.

In Table II and Fig. 2 the average potentials measured for various membranes and solution concentrations are

(6) I. H. Spinner, J. Ciric and W. F. Graydon, *Can. J. Chem.*, **32**, 143 (1954).

(7) J. T. Clarke, J. A. Marinsky, W. Juda, N. W. Rosenberg and S. Alexander, THIS JOURNAL, **56**, 100 (1952).

(8) T. R. E. Kressman, *J. Appl. Chem.*, **4**, 123 (1954).

TABLE II

MEMBRANE POTENTIALS

Membrane no.	$[RSO_3^-]$ resinate, M	Approx. 0.05–0.1 N % ideal $\times 10^{-2}$	Approx. 0.1–0.2 N % ideal $\times 10^{-2}$	Approx. 0.2–0.4 N % ideal $\times 10^{-2}$	Approx. 0.4–0.8 N % ideal $\times 10^{-2}$
1–6	3.33	0.998	0.995	0.983	0.967
2–6B	3.50	.994	.990		
3–6A	3.01	.989	.986	.954	.905
3–4	2.18	.975	.965	.909	.837

Calcd. ideal potentials:

0.5 − 0.1 = 33.13 mv.
0.1 − 0.2 = 32.31 mv.
0.2 − 0.4 = 31.84 mv.
0.4 − 0.8 = 32.94 mv.

The electrical resistance of the 2–4 membrane was measured using a Solubridge, as described by Juda.[4] The resistance measured was not greater than 4 ohms per cm.^{2} at 1000 cps.

given. The numbers in the columns headed % Ideal were calculated by dividing the measured potential by the value of 0.11834 log a_1/a_2. The solution activities were calculated from the measured concentrations using the data of Harned and Owen.[9]

Discussion

The difficulty encountered in attempts to prepare ion-exchange membranes by the sulfonation of polystyrene sheets is consistent with the data obtained for the tensile strength of the ester polymer membranes. As may be seen from Fig. 1, the tensile strength of these materials decreases rapidly with increasing capacity. The product obtained after sulfonation of polystyrene sheet must have a capacity of the order of five meq./g. if the sulfonation is uniform throughout the resin. The data of Fig. 1 indicate that such a resin would have a very low tensile strength.

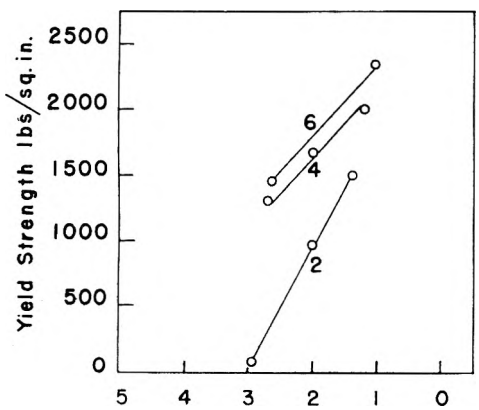

Fig. 1.—Yield strength, lb./sq. in. *vs.* capacity, meq./g., The numbers on the plots represent mole % divinylbenzene.

The extent to which these ester polymer membranes approach the primary requirement of transferring only cationic species may be seen from Table II.

The ideal potential is calculated in each case for a hypothetical membrane permeable only to cations.

$$\text{Ag/AgCl/NaCl, } a_1\text{/M/NaCl, } a_2\text{/AgCl/Ag}$$

$$E_i = \frac{2RT}{F} \ln \frac{a_1}{a_2} \qquad (1)$$

where a_1 and a_2 are mean activities for NaCl.

(9) H. S. Harned and B. B. Owen, "The Physical Chemistry of Electrolytic Solutions," Reinhold Publ. Corp., New York, N. Y., 1950.

The measured potentials which are lower than the ideal potentials show that the ideal cell reaction is not a sufficient description of the laboratory cell reaction. It must be noted that membrane cell potentials are not reversible potentials unless the membranes used are impermeable to water. However, since the potentials for most of the cells measured are reproducible to within ±0.02 mv. over periods of at least five minutes, the amount of osmotic degradation is small. The 3-2 and 2-2 membrane potentials decreased much more rapidly with time and there is some doubt that the potential measured is within 0.02 mv. of the reversible potential. Even if the osmotic flow of water is negligibly small, water may be transferred reversibly by electroösmosis and contribute to the cell reaction. In addition there is the possibility of anion transfer. Hence we assume that the membrane cell reaction is

$$a_1 \xrightarrow{(1 - t_{Cl}) \text{ moles NaCl}} a_2$$

$$a_{w1} \xrightarrow{t_w \text{ moles } H_2O} a_{w2}$$

$$\xrightarrow[\text{positive electricity}]{1 \text{ Faraday of}}$$

and assuming that osmotic degradation is negligible, write the measured cell potential

$$E_c = E_i - 2t_{Cl} \frac{RT}{F} \ln \frac{a_1}{a_2} + t_w \frac{RT}{F} \ln \frac{a_{w1}}{a_{w2}} \qquad (2)$$

where t_{Cl} and t_w represent moles of chloride and water transferred per Faraday.

It has been customary to neglect water transfer in the consideration of membrane potentials[10] and to refer to the ratio of measured to ideal potentials as the cation transport number.[4]

A number of authors have noted that this procedure may result in erroneous values.[11,12] Our calculations indicate that in some circumstances the water transfer term is greater than the anion transfer term in equation 2.

The value to be assigned to the anion transfer term in equation 2 may be estimated using the assumptions of Meyer–Sievers[10] and Teorell.[13]

The appropriate portion of the Donnan potential and the Henderson potential is substituted for the

(10) K. H. Meyer and J. F. Sievers, *Helv. Chim. Acta*, **19**, 649 (1936).
(11) G. Scatchard, *J. Am. Chem. Soc.*, **75**, 2883 (1953).
(12) K. S. Spiegler, *J. Electrochem. Soc.*, **100**, 303C (1953).
(13) J. Teorell, *Proc. Soc. Exptl. Biol. Med.*, **33**, 282 (1935).

anion transfer term in equation 2 to give equation 3.

$$E_c = E_1 - \frac{RT}{F} \ln \frac{[Cl_i^-]_1 + [RSO_3^-]}{[Cl_i^-]_2 + [RSO_3^-]} + \left(\frac{U_c - U_a}{U_c + U_a}\right) \frac{RT}{F} \ln \frac{\left(\frac{U_c + U_a}{U_c}\right)[Cl_i^-]_1 + [RSO_3^-]}{\left(\frac{U_c + U_a}{U_c}\right)[Cl_i^-]_2 + [RSO_3^-]} + t_w \frac{RT}{F} \ln \frac{a_{w1}}{a_{w2}} \quad (3)$$

where

U_c = cation mobility
U_a = anion mobility
$[Cl_i^-]_1$ = chloride concn. internal on side 1 of the membrane
$[Cl_i^-]_2$ = chloride concn. internal on side 2 of the membrane
$[RSO_3^-]$ = capacity meq./g./moisture g. H_2O/g.

For the evaluation of the anion transfer term the values of sodium and chloride ion mobilities have been assumed proportional to the water mobilities of these species. Activity coefficients have been assumed unity and $[Cl_i^-] = [NaCl_0]^2/[RSO_3^-]$.

Using equation 3, values of the water transference number t_w have been calculated and are listed in Table III.

TABLE III

Membrane no.	Nominal soln. molarities	Calcd. anion transfer term, mv.	Water transfer term, mv.	t_w
1-6	0.1-0.05	0.009	0.051	1.2
1-6	.2- .1	.039	.121	1.4
1-6	.4- .2	.148	.382	2.3
1-6	.8- .4	.60	.49	1.4
1-4	.1- .05	.010	.080	1.9
1-2	.1- .05	.028	.902	21.5
2-6A	.1- .05	.009	.271	6.5
2-6B	.1- .05	.008	.182	4.3
2-6B	.2- .1	.023	.317	3.8
2-4	.1- .05	.014	.516	12.3
2-2	.1- .05	.038	1.64	39.0
3-6A	.1- .05	.010	0.36	8.6
3-6A	.2- .1	.044	0.416	5.0
3-6A	.4- .2	.182	1.288	7.9
3-6A	.8- .4	.73	2.40	7.1
3-6B	.1- .05	.010	.26	6.2
3-4	.1- .05	.020	.81	19.3
3-4	.2- .1	.084	1.056	12.9
3-4	.4- .2	.356	2.534	15.6
3-4	.8- .4	1.41	3.94	11.7
3-2	.1- .05	0.053	2.83	66.4

The difference between the ideal and the measured potentials is small and the uncertainty of the measurement is a significant fraction of the difference, in some cases as high as a factor of 0.5. In addition, the approximations involved in the calculation of the anion transfer term result in errors which may be of the same order of magnitude. For example, activity coefficients for the Donnan equation may differ widely from unity[14] for sulfonated polystyrene ion-exchange materials. Hence the absolute values of t_w are regarded as indicative only. It is probable that the relative values of t_w for various membranes are more precise.

The values obtained for t_w may be compared to values estimated from other experimental data. Preliminary measurements of electroösmotic water transfer across membranes in 0.1 M NaCl solution gave a value of $t_w = 4.25$ moles per Faraday for a 2-6B membrane. The value of $t_w = 17.0$ has been reported by Rosenberg[15] for a membrane which shows a membrane potential 0.96 of the ideal potential in dilute solution.

It is to be expected that the water transfer through a membrane should be a function of the water content of the membrane. For the potentials measured between 0.05 and 0.10 N solutions the approximation indicates that the water transfer is the major term in the deviation from ideality. Thus the potential measured would be a function of the water content of the membrane. Empirically the potential has been found to be inversely proportional to the cross-linking of the membrane at constant water content. This empirical correlation of the experimental data is given in Fig. 2. The

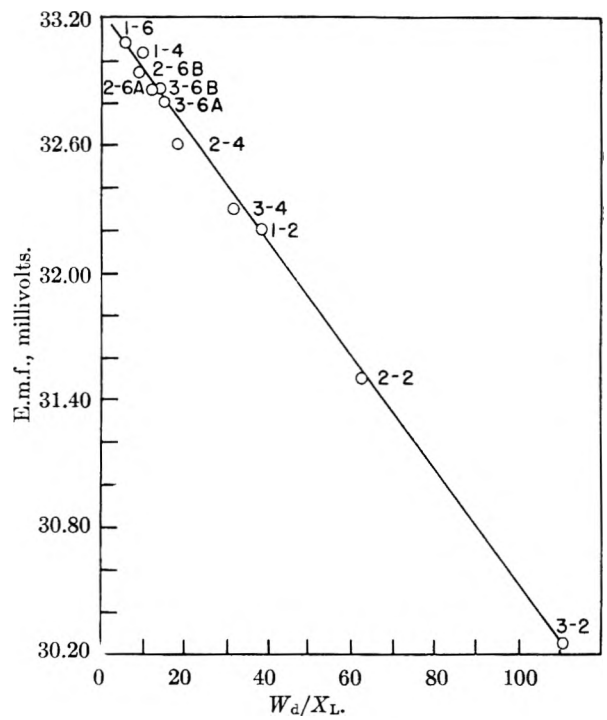

Fig. 2.—Membrane potential developed between 0.099 and 0.0492 N sodium chloride solutions. Wd represents % moisture in the membrane on a dry-weight basis and XL represents mole % divinylbenzene in the membrane. The numbers on the points are membrane numbers.

slope of the line is somewhat doubtful because of the possibility of osmotic degradation of the cell which presumably is also a function of the water content of the membrane. However, the data indicates that for these membranes

$$t_w = K(W_D/X_L)$$

where W_D is grams of water per gram of dry membrane, X_L is the nominal cross-linking in mole % divinylbenzene.

Acknowledgment.—The authors are indebted to the Research Council of Ontario and to the Advisory Committee on Scientific Research, University of Toronto, for financial support.

(14) H. P. Gregor and M. H. Gottlieb, *J. Am. Chem. Soc.*, **75**, 3539 (1953).

(15) Rosenberg quoted by K. S. Spiegler, *J. Electrochem. Soc.*, **100**, 303C (1953).

EXTRACTION OF INORGANIC SALTS BY 2-OCTANOL. I. COBALT(II) AND NICKEL(II) PERCHLORATES[1]

BY T. E. MOORE, ROY J. LARAN AND PAUL C. YATES

Contribution from the Department of Chemistry, Oklahoma A. and M. College, Stillwater, Oklahoma

Received August 13, 1954

The 2-octanol extractions of $Ni(ClO_4)_2$ and $Co(ClO_4)_2$ from aqueous solutions have been studied at 30°. The distribution coefficients of these salts are almost alike and much higher than those of the corresponding chlorides. By studying the extraction of $Co(ClO_4)_2$ at constant initial aqueous concentration in the presence of varying concentrations of $LiClO_4$, $Ca(ClO_4)_2$ and $Al(ClO_4)_3$, the effect of the latter perchlorates in promoting the extraction of $Co(ClO_4)_2$ has been shown to be primarily the mass action of the perchlorate ions. The ratio of the octanol and aqueous phase activities of $Co(ClO_4)_2$ in mixed extractions with $Ca(ClO_4)_2$ have been calculated by making certain assumptions regarding the activity coefficients in each phase. Values of the ratio are reasonably constant. It is concluded that the differences in the chloride-promoted 2-octanol extractions of $CoCl_2$ and $NiCl_2$ are not the result of differences in the extraction behavior of the nickel and cobalt ions but arise from specific promoting salt-transition metal salt interactions.

Garwin and Hixson[2] have reported the separation of $NiCl_2$ from $CoCl_2$ through the selective extraction of the latter by 2-octanol from solutions containing HCl or $CaCl_2$ at high concentrations. Further study in these laboratories has shown that LiCl is also a very effective extraction-promoting electrolyte for $CoCl_2$. The role of the promoting electrolytes in this and other similar systems is unquestionably very complex. For example the promoting electrolytes are usually themselves readily extracted, and spectrophotometric studies on the $CoCl_2$–LiCl–octanol–H_2O system[3] have provided evidence of extensive interaction of LiCl with $CoCl_2$ in octanol. Reactions of $NiCl_2$ with LiCl in octanol appear to be of much less importance.[3] To support the hypothesis that the differences in the behavior of cobalt and nickel salts with respect to extraction by 2-octanol are primarily the result of differences in specific interactions of transition metal salt with promoting salt, a study was undertaken of the 2-octanol extraction of the perchlorates of cobalt and nickel. Complex formation between perchlorate ions and transition metal ions would be expected to be at a minimum in both phases in such systems.

Experimental

Materials.—All chemicals were C.P. or reagent grades. Stock solutions of $Co(ClO_4)_2$ or $Ni(ClO_4)_2$ were prepared from the corresponding metal carbonates and $HClO_4$, and stock solutions of $LiClO_4$ and $Al(ClO_4)_3$ were prepared by metathesis from the metal sulfates and $Ba(ClO_4)_2$. The octanol was the best grade furnished by the Matheson Coleman and Bell Co. It was found to be ketone-free and to have the boiling point and refractive index reported in the literature for the pure compound.[4] No further purification was considered necessary.

Extraction Procedure.—The first set of experiments was concerned with the variations in the distribution coefficients of $Co(ClO_4)_2$ and $Ni(ClO_4)_2$ with concentration while the other series of experiments were designed to study the promoting effects of perchlorates of varying cationic charge types on the distribution coefficients of $Co(ClO_4)_2$. Three stock solutions having constant $Co(ClO_4)_2$ concentration (0.243 *m*) and known concentrations of either $LiClO_4$, $Ca(ClO_4)_2$ or $Al(ClO_4)_3$ were diluted with 0.243 *m* $Co(ClO_4)_2$ solution. The series of solutions so prepared were used in the promoted-extraction experiments. A similar series of solutions containing 0.243 *m* $CoCl_2$ mixed with $CaCl_2$ was prepared. For the unpromoted experiments concentrated stock solutions of $Co(ClO_4)_2$ or $Ni(ClO_4)_2$ were diluted with water.

The equilibrations were made from equal weights of the aqueous mixtures and 2-octanol sealed in glass-stoppered flasks and mechanically agitated overnight at 30.0 ± 0.1°. The phases were separated and analyzed.

Analytical Procedures.—The analytical procedures employed on the aqueous phases were for the most part the ordinary methods: cobalt, spectrophotometric using the absorption peak at 510 mμ or electrolysis; nickel, spectrophotometric using the 720 mμ peak; perchlorate, precipitation as $KClO_4$; calcium, precipitation as CaC_2O_4 and titration with $KMnO_4$; chloride, titration with $AgNO_3$. Lithium and aluminum were determined by difference. Methods of analysis of the octanol phases varied according to the concentrations of the extracted salts. At the higher concentrations both cobalt and nickel were directly determined spectrophotometrically at the same wave lengths used for the aqueous phases, by means of the Beckman Model B spectrophotometer. It was observed, however, that the extinction coefficient at 510 mμ in the case of $Co(ClO_4)_2$ was somewhat dependent upon the water concentration in octanol. Since the extraction phases had a variable water content, efforts were made to allow for this in making the spectrophotometric standard curve. Sufficient hydrous octanol was used in the preparation of the standard solutions to correspond approximately to the experimentally determined water content of the phases.

In the determination of the lower concentrations of $Co(ClO_4)_2$ (10^{-3} molal and under) use was made of the very high extinction coefficient of the 680 mμ absorption peak found in concentrated LiCl solutions in octanol containing $CoCl_2$. A saturated solution of LiCl was added to give a Cl/Co ratio of approximately 1000. Although Beaver, *et al.*,[3] showed that above a Cl/Co ratio of 100 water has little effect upon the spectrum, the spectrophotometric standard solutions were again prepared using hydrous octanol.

Perchlorate was determined as $KClO_4$ by direct precipitation from octanol (after preliminary results had shown that this procedure gave as satisfactory results as back-extraction into water prior to precipitation). The lowest concentrations of nickel were back-extracted and determined polarographically.[5] Water was found by the Karl Fischer method with a dead-stop end-point.

Results and Discussion

Figure 1 shows that while the distribution coefficients k_d of $Co(ClO_4)_2$ and $Ni(ClO_4)_2$, defined as the ratio of the number of moles of salt per 1000 g. of octanol + water in the non-aqueous phase to the aqueous phase molality, are strongly concentration-dependent, they are almost equal and markedly higher than those of $CoCl_2$ and $NiCl_2$. This result

(1) Presented in part at the 9th Southwest Regional meeting of the American Chemical Society, New Orleans, La., 1953. Supported under Contract AT(11-1)-71 No. 1 with the U. S. Atomic Energy Commission.

(2) L. Garwin and A. N. Hixson, *Ind. Eng. Chem.*, **41**, 2303 (1949).

(3) W. D. Beaver, L. E. Trevorrow, W. E. Estill, P. C. Yates and T. E. Moore, *J. Am. Chem. Soc.*, **75**, 4556 (1953).

(4) G. L. Dorough, H. B. Glass, T. L. Gresham, G. B. Malone and E. B. Reid, *ibid.*, **63**, 3100 (1941).

(5) I. M. Kolthoff and J. J. Lingane, "Polarography," Interscience Publishers Inc., New York, N. Y., 1941, p. 281.

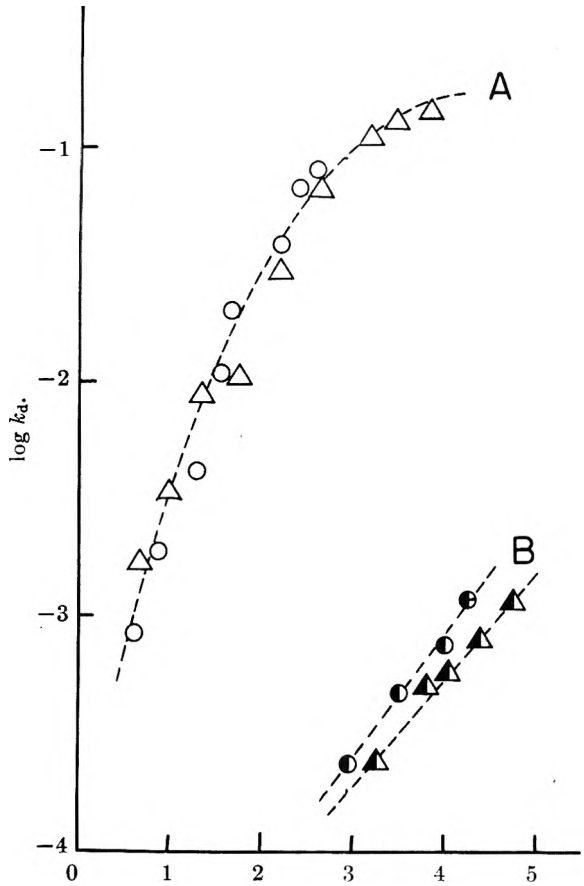

Fig. 1.—Distribution coefficients k_d of salts between 2-octanol and water at 30°: A, ○, $Co(ClO_4)_2$; △, $Ni(ClO_4)_2$; B, ◐, $CoCl_2$; ◭, $NiCl_2$.

indicates a close similarity in the salt–solvent interactions for $Co(ClO_4)_2$ and $Ni(ClO_4)_2$ in octanol. It seems probable, owing to the small tendency of perchlorate ions to associate with cations into complexes and to the greater base strength of water compared to octanol, that cobalt and nickel perchlorates exist largely as hydrated ions and ion-pairs in the octanol phases. This is supported by the high but similar hydration numbers (~12) reported by Yates, *et al.*,[6] and by the shift in the principal absorption peak from 525–530 mμ characteristic of anhydrous $Co(ClO_4)_2$ in anhydrous octanol to 510 mμ characteristic of both aqueous and hydrous-octanol solutions of $Co(ClO_4)_2$.

The promoting effect of added perchlorates was found to depend only upon the total perchlorate concentration and to be independent of the charge type of the promoting salt cations. This relatively simple result is illustrated in Fig. 2 where the distribution coefficients of $Co(ClO_4)_2$ alone and in mixtures can be seen to lie on a common curve as a function of the total perchlorate concentration.

By assuming that at equal concentrations the values of $\gamma\pm$ for 2:1 metal perchlorates are approximately equal and also that the values of $\gamma\pm$ for $Co(ClO_4)_2$ in a mixture of 2:1 metal perchlorates are equal to those of $Co(ClO_4)_2$ alone at the same total concentration as the mixture, values of the

(6) Paul C. Yates, R. J. Laran, R. E. Williams and T. E. Moore, *J. Am. Chem. Soc.*, **75**, 2212 (1953).

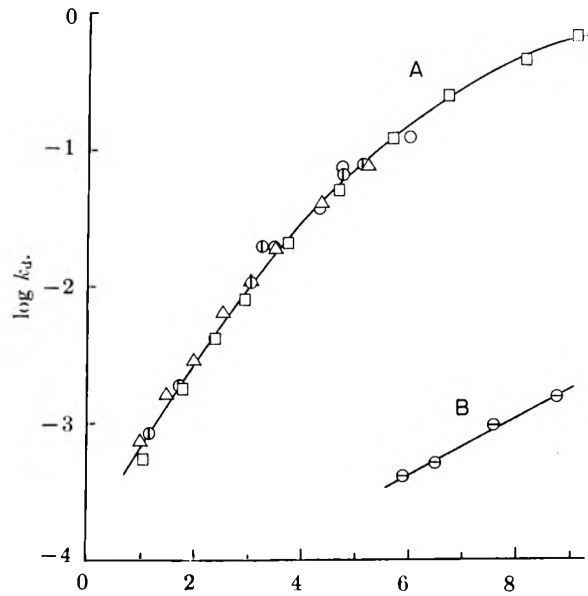

Fig. 2.—Distribution coefficients k_d of $Co(ClO_4)_2$ or $CoCl_2$ between 2-octanol and aqueous mixtures of promoting electrolytes at 30°: A, (|), $Co(ClO_4)_2$ alone; ○, $Co(ClO_4)_2$ + $Al(ClO_4)_3$; □, $Co(ClO_4)_2$ + $Ca(ClO_4)_2$; △, $Co(ClO_4)_2$ + $LiClO_4$; B, ⊖, $CoCl_2$ + $CaCl_2$.

equilibrium distribution constant for the $Ca(ClO_4)_2$-promoted extractions were calculated.

$$K_d = \frac{\{[Co][ClO_4]^2\gamma\pm^3\}_{oct}}{\{[Co][ClO_4]^2\gamma\pm^3\}_{aq}} = k_m \frac{(\gamma\pm^3)_{oct}}{(\gamma\pm^3)_{aq}} \quad (1)$$

In making the calculations the octanol-phase activity coefficient of $Co(ClO_4)_2$ in the unpromoted series was arbitrarily made unity at the lowest concentration. The results (Table I) show no significant trend and have an average deviation of 37% from the average value.

TABLE I

EQUILIBRIUM DISTRIBUTION CONSTANTS FOR THE $Ca(ClO_4)_2$-PROMOTED 2-OCTANOL EXTRACTION OF $Co(ClO_4)_2$

Aqueous phase total salt molality	$k_m \times 10^9$	$K_d \times 10^9$
0.52	0.23	0.91
0.88	0.44	1.29
1.17	2.65×10	1.31
1.47	1.93×10^2	1.53
1.86	2.19×10^3	1.92
2.35	3.93×10^4	0.46
2.84	2.92×10^5	0.44
3.36	1.50×10^6	1.59
4.09	6.20×10^6	0.89
4.56	1.59×10^7	2.22

The fact that equation 1 expresses the concentration dependence of the $Ca(ClO_4)_2$-promoted extractions over a wide range of perchlorate concentrations suggests that extraction promotion in perchlorate systems is largely a common-ion effect. It is concluded from this research that the differences observed in the chloride-promoted 2-octanol extractions of $CoCl_2$ and $NiCl_2$ are the result of specific interactions of $CoCl_2$ with the promoting chlorides rather than fundamental differences in the extraction behavior of cobalt and nickel ions.

NOTES

TORSIONAL BARRIERS IN MOLECULES $C_2H_mF_nCl_{6-m-n}$.

By N. W. Luft

Ladybridge Road, Cheadle Hulme, Cheshire, England

Received June 7, 1954

There appears to be hardly a group of chemical compounds for which more experimental data on intramolecular rotational barriers are available than the series of halogenated ethanes of the general composition of $C_2H_mF_nCl_{6-m-n}$. This is especially due to the extensive spectroscopic investigations by Nielsen and co-workers.[1-5] However, on occasions it has been found necessary[6] to revise some of the reported information on threefold barrier heights and torsional frequencies of these compounds. A more careful scrutiny has revealed certain additional inconsistencies in the torsional assignments, which lead to discrepancies with the additivity rule[7] for the increments, B, of threefold torsional barriers V_0, *viz.*

$$V_0(i_3 - k_rl_{3-r}) = rB(i\ldots k) + (3 - r)B(i\ldots l) \quad (1)$$

for ethane derivatives $(i_3 - k_rl_{3-r})$. Thus a reexamination of the torsional data seems unavoidable.

Usually torsional frequencies, δ_t, are related to barrier heights, V_0, by means of the harmonic oscillator approximation

$$\delta_t = (n/2\pi c)(V_0/2I_r)^{1/2} \quad (2)$$

where I_r = reduced moment of inertia about the n-fold axis of internal rotation and $n = 3$ in the present cases. Recently[1] an alternative graphical evaluation, by way of correlation of observed energy levels with actual eigen-values of the Mathieu equation, has been proposed which is likely to be more accurate for sinusoidal barriers of low height; *cf.* figures in brackets [] in Table I.

The data for threefold torsional barriers of fluorinated and chlorinated ethanes are given in Table I. Ethane and trifluoroethane are well investigated molecules which need no further comment. Their barriers determine the barrier increments, B(H . . . H) = 0.96 ± 0.05 and B(H . . . F) = 1.22 ± 0.05 kcal./mole, for internal rotation, opposite a CH_3 group, of a CH and CF bond, respectively, and thus the barriers in H_3C–CH_2F and H_3C–CHF_2. The result for the latter molecule is $V_0 = 3.40$ kcal./mole and $\delta_t \simeq 240$ cm.$^{-1}$, whereas previously $\delta_t \simeq 250$ cm.$^{-1}$ and $V_0 \simeq 3.94$ kcal./mole was proposed, from a rather uncertain interpolation of torsional frequencies of methyl fluoromethanes, although neither this fundamental nor its overtone has been observed. It seems possible now that the band $\nu(A') \sim 475$ cm.$^{-1}$ overlaps $2\delta_t$. In a recent note[6] the writer proposed $\delta_t \sim 93$ cm.$^{-1}$ and $V_0 \sim 10.1$ kcal./mole for F_3C–$CHCl_2$ instead of an earlier V_0 value about twice as high. Together with the above value of B(H . . . F) this leads to B(F . . . Cl) ≃ 4.4 kcal. and results in $V_0(F_3C$–$CH_2Cl) \simeq 6.8$ and the somewhat high $V_0(F_3C$–$CCl_3) \sim 13.2$ kcal./mole. Thus $\delta_t \sim 96$ cm.$^{-1}$ for F_3C–CCl_3, so that the higher value[4] $\delta_t = 173$ cm.$^{-1}$ is definitely ruled out. For F_3C–CH_2Cl Nielsen, *et al.*,[3] gave $\delta_t = 109$ cm.$^{-1}$ and $V_0 = 5.7$ kcal./mole, whereas with the same frequency and an estimated $I_r = 78.1 \times 10^{-40}$ g. cm.^{2} actually $V_0 \simeq 10.5$ kcal./mole is obtained. Therefore the frequency of 109 cm.$^{-1}$ is suspect of being slightly high.

The recent value $V_0(F_3C$–$CF_3) = 3.92$ kcal./mole gives B(F . . . F) = 1.31 kcal./mole and furthermore $V_0(F_3C$–$CF_2Cl) = 7.0$ and $V_0(F_3C$–$CFCl_2) = 10.1$ kcal./mole. This results in the estimated torsional frequencies $\delta_t \sim 80$ and 92 cm.$^{-1}$ in good agreement with the following assignments of overtone bands, *viz.*, 532 Ivw, liq. = 454 + δ_t, 828 Ivw, liq. = 648 + δ_t and 487 Ivwb = 399 + δ_t, respectively.

Moreover $V_0(Cl_3C$–$CCl_3) \sim 12 \pm 2$ kcal./mole[8] leads to B(Cl . . . Cl) ~ 4.0 kcal./mole and $V_0(Cl_3C$–$CCl_2F) = 12.4$ and $V_0(Cl_3C$–$CClF_2) = 12.8$ kcal./mole in reasonable agreement with previous values.[5]

For the evaluation of the remaining increment B(H . . . Cl) the following three spectroscopically determined[2,17] barrier heights are at our disposal, which yield three slightly different B-values, *viz.*

H_3C–CF_2Cl V_0 =	[3.705] kcal./mole	B(H . . . Cl) = 1.27 kcal.
H_3C–$CFCl_2$	[3.47]	1.13
H_3C–CCl_3	[2.967]	0.99

Derivation of the first two B's involves use of the above B(H . . . F) = 1.22 kcal./mole. The last figure is a more direct one and supported by the impressive interpretation, due to Pitzer and Hollenberg,[17] of the six infrared bands of H_3C–CCl_3 at 137, 154, 172, ~ 533, 548 and 565 cm.$^{-1}$ as difference and sum combinations of $\nu_{11}(E) = 351$ cm.$^{-1}$ and various torsional levels ν_6. The inactive $\delta_t \sim \nu(0 - 1) = 214$ is obtained from the largest frequency in the series, 565 = 351 + $\nu_6(0 - 1)$. All three V_0's were evaluated[1,17] by special methods from actual levels. If instead, eq. 2 is used for δ_t's of the first two molecules then the resulting V_0's are smaller and B(H . . . Cl) ≃ 1.0 kcal./mole for all three. The slightly higher alternatives are not completely ruled out, since, *e.g.*, the above frequency of 214 cm.$^{-1}$ in H_3C–CCl_3 might perhaps be ν_5 (1 − 2), etc., and ν_5 (0 − 1) still larger (~240 ~588 Iw − 351, ?). But then B(H . . . Cl) ~ 1.3

(1) D. C. Smith, R. A. Saunders, J. R. Nielsen and E. E. Ferguson, *J. Chem. Phys.*, **20**, 847 (1952).

(2) D. C. Smith, G. M. Brown, J. R. Nielsen, R. M. Smith and C. Y. Liang, *ibid.*, **20**, 473 (1952).

(3) J. R. Nielsen, C. Y. Liang and D. C. Smith, *ibid.*, **21**, 1060 (1953).

(4) J. R. Nielsen, C. Y. Liang, D. C. Smith and R. M. Smith, *ibid.*, **21**, 383 (1953).

(5) J. R. Nielsen, C. Y. Liang, D. C. Smith and M. Alpert, *ibid.*, **21**, 1070 (1953).

(6) N. W. Luft, *ibid.*, **22**, 155 (1954).

(7) N. W. Luft, *Faraday Soc. Discs.*, **10**, 117 (1951); *J. Chem. Phys.*, **21**, 179 (1953).

TABLE I

TORSIONAL OSCILLATIONS IN MOLECULES $C_2H_mF_nCl_{6-m-n}$

Molecule	Previous values: V_0 (kcal./mole)	Previous values: δ_t (cm.$^{-1}$)	Ref.	Present data: V_0 (kcal./mole)	Present data: δ_t (cm.$^{-1}$)
H_3C–CH_3	2.75–3.05	280 ± 10	1, 9	2.90	290[a]
H_3C–CH_2F	[3.959]	278	1	3.15	(250)
H_3C–CHF_2	(3.94)	(250)	1	3.40	(240)
H_3C–CF_3	3.66	238	2,10	3.66	238
H_3C–CH_2Cl	2.7–4.7	(215–280)	11, 12	2.9	(220)
H_3C–$CHCl_2$	...	...	...	2.9_5	(215)
H_3C–CCl_3	(2.7–3.045)	(205)	13, 1		
	2.967	(214)	17	3.0	(214)
H_3C–CF_2Cl	[3.705]	238	1	3.4_4	~230
H_3C–$CFCl_2$	[3.470]	229	1	3.2	~220
F_3C–CH_2F	...	...	...	3.75	(87)
F_3C–CHF_2	...	...	...	3.85	(74)
F_3C–CF_3	3.92 (−4.35)	(68–70)	14, 15	3.9	(68)
F_3C–CH_2Cl	(10.5)	109	3	6.8	(90)
F_3C–$CHCl_2$	22.3	141	3	10.1	93
F_3C–CCl_3	(<38.7 or 13.2)	<173 or 96	4	(10.7–)13.2	(90–)96
F_3C–CF_2Cl	(<30.4 or 9.1)	<168 or 91	4	7.0(–9.1)	80(–91)
F_3C–$CFCl_2$	(<39.5)	<180	4	~10.1	~92
Cl_3C–$CClH_2$	...	...	...	6	(70)[b]
Cl_3C–CCl_2H	...	...	...	9	(65)
Cl_3C–CCl_3	12.0 ± 2.0	(65)	8	12.0	(65)
Cl_3C–CH_2F	...	...	...	6.4	(105)
Cl_3C–CHF_2	...	...	...	9.8	(100)
Cl_3C–CF_2Cl	(12.8)	81	5	12.8	81
Cl_3C–$CFCl_2$	(14.4)	77	5, *cf.* 16	12.4	~70

[a] L. G. Smith, *J. Chem. Phys.*, **17**, 139 (1949); *cf.* ref. 9. [b] *Cf.* the Raman shift at 85 cm.$^{-1}$, Landolt–Börnstein, Zahlenwerte & Funktionen, I, Springer, 1951, p. 3.

kcal. would call for yet another revision of assignments of two bands of H_3C–$CFCl_2$, *viz.*, 458 = 2 $\nu(A')$ instead of $2\delta_t$, and 256 = δ_t instead of $\nu(A')$. For these reasons B(H . . . Cl) = 1.0 kcal./mole is chosen.

The above B values have been used to estimate a number of unknown barriers which are also listed in Table I. The actual values of barrier increments B do not exhibit any obvious regularities and it is particularly surprising that the barrier in C_2Cl_6 is smaller than in C_2Cl_5F and $C_2Cl_4F_2$. It would be possible, at least in principle, to reverse this situation, *e.g.*, by assuming a barrier height in H_3C–CCl_3 comparable to Gordon and Giauque's[12] figure and for Cl_3C–CCl_3 one of the order of the upper limit of Mizushima, *et al.*[8], value. Because of additivity of barrier increments, however, such attempt would call for modifications of a number of barrier heights of related molecules, which seem less justified in the light of the most recent spectroscopic results.

(8) S. Mizushima, Y. Morino, T. Simanouchi and K. Kuratani, *J. Chem. Phys.*, **17**, 838 (1949).

(9) *Cf.* K. S. Pitzer, *Faraday Soc. Discs.*, **10**, 66 (1951).

(10) B. P. Dailey, *Ann. N. Y. Acad. Sci.*, **55**, 915 (1952).

(11) H. J. Bernstein, *J. Chem. Phys.*, **17**, 262 (1949); *cf.* A. Tang, *J. Chinese Chem. Soc.*, **18**, 2 (1951).

(12) J. Gordon and W. F. Giauque, *J. Am. Chem. Soc.*, **70**, 1506 (1948).

(13) T. R. Rubin and B. H. Levedahl, D. M. Yost, *ibid.*, **66**, 279 (1944).

(14) D. E. Mann and E. K. Plyler, *J. Chem. Phys.*, **21**, 1111 (1953); *cf.* J. S. Wicklund, H. W. Flieger and J. F. Masi, *J. Research Natl. Bur. Standards*, **51**, 91 (1953).

(15) E. L. Pace and J. G. Aston, *J. Am. Chem. Soc.*, **70**, 566 (1948).

(16) D. Simpson and E. K. Plyler, *J. Research Natl. Bur. Standards*, **50**, 223 (1953).

(17) K. S. Pitzer and J. L. Hollenberg, *J. Am. Chem. Soc.*, **75**, 2219 (1953).

LOW PRESSURE HYDROGEN SOLUBILITY IN URANIUM

BY H. C. MATTRAW

Knolls Atomic Power Laboratory,[1] General Electric Company, Schenectady, N. Y.

Received August 16, 1954

As is well known,[2] uranium forms a compound UH_3, with hydrogen, and the equilibrium pressure for the reaction

$$UH_3 \text{ (solid phase 1)} = U \text{(solid phase 2)} + 3/2\ H_2\text{(gas)}$$

is satisfactorily expressed by

$$\log P_{mm} = -\frac{4500}{T} + 9.28 \qquad (1)$$

Solid phase 1 is solid solution rich in UH_3 and low in U. Solid phase 2 is solid solution rich in U and low in H. For the very low hydrogen concentration region, phase 1 is absent. At 295°, the dissociation pressure of the hydride is 23 to 24 mm. (at 436° UH_3 has a dissociation pressure of 1 atmosphere); however, at pressures below this there exists appreciable solubility of hydrogen in uranium. Qualitatively the system is similar to the palladium–hydrogen system, and behaves as the metals which Dushman[3] terms the group B, that is, lowered solubility with increased temperature.

(1) The Knolls Atomic Power Laboratory is operated by the General Electric Co. for the Atomic Energy Commission. The work reported here was carried out under Contract W-31-109 Eng-52.

(2) (a) F. H. Spedding, A. S. Newton, *et al.*, *Nucleonics*, **4**, 4 (1949); (b) J. J. Katz and E. Rabinowitch, "The Chemistry of Uranium, NNEW VIII-5," McGraw-Hill Book Co., Inc., New York, N. Y., 1951.

(3) S. Dushman, "Scientific Foundations of Vacuum Technique," Chap. 9, John Wiley and Sons, Inc., New York, N. Y., 1949.

TABLE I

SOLUBILITY OF HYDROGEN IN URANIUM AT 295°

P, μ	S, cc./10 g.	$S/\sqrt{P}$	P, μ	S, cc./10 g.	$S/\sqrt{P}$
	Run 1			Run 2	
150	0.41	0.0335	103	0.34	0.0335
135	.35	.0301	82	.29	.0320
100	.31	.0310	56	.28	.0374
79	.28	.0315	47	.23	.0335
69	.25	.0301	38	.22	.0357
57	.23	.0305	34	.20	.0343
46	.21	.0310			
35	.20	.0338			
30	.19	.0347			
26	.18	.0353			

In this work, the solubilities at various low pressures were determined at 295° using 10 g. of powdered uranium. For this low hydrogen concentration region the solubility may be expressed by

$$S = K\sqrt{P} \qquad (2)$$

where S is in standard cc./g. of uranium, P in microns. The data presented below show that equation 2 is obeyed

This square root relation has been shown by Battelle[2b] to hold for α,β,γ-forms of uranium at temperatures from 600–800° at pressures up to 100 mm. The average value of $S/\sqrt{P}$ for 10 g. of uranium is 0.033 with a standard deviation of ± 0.0022. Thus for 1 g. of uranium at 295° the hydrogen solubility obeys equation 2 and K has a value of $3.30 \pm 0.22 \times 10^{-3}$.

Hydrogen must go into solution in the dilute region as H atoms or negative H ions or as UH.

Experiments at other temperatures, though not designed to find the true heat of solution, show the heat of solution of hydrogen in α uranium (solid phase 2) at infinite dilution is approximately -13 kcal./mole H_2. The heat of solution of hydrogen in α-uranium (solid phase 2) at the composition where the uranium hydride phase begins to separate is calculated from equation 1 to be about -20 kcal./mole H_2.

The Battelle work[2b] indicates that for β, γ- and liquid uranium the heat of solution of hydrogen becomes positive in contrast with the negative heat of solution found for the α uranium in this study.

COMMUNICATIONS TO THE EDITOR

MONOLAYER STRUCTURE AS REVEALED BY ELECTRON MICROSCOPY

Sir:

Little is known about the detailed structure of monolayers, the process of monolayer collapse and the nature of collapsed films. Films of fatty acids on water, before and after collapse, have recently been transferred from a Langmuir–Adam–Harkins film balance[1,2] to a collodion support, shadowcast with chromium, and examined in an RCA Type EMU electron microscope. Remarkable structures were revealed.

Monolayers of *n*-hexatriacontanoic acid[3] give pressure–area isotherms similar to those of stearic acid. At zero pressure, the molecule has an extrapolated cross-sectional area of 20.4 Å.^{2}, essentially identical to the 20.3 Å.^{2} for stearic acid.[4] It differs principally in that the film collapses at 58 dynes per cm., as compared with 42 dynes for that of stearic acid.

Samples of *n*-hexatriacontanoic acid films were taken[5] at 15 dynes per cm., at 25 dynes per cm., and after collapse. They were shadowcast with chromium at an angle of 15° to the surface. Electron micrographs are shown in Fig. 1. A blank water sample, which had been transferred from the film balance to a collodion support, is shown in A.

Throughout B, the widths of the shadows correspond to a film thickness close to the 50 Å. expected for a monolayer of vertically oriented *n*-hexatriacontanoic acid. Many islands or aggregates of irregular shape and size characterize the partly compressed monolayer. Movement of islands may account for the unstable pressures in this region of the isotherm often observed for fatty acid monolayers.

In C, a transition stage between monolayer islands and collapsed film is shown. The monolayer has become a continuous phase; the bare portions are now discontinuous. Islands have sometimes been seen at this pressure, possibly because the film had been disturbed during the transfer process.

In both B and C, the monolayer surface appears coarser than that of the collodion support. The texture may reflect the structure of the condensed monolayer. Bare portions may contain film molecules that are less closely packed.

Across D, several long flat fiber-like structures appear. They rest on a continuous monolayer substrate and are about 100 Å. or two molecules thick.

(1) N. K. Adam, "The Physics and Chemistry of Surfaces," Third Edition, Oxford University Press, Oxford, 1941.

(2) W. D. Harkins, "The Physical Chemistry of Surface Films," Reinhold Publ. Corp., New York, N. Y., 1952.

(3) A 36-carbon acid prepared in 99.99% purity by Dr. R. J. Meyer of our laboratories.

(4) H. E. Ries, Jr., and H. D. Cook, *J. Colloid Sci.*, in press.

(5) A small ring was raised through the film and lowered over a collodion support. Two more-refined techniques have reproduced the main features of the micrographs. In one, shallow cups containing collodion supports are raised through the film. In the other, metal-coated collodion supports are raised vertically through the film as in the Langmuir–Blodgett technique.

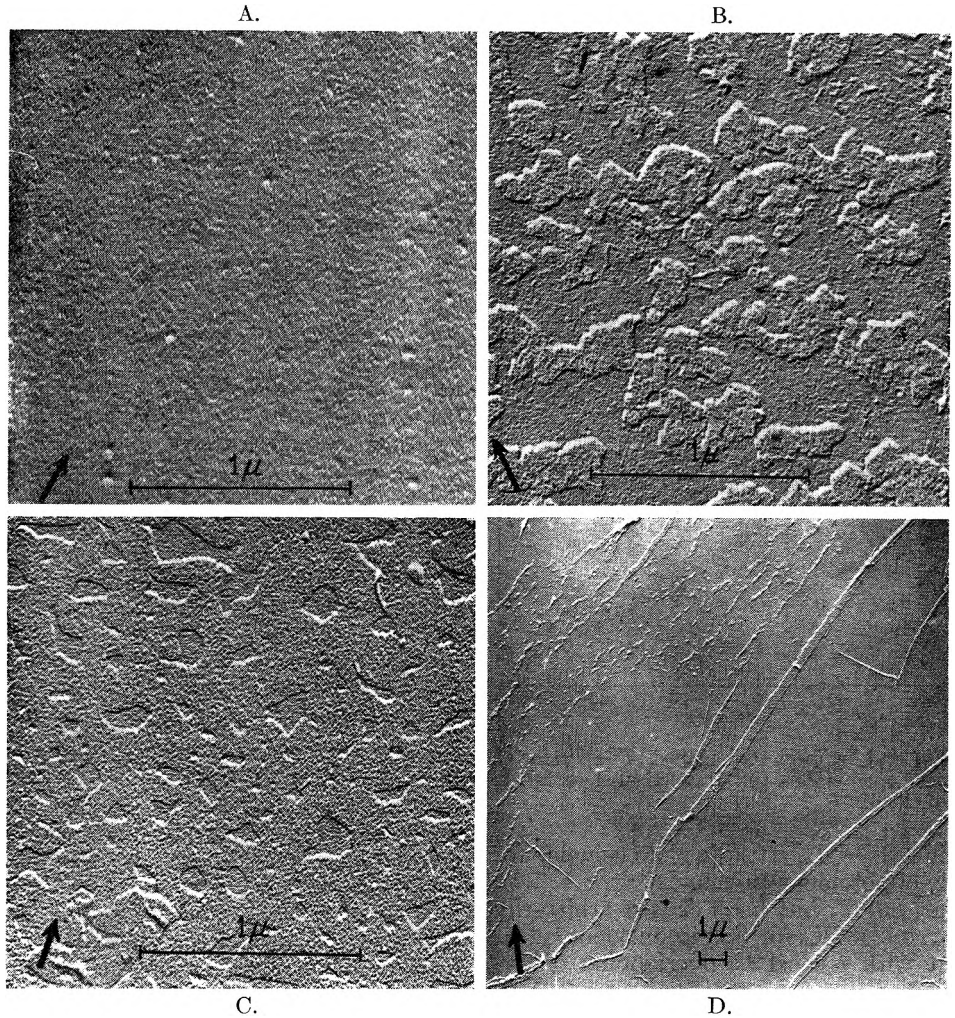

Fig. 1.—Electron micrographs of monolayer films of *n*-hexatriacontanoic acid: A, blank, no film; B, at −15 dynes per cm.; C, at 25 dynes per cm.; D, after collapse. Shadows are light, and arrows indicate the direction of chromium shadowcasting.

Shadows at a small break through the substrate showed that it remained 50 Å. thick. A mechanism for collapse is clearly suggested: as the pressure increases, the monolayer rises from the surface along a line of rupture, folds polar face to polar face, and falls over to form long flat structures, two molecules thick.

When *n*-hexatriacontanoic acid was deposited directly on the collodion support rather than on water, different structures were observed. A solution in benzene of less hexatriacontanoic acid than needed for a closely packed monolayer was deposited on collodion. After evaporation of the benzene and shadowcasting, micrographs showed many platelets or flat micelles with rounded edges and a thickness of two molecules. No monolayer structures were observed.

Such observations of monolayer islands, collapsed films and platelets deposited directly from solution provide information basic to two-dimensional and three-dimensional nucleation, crystallization and micelle formation.

RESEARCH DEPARTMENT
STANDARD OIL COMPANY (INDIANA) HERMAN E. RIES, JR.
WHITING, INDIANA WAYNE A. KIMBALL

RECEIVED NOVEMBER 26, 1954

THE TEMPERATURE DEPENDENCE OF MECHANICAL AND ELECTRICAL RELAXATIONS IN POLYMERS[1]

Sir:

The temperature dependence of both viscoelastic[2,3] and dielectric[4] properties of a polymeric system can be described by a single temperature-dependent parameter which represents the ratio of any relaxation time at temperature T to its value at an arbitrary reference temperature T_0. When different systems are compared using the same T_0 for all (*e.g.*, 298°K.), plots of this parameter (a_T or κ from viscoelastic measurements, b_T from dielectric) against T exhibit little resemblance. However, we have found that, by selecting a different reference temperature T_s for each system and plotting

(1) This work was supported by Picatinny Arsenal, Ordnance Corps, Department of the Army. The author wishes to express to Prof. John D. Ferry and Dr. Robert F. Landel his appreciation for many helpful discussions.

(2) (a) R. D. Andrews, N. Hofman-Bang and A. V. Tobolsky, *J. Polymer Sci.*, **3**, 669 (1948); (b) A. V. Tobolsky and J. R. McLoughlin, *ibid.*, **8**, 543 (1952).

(3) J. D. Ferry, *J. Am. Chem. Soc.*, **72**, 3746 (1950).

(4) (a) J. D. Ferry and E. R. Fitzgerald, *J. Colloid Sci.*, **8**, 224 (1953); (b) J. D. Ferry, M. L. Williams and E. R. Fitzgerald, THIS JOURNAL, in press.

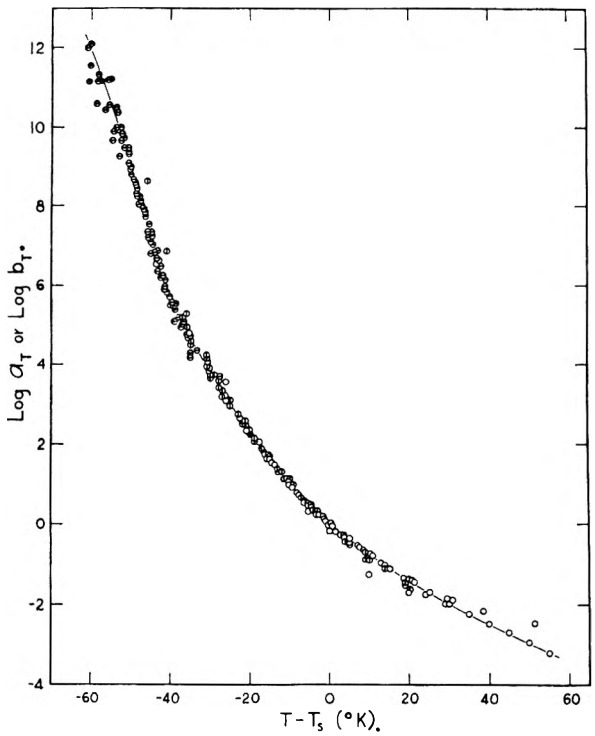

Fig. 1.—Log a_T and log b_T plotted against $(T - T_s)$ for 17 polymer systems: open circles, ref. 5; vertical slots, ref. 4; horizontal slots, ref. 6.

a_T or b_T against $T - T_s$, all such plots coincide for a wide variety of polymer systems.

For comparison, T_s has been chosen arbitrarily for one system—243°K. for polyisobutylene, a favorable point with respect to overlapping of dynamic mechanical data from this Laboratory. Values of T_s for 16 other systems have been obtained by comparing the temperature dependence of their dynamic mechanical,[4a,5] stress relaxation,[1,6] steady flow viscosity,[5a,b,d] and dielectric properties[4] with that of polyisobutylene, and are listed in Table I. In Fig. 1, a_T and b_T are plotted logarithmically against $T - T_s$ for all 17 systems, and fall quite closely on a single composite curve.

(5) (a) J. D. Ferry, L. D. Grandine, Jr., and E. R. Fitzgerald, *J. Appl. Phys.*, **24**, 911 (1953); (b) L. D. Grandine, Jr., and J. D. Ferry, *ibid.*, **24**, 679, (1953); (c) M. L. Williams and J. D. Ferry, *J. Colloid Sci.*, **9**, 479 (1954); (d) M. L. Williams and J. D. Ferry, *ibid.* (in press); (e) R. F. Landel and J. D. Ferry, (unpublished experiments); (f) M. L. Williams, J. D. Ferry, S. Axelrod, S. N. Chinai, J. D. Matlack and A. L. Resnick, Presented at the 126th Meeting of the American Chemical Society, Sept. 1954.

(6) (a) J. Bischoff, E. Catsiff and A. V. Tobolsky, *J. Am. Chem. Soc.*, **74**, 3378 (1952); (b) E. Catsiff and A. V. Tobolsky, *J. Appl. Phys.*, **25**, 1092 (1954); (c) A. V. Tobolsky and E. Catsiff, *J. Am. Chem. Soc.*, **76**, 4204 (1954).

TABLE I

System	Measurement[a]	Reference	T_s, °K.
Polyisobutylene	D, S, V	5a, 1	243
Polystyrene	D	5b	408
Polyvinyl acetate	D, E	5c	349
Polymethyl acrylate	D, E	5f, 4b	324
Polyvinyl chloroacetate	E	4b	346
Polyvinyl acetal	E	4b	380
Butadiene–styrene			
75/25	S	6a	268
60/40	S	6b	283
50/50	S	6b	296
30/70	S	6b	328
Paracril 26	S	6b	288
Polymethyl methacrylate	S	6a	433
Polystyrene–Decalin 62%	D, V	5b	291
Polyvinyl acetate–tricresyl phosphate 50%	D, V	5d	293
Polyvinyl chloride–dimethyl-thianthrene			
10%	D, E	4a	293
40%	D, E	4a	313
Cellulose tributyrate dimethyl phthalate 21%	D	5e	247

[a] D = dynamic mechanical, S = stress relaxation, V = steady flow viscosity, E = dielectric.

Our reference temperature T_s is 50 ± 4° above the glass transition temperature for 7 of these systems, and it is 46 ± 3° above the distinctive temperature T_d of Tobolsky[6c,7] for the 6 systems he has analyzed. This suggests that the arbitrary T_s might be replaced by an absolute T_g (from thermal expansion measurements) or T_d (from the inflection of a plot of log a_T against temperature). However, because of the difficulty of experimental measurements near T_g or T_d, we prefer to base our comparison on one arbitrary selection of T_s at present.

It should be mentioned that divergences may be expected at lower temperatures where properties are affected by thermal history. A later communication will discuss the relation of this treatment to various theoretical formulations of the temperature dependence of relaxation and viscosity.

DEPARTMENT OF CHEMISTRY
UNIVERSITY OF WISCONSIN MALCOLM L. WILLIAMS
MADISON 6, WIS.

RECEIVED NOVEMBER 17, 1954

(7) The reduced viscoelastic equations of Tobolsky and Catsiff,[6] which also involve a correlation of temperature dependence in different polymers, are based on a function $f(T/T_d)$ rather than a difference $T - T_s$. Within the temperature range where f is a linear function of T/T_d (roughly between −60 and −30° in Fig. 1), it can be shown that log a_T is actually a linear function of $(T - T_d)$. Thus in this range the two treatments predict the same temperature dependence. At higher temperatures, however, they would differ.

to those qualified
in the techniques of

PLASTICS

as applied to the
field of advanced

GUIDED MISSILES

The Laboratories are engaged, among other projects, in a highly advanced research and development program devoted to production of the Hughes guided missile.

ENGINEERS or APPLIED PHYSICISTS

familiar with non-metallic materials are required to plan, coordinate, and conduct special laboratory and field test programs on missile components. These men should have experience in materials development, laboratory instrumentation, and the design of test fixtures.

RESEARCH CHEMIST

The Plastics Department of the Microwave Laboratory has need for an individual with a Ph.D. Degree, or equivalent experience in organic or physical chemistry, to investigate the basic properties of plastics. The work involves research into the properties of flow, the mechanisms of cure, vapor transmission, and the electrical and physical characteristics of plastics.

Scientific and Engineering Staff

HUGHES

RESEARCH AND DEVELOPMENT LABORATORIES

Culver City
Los Angeles County
California